APPLICATION OF MECHANISTIC REVELATIONS TOWARDS DEVELOPMENT OF NOVEL REACTIONS

By

Kumar Dilip Ashtekar

A DISSERTATION

Submitted to
Michigan State University
in partial fulfillment of the requirements
for the degree of

Chemistry – Doctor of Philosophy

2014

ABSTRACT

APPLICATION OF MECHANISTIC REVELATIONS TOWARDS DEVELOPMENT OF NOVEL REACTIONS

By

Kumar Dilip Ashtekar

Mechanistic investigations of the sought-after organic reactions-the Morita Baylis Hilman reaction and halofunctionalization of olefins has led to insightful and critical mechanistic discernments. Tools such as quantum chemical computational analysis, labeling experiments, kinetic isotopic effects, and kinetics studies (RPKA) were employed towards a comprehensive analysis of these reactions. These mechanistic revelations were applied towards development of three novel reactions a.) [4+2] formal cycloaddition towards asymmetric synthesis of dihydropyrans, b.) halenium ion initiated diastereoselective cascade spiroketalization of alkenoic ketones and c.) Iodenium ion initiated cascade towards a diastereoselective synthesis of tricyclic molecules with an octahydroquinoline core. This dissertation describes in detail the tools that were involved in probing the mechanistic nuances and a rational approach designed towards reaction discovery and optimization endeavors.

ACKNOWLEDGEMENTS

I can never thank enough the people that have been a part of my everyday life during my doctoral studies. Certainly, I won't be here in the first place if it wasn't for my parents. Everything I have and what I am today, is because of their unconditional love and support. It is not the discoveries that I made or the knowledge I have gained are important to me, but the contribution of everyone who made this journey possible is invaluably an integral part of my life and I am indebted to all of them. It will be the memories with everyone that I have amassed at Michigan State University will define the true treasure I have earned during my doctoral studies.

The Borhan group has always been more of family rather than a 'lab', held together and nurtured by Babak and Chrysoula. It is the comfort of being a part of this family and enjoying chemistry with all my friends kept me going all these years. I never felt I was working for a boss, rather I worked with a very good friend. Although new members become a part of this group every year, I never liked that old members had to leave, and now it is my turn. I do not know if I will remember all the experiments I ever performed in this lab, but I will always cherish the memories I have with everyone and I am grateful to all of them for making my journey at MSU an unforgettable and treasured experience.

TABLE OF CONTENTS

LIST OF TABLES

LIST OF FIGURES

LIST OF SCHEMES

KEY TO SYMBOLS AND ABBREVIATIONS

Symbols

Å	Angstrom
cm^{-1}	Wavenumber
M	Molar
mM	Millimolar
mg	Milligram
mmol	Millimole
>	Larger than
<	Less than
$CHCl_3$	Chloroform
DMF	Dimethylformamide
ESI	Electrospray Ionization
Et_3N	Triethylamine
EtOAc	Ethyl Acetate
HalA	Halenium Affinity
HOMO	Highest Occupied Molecular Orbital
HRMS	High-Resolution Mass Spectrometry
LUMO	Lowest Unoccupied Molecular Orbital
m. p.	Melting Point
mbar	Milibarr
$MgSO_4$	Magnesium Sulfate
NAAA	Nucleophile Assisted Alkene Activation
n.a.	Not Applicable
n.d.	Not Determined

Na_2SO_4	Sodium Sulfate
NaH	Sodium Hydride
NaHMDS	Sodium bis(trimethylsilyl)amide
NaOH	Sodium Hydroxide
NMR	Nuclear Magnetic Resonance
IR	Infrared

CHAPTER I: A MECHANISTICALLY INSPIRED APPROACH TOWARDS THE DEVELOPMENT OF A CATALYTIC ASYMMETRIC FORMAL [4+2] ADDITION OF ETHYL-2,3-BUTADIENOATE WITH ACYCLIC ENONES

I.1. Introduction.

The Morita Baylis-Hillman reaction has been extensively studied for its utility to forge C-C bonds catalyzed by nitrogen and phosphorus based Lewis bases.[1-3] Recent advancements include the development of catalytic asymmetric variants.[4-7] A stereotypical Morita Baylis-Hillman reaction and its established mechanism are depicted in Figure I-1. The robustness of this reaction in terms of its atom economy and utility of the resulting products have led towards an extensive exploration of electrophiles that can serve as good Michael acceptors. Allene esters are one such class of Michael acceptors, which expand the repertoire of products resulting from the Baylis-

Figure I-1. A prototypical Morita Baylis-Hillman reaction

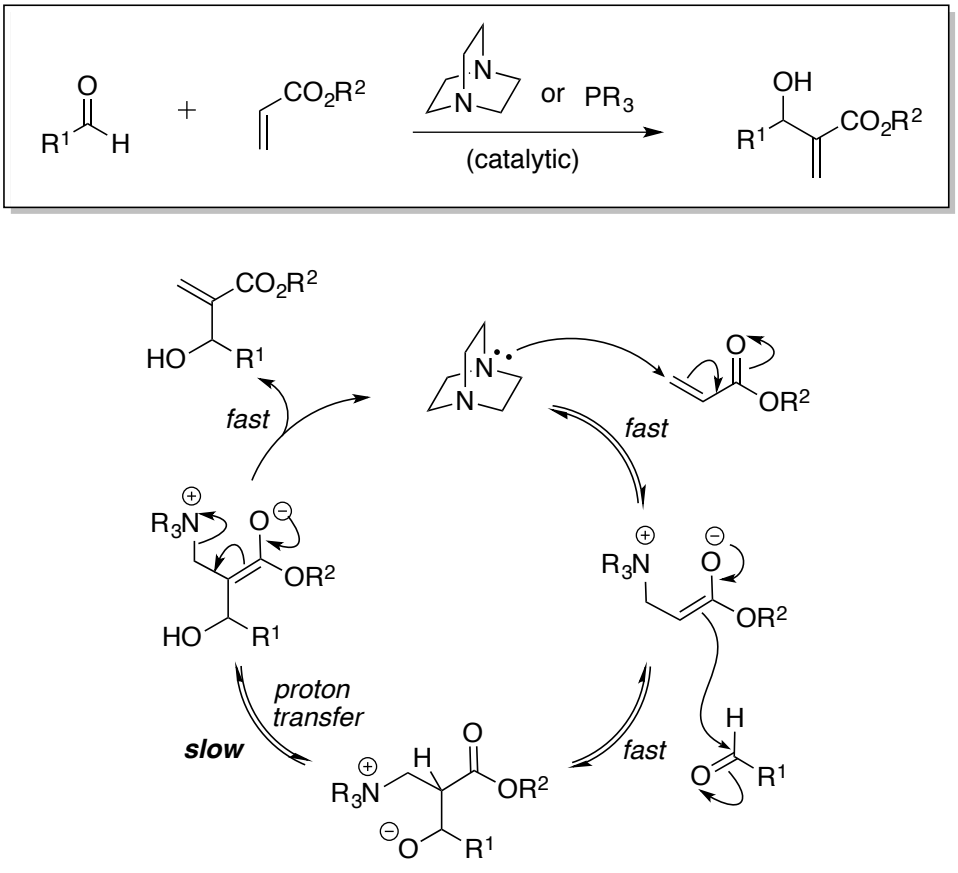

Hillman reaction. The subsequent reactions add to the complexity of the final structures.[7] In the latter context, the use of chiral nitrogen or phosphorus based Lewis bases have been reported with various secondary electrophiles;[8-15] however development of a reaction with acyclic enones as secondary electrophiles has not been explored until recently.[16]

Figure I-2. Phosphine[8] and quinuclidine[9] catalytic pathway for allene ester mediated addition reaction.

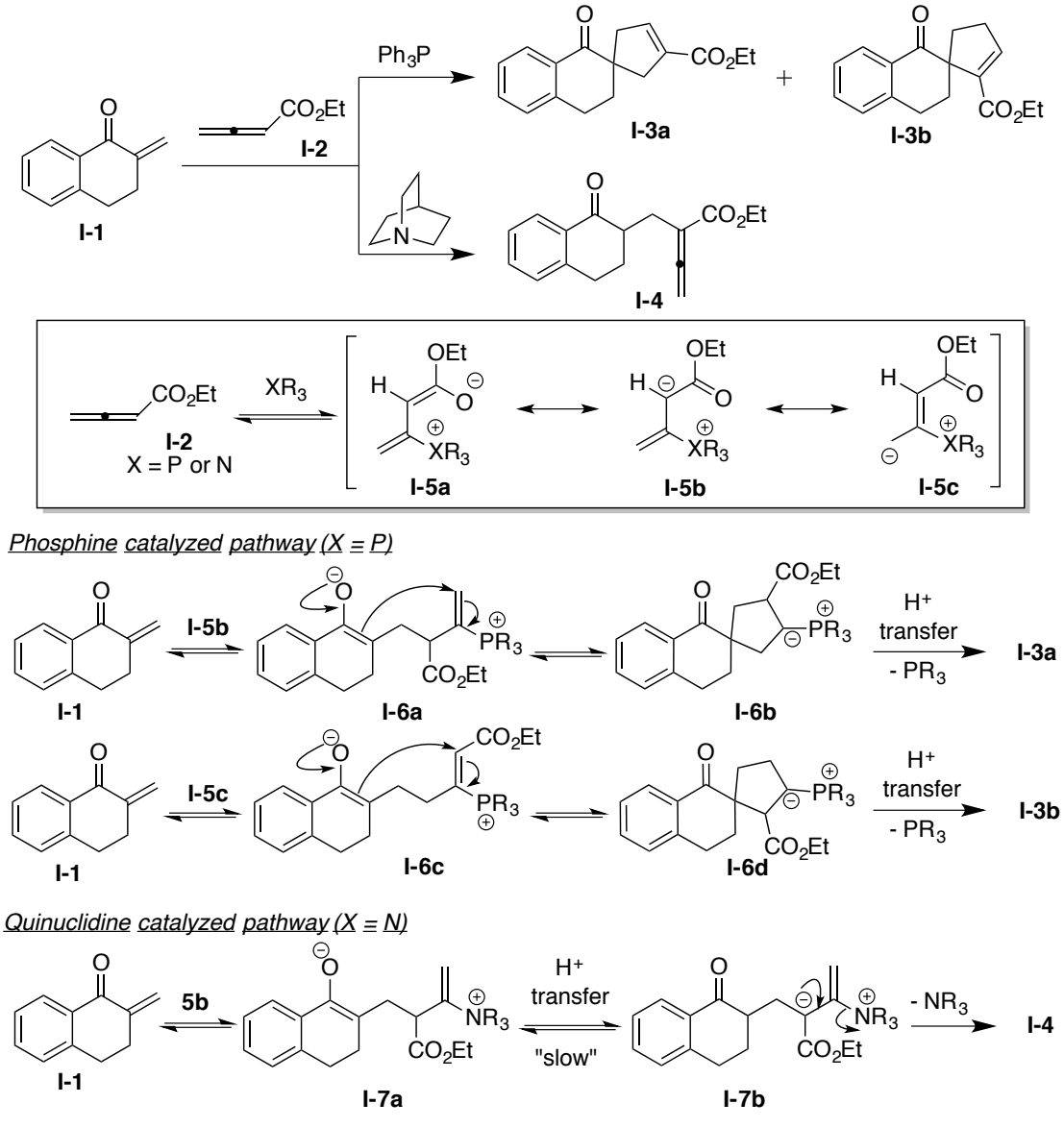

I.2. Mechanistically inspired approach.

As shown in Figure I-1, the rate determining step (RDS) in a Baylis-Hillman reaction is the proton transfer step followed by a '*fast*' expulsion of the catalyst. Considering our endeavor in developing synthetic routes to heterocyclic nuclei,[17-19] our interest was piqued by the possibility of exploiting the slow proton transfer event associated with an amine catalyzed Baylis-Hillman reaction and syphoning the reaction pathway towards a cyclized product. This can be implemented by an appropriate choice of secondary electrophile, thus allowing a robust access to a library of complex dihydropyrans as key intermediates for constructing complex motifs.[20-26]

Figure I-2 illustrates the divergence in products obtained from the reaction of **I-1** with allenoate **I-2**, catalyzed with either phosphines[8] or amines.[9] Two main factors seem to contribute to the formation of cyclic products in the phosphine catalyzed pathway: (a) the presence of *'d'* orbitals on phosphorus that support an expanded valence shell, enable the reaction of the transient enolates **I-6a** and **I-6c** in the manner depicted to generate ylides **I-6b** and **I-6d**; (b) a rapid proton transfer in ylides **I-6b** and **I-6d** initiates catalyst turnover. Nitrogen, on the other hand, cannot exhibit similar genre of reactivity, as the lack of *'d'* orbitals precludes ylide formation under

Figure I-3. Hypothetical pathways for a *formal* [4+2] addition reaction.

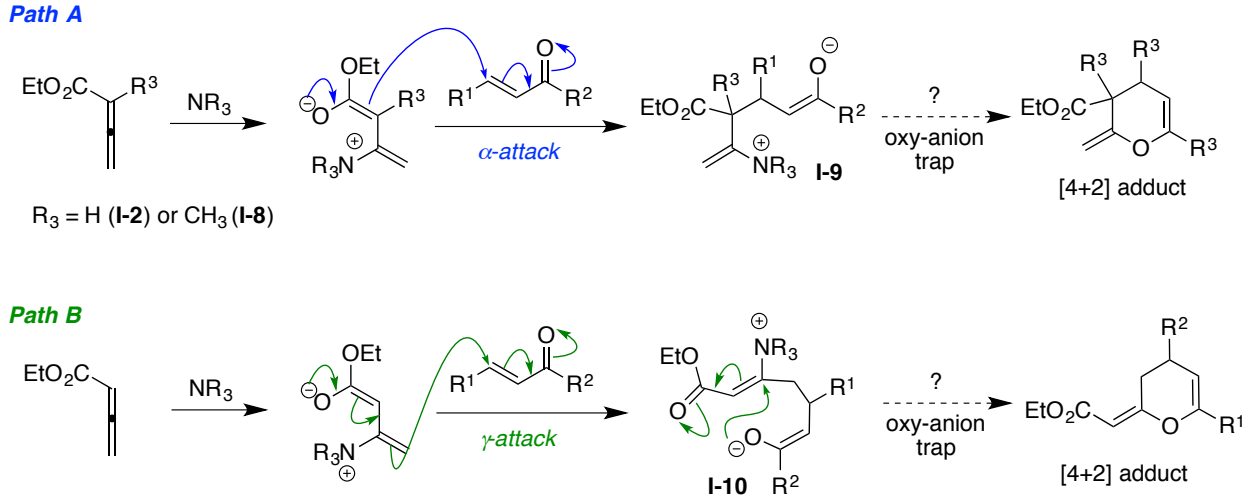

the mild reaction conditions. Consequently, proton transfer leading to the illustrated elimination (Figure I-2, **I-7a**→ **I-7b**), albeit slowly,[27] results in the formation of α-substituted allenes.

Our venture into the use of acyclic enones was based on the assumption that the increased conformational flexibility of the enolate intermediate could lead to a facile ring closure in preference to the slow proton transfer. As depicted Figure I-3, cyclization of the *hard* oxyanion onto the *hard* enamine, as opposed to that observed with phosphine catalysis (cyclization of the *softer* carbon onto the *softer* vinylphosphonium, see Figure I-2) would yield a specific dihydropyran product based on whether the reaction proceeds through path A or path B. Either pathway will be a manifestation of a regioselective attack of the amine-allene ester adduct on the secondary electrophile-chalcone. An α-attack of the amine-allene ester adduct on the chalcone will result in the formation of **I-9** whereas, a γ-attack of the same adduct on the chalcone will yield intermediate **I-10**. Cyclization of this intermediate oxyanion (**I-10**) via interamolecular Michael addition seems more feasible in comparison to its counterpart **I-9,** which would require intermediacy of a putative primary methylene anion.

I.3. Results and discussions.

I.3.1. Preliminary results.

To probe the experimental outcome and validate our hypothesis, a variety of enones as possible secondary electrophiles were screened for reactivity with allene ester **I-2**. Allene ester **I-8**, incapable of proton transfer, was also chosen to further facilitate the cyclization of **I-9** or **I-10**. In the event, treatment of acyclic enones (see Table I-1) with ethyl-2-methyl-2,3-butadienoate (**I-8**) in the presence of 20 mol % DABCO provided no product and the secondary electrophile was recovered unreacted. The inertness of **I-8** in this reaction may be attributed to sterics as a result of the α-methyl group substitution, rendering the intermediate enolate incapable of attacking the

secondary electrophile (enone). To the contrary, ethyl-2,3-butadienoate (**I-2**) provided good yields of the *formal* [4 + 2] adducts, albeit via the unanticipated attack of the γ-enolate derived from the activation of **I-2** with DABCO (Figure 3, enolate **I-2a**). In fact, previous studies with **I-2** only report products that arise from α-substitution during the Baylis-Hillman reaction.[9,10] Figure **I-4** illustrates

Table I-1. Preliminary results for [4+2] addition reaction.

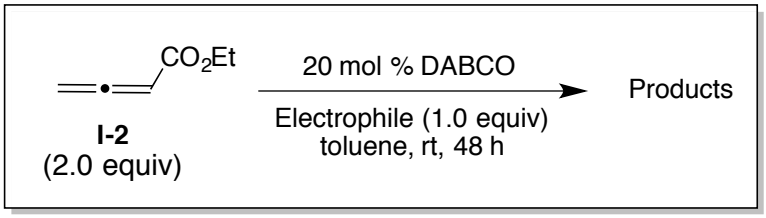

entry	electrophile	products	yields[a]
1	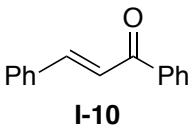 **I-10**	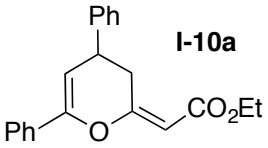 **I-10a**	70% (76%)[b]
		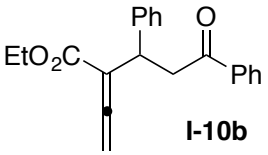 **I-10b**	15%[c]
2	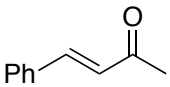 **I-11**	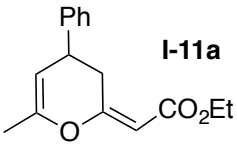 **I-11a**	55%
3	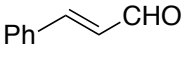 **I-12**	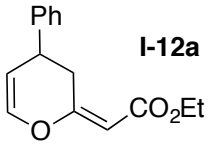 **I-12a**	75%
4	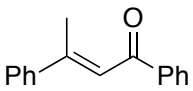 **I-13**	No Reaction	---

[a]Isolated yields after column chromatography. Due to thermal sensitivity of the products solvents were removed under vacuum without heating. [b]Reaction was performed in presence of 4 Å MS. [c]Not observed under anhydrous conditions.

the proposed mechanism leading to the observed products in Table I-1, highlighting the γ-substitution of the allene ester (**I-2a**→ **I-2b**) and subsequent oxygen trap (**I-2b**→ **I-2c**) to yield the dihydropyran without proton transfer. Although product **I-10a**, formed by the γ-attack of the allene predominates, a minor fraction of α-substituted allene product **I-10b** was observed (Table I-1, entry 1). Optimization of reaction conditions revealed that the presence of adventitious water leads to the formation of **I-10b**. The same reaction charged with 4Å molecular sieves under argon atmosphere yields **I-10a** exclusively. As shown in Table I-1, several secondary electrophiles with varying substitution patterns were employed to investigate the scope of this reaction. Enones **I-11** and **I-12** provide the corresponding dihydropyran product as anticipated (Table I-1, entries 2 and 3). Dypnone (**I-13**), a β,β-disubstituted enone (entry 4), did not yield product, presumably

Figure I-4. Proposed mechanism for the *formal* [4+2] addition.

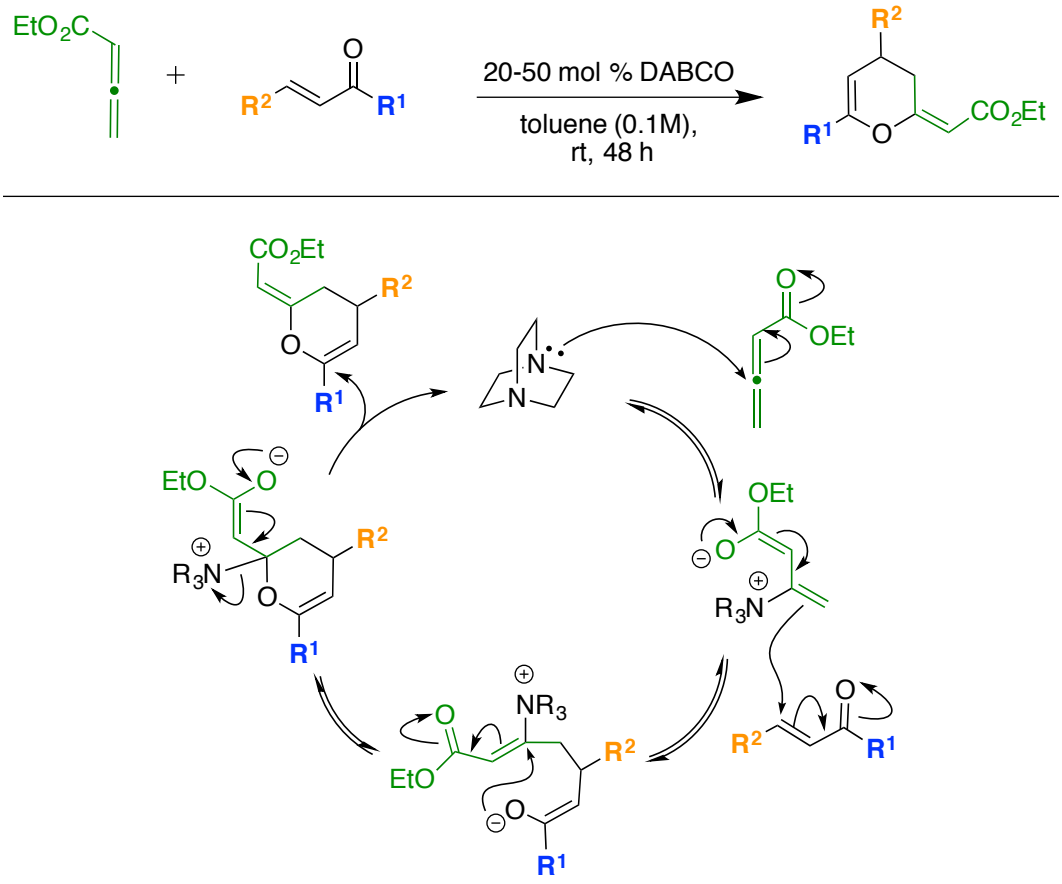

indicating the intolerance of the reaction to increased sterics at the *β*-position of the enone. It is noteworthy that the isolated mass balance of the latter reactions was the unreacted enone. The allene ester **I-2** does decompose at room temperature regardless of the absence or presence of the secondary electrophile, an observation that was helpful in further optimization of this reaction, leading to high yields of products as will be described below.

I.3.2. Optimization of reaction variables and development of an asymmetric protocol.

To explored the possibility of enantiocontrol at C4, several cinchona alkaloids (and their derivatives) were employed as chiral amine catalysts for the Baylis-Hillman reaction. Chalcone **I-10** was chosen as the model substrate in the reaction of **I-2** as the primary electrophile using 10 mol % of the chiral amine for initial screening efforts; the reactions were performed in toluene at room temperature. Preliminary results were encouraging since every catalyst that furnished the desired product displayed enantioselectivity, with most surpassing 90% *ee*. Not surprisingly, the monohydrochloride salts of cinchonine (**I-G**) and cinchonidine (**I-H**) did not yield product, suggesting that the quinuclidine nitrogen is necessary to carry out catalysis.

Although the initial screening delivered the desired products in good enantiomeric excess, the low yields (10-20%) were clearly a problem. Surprisingly, increasing catalyst loading up to 30 mol % did not make any quantifiable difference in the isolated yields. Hatekeyama's catalyst (**I-E**), which reportedly enhances the rate of reaction through hydrogen bonding with secondary electrophiles,[6] marginally improved the yield (30%), although the *ee* suffered in the process (59%). Any attempt to externally activate the secondary electrophile by addition of acidic or basic additives led to faster decomposition of **I-2**. A screen of different solvents with a large range of polarities was not conclusive, with comparable efficiencies for both polar and nonpolar solvents.

We next resorted to a concentration study, mindful of the tendency for cinchona alkaloids to aggregate at high concentrations (which often leads to deterioration of their catalytic and

stereoinductive ability).[28,29] Gratifyingly, the highest yields were obtained under neat reaction conditions (see Table I-2), providing the products in both synthetically useful quantities, and also, maintaining high enantiomeric excess. Since, the catalyst and chalcone are both solids, the loading of **I-2** up to 3-4 equivalents was necessary to provide medium with efficient mixing.

Figure I-5. Catalyst screening for development of asymmetric *formal* [4+2] addition.

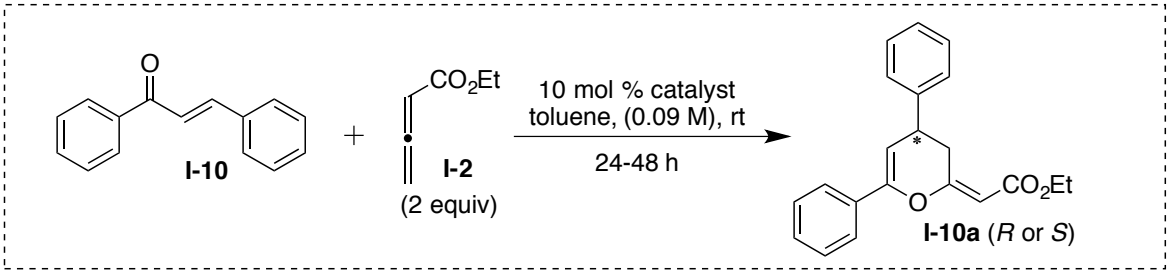

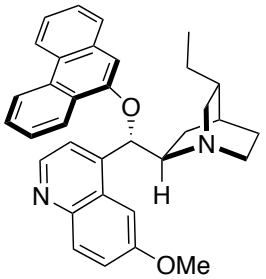

Hydroquinidine-9-phenanthryl ether (**I-A**)
I-10a-*S*, 20% yield, 98% *ee*

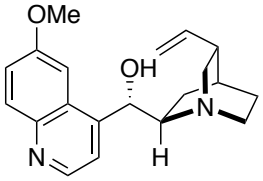

(+)-Quinidine (**I-B**)
I-10a-*S*, 19% yield, 94% *ee*

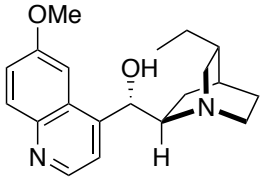

Dihydroquinidine (**I-C**)
I-10a-*S*, 17% yield, 96% *ee*

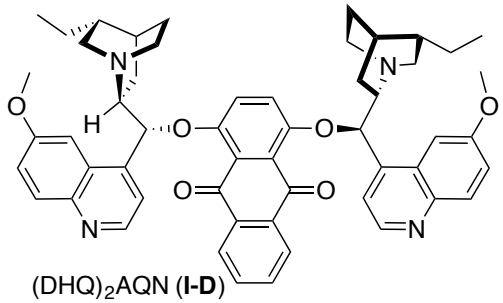

$(DHQ)_2AQN$ (**I-D**)
I-10a-*R*, 15% yield, 94% *ee*

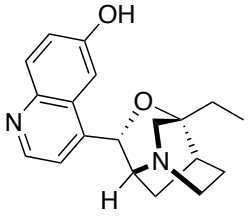

Hatekeyama's catalyst (**I-E**)
I-10a-*S*, 30% yield, 59% *ee*

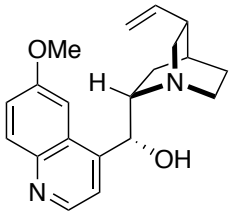

(-)-Quinine (**I-F**)
I-10a-*R*, 12% yield, 82% *ee*

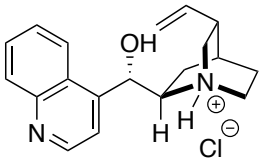

(+)-Cinchonine Hydrochloride (**I-G**)
no reaction

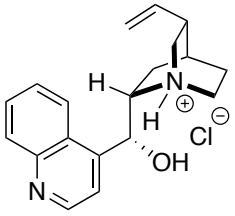

(-)-Cinchonidine Hydrochloride (**I-H**)
no reaction

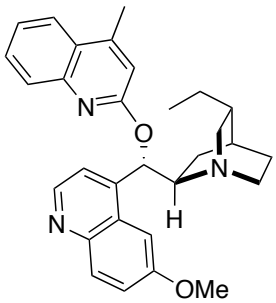

Hydroquinidine-4-methyl-2-quinolyl ether (**I-I**)
I-10a-*S*, 10% yield, 97% *ee*

Table I-2. Solvent screening and concentration studies.

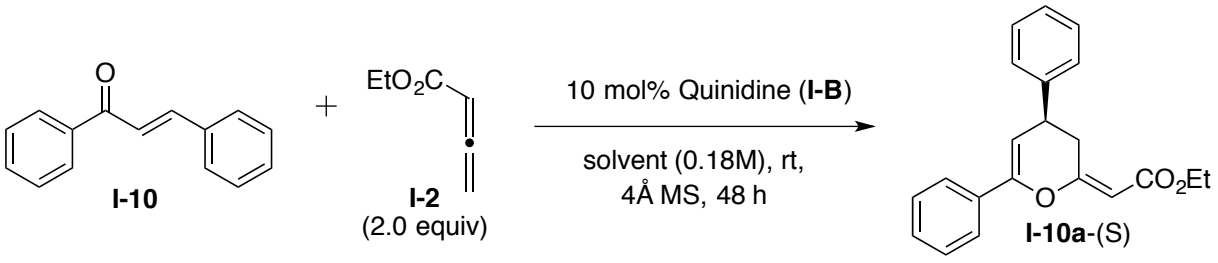

Entry	Solvent/Conditions	Rel. Polarity[d]	Yield	Product	% *ee*[c]
1	MeOH (3Å MS)	0.762	10%	**I-10a**-*S*	33
2	CH_3CN	0.460	17%	**I-10a**-*S*	95
3	DMF (3Å MS)	0.386	N.R.	**---**	---
4	Acetone	0.355	20%	**I-10a**-*S*	98
5	CH_2Cl_2	0.309	Trace	**I-10a**-*S*	N.D.
6	$CHCl_3$	0.259	Trace	**I-10a**-*S*	N.D.
7	EtOAc	0.228	N.R.	---	---
8	THF	0.207	N.R.	---	---
9	Ether	0.117	15%	**I-10a**-*S*	N.D.
10	Benzene	0.111	Trace	**I-10a**-*S*	N.D.
11	Hexanes	0.009	N.R.	---	---
12	Cyclohexane	0.006	N.R.	---	---
13	Toluene (0.09M)	0.099	19%	**I-10a**-*S*	94
14	Toluene (0.9M)	0.099	52%	**I-10a**-*S*	96
15	Toluene (1.8M)	0.099	61%	**I-10a**-*S*	95
16	Toluene (3.0M)	0.099	65%	**I-10a**-*S*	95
17	Toluene (9.0M)	0.099	80%	**I-10a**-*S*	95
18	neat, 5 equiv. **I-2**[a]	---	91%	**I-10a**-*S*	95
19	neat, 3 equiv. **2**, cat. **I-A**	---	93%	**I-10a**-*S*	97
20	neat, 3 equiv. **2**, cat. **I-F**[a]	---	67%	**I-10a**-*R*	84
21	neat, 3 equiv. **2**, cat. **I-C**[a]	---	89%[b]	**I-10a**-*S*	94
22	neat, 3 equiv. **2**, cat. **I-D**	---	89%	**I-10a**-*R*	88

[a]catalyst loading was 20 mol%. [b]reaction was performed on 1g scale of chalcone. [c]ratios were determined by chiral HPLC analysis. [d]Polarity relative to water (H_2O = 1.000)[2b]. (N.R. = No Reaction, N.D. = Not Determined).

The increased concentration along with the higher equivalence of **I-2** leads to a faster reaction rate prior to its degradation via non-productive pathways. It is also noteworthy that no significant deleterious effects result from the self-aggregation of cinchona alkaloids or their derivatives, most probably because stereochemical induction results after the addition of the catalyst to the allenoate (**I-2**). Aggregation of the zwitterionic intermediate is less likely as compared to the neutral catalyst.

The scope of the reaction was tested with a number of enones as secondary electrophiles, employing the best four catalysts (**I-A** through **1-D**) displayed in Figure I-5. It is evident from the results that electron donation through R^1 does not favor the formation of transient oxyanion upon attack of the amine-allenoate adduct and therefore furnishes low product yield (Table I-3, entries 2 and 9). Although, electron withdrawing R^2 groups gave better yields (entries 4, 5 and 8), the yields are not affected dramatically by electron donating groups (entries 6, 7, 11 and 16). Aliphatic enones provided the desired products in lower yields (Table I-3, entries 13-15); presumably, under basic condition, the rate of self-condensation *via* aldol reaction is faster than the desired *formal* [4+2] addition. ^{1}H NMR studies of the crude reaction mixture validates this premise.

Aromatic and heteroaromatic enones were stable under the reaction condition and furnished good yields of the desired products with excellent enantioselectivity. Moreover, we were able to access both enantiomers by a simple switch of the pseudo-enantiomeric catalyst. Regardless of electronic and steric factors, the enantioselectivity of the reaction was not greatly influenced by the substitution pattern on either R^1 or R^2.

Table I-3. Substrate scope for the catalytic asymmetric *formal* [4+2] addition.

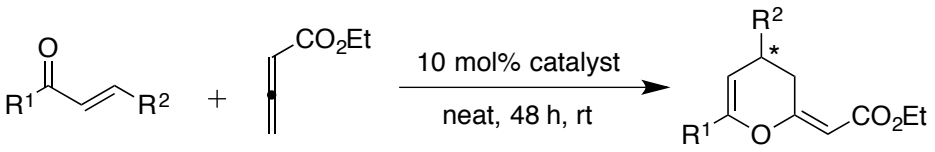

(1.0 equiv) (3 equiv) (*R* or *S*)

Entry	R^1	R^2	Catalyst	Product	Yield	%*ee*
1	Ph	Ph	**I-A**	**10a-***S*	93%	97
			I-B[a]	**10a-***S*	87%	95
			I-C[a]	**10a-***S*	89%	94[b]
			I-D	**10a-***R*	89%	88
2	*p*-OMe-C_6H_4	Ph	**I-A**	**14a-***S*	39%	96
			I-B[a]	**14a-***S*	31%	96
			I-C[a]	**14a-***S*	N.D.	N.D.
			I-D	**14a-***R*	42%	82
3	*p*-NO_2-C_6H_4	α-naphthyl	**I-A**	**15a-***S*	97%	97
			I-B[a]	**15a-***S*	>99%	97[b]
			I-C[a]	**15a-***S*	94%	97
			I-D	**15a-***R*	94%	90
4	Ph	*p*-CN-C_6H_4	**I-A**	**16a-***S*	81%	97
			I-B[a]	**16a-***S*	74%	90
			I-C[a]	**16a-***S*	81%	91
			I-D	**16a-***R*	55%	89
5	Ph	*p*-Br-C_6H_4	**I-A**	**17a-***S*	92%	96[d]
			I-B[a]	**17a-***S*	94%	93[d]
			I-C[a]	**17a-***S*	89%	93[d]
			I-D	**17a-***R*	82%	91[d]
6	Ph	*p*-OMe-C_6H_4	**I-A**	**18a-***S*	60%	96[d]
			I-B[a]	**18a-***S*	62%	95[d]
			I-C[a]	**18a-***S*	68%	95[d]
			I-D	**18a-***R*	52%	83[d]

Enantiomeric ratios were determined by chiral HPLC. [a]Catalyst loading was 20 mol%. [b]Reactions were performed on 1 g scale of chalcone. [c]Enantiomers could not be resolved by HPLC analysis. [d]Reactions were performed using 4 equiv of allenoate (**I-2**).

Table I-3. (cont'd)

Entry	R^1	R^2	Catalyst	Product	Yield	%*ee*
7	*p*-NO_2-C_6H_4	*p*-OMe-C_6H_4	**I-A**	**19a**-*S*	58%	95[d]
			I-B[a]	**19a**-*S*	61%	93[d]
			I-C[a]	**19a**-*S*	64%	93[d]
			I-D	**19a**-*R*	49%	84[d]
8	*p*-CH_3-C_6H_4	*p*-Cl-*m*-NO_2-C_6H_3	**I-A**	**20a**-*S*	66%	90[d]
			I-B[a]	**20a**-*S*	60%	88[d]
			I-C[a]	**20a**-*S*	63%	86[d]
			I-D	**20a**-*R*	50%	92[d]
9	*p*-MeO-C_6H_4	*p*-Br-C_6H_4	**I-A**	**21a**-*S*	16%	95
			I-B[a]	**21a**-*S*	16%	94
			I-C[a]	**21a**-*S*	N.D.	N.D.
			I-D	**21a**-*R*	15%	85
10	*o*-MeO-C_6H_4	*p*-F-C_6H_4	**I-A**	**22a**-*S*	>99%	97[d]
			I-B[a]	**22a**-*S*	63%	96[d]
			I-C[a]	**22a**-*S*	85%	95[d]
			I-D	**22a**-*R*	63%	81[d]
11	*o*-Br-C_6H_4	2-furanyl	**I-A**	**23a**-*S*	61%	96
			I-B[a]	**I-23a**-*S*	46%	93
			I-C[a]	**I-23a**-*S*	68%	93
			I-D	**I-23a**-*R*	52%	79
12	*m*-Br-C_6H_4	*p*-Ph-C_6H_4	**I-A**	**I-24a**-*S*	98%	98[b]
			I-B[a]	**I-24a**-*S*	96%	96
			I-C[a]	**I-24a**-*S*	98%	96
			I-D	**I-24a**-*R*	70%	79
13	CH_3	*n*-C_5H_{11}	**I-A**	**I-25a**-*S*	12%	86
			I-B[a]	**I-25a**-*S*	10%	87
			I-C[a]	**I-25a**-*S*	N.D.	N.D.
			I-D	**I-25a**-*R*	11%	77

Enantiomeric ratios were determined by chiral HPLC. [a]Catalyst loading was 20 mol%. [b]Reactions were performed on 1 g scale of chalcone. [c]Enantiomers could not be resolved by HPLC analysis. [d]Reactions were performed using 4 equiv of allenoate (**I-2**).

Table I-3. (cont'd)

Entry	R^1	R^2	Catalyst	Product	Yield	%*ee*
14	H	Ph	**I-A**	**I-12a-***S*	45%	95
			I-B[a]	**I-12a-***S*	36%	96
			I-C[a]	**I-12a-***S*	38%	95
			I-D	**I-12a-***R*	30%	80
15	H	*n*-C_3H_7	**I-A**	**I-26a-***S*	13%	N.D.[c]
			I-B[a]	**I-26a-***S*	18%	N.D.[c]
			I-C[a]	**I-26a-***S*	17%	N.D.[c]
			I-D	**I-26a-***R*	12%	N.D.[c]
16	*o*-Cl-C_6H_4	*p*-OMe-C_6H_4	**I-A**	**I-27a-***S*	>99%	97[d]
			I-B[a]	**I-27a-***S*	85%	94[d]
			I-C[a]	**I-27a-***S*	91%	95[d]
			I-D	**I-27a-***R*	58%	77[d]
17	*p*-I-C_6H_4	*p*-Br-C_6H_4	**I-A**	**I-28a-***S*	51%	95[d]
			I-B[a]	**I-28a-***S*	48%	92[d]
			I-C[a]	**I-28a-***S*	42%	92[d]
			I-D	**I-28a-***R*	36%	87[d]

Enantiomeric ratios were determined by chiral HPLC. [a]Catalyst loading was 20 mol%. [b]Reactions were performed on 1 g scale of chalcone. [c]Enantiomers could not be resolved by HPLC analysis. [d]Reactions were performed using 4 equiv of allenoate (**I-2**).

I.3.3. Elucidation of mechanistic nuances of the *formal* [4+2] addition.

Figure I-4 depicts a putative mechanism for the formation of the desired dihydropyran products. Several attempts to investigate the mechanistic underpinnings *via* NMR studies failed to provide any conclusive evidence. The transient adducts could not be observed as individual species under the NMR time scale as evident by broadning of the spectral lines. Gratifyingly, evidence for the proposed mechanism was obtained from ESI-MS analyses of reaction intermediates. Figure I-6a depicts mass spectrum of a 1:1 mixture of quinidine (**I-B**) with allene ester **I-2**. Present in the mass spectrum is clear evidence for addition of the cinchona alkaloid **I-B**

to allene ester **I-2** (structure **I- B1**). In the absence of an enone, a second equivalent of allenoate **I-2** functions as the secondary electrophile (structure **I-B2**). Addition of 1.0 equiv of enone **I-15** to the latter mixture yields the spectrum in Figure I-6b, with evidence for the anticipated intermediate

Figure I-6. ESI-MS based analysis during the formation of **I-15a**-(*S*).

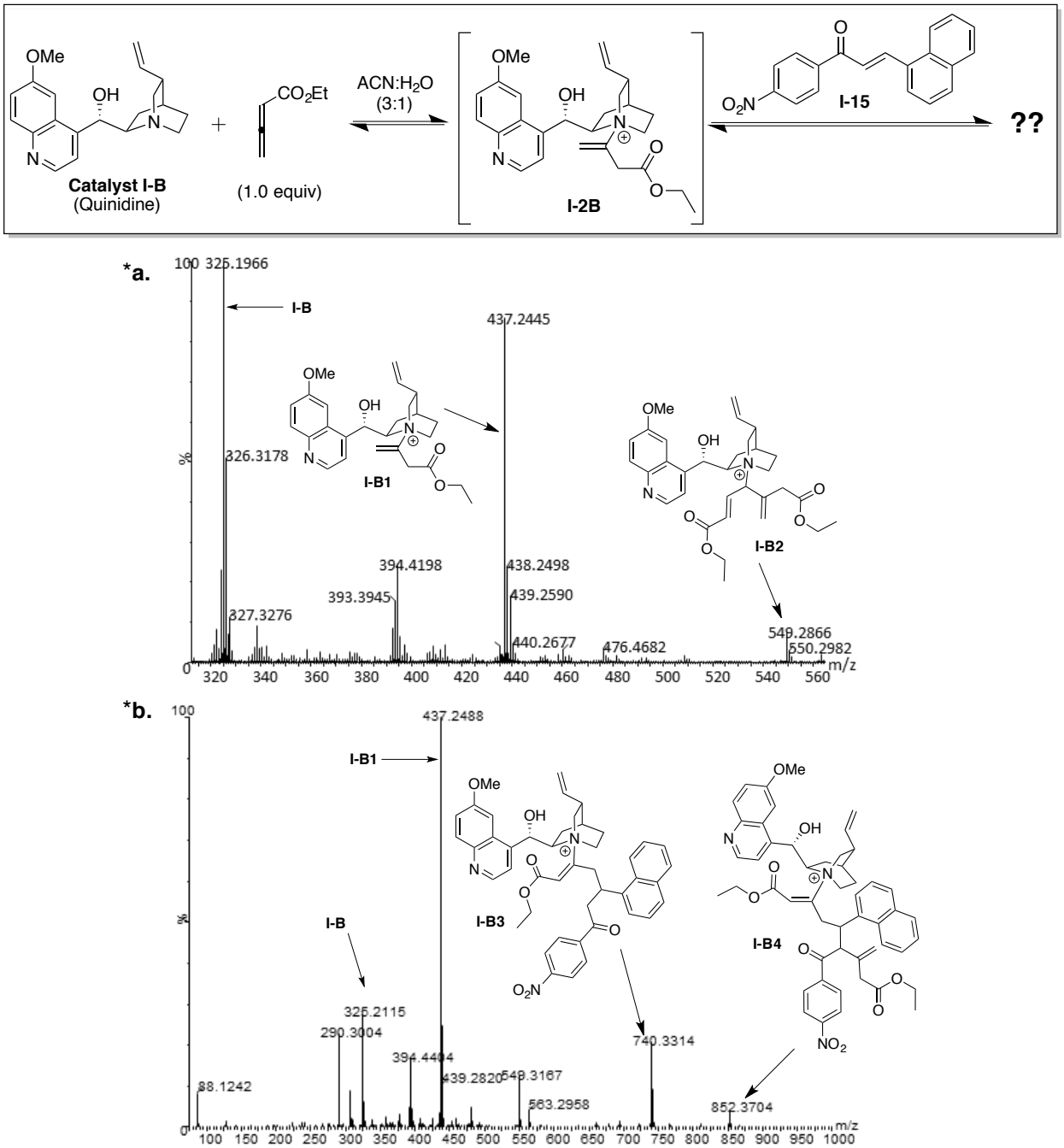

*The samples were injected within 2 min after the mixing of reactants.

Figure I-7. Putative intermediates in the formal [4+2] addition reaction.

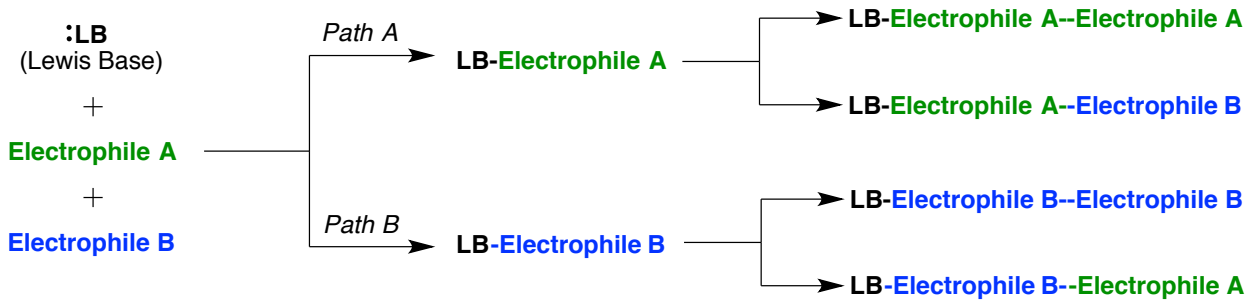

(structure **I-B3**) on route to the observed product (**I-15a**-*S*). Under the reaction conditions employed, a second addition of **I-2** to the adduct **I-B3** is also observable (structure **I-B4**). Furthermore, the relative ratio of **I-B**:**I-B1** changes dramitically upon inclusion of enone **I-15** in the reaction mixture, as observed by the intensity of corresponding spectral lines. As depicted in Figure I-7, the results obtained from ESI-MS studies clearly indicate that the reaction mixture comprises of several adducts in equilibrium, which syphon into the final product *via* an irreversible ring closure of the oxyanion. A detailed computational work on this reaction was recently published by Yu and co-workers[27] which supports the initially proposed mechanism (Figure I-4).

To probe the basis for stereoinduction, an exhaustive DFT calculation at the B3LYP/6-31G* level using toluene as solvent, was performed. A large number of possible reaction trajectories (>20) for the approach of chalcone relative to the adduct of catalyst **I-B** and **I-2** were examined. The results revealed that the difference in energy for the two diastereomeric transition states is 2.5 kcal/mol in favor of the observed (*S*)- enantiomer (Figure I-8). This is in excellent agreement with the experimentally observed selectivity of 98:2 *er*. The two transition states in Figure I-8 orient the reacting molecules such that a close proximity of the counter ions (electrostatic stabilization) is achieved. The gauche interaction encountered in **TS2** (highlighted bonds in red) makes this transition state energetically more demanding than the orientation suggested in **TS1**.

Figure I-8. Origin of enantioselectivity (diastereomeric transition states **TS1** and **TS2** determined at B3LYP/6-31G*/SM8 level). The gauche interactions (highlighted in red bonds) makes **TS2** energetically less favored than **TS1**.

experimental result:

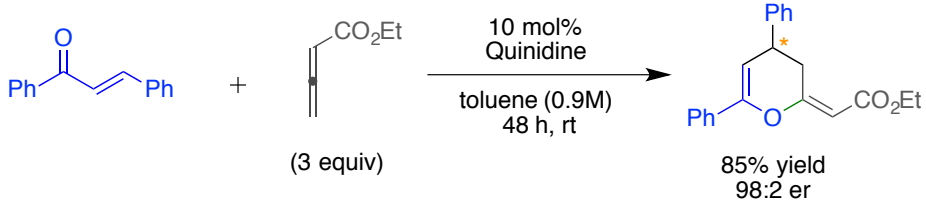

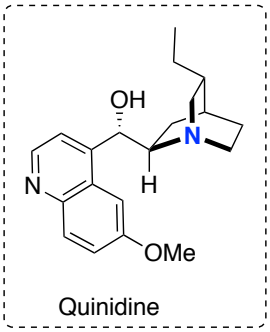

theoretical result:

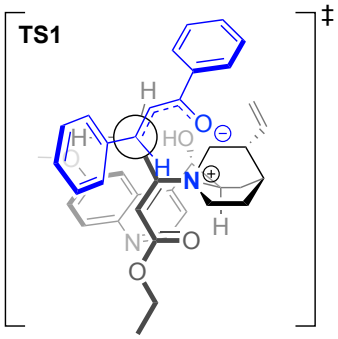

Re face attack on chalcone
(*S*)-enantiomer
(favored by ~2.5 kcal/mol)

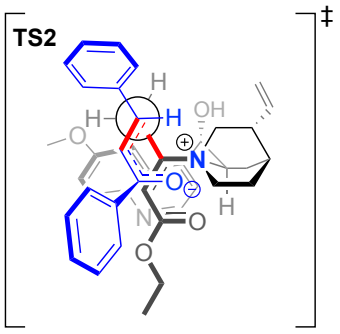

Si face attack on chalcone
(*R*)-enantiomer

$\Delta\Delta G^{\ddagger}_{(experimental)}$ = **2.4 Kcal/mol**

$\Delta\Delta G^{\ddagger}_{(calculated)}$ = **2.5 Kcal/mol** B3LYP/6-31G*SM8 (Toluene)

In summary, exploiting the key mechanistic disparity (rate of proton tranfer) between phosphine and amine catalysis, a hypothetical *formal* [4+2] reaction was designed and successfully executed towards the construction of novel dihydropyrans. Gratifyingly, the commercially available cinchona alkaloids catalysts displayed excellent levels of enantioinduction to render this process catalytic and asymmetric. The insights gained upon development of this mechanistically inspired approach towards syphoning a reaction pathway based on differencial rates of proton transfer, offered us as well as several other research groups with novel

approaches for extension of this methodology towards accessing different heterocyclic cores in a catalytic asymmetric manner. [30-38]

I.3.4. Stereoselective functionalization of substituted dihydropyrans.

The synthetic utility of this transformation is dictated by its ability to access both enantiomers with excellent selectivity and its tolerance to various functional groups under solvent free conditions at room temperature. Interestingly, by exploiting the stereocenter and the rigid framework of these molecules one can imagine a plethora of electrophiles reacting at the nucleophilic 'enol ether' in a stereoselective mode, moreover, upon electrophilic functionalization at C3, the resulting oxacarbenium can undergo attack by nucleophiles, also in a stereoselective manner. As a demonstration of its applicability, $Rh_2(OAc)_4$ mediated cyclopropanation of **I-24a**-(*S*) provided product **I-24b** in 74% isolated yield as a single isomer by NMR (Scheme I-1). The crystal structure of **I-24b** provides the absolute stereochemistry of the product, suggesting that the C4 substituent is the stereochemical driver in this reaction. It is noteworthy that the stereocenter at the methine carbon, α to the carbethoxy group, is also controlled by the C4 substituent.

Scheme I-1. Rh (II) mediated cyclopropanation of **I-24a**-*S* and crystal structure of **I-24b**.

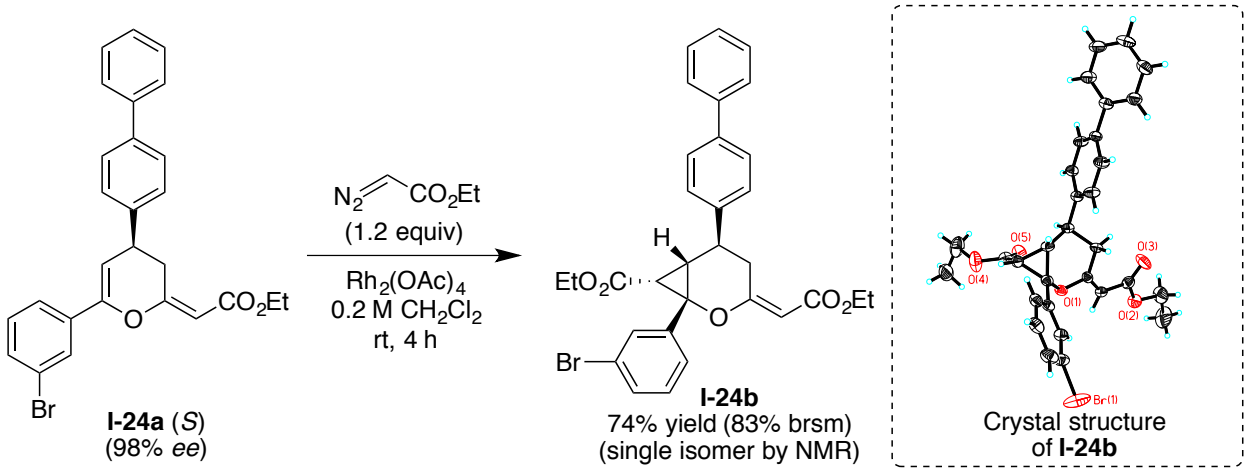

I.4.1. Application towards synthesis of 'Danishefsky-type' chiral dienes.

Scheme I-2. One-pot protocol for consecutive [4+2] additions.

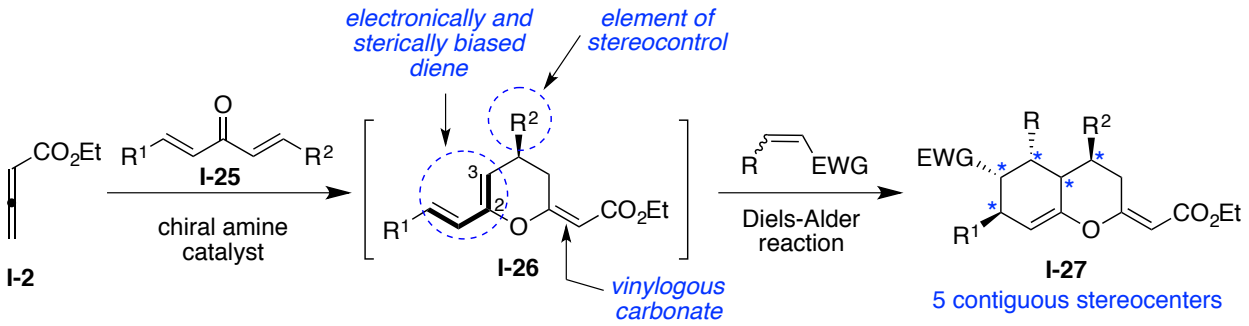

As depicted in Scheme I-1, employment of cinchona alkaloid catalyzed *formal* [4+2] addition of acyclic enones and allenoate **I-2** creates an asymmetric center at C4 with efficient stereocontrol, providing a handle for further stereochemical functionalizations of the dihydropyrans. The encouraging result obtained from Rh (II) catalyzed cyclopropanation of **I-24a** led us to expanding this methodology towards construction of 'Danishefsky type' dienes. As shown in Scheme I-2, use of dibenzal acetones in place of simple enones should yield the corresponding dihydropyrans (**I-26**) with tethered dienes that can be subjected to a concomitant Diels-Alder reaction. This would furnish highly functionalized stereopentads such as **I-27,** incorporating 5 contiguous stereocenters. The goal is to develop a one pot protocol to access compounds **I-27**.

Table I-4 depicts the current substrate scope for formation of the intermediate dienes (**I-26**). Although, these dienes displayed lower efficiency towards Diels-Alder reactions in comparison to Danishefsky diene, elevated temperatures indeed furnished the desired Diels-Alder adducts in high yields. The current 'one-pot' optimized conditions involve stirring a neat mixture comprising of 10 mol% DHQD-9-phenanthryl ether as a chiral amine catalyst, 2.0-3.0 equiv. of allene ester **I-2** with enones **I-26** at room temperature for 24-48 h. This is followed by an addition of 1.5 equiv. dienophile in toluene (1M) to furnish the adducts **I-27** in excellent yields and enantioinduction. These products are excellent synthons for diastereoselective functionalization

Table I-4. Substrate scope for the catalytic asymmetric *formal* [4+2] addition of dienones

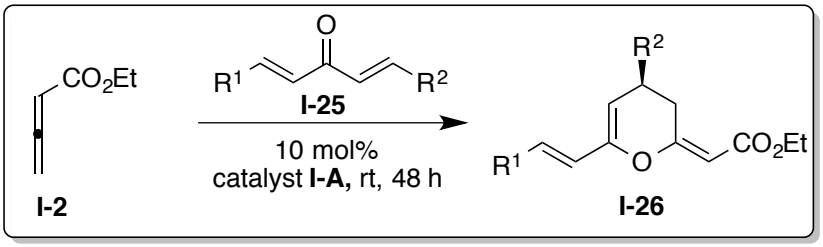

entry	$R^1 = R^2$	product	yield	% *ee*
1	C_6H_5	**I-26a**	98%	98
2	*p*-OMe-C_6H_4	**I-26b**	50%	94
3	*o*-Br-C_6H_4	**I-26c**	93%	88
4	1-naphthyl	**I-26d**	77%	92
5	*p*-Br-C_6H_4	**I-26e**	92%	94

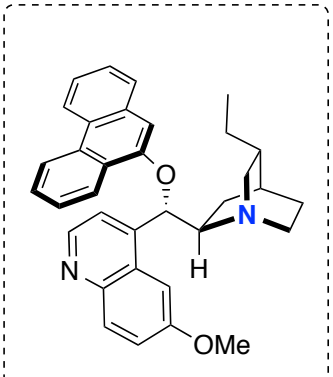

Hydroquinidine-9-phenanthryl ether (**I-A**)

Enantiomeric ratios were determined by chiral HPLC. Yields displayed are isolated yields. Reaction represented in entry 1 was performed twice on 1.0 g scale of dibenzalacetone.

towards assembly of natural products incorporating the tetrahydropyranyl core. Table **I-5** represents the results of the 'one-pot' protocol using dibenzalacetone **I-25**. Current efforts are focused on exploring the scope of substituted dibenzal acetones and the dienophiles. The mechanistic studies and substrate scope exploration related to this project is currently pursued by Mr. Xinliang Ding (graduate student) and Mr. Christopher Rahn (undergraduate student) in Prof. Borhan's lab (MSU).

Table I-5. Preliminary results for one-pot protocol for consecutive [4+2] addition.

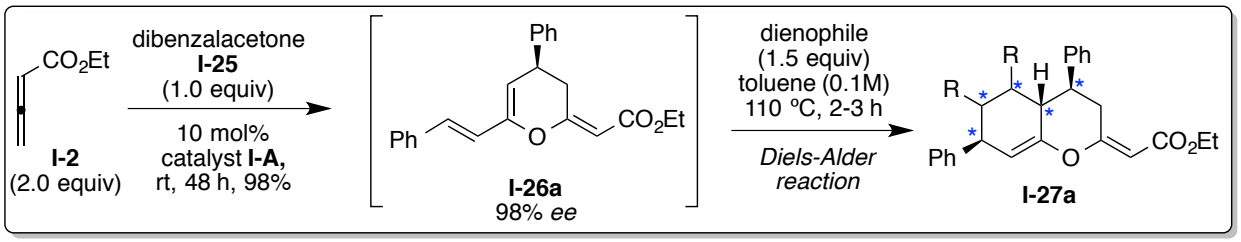

entry	*dienophile*	*product*	*yield*
1	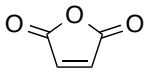	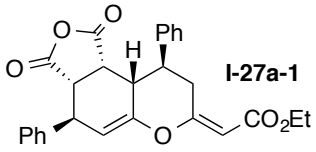 **I-27a-1**	78%
2	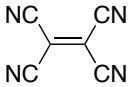	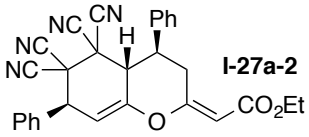 **I-27a-2**	92%

I.5. Experimental section.

I.5.1. General information.

All reactions were carried out in flame dried glassware under an atmosphere of dry nitrogen or argon. 4 Å molecular sieves were dried at 160 °C under 0.25 mtorr pressure prior to use. Unless otherwise mentioned, solvents were purified as follows. THF and diethyl ether were distilled from sodium benzophenone ketyl. Methylene chloride, acetonitrile and triethylamine were dried over CaH_2 and freshly distilled prior to use. DMF was dried over $MgSO_4$, distilled and stored over 4 Å molecular sieves. $CHCl_3$ was initially washed with water to remove ethanol, distilled and stored over 4 Å molecular sieves. Toluene was dried over CaH_2, distilled and stored over 4 Å molecular sieves at least for 48 hours prior to use. Where ever necessary, commercially available enones were either distilled or recrystallized from appropriate solvents prior to use. Ethyl-2,3-butadienoate was synthesized as per reported procedure.[39] All the other commercially available reagents and solvents were used as received unless otherwise mentioned.

^{1}H NMR spectra were obtained using either 300 MHz Inova, 500 MHz Varian or 600 MHz Varian NMR spectrometer, while ^{13}C NMR spectra were measured on 75 MHz Inova, 125 MHz Varian or 150 MHz Varian NMR spectrometer and referenced using deuterated chloroform, unless otherwise mentioned. The corresponding chemical shifts are reported relative to chemical shift of the residual solvent. Infrared spectra were reported on a Nicolet IR/42 spectrometer FT-IR (thin film, NaCl cells). For HRMS (ESI) analysis, Waters 2795 (Alliance HT) instrument was used and the reference used was Polyethylene Glycol (PEG).

Column chromatography was performed using Silicycle 60Å, 35-75 μm silica gel. Pre-coated 0.25 mm thick silica gel 60 F254 plates were used for analytical TLC and visualized using UV light, iodine, potassium permanganate stain, *p*-anisaldehyde stain or phosphomolybdic acid in EtOH stain. Chiral HPLC analysis was done using DAICEL CHIRALPAK OJ-H and OD-H

columns. Optical rotations were measure in chloroform and acquired on a Jasco P-2000 polarimeter at 20 °C and 589 nm.

I.5.2. General procedure for *formal* [4+2] addition of ethyl 2,3-butadienoate and acyclic enones.

Asymmetric variant.

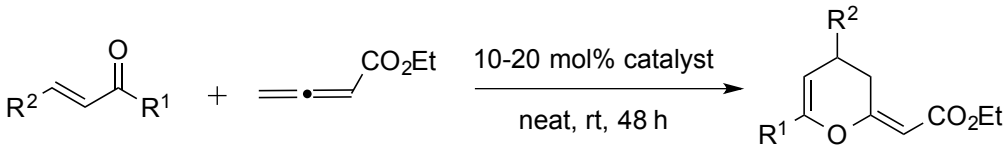

I-10 to **I-28**

I-2
(3-4 equiv)

I-10a to **I-28a**
(*R* or *S*)

At room temperature, in a 1 dram vial flushed under nitrogen, 0.09 mmol of the enone was transferred followed by 0.27-0.36 mmol (3-4 equiv) of ethyl-2,3-butadienoate. To this resulting slurry was added 10-20 mol% of the corresponding catalyst (changing the order of addition of reagents and catalyst does not make any difference in the isolated yields and enantioselectivity) and the mixture was stirred at room temperature for 48 h. The resulting viscous dark brown gel was diluted with 2-3 drops of dichloromethane and directly purified by silica gel chromatography using hexanes-ethyl acetate as eluents.

Racemic variant.

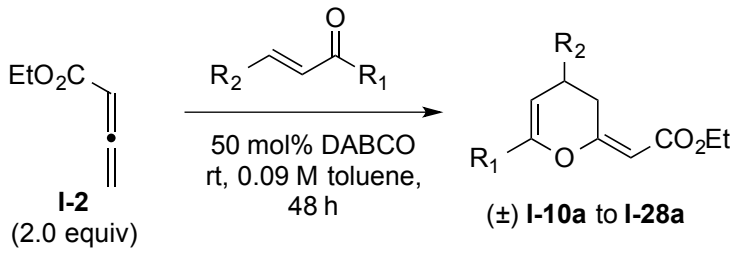

I-2
(2.0 equiv)

(±) **I-10a** to **I-28a**

At room temperature, in a 1 dram vial, 0.18 mmol (2 equiv.) of ethyl-2,3-butadienoate was dissolved in dry toluene (1 mL, 0.09M). To this solution were added 0.09 mmol of the secondary electrophile along with 2-5 mg (10-50 mol%) of 1,4-diazabicyclo [2,2,2] octane (DABCO) and the resulting mixture was stirred at room temperature. The reaction was monitored by TLC. Usually in about 48 h, the solvent was removed under a stream of nitrogen or under vacuum (do not heat over a water bath) and residue was directly purified by silica gel chromatography using hexanes-ethyl acetate as eluents

Note: Do not heat the collective fractions (from silica gel chromatography) to remove the eluents. The fractions should be concentrated mostly under the influence of vacuum.

I.5.3. Characterization of products.

Analytical data for dihydropyrans **I-10a** to **I-28a**:

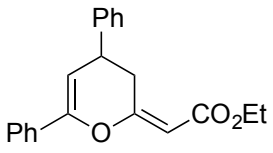

I-10a

***(E)*-ethyl-2-(4,6-diphenyl-3,4-dihydro-2H-pyran-2-ylidene)acetate (I-10a)**: Using 10 mol% catalyst **I-A**, 27.0 mg of pure product was isolated (93% yield). Pale yellow solid, mp 82 °C; ^{1}H

NMR (300 MHz, $CDCl_3$) δ 7.62-7.65 (2H, m.), 7.22-7.41 (8H, m.), 5.78 (1H, d, *J* = 3.6 Hz), 5.71 (1H, s.), 4.08-4.15 (2H, m.), 3.69-3.78 (2H, m.), 3.16 (1H, dd, *J* = 10.2, 6.6 Hz.), 1.25 (3H, t, *J* = 7.2 Hz.) ppm; ^{13}C NMR (75 MHz, $CDCl_3$) δ 167.3, 166.4, 149.3, 143.1, 133.4, 128.7, 128.6, 128.4, 127.3, 126.9, 124.5, 103.4, 99.4, 59.6, 35.9, 30.8, 14.3 ppm; IR (film) 3080, 2980, 1707 (s), 1660 (s), 1643 (s), 1495, 1282, 1167, 1119 (s) 758 cm^{-1}. HRMS (ESI) Calculated Mass for $C_{21}H_{21}O_3$: 321.1491 ($[M+H]^+$), Found 321.1505 ($[M+H]^+$), chiral HPLC analysis was done using DAICEL CHIRALPAK OJ-H column, R_t = 21.8 min (minor) and 26.6 min (major), **I-10a**-*S* (94% *ee*)**:** $[\alpha]_D^{20}$= -139 (c = 0.1, $CHCl_3$).

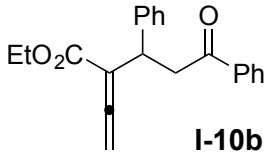

I-10b

***(E)*-ethyl-5-oxo-3,5-diphenyl-2-vinylidenepentanoate** (**I-10b**)**:** Using 20 mol% DABCO, 4.5 mg of **10b** was isolated as a side product (15% yield). Colorless oil, ^1H NMR (500 MHz, $CDCl_3$) δ 7.90-7.93 (2H, m.), 7.5-7.54 (1H, m.), 7.40-7.44 (2H, m.), 7.25-7.32 (2H, m.), 7.16-7.20 (1H, m.), 5.25 (1H, dd, *J* = 2.5, 14.0 Hz), 5.15 (1H, dd, *J* = 3.0, 14.0 Hz), 4.23-4.54 (1H, m.), 4.06-4.15 (2H, m.), 3.56 (1H, dd, *J* = 9, 17.5 Hz), 3.24 (1H, m.), 1.17 (3H, t, *J* = 7.0 Hz.) ppm; ^{13}C NMR (125 MHz, $CDCl_3$) δ 213.1, 197.5, 166.0, 142.7, 137.0, 133.0, 128.6, 128.4, 128.1, 127.9, 127.8, 126.7, 104.3, 81.5, 61.1, 44.3, 39.0, 14.1 ppm; IR (film) 3080, 2982, 1942, 1713 (s), 1688 (s), 1597, 1448, 1248(s), 1101, 1047, 752 cm^{-1}. HRMS (ESI) Calculated Mass for $C_{21}H_{21}O_3$: 321.1491 ($[M+H]^+$), Found 321.1487 ($[M+H]^+$).

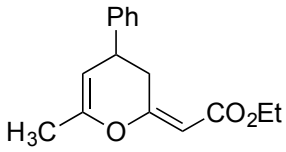

I-11a

***(E)*-ethyl-2-(6-methyl-4-phenyl-3,4-dihydro-2H-pyran-2-ylidene)acetate** (**I-11a**)**:** Using 20 mol% DABCO, 13.0 mg of pure product was isolated (55% yield). Colorless oil, ^{1}H NMR (500 MHz, $CDCl_3$) δ 7.18-7.29 (5H, m.), 5.48 (1H, s.), 4.93 (1H, d, *J* = 0.5 Hz), 4.05-4.09 (2H, m.), 3.41-3.59 (2H, m.), 3.30 (1H, dd, *J* = 8, 14.5 Hz), 1.90 (3H, t, *J* = 1 Hz.), 1.17-1.24 (3H, m.) ppm; ^{13}C NMR (125 MHz, $CDCl_3$) δ 167.4, 166.9, 148.7, 143.6, 128.5, 127.2, 126.7, 102.8, 98.7, 59.5, 35.5, 30.8, 19.1, 14.3 ppm; IR (film) 3085, 2982, 1711 (s), 1649 (s), 1373, 1269, 1176, 1110 (s), 846 cm^{-1}. HRMS (ESI) Calculated Mass for $C_{16}H_{19}O_3$: 259.1334 ($[M+H]^+$), Found 259.1331 ($[M+H]^+$).

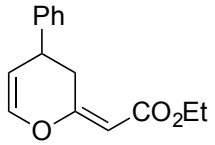

I-12a

***(E)*-ethyl-2-(4-phenyl-3,4-dihydro-2H-pyran-2-ylidene)acetate** (**I-12a**): Using 10 mol% catalyst **I-A**, 10.0 mg of pure product was isolated (45% yield). Colorless oil, ^{1}H NMR (300 MHz, $CDCl_3$) δ 7.23-7.36 (4H, m.), 6.58 (1H, dd, *J* = 2.1, 6.3 Hz.), 5.41 (1H, s.), 5.22-5.25 (1H, m.), 4.07-4.20 (2H, m.), 3.58-3.69 (1H, m.), 3.15 (1H, dd, *J* = 7.5, 14.4 Hz.), 1.22-1.34 (3H, m.) ppm; ^{13}C NMR (125 MHz, $CDCl_3$) δ 167.2, 166.0, 142.8, 140.9, 128.6, 127.2, 126.8, 107.8, 99.3, 77.2, 59.6, 34.8, 31.0, 14.3 ppm; IR (film) 3080, 2982, 1711 (s), 1653 (s), 1371, 1223, 1163 (s), 1109 (s), 846, 756 cm^{-1}. HRMS (ESI) Calculated Mass for $C_{15}H_{17}O_3$: 245.1178 ($[M+H]^+$), Found 245.1176 ($[M+H]^+$). Chiral HPLC analysis was done using DAICEL CHIRALPAK OJ-H column (1% isopropanol in *n*-

hexanes at 1.0 mL/min), R_t = 11.5 min (minor) and 17.5 min (major), **I-12a-*S*** (95% *ee*)**:** $[\alpha]_D^{20}$= -139 (c = 0.1, $CHCl_3$).

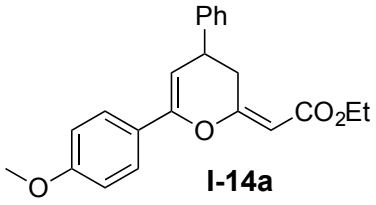

I-14a

(E)*-ethyl-2-(6-(4-methoxyphenyl)-4-phenyl-3,4-dihydro-2H-pyran-2-ylidene)acetate** (**I-14a**): Using 10 mol% catalyst **I-A**, 12.0 mg of pure product was isolated (39% yield). White solid, mp 91 °C, ^{1}H NMR (500 MHz, $CDCl_3$) δ 7.59-7.57 (2H, dd, *J* = 10.0, 3.0 Hz.), 7.32-7.35 (2H, m.), 7.24-7.30 (3H, m.), 6.91-7.93 (2H, dd, *J* = 10.0, 3.0 Hz.), 5.70 (1H, s.), 5.61 (1H, d, *J* = 4.0 Hz), 4.17-4.10 (2H, m.), 3.85 (3H, s.), 3.76-3.70 (2H, m.), 3.19-3.13 (1H, m.), 1.26 (3H, t, *J* = 7.5 Hz.) ppm; ^{13}C NMR (125 MHz, $CDCl_3$) δ 167.3, 166.6, 160.1, 149.1, 143.4, 128.6,127.3, 126.8, 126.1, 125.9, 113.8, 101.6, 99.2, 59.6, 55.3, 35.9, 30.9, 14.3 ppm; IR (film) 3062, 2980, 2838, 1707 (s), 1646 (s), 1513, 1373, 1282, 1253(s), 1175, 1120(s), 1045, 836 cm^{-1}. HRMS (ESI) Calculated Mass for $C_{22}H_{23}O_4$: 351.1596 ($[M+H]^+$), Found 351.1586 ($[M+H]^+$). Chiral HPLC analysis was done using DAICEL CHIRALPAK OJ-H column (5% isopropanol in *n*-hexanes at 1.0 mL/min), R_t = 37.3 min (minor) and 54.7 min (major), **I-14a-*S (96% *ee*)**:** $[\alpha]_D^{20}$= -161 (c = 0.05, $CHCl_3$).

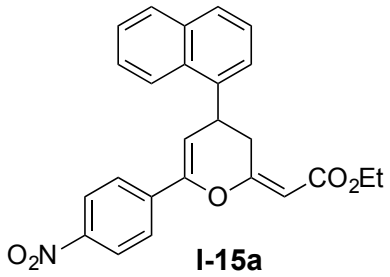

I-15a

(E)*-ethyl-2-(4-(naphthalen-1-yl)-6-(4-nitrophenyl)-3,4-dihydro-2H-pyran-2-ylidene) acetate** (**I-15a**): Using 1 g of enone **I-15** and 20 mol% catalyst **I-B**, 1.36 g of pure product was isolated (>99% yield). Yellowish orange solid, mp 125 °C. ^{1}H NMR (600 MHz, $CDCl_3$) δ 8.23 (2H, d, *J* = 9.0 Hz.), 8.10 (1H, d, *J* = 9.0 Hz.), 7.90 (1H, d, *J* = 8.4 Hz.), 7.80 (2H, d, *J* = 9.0 Hz.), 7.78 (1H, d, *J* = 7.8 Hz.), 7.57 (1H, t, *J* = 7.2 Hz.), 7.51 (1H, t, *J* = 6.6 Hz), 7.43 (1H, t, *J* = 7.2 Hz.), 7.38 (1H, t, *J* = 6.0 Hz.), 6.08 (1H, d, *J* = 4.2 Hz.), 5.77 (1H, s.), 4.61-4.58 (1H, m.), 4.08-4.04 (2H, m.), 3.92 (1H, dd, *J* = 15.0, 6.0 Hz.), 3.34 (1H, dd, *J* = 15.0, 8.4 Hz.), 1.17 (3H, t, *J* = 7.2 Hz.) ppm; ^{13}C NMR (150 MHz, $CDCl_3$) δ 166.8, 165.4, 147.9, 147.7, 139.3, 137.6, 134.1, 131.0, 129.2, 128.0, 126.6, 125.8, 125.5, 125.1, 124.3, 123.8, 122.7, 107.6, 100.6, 59.9, 32.0, 29.4, 14.2 ppm; IR (film) 3056, 2925, 2855, 1703 (s), 1656 (s), 1597, 1518 (s), 1344 (s), 1286, 1119(s), 1051, 858, 777 $cm^{-1.}$ HRMS (ESI) Calculated Mass for $C_{25}H_{22}NO_5$: 416.1498 ($[M+H]^+$), Found 416.1492 ($[M+H]^+$). Chiral HPLC analysis was done using DAICEL CHIRALPAK OD-H column (30% isopropanol in *n*-hexanes at 1.0 mL/min), R_t = 30.2 min (minor) and 39.8 min (major), **I-15a-*S (97% *ee*)**:** $[\alpha]_D^{20}$= -10 (c = 0.1, $CHCl_3$).

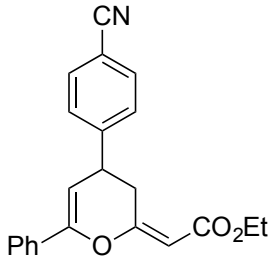

I-16a

(E)*-ethyl-2-(4-(4-cyanophenyl)-6-phenyl-3,4-dihydro-2H-pyran-2-ylidene)acetate** (**I-16a**): Using 10 mol% catalyst **I-A**, 25.0 mg of pure product was isolated (81% yield). Crystalline pale yellow solid, mp 123 °C. ^{1}H NMR (600 MHz, $CDCl_3$) δ 7.62-7.59 (4H, m.), 7.40-7.34 (5H, m.), 5.71-5.70 (2H, m.), 4.13-4.06 (2H, m.), 3.81 (1H, dd, *J* = 12.0, 6.6 Hz.), 3.55 (1H, dd, *J* = 15.0, 6.0 Hz.), 3.35 (1H, dd, *J* = 15.6, 7.2 Hz.), 1.23 (3H, t, *J* = 7.2 Hz.) ppm; ^{13}C NMR (125 MHz, $CDCl_3$) δ 167.1, 165.1, 150.3, 148.5, 133.0, 132.5, 129.1, 128.5, 128.3, 124.6, 118.8, 110.9, 101.2, 100.3, 59.8, 36.0, 30.2, 14.3 ppm; IR (film) 3063, 2981, 2228, 1706 (s), 1649 (s), 1608, 1374, 1281, 1166, 1120(s), 1048, 846, 761 $cm^{-1.}$ HRMS (ESI) Calculated Mass for $C_{22}H_{20}NO_3$: 346.1443 ($[M+H]^+$), Found 346.1447 ($[M+H]^+$). Chiral HPLC analysis was done using DAICEL CHIRALPAK OD-H column (13% isopropanol in *n*-hexanes at 1.0 mL/min), R_t = 13.9 min (minor) and 17.3 min (major), **I-16a-*S (97% *ee*)**:** $[\alpha]_D^{20}$= -94 (c = 0.1, $CHCl_3$).

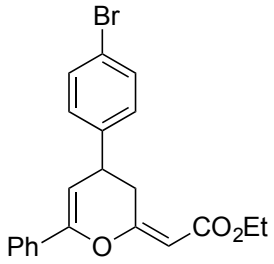

I-17a

(E)*-ethyl-2-(4-(4-bromophenyl)-6-phenyl-3,4-dihydro-2H-pyran-2-ylidene)acetate** (**I-17a**): Using 10 mol% catalyst **I-A**, 33.4 mg of pure product was isolated (96% yield). White solid, mp 129 °C. ^{1}H NMR (600 MHz, $CDCl_3$) δ 7.61 (2H, d, *J* = 6.6 Hz.), 7.42 (2H, dd, *J* = 11.4, 3.0 Hz.), 7.38-7.32 (3H, m.), 7.14-7.12 (2H, m.), 5.71 (1H, d, *J* = 4.8 Hz.), 5.69 (1H, s.), 4.13-4.07 (2H, m.), 3.72-3.69 (1H, m.), 3.58 (1H, dd, *J* = 15.0, 6.0 Hz.), 1.23 (3H, t, *J* = 7.2 Hz.) ppm; ^{13}C NMR (150 MHz, $CDCl_3$) δ 167.2, 165.8, 149.7, 142.1, 133.2, 131.8, 129.1, 128.9, 128.5, 124.6, 120.7, 102.4, 99.8, 59.8, 35.4, 30.6, 14.3 ppm; IR (film) 3061, 2980, 1706 (s), 1648 (s), 1489, 1374, 1281, 1166, 1120(s), 1050, 847, 820, 760 $cm^{-1.}$ HRMS (ESI) Calculated Mass for $C_{21}H_{21}O_3Br$: 399.0596 ($[M+H]^+$), Found 399.0592 ($[M+H]^+$). Chiral HPLC analysis was done using DAICEL CHIRALPAK OJ-H column (5% isopropanol in *n*-hexanes at 1.0 mL/min), R_t = 23.9 min (minor) and 34.1 min (major), **I-17a-*S (96% *ee*)**:** $[\alpha]_D^{20}$= -76 (c = 0.07, $CHCl_3$).

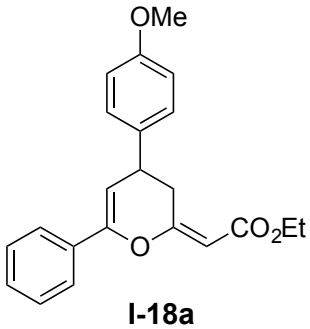

I-18a

***(E)*-ethyl-2-(4-(4-methoxyphenyl)-6-phenyl-3,4-dihydro-2H-pyran-2-ylidene)acetate** (**I-18a**)**:** Using 10 mol% catalyst **I-A**, 19.0 mg of pure product was isolated (60% yield). White solid, mp 86

°C. ^{1}H NMR (600 MHz, $CDCl_3$) δ 7.61 (1H, t, *J* = 2.4 Hz.), 7.38-7.35 (2H, m.), 7.32 (1H, tt, *J* = 7.2, 4.8, 1.8 Hz.), 7.18-7.16 (2H, m), 6.84 (2H, dt, *J* = 9.6, 5.4, 3.0 Hz.), 5.74 (1H, d, *J* = 4.2 Hz.), 5.68 (1H, s.), 4.14-4.08 (2H, m.), 3.78 (3H, s.), 3.70-3.67 (1H, m.), 3.64 (1H, dd, *J* = 15.0, 6.0 Hz.), 3.15 (1H, dd, *J* = 15.0, 7.8 Hz.), 1.23 (3H, t, *J* = 6.6 Hz.) ppm; ^{13}C NMR (150 MHz, $CDCl_3$) δ 167.3, 166.6, 158.5, 149.2, 135.2, 133.5, 128.7, 128.4, 124.5, 114.1, 103.7, 99.4, 59.6, 55.3, 35.1, 31.0, 14.3 ppm; IR (film) 3028, 2928, 1704 (s), 1649 (s), 1512, 1374, 1251, 1118 (s), 1046, 829, 761 cm^{-1}. HRMS (ESI) Calculated Mass for $C_{22}H_{23}O_4$: 351.1596 ($[M+H]^+$), Found 351.1591 ($[M+H]^+$). Chiral HPLC analysis was done using DAICEL CHIRALPAK OJ-H column (15% isopropanol in *n*-hexanes at 1.0 mL/min), R_t = 18.3 min (minor) and 30.5 min (major), **I-18a-*S*** (96% *ee*)**:** $[\alpha]_D^{20}$= -179 (c = 0.1, $CHCl_3$).

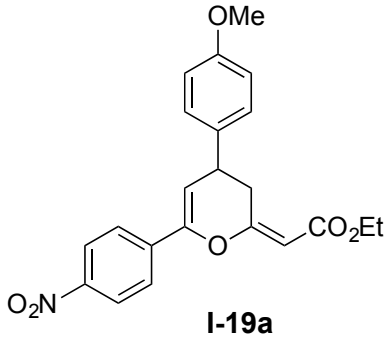

I-19a

***(E)*-ethyl-2-(4-(4-methoxyphenyl)-6-(4-nitrophenyl)-3,4-dihydro-2H-pyran-2-ylidene) acetate** (**I-19a**)**:** Using 10 mol% catalyst **I-A**, 21.0 mg of pure product was isolated (58% yield). Thick yellow oil. ^{1}H NMR (600 MHz, $CDCl_3$) δ 8.31-8.09 (1H, m.), 7.76 (2H, dd, *J* = 11.4, 2.4 Hz.), 7.15 (2H, dd, *J* = 12.0, 3.0 Hz.), 6.87-6.84 (2H, m), 5.95 (1H, d, *J* = 4.2 Hz.), 5.72 (1H, s.), 4.15-4.09 (2H, m.), 3.78 (3H, s.), 3.74-3.74 (1H, m.), 3.67 (1H, dd, *J* = 15.6, 6.0 Hz.), 3.17 (1H, dd, *J* = 15.0, 7.8 Hz.), 1.24 (3H, t, *J* = 7.2 Hz.) ppm; ^{13}C NMR (150 MHz, $CDCl_3$) δ 166.9, 165.5, 158.7, 147.7, 147.4, 139.4, 134.3, 128.3, 125.1, 123.8, 114.2, 107.9, 100.3, 59.9, 55.3, 35.3, 30.6, 14.3 ppm; IR

(film) 3076, 2981, 1708 (s), 1659 (s), 1515 (s), 1344 (s), 1286, 1171, 1119 (s), 860, 752 cm^{-1}. HRMS (ESI) Calculated Mass for $C_{22}H_{22}NO_6$: 396.1447 ($[M+H]^+$), Found 396.1447 ($[M+H]^+$). Chiral HPLC analysis was done using DAICEL CHIRALPAK OD-H column (10% isopropanol in *n*-hexanes at 1.0 mL/min), R_t = 22.6 min (minor) and 42.9 min (major), **I-19a-*S*** (95% *ee*)**:** $[\alpha]_D^{20}$= -262 (c = 0.15, $CHCl_3$).

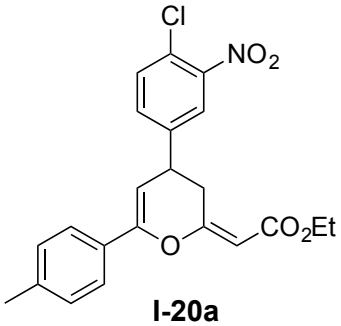

I-20a

***(E)*-ethyl-2-(4-(4-chloro-3-nitrophenyl)-6-(p-tolyl)-3,4-dihydro-2H-pyran-2-ylidene)acetate** (**I-20a**): Using 10 mol% catalyst **I-A,** 24.4 mg of pure product was isolated (66% yield). Viscous yellow oil. ^{1}H NMR (600 MHz, $CDCl_3$) δ 7.76 (1H, d, *J* = 2.4 Hz.), 7.51-7.48 (3H, m.), 7.41 (1H, dd, *J* = 8.4, 2.4 Hz.), 7.19 (2H, d, *J* = 8.4 Hz.), 5.72 (1H, s.), 5.63 (1H, d, *J* = 2.4 Hz.), 4.12-4.08 (2H, m.), 3.80 (1H, dd, *J* = 11.4, 6.6 Hz.), 3.50 (1H, dd, *J* = 15.6, 6.6 Hz.), 3.41 (1H, dd, *J* = 15.0, 6.6 Hz.), 2.36 (3H, s.), 1.23 (3H, t, *J* = 7.2 Hz.) ppm; ^{13}C NMR (150 MHz, $CDCl_3$) δ 167.0, 164.7, 150.7, 143.8, 139.4, 132.2, 132.1, 130.0, 129.2, 125.4, 124.6, 124.4, 100.5, 99.6, 59.9, 35.1, 30.0, 21.3, 14.3 ppm; IR (film) 3071, 2982, 2927, 1707 (s), 1650 (s), 1537 (s), 1478, 1352, 1282, 1175, 1121(s), 1048, 823, 731 $cm^{-1.}$ HRMS (ESI) Calculated Mass for $C_{22}H_{21}NO_5Cl$: 414.1108 ($[M+H]^+$), Found 414.1109 ($[M+H]^+$). Chiral HPLC analysis was done using DAICEL CHIRALPAK

OD-H column (5% isopropanol in *n*-hexanes at 0.7 mL/min), R_t = 20.0 min (minor) and 26.5 min (major), **I-20a-*S*** (90% *ee*)**:** $[\alpha]_D^{20}$= -275 (c = 0.07, $CHCl_3$).

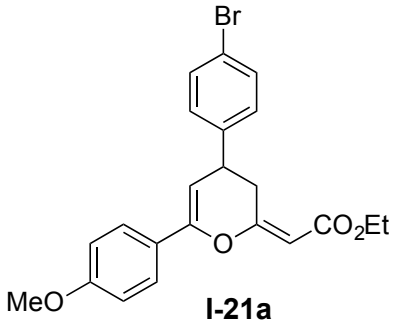

I-21a

(E)*-ethyl-2-(4-(4-bromophenyl)-6-(4-methoxyphenyl)-3,4-dihydro-2H-pyran-2-ylidene) acetate** (**I-21a**): Using 10 mol% catalyst **I-A**, 6.2 mg of pure product was isolated (16% yield). Brown yellow oil. ^{1}H NMR (600 MHz, $CDCl_3$) δ 7.53 (2H, d, *J* = 9.0 Hz.), 7.41 (2H, d, *J* = 8.4 Hz.), 7.13 (2H, d, *J* = 8.4 Hz.), 7.89 (2H, d, *J* = 9.0 Hz.), 5.67 (1H, s.), 5.57 (1H, d, *J* = 4.2 Hz.), 4.15-4.07 (2H, m.), 3.81 (3H, s.), 3.69-3.58 (1H, m.), 3.56 (1H, dd, *J* = 15.0, 6.0 Hz.), 3.21 (1H, dd, *J* = 15.6, 8.4 Hz.), 1.23 (3H, t, *J* = 7.2 Hz.) ppm; ^{13}C NMR (150 MHz, $CDCl_3$) δ 167.3, 166.0, 160.1, 149.5, 142.3, 131.7, 129.1, 126.0, 125.9, 120.7, 113.8, 100.65, 99.6, 59.7, 55.4, 35.4, 30.7, 14.3 ppm; IR (film) 3072, 2980, 2937, 1733 (s), 1602 (s), 1512, 1490, 1371, 1257(s), 1173(s), 1117, 1028, 836, 732 $cm^{-1.}$ HRMS (ESI) Calculated Mass for $C_{22}H_{22}O_4Br$: 429.0701 ($[M+H]^+$), Found 429.0693 ($[M+H]^+$). Chiral HPLC analysis was done using DAICEL CHIRALPAK OJ-H column (32% isopropanol in *n*-hexanes at 1.0 mL/min), R_t = 20.9 min (minor) and 33.7 min (major), **I-21a-*S (95% *ee*)**:** $[\alpha]_D^{20}$= -123 (c = 0.1, $CHCl_3$).

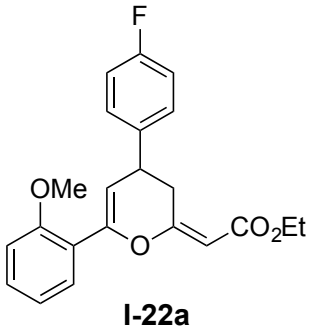

I-22a

(E)*-ethyl-2-(4-(4-fluorophenyl)-6-(2-methoxyphenyl)-3,4-dihydro-2H-pyran-2-ylidene) acetate** (**I-22a**)**:** Using 10 mol% catalyst **I-A**, 32.8 mg of pure product was isolated (>99% yield). Thick pale yellow oil. ^{1}H NMR (600 MHz, $CDCl_3$) δ 7.59 (1H, dd, *J* = 7.8, 1.8 Hz.), 7.30 (1H, m.), 7.26-7.23 (2H, m.), 7.00-6.97 (3H, m.), 6.94 (1H, d, *J* = 8.4Hz.), 5.97 (1H, d, *J* = 4.2 Hz.), 5.61 (1H, s.), 4.11-4.07 (2H, m.), 3.84 (3H, s.), 3.74-3.72 (1H, m.), 3.61 (1H, dd, *J* = 15.0, 6.0 Hz.), 3.18 (1H, dd, *J* = 15.6, 8.4 Hz.), 1.22 (3H, t, *J* = 7.2 Hz.) ppm; ^{13}C NMR (150 MHz, $CDCl_3$) δ 167.4, 166.7, 162.5 (d, $^{1}J_{C,F}$ = 243.2 Hz.), 157.1, 146.4, 139.1 (d, $^{4}J_{C,F}$ = 3.5 Hz.), 129.7, 128.9 (d, $^{3}J_{C,F}$ = 8.0 Hz.), 128.2, 122.5, 120.5, 115.4 (d, $^{2}J_{C,F}$ = 21.2 Hz.), 111.3, 108.2, 98.9, 59.6, 55.6, 35.3, 31.1, 14.3 ppm; IR (film) 3071, 2979, 1706 (s), 1645 (s), 1508 (s), 1374, 1257, 1119 (s), 1051, 1023, 835, 755 cm^{-1}. HRMS (ESI) Calculated Mass for $C_{22}H_{22}O_4F$: 369.1502 ([M+H]$^+$), Found 369.1515 ([M+H]$^+$). Chiral HPLC analysis was done using DAICEL CHIRALPAK OD-H column (1% isopropanol in *n*-hexanes at 0.7 mL/min), R_t = 15.9 min (minor) and 18.7 min (major), **I-22a-*S (97% *ee*)**:** $[\alpha]_D^{20}$= -144 (c = 0.1, $CHCl_3$).

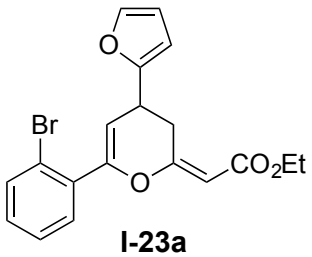

I-23a

(E)*-ethyl-2-(6-(2-bromophenyl)-4-(furan-2-yl)-3,4-dihydro-2H-pyran-2-ylidene)acetate** (**I-23a**)**:** Using 10 mol% catalyst **I-A**, 21.4 mg of pure product was isolated (61% yield). Thick brown oil. ^{1}H NMR (600 MHz, $CDCl_3$) δ 7.59 (1H, d, *J* = 6.6 Hz.), 7.40 (1H, dd, *J* = 7.8, 1.8 Hz.), 7.34 (1H, dd, *J* = 2.4, 1.2 Hz.), 7.30 (1H, dt, *J* = 4.8, 1.2 Hz), 7.21 (1H, m.), 6.29 (1H, t, *J* = 3.0 Hz.), 6.16 (1H, d, *J* = 3.0 Hz.), 5.61 (1H, s.), 5.49 (1H, d, *J* = 4.8 Hz.), 4.15-4.12 (2H, m.), 3.83-3.80 (1H, m.), 3.58 (1H, dd, *J* = 15.0, 6.0 Hz.), 3.47 (1H, dd, *J* = 15.0, 7.2 Hz.), 1.25 (3H, t, *J* = 6.6 Hz.) ppm; ^{13}C NMR (150 MHz, $CDCl_3$) δ 167.2, 165.8, 155.1, 150.1, 141.8, 135.4, 133.3, 130.9, 130.4, 127.3, 122.5, 110.2, 105.4, 105.38, 99.9, 59.8, 29.7, 27.4, 14.3 ppm; IR (film) 3064, 2976, 1735, 1701 (s), 1651 (s), 1560, 1292, 1173, 1116 (s), 1045, 1021, 847, 780 cm^{-1}. HRMS (ESI) Calculated Mass for $C_{19}H_{18}O_4Br$: 389.0388 ($[M+H]^+$), Found 389.0387 ($[M+H]^+$). Chiral HPLC analysis was done using DAICEL CHIRALPAK OJ-H column (2% isopropanol in *n*-hexanes at 1.0 mL/min), R_t = 19.7 min (minor) and 24.2 min (major), **I-23a-*S (96% *ee*)**:** $[\alpha]_D^{20}$= -112 (c = 0.1, $CHCl_3$).

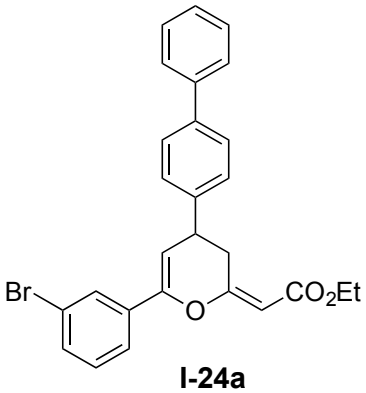

I-24a

(E)*-ethyl-2-(4-([1,1'-biphenyl]-4-yl)-6-(3-bromophenyl)-3,4-dihydro-2H-pyran-2-ylide-ne) acetate** (**I-24a**): Using 1 g of enone **I-24** and 10 mol% catalyst **I-A**, 1.28 g of pure product was isolated (98% yield). Pale yellow solid, mp 102 °C. ^{1}H NMR (600 MHz, $CDCl_3$) δ 7.78 (1H, t, *J* = 1.2 Hz.), 7.57 (1H, t, *J* = 1.8 Hz.), 7.56-7.53 (4H, m.), 7.46 (1H, d, *J* = 6.0 Hz.), 7.42 (2H, t, *J* = 7.8 Hz.), 7.34-7.32 (3H, m.), 7.24 (1H, t, *J* = 6.6 Hz), 5.81 (1H, d, *J* = 3.6 Hz.), 5.73 (1H, s.), 4.16-4.08 (2H, m.), 3.80-3.77 (1H, m.), 3.72 (1H, dd, *J* = 15.0, 6.0 Hz.), 3.22 (1H, dd, *J* = 15.6, 8.4 Hz.), 1.24 (3H, t, *J* = 6.0 Hz.) ppm; ^{13}C NMR (150 MHz, $CDCl_3$) δ 167.1, 165.9, 148.0, 141.8, 140.8, 140.0, 135.4, 131.7, 129.9, 128.8, 127.7, 127.6, 127.5, 127.2, 127.0, 123.1, 122.7, 104.5, 99.9, 59.8, 35.6, 30.6, 14.3 ppm; IR (film) 3062, 2980, 2902, 1706 (s), 1658 (s), 1562, 1483, 1374, 1277, 1167, 1119(s), 1050, 847, 765 $cm^{-1.}$ HRMS (ESI) Calculated Mass for $C_{27}H_{24}O_3Br$: 475.0909 ($[M+H]^+$), Found 475.0901 ($[M+H]^+$). Chiral HPLC analysis was done using DAICEL CHIRALPAK OJ-H column (40% isopropanol in *n*-hexanes at 1.0 mL/min), R_t = 29.7 min (minor) and 77.6 min (major), **I-24a-*S (98% *ee*)**:** $[\alpha]_D^{20}$= -93 (c = 0.1, $CHCl_3$).

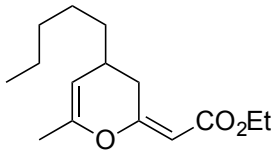

I-25a

(E)*-ethyl-2-(6-methyl-4-pentyl-3,4-dihydro-2H-pyran-2-ylidene)acetate** (**I-25a**): Using 10 mol% catalyst **I-A**, 3.0 mg of pure product was isolated (12% yield). Colorless oil, ^{1}H NMR (600 MHz, $CDCl_3$) δ 5.34 (1H,s.), 4.75 (1H, d, *J* = 3.6 Hz.), 4.12 (2H, q, *J* = 7.2 Hz.), 3.26 (1H, dd, *J* = 15.0, 6.0 Hz.), 2.73 (1H, dd, *J* = 15.0, 7.8 Hz.), 2.16 (1H, m.), 1.80 (3H, dd, *J* = 1.8, 1.2 Hz.), 1.32-1.27 (5H, m.), 1.25-1.20 (6H, m.), 0.86 (3H, t, *J* = 6.6 Hz.) ppm; ^{13}C NMR (150 MHz, $CDCl_3$) δ 168.4, 167.8, 147.4, 104.2, 98.0, 59.5, 35.4, 31.8, 29.7, 29.3, 28.4, 26.3, 22.5, 19.0, 14.4, 14.0 ppm; IR (film) 2956, 2924, 2853, 1711 (s), 1647 (s), 1379, 1267, 1116(s), 1050 cm^{-1}. HRMS (ESI) Calculated Mass for $C_{15}H_{25}O_3$: 253.1804 ($[M+H]^+$), Found 253.1804 ($[M+H]^+$). Chiral HPLC analysis was done using DAICEL CHIRALPAK OJ-H column (100% *n*-hexanes at 0.7 mL/min), R_t = 21.6 min (minor) and 27.1 min (major), **I-25a-*S (86% *ee*): $[\alpha]_D^{20}$= -25 (c = 0.05, $CHCl_3$).

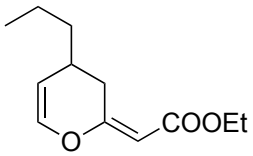

I-26a

(*E*)-ethyl-2-(4-propyl-3,4-dihydro-2H-pyran-2-ylidene)acetate (**I-26a**): Using 20 mol% catalyst **I-B**, 3.5 mg of pure product was isolated (18% yield). Colorless oil, ^{1}H NMR (600 MHz, $CDCl_3$) δ 6.33 (1H, d, *J* = 6.6 Hz.), 5.45 (1H, s.), 5.02 (1H, dd, *J* = 6.0, 4.2 Hz.), 4.15-4.11 (2H, m.), 3.29 (1H, dd, *J* = 6.0, 15.0 Hz.), 2.86 (1H, dd, *J* = 15.0, 7.8 Hz.), 2.36-2.31 (1H, m.), 0.89 (3H, t, *J* = 7.2 Hz.) ppm; ^{13}C NMR (150 MHz, $CDCl_3$) δ 167.54, 167.48, 139.8, 109.2, 98.6, 59.6, 37.3, 28.43,

28.37, 19.8, 14.4, 14.0 ppm; IR (film) 3076, 2989, 1710 (s), 1651 (s), 1220, 1167, 1100 (s), 845 cm^{-1}. HRMS (ESI) Calculated Mass for $C_{12}H_{19}O_3$: 211.1329 ($[M+H]^+$), Found 211.1331 ($[M+H]^+$). Chiral HPLC analysis could not be done as analytically desirable resolution of the enantiomers was not possible using various chiral columns.

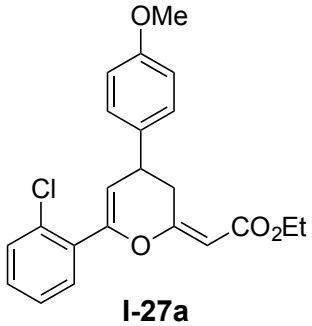

I-27a

(E)*-ethyl-2-(6-(2-chlorophenyl)-4-(4-methoxyphenyl)-3,4-dihydro-2H-pyran-2-ylidene) acetate** (**I-27a**)**:** Using 10 mol% catalyst **I-A**, 35.0 mg of pure product was isolated (>99% yield). Thick colorless oil. ^{1}H NMR (500 MHz, $CDCl_3$) δ 7.47-7.45 (1H, m.), 7.42-7.40 (1H, m.), 7.30-7.25 (2H, m.), 7.23-7.20 (2H, m), 6.86-6.84 (2H, m.), 5.59 (1H, s.), 5.53 (1H, d, *J* = 3.5 Hz.), 4.12-4.06 (2H, m.), 3.78 (3H, s.), 3.70-3.62 (2H, m.), 3.18 (1H, dd, *J* = 15.0, 7.0 Hz.), 1.22 (3H, t, *J* = 7.0 Hz.) ppm; ^{13}C NMR (125 MHz, $CDCl_3$) δ 167.3, 166.5, 158.6, 148.2, 135.0, 133.6, 133.0, 130.5, 130.2, 130.0, 128.4, 126.7, 114.1, 109.1, 99.4, 59.6, 55.3, 35.2, 31.1, 14.3 ppm; IR (film) 3064, 2980, 1704 (s), 1649 (s), 1512, 1350, 1251, 1116 (s), 1039, 850, 760 cm^{-1}. HRMS (ESI) Calculated Mass for $C_{22}H_{22}O_4Cl$: 385.1207 ($[M+H]^+$), Found 385.1209 ($[M+H]^+$). Chiral HPLC analysis was done using DAICEL CHIRALPAK OD-H column (1% isopropanol in *n*-hexanes at 0.7 mL/min), R_t = 19.4 min (minor) and 22.9 min (major), **I-27a-*S (97% *ee*)**:** $[\alpha]_D^{20}$= -114 (c = 1.6, $CHCl_3$).

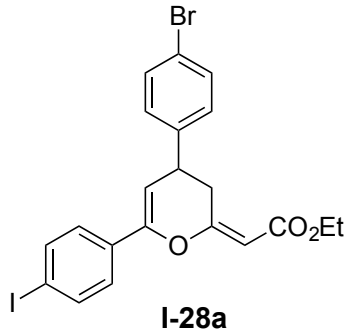

I-28a

(E)*-ethyl-2-(4-(4-bromophenyl)-6-(4-iodophenyl)-3,4-dihydro-2H-pyran-2-ylidene) acetate** (**I-28a**)**:** Using 10 mol% catalyst **I-A**, 24.0 mg of pure product was isolated (51% yield). Yellow solid, mp 74 °C. ^{1}H NMR (500 MHz, $CDCl_3$) δ 7.70 (2H, dt, J = 9.0, 4.0, 2.5 Hz.), 7.42 (2H, dt, *J* = 9.0, 4.5, 2.5 Hz.), 7.33 (2H, dt, *J* = 9.2, 4.5, 2.5 Hz.), 7.10 (2H, dt, *J* = 9.0, 4.0, 2.5 Hz.), 5.71 (1H, d, *J* = 4.5 Hz.), 5.68 (1H, s.), 4.13-4.08 (2H, m.), 4.07-3.66 (1H, m.), 3.58 (1H, dd, *J* = 15.0, 6.0 Hz.), 3.21 (1H, dd, *J* = 15.0, 7.5 Hz.), 1.23 (3H, t, *J* = 7.0 Hz.) ppm; ^{13}C NMR (125 MHz, $CDCl_3$) δ 167.0, 165.4, 148.9, 141.8, 137.6, 132.8, 131.8, 129.1, 126.2, 120.8, 103.0, 100.1, 94.6, 59.8, 35.4, 30.4, 14.3 ppm; IR (film) 3076, 2924, 1703 (s), 1652 (s), 1487, 1282, 1118 (s), 1005, 887, 853 cm^{-1}. HRMS (ESI) Calculated Mass for $C_{21}H_{19}O_3BrI$: 524.9562 ($[M+H]^+$), Found 524.9558 ($[M+H]^+$). Chiral HPLC analysis was done using DAICEL CHIRALPAK OD-H column (1% isopropanol in *n*-hexanes at 1.0 mL/min), R_t = 15.7 min (minor) and 23.6 min (major), **I-28a-*S (95% *ee*)**:** $[\alpha]_D^{20}$= -117 (c = 0.8, $CHCl_3$).

I.5.4. Synthesis of I-24b.

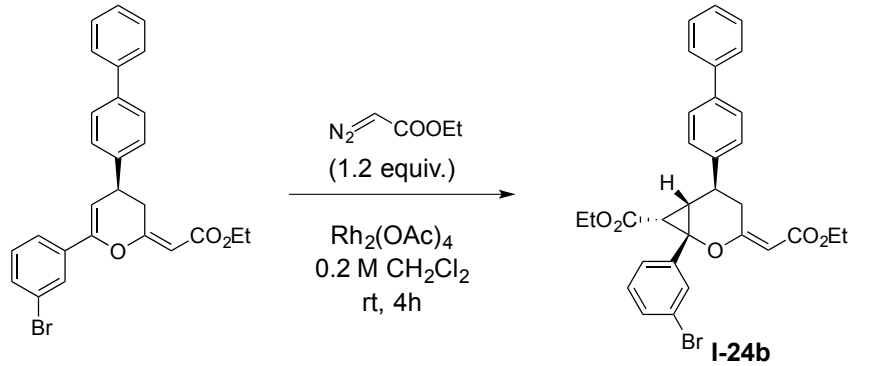

I-24a-*S*
(98% *ee*)

I-24b
74% yield (83% brsm)
(single isomer by NMR)

In a 1 dram vial, initially purged with argon, was taken 100 mg (0.21 mmol) of **I-24a-***S* along with 5 mol% of $Rh_2(OAc)_4$ in CH_2Cl_2 (0.5 mL). The resulting green suspension containing 4Å MS (10% by weight) was stirred at room temperature while a solution of 29 mg (0.25 mmol, 1.2 equiv.) of ethyl diazoacetate in CH_2Cl_2 (0.5 mL) was added drop wise over a period of 3 h (Note: The addition has to be slow and dropwise or else significant amount of diethyl fumarate is formed which co-elutes with the desired product during silica gel column chromatography and can only be separated after successive recrystallizations of **I-24b**). After the addition was complete, the resulting mixture was allowed to stir at room temperature for another hour. The solvent was then partially evaporated under a stream of nitrogen and the slurry was loaded directly on a silica gel column. A flash silica gel chromatography using ethyl acetate and hexanes as eluents afforded **I-24b** as a crystalline white solid (88 mg, 74% yield).

Analytical data for **I-24b:**

Crystalline white solid, mp 147 °C. ^{1}H NMR (600 MHz, $CDCl_3$) δ 7.58-7.56 (4H, m.), 7.44-7.41 (3H, m.), 7.40-7.38 (2H, m.), 7.36 (1H, t, *J* = 1.2 Hz.), 7.34 (1H, tt, *J* = 6.6, 2.4, 1.2 Hz.), 7.22 (1H,

d, *J* = 7.8 Hz.), 7.16-7.14 (1H, m.), 5.63 (1H, s.), 4.25-4.20 (2H, m.), 4.11 (2H, q, *J* = 7.2 Hz.), 3.98-3.94 (1H, m.), 2.44-2.39 (1H, m.), 2.30-2.25 (2H, m.), 1.29 (3H, t, *J* = 6.6 Hz.), 1.24 (3H, t, *J* = 6.6 Hz.) ppm; ^{13}C NMR (150 MHz, $CDCl_3$) δ 171.0, 167.6, 167.0, 142.2, 142.1, 140.7, 140.2, 130.9, 130.3, 128.8, 127.63, 127.61, 127.3, 127.1, 123.1, 122.7, 97.7, 63.3, 61.0, 59.6, 35.1, 31.0, 30.5, 14.4, 14.3 ppm; IR (film) 3057, 2981, 1730 (s), 1704 (s), 1644 (s), 1596, 1486, 1375, 1348, 1231, 1170 (s), 1119 (s), 1049, 763, 659 cm^{-1}. HRMS (ESI) Calculated Mass for $C_{31}H_{30}O_5Br$: 561.1276 ([M+H]$^+$), Found 561.1271 ([M+H]$^+$), $[\alpha]_D^{20}$= -50 (c = 0.15, $CHCl_3$).

I.5.5. General Procedure for synthesis of chalcones.

(Enones **I-10** through **I-14**, **I-25,** and **I-26** were procured from commercial sources.)

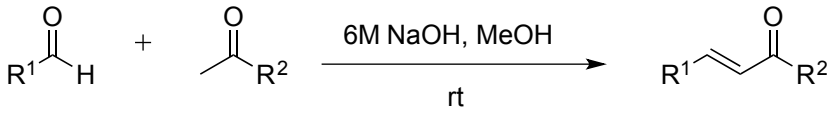

In a 50 ml round bottom flask, 8.56 mmol of the respective acetophenone was charged with the *corresponding* benzaldehyde (8.56 mmol) and the mixture was then dissolved in methanol (8.0 mL). This solution was rapidly stirred at room temperature when, 6M NaOH (4.3 mL) was added dropwise. The reaction mixture warmed up rapidly forming a cloudy suspension. Even though, in most cases the product crashed out of the solution within 5-10 min, the reaction mixture was allowed to stir at room temperature for another hour (overnight in case of **I-22**). The precipitated solid was filtered through a Buchner funnel, washed with water (50.0 mL) to remove the alkali, dried and then recrystallized using appropriate solvents. For isolation of product **I-22** (oil), the reaction mixture was allowed to stir overnight. It was then poured over ice (20 g) and the resulting mixture was extracted with ethyl acetate (10 x 3 mL). The combined extracts were

washed with brine, dried over sodium sulfate, concentrated and finally subjected to purification by silica gel flash column chromatography.

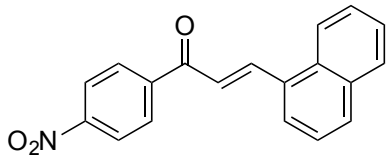

I-15

(*E*)-3-(naphthalen-1-yl)-1-(4-nitrophenyl)prop-2-en-1-one (**I-15**)**:** 71% yield, recrystallized from hot ethyl acetate and MeOH (EtOAc: MeOH = 5:1), bright yellow solid, mp 150-151 °C (lit.[40] 144-146 °C) ^{1}H NMR (600 MHz, $CDCl_3$) δ 8.71 (1H, d, *J* = 15.6 Hz.), 8.36-8.34 (2H, m.), 8.22-8.17 (3H, m.), 7.96-7.89 (3H, m.), 7.61-7.52 (4H, m.) ppm; ^{13}C NMR (150 MHz, $CDCl_3$) δ 188.9, 150.3, 143.8, 143.2, 134.0, 132.0, 131.9, 131.8, 129.7, 129.1, 127.5, 126.7, 125.6, 125.6, 124.1, 123.9, 123.4 ppm.

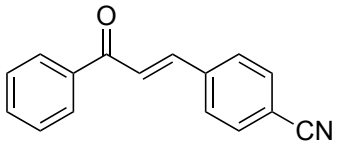

I-16

(*E*)-4-(3-oxo-3-phenylprop-1-en-1-yl)benzonitrile (**I-16**)**:** 91% yield, recrystallized from hot ethanol, pale yellow solid, mp 157 °C (lit.[41] 140-141 °C) ^{1}H NMR (500 MHz, $CDCl_3$) δ 8.02-8.00 (2H, m.), 7.76 (1H, d, *J* = 15.5 Hz.), 7.75-7.69 (4H, m.), 7.62-7.58 (2H, m.), 7.53-7.50 (2H, m.) ppm; ^{13}C NMR (125 MHz, $CDCl_3$) δ 189.7, 142.1, 139.2, 137.7, 133.3, 132.7, 128.8, 128.7, 128.6, 125.1, 118.4, 113.5 ppm.

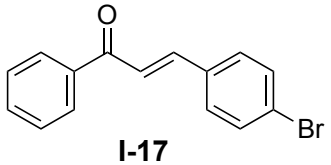

I-17

(*E*)-3-(4-bromophenyl)-1-phenylprop-2-en-1-one (**I-17**)**:** 71% yield, recrystallized from hot ethanol, pale yellow solid, mp 125 °C (lit.[42] 127-128 °C) ^{1}H NMR (600 MHz, $CDCl_3$) δ 8.00 (2H, m.), 7.72 (1H, d, *J* = 18.6 Hz.), 7.60-7.56 (1H, m.), 7.56-7.48 (7H, m.) ppm; ^{13}C NMR (125 MHz, $CDCl_3$) δ 190.2, 143.3, 138.0, 133.8, 132.9, 132.2, 129.8, 128.7, 128.5, 124.8, 122.6 ppm.

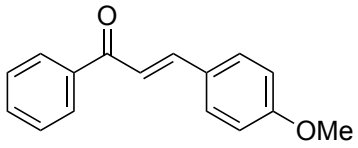

I-18

(*E*)-3-(4-methoxyphenyl)-1-phenylprop-2-en-1-one (**I-18**)**:** 71% yield, recrystallized from hot ethanol, pale yellow solid, mp 78 °C (lit.[43] 76-77.5 °C) ^{1}H NMR (500 MHz, $CDCl_3$) δ 8.00-7.98 (2H, m.), 7.71 (1H, d, *J* = 15.5 Hz.), 7.60-7.54 (3H, m.), 7.49-7.46 (2H, m.), 7.40 (1H, d, *J* = 15.5 Hz.), 6.92 (2H, dt, *J* = 9.5, 5.0, 3.0 Hz.), 3.84 (3H, s.) ppm; ^{13}C NMR (125 MHz, $CDCl_3$) δ 190.6, 161.7, 144.7, 138.5, 132.5, 130.2, 128.5, 128.4, 127.6, 119.8, 114.4, 55.4 ppm.

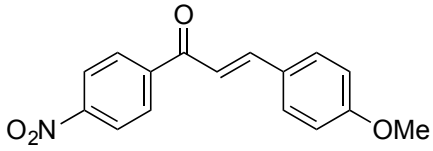

I-19

(*E*)-3-(4-methoxyphenyl)-1-(4-nitrophenyl)prop-2-en-1-one (**I-19**)**:** 71% yield, recrystallized from hot ethanol, pale yellow solid, mp 185 °C (lit.[44] 177-178 °C) ^{1}H NMR (500 MHz, $CDCl_3$) δ

8.32 (2H, d, *J* = 7.5 Hz.), 8.10 (2H, d, *J* = 7.0 Hz.), 7.80 (1H, d, *J* = 13.0 Hz.), 7.60 (2H, d, *J* = 7.5 Hz.), 7.34 (1H, d, *J* = 13.0 Hz.), 6.93 (2H, d, *J* = 7.0 Hz.), 3.85 (3H, s.) ppm; ^{13}C NMR (125 MHz, $CDCl_3$) δ 189.0, 162.3, 149.9, 146.7, 143.5, 130.6, 129.3, 127.0, 123.8, 118.9, 114.6, 55.5 ppm.

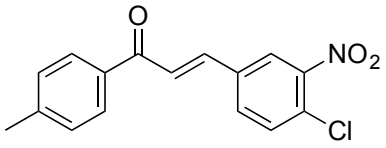

I-20

(*E*)-3-(4-chloro-3-nitrophenyl)-1-(*p*-tolyl)prop-2-en-1-one (**I-20**)**:** 82% yield, recrystallized from hot ethyl acetate, crystalline dirty yellow solid, mp 158 °C. ^{1}H NMR (600 MHz, $CDCl_3$) δ 8.11 (1H, d, *J* = 1.8 Hz.), 7.92 (2H, dd, *J* = 6.6, 1.8 Hz.), 7.72-7.69 (2H, m.), 7.59-7.56 (2H, m.), 7.30 (1H, d, *J* = 8.4 Hz.), 2.43 (3H, s.) ppm; ^{13}C NMR (150 MHz, $CDCl_3$) δ 188.8, 148.3, 144.4, 139.9, 135.2, 134.9, 132.5, 132.4, 129.5, 128.7, 128.2, 124.9, 124.4, 21.7 ppm. IR (film) 3070, 2914, 1660 (s), 1602 (s), 1527(s), 1476, 1339 (s), 1310, 1183, 979, 809 cm^{-1}. HRMS (ESI) Calculated Mass for $C_{16}H_{13}NO_3Cl$: 302.0584 ($[M+H]^+$), Found 302.0578 ($[M+H]^+$).

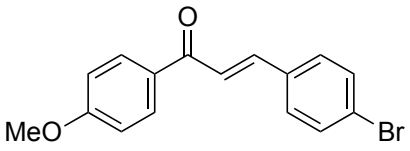

I-21

(*E*)-3-(4-bromophenyl)-1-(4-methoxyphenyl)prop-2-en-1-one (**I-21**)**:** 90% yield, recrystallized from hot ethyl acetate, crystalline white solid, mp 157 °C (lit.[45] 152-153 °C). ^{1}H NMR (600 MHz, $CDCl_3$) δ 8.01 (2H, dd, *J* = 7.2, 1.8 Hz.), 7.71 (1H, d, *J* = 15.6 Hz.), 7.53-7.47 (5H, m.), 6.97 (2H, dd, *J* = 7.2, 2.4 Hz.), 3.87 (3H, s.) ppm; ^{13}C NMR (150 MHz, $CDCl_3$) δ 188.3, 163.5, 142.5, 134.0, 132.1, 130.9, 130.8, 129.7, 124.5, 122.4, 113.9, 55.5 ppm.

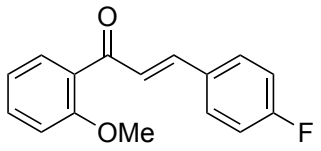

I-22

(*E*)-3-(4-fluorophenyl)-1-(2-methoxyphenyl)prop-2-en-1-one (**I-22**)**:** 87% yield, pale yellow oil. ^{1}H NMR (600 MHz, $CDCl_3$) δ 7.60 (1H, dd, *J* = 7.2, 1.8 Hz.), 7.58-7.53 (3H, m.), 7.46-7.43 (1H, m.), 7.29 (1H, d, *J* = 15.6 Hz.), 7.07-7.04 (2H, m.), 7.03-7.00 (1H, m.), 7.97 (1H, d, *J* = 8.4 Hz.), 3.87 (3H, s.) ppm; ^{13}C NMR (150 MHz, $CDCl_3$) δ 192.6, 163.8 (d, $^{1}J_{C,F}$ = 250.1 Hz.), 158.1, 141.7, 132.9, 131.3 (d, $^{4}J_{C,F}$ = 2.9 Hz.), 130.3, 130.2 (d, $^{3}J_{C,F}$ = 8.6 Hz.), 129.1, 126.7 (d, $^{5}J_{C,F}$ = 2.3 Hz.), 120.7, 115.9 (d, $^{2}J_{C,F}$ = 21.8 Hz.), 111.6, 55.7 ppm. IR (film) 3072, 2934, 1658 (s), 1599 (s), 1507 (s), 1485, 1327, 1235 (s), 1159, 1021, 830, 759 cm^{-1}. HRMS (ESI) Calculated Mass for $C_{16}H_{14}O_2F$: 257.0978 ($[M+H]^+$), Found 257.0980 ($[M+H]^+$).

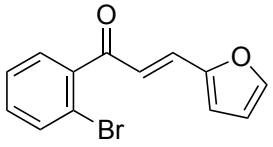

I-23

(*E*)-1-(2-bromophenyl)-3-(furan-2-yl)prop-2-en-1-one (**I-23**)**:**[46] 98% yield, brown oil, ^{1}H NMR (600 MHz, $CDCl_3$) δ 7.61 (1H, d, *J* = 7.8 Hz.), 7.51 (1H, s.), 7.40-7.35 (2H, m.), 7.31-7.28(1H, m.), 7.18 (1H, d, *J* = 15.6 Hz.), 6.67 (1H, d, *J* = 3.6 Hz.), 6.48-6.47 (1H, m.) ppm; ^{13}C NMR (150 MHz, $CDCl_3$) δ 190.1, 151.0, 145.5, 141.1, 133.4, 132.2, 131.3, 129.1, 127.3, 123.5, 119.4, 116.7, 112.8 ppm.

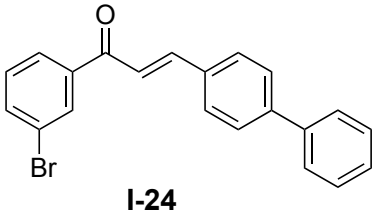

I-24

(*E*)-3-([1,1'-biphenyl]-4-yl)-1-(3-bromophenyl)prop-2-en-1-one (**I-24**)**:** 84% yield, recrystallized from hot ethyl acetate and dichloromethane (EtOAc : DCM = 5:1), needle shaped crystalline yellow solid, mp 132 °C. ^{1}H NMR (600 MHz, $CDCl_3$) δ 8.14 (1H, t, *J* = 1.8 Hz.), 7.95-7.93 (1H, m.), 7.85 (1H, d, *J* = 15.6 Hz.), 7.72-7.69 (3H, m.), 7.66-7.64 (2H, m.), 7.63-7.61 (2H, m.), 7.50-7.44 (3H, m.), 7.39-7.36 (2H, m.) ppm; ^{13}C NMR (150 MHz, $CDCl_3$) δ 188.9, 145.2, 143.6, 140.1, 140.0, 135.6, 133.6, 131.5, 130.2, 129.1, 128.9, 128.0, 127.6, 127.1, 127.0, 123.0, 121.2 ppm. IR (film) 3067, 2921, 1656 (s), 1606 (s), 1561, 1486, 1417, 1312, 1209, 763 cm^{-1}. HRMS (ESI) Calculated Mass for $C_{21}H_{16}OBr$: 363.0385 ($[M+H]^+$), Found 363.0389 ($[M+H]^+$).

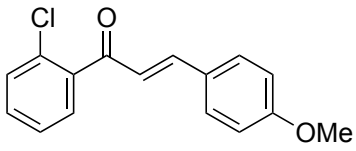

I-27

(*E*)-1-(2-chlorophenyl)-3-(4-methoxyphenyl)prop-2-en-1-one (**I-27**)**:** 89% yield, recrystallized from hot ethanol, crystalline yellow solid, mp 81 °C (lit.[47] 80-81 °C). ^{1}H NMR (500 MHz, $CDCl_3$) δ 7.51-7.48 (2H, m.), 7.45-7.37 (4H, m.), 7.33 (1H, dt, *J* = 9.0, 7.5, 1.0 Hz.), 6.98 (1H, d, *J* = 16.0 Hz.), 6.90 (2H, dt, *J* = 10.0, 5.0, 3.0 Hz.), 3.82 (3H, s.) ppm; ^{13}C NMR (125 MHz, $CDCl_3$) δ 193.9, 162.0, 146.4, 139.4, 131.2, 131.1, 130.4, 130.2, 129.2, 127.1, 126.8, 124.1, 114.5, 55.4 ppm.

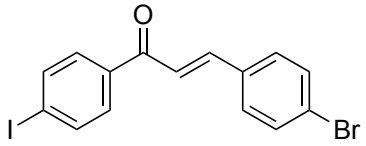

I-28

(*E*)-3-(4-bromophenyl)-1-(4-iodophenyl)prop-2-en-1-one (**I-28**)**:**[48] 64% yield, recrystallized from hot chloroform, flaky crystalline light brown solid, mp 190 °C. ^{1}H NMR (500 MHz, $CDCl_3$) δ 7.85 (2H, dt, *J* = 8.5, 4.0, 2.0 Hz.), 7.74-7.69 (3H, m.), 7.55-7.53 (2H, m.), 7.48 (2H, dt, *J* = 8.5, 3.5, 1.5 Hz.), 7.43 (2H, d, *J* = 16.0 Hz.) ppm; ^{13}C NMR (125 MHz, $CDCl_3$) δ 189.3, 143.9, 138.0, 137.3, 133.6, 132.3, 129.9, 129.8, 125.1, 122.0, 100.8 ppm.

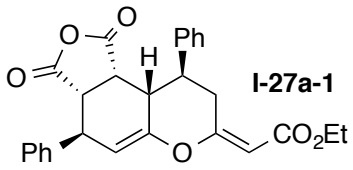

I-27a-1

ethyl (*E*)-2-((3a*S*,4*R*,9*S*,9a*S*,9b*R*)-1,3-dioxo-4,9-diphenyl-1,3,3a,4,8,9,9a,9b-octahydro-7*H*-furo[3,4-*f*]chromen-7-ylidene)acetate: Crystalline white solid, mp 184-188 °C. ^{1}H NMR (500 MHz, $CDCl_3$) δ 7.44-7.43 (4H, m.), 7.42-7.40 (2H, m.), 7.38-7.34 (2H, m.), 7.23-7.22 (2H, m.), 5.73 (1H, dd, *J* = 3.0, 3.5 Hz.), 5.54 (1H, d, *J* = 2.0 Hz.), 4.33 (1H, dd, *J* = 3.0, 16.0 Hz.), 4.16 (2H, ddd, *J* = 1.0, 7.0, 15.0 Hz.), 3.95 (1H, dddd, *J* = 3.0, 12.0, 13.5, 15.0 Hz.), 3.80-3.77 (1H, m.), 3.46 (1H, t, *J* = 9.5 Hz.), 3.33 (1H, dd, *J* = 5.0, 9.0 Hz.), 2.89 (1H, dddd, *J* = 3.0, 5.0, 7.0, 10.0 Hz.), 2.58 (1H, dddd, *J* = 2.0, 13.5, 16.0, 16.0 Hz.), ppm; ^{13}C NMR (125 MHz, $CDCl_3$) δ 170.7, 168.7, 167.3, 166.9, 151.5, 140.2, 137.5, 133.0, 129.7, 129.2, 128.7, 128.5, 128.3, 128.0, 127.9, 127.5, 104.7, 98.0, 69.2, 64.0, 59.8, 47.8, 42.9, 42.8, 41.3, 35.1, 31.5, 14.3 ppm; IR (film) 3062, 2928, 2854, 1779 (s), 1701, 1629 (s), 1337, 1170, 1135 (s), 939, 703 cm^{-1}. HRMS (ESI) Calculated Mass for $C_{27}H_{25}O_6$: 445.1651 ($[M+H]^+$), Found 445.1653 ($[M+H]^+$), $[\alpha]_D^{20}$= +74.5 (c = 1.0, CH_2Cl_2). The relative stereochemistry is assigned based on NOESY experiments.

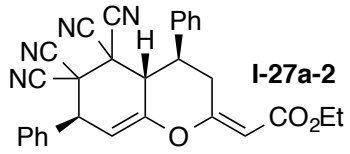

I-27a-2

ethyl 2-((4S,4aS,7S,E)-5,5,6,6-tetracyano-4,7-diphenyl-3,4,4a,5,6,7-hexahydro-2H-chromen-2-ylidene)acetate: Off white solid, decomposes above 160 °C. ^{1}H NMR (500 MHz, $CDCl_3$) δ 7.51-7.46 (5H, m.), 7.42-7.37 (5H, m.), 5.75 (1H, dd, *J* = 2.0, 3.0 Hz.), 5.67 (1H, br. s.), 4.45 (1H, t, *J* = 3.0 Hz.), 4.09-4.05 (2H, m.), 3.66-3.58 (3H, m.), 3.54 (1H, ddd, *J* = 0.5, 7.0, 15.0 Hz.), 1.18 (3H, t, *J* = 5.5 Hz.) ppm; ^{13}C NMR (125 MHz, $CDCl_3$) δ 166.3, 164.4, 146.2, 137.7, 132.1, 130.5, 130.5, 129.6, 129.4, 129.0, 127.9, 111.0, 109.9, 109.3, 108.3, 105.6, 101.1, 60.1, 46.3, 44.9, 44.7, 41.5, 40.5, 32.7, 14.2 ppm; HRMS (ESI) Calculated Mass for $C_{29}H_{23}N_4O_3$: 475.1770 ($[M+H]^+$), Found 475.1770 ($[M+H]^+$).

I.5.6. Quantum Mechanical Modeling Studies.

Full optimizations on all conformations of the model systems in simulated toluene as a solvent were performed at the B3LYP/6-31G*/SM8 (toluene) level using the Spartan-10 software running on Macintosh platform. To verify convergence and consistency of the optimizations, a number of examples were re-optimized from multiple starting points; energetic variations of 0.02 kcal/mol or less were found among these calculated structures. To confirm that each structure was a true minimum, vibrational analyses were performed; because analytical second derivatives are not available in SM8 solvated wavefunctions, these analyses relied on finite difference calculations. Their consistency was checked in multiple runs, and showed negligible variation. For comparison, the relative enthalpies ($\Delta H°_{rel}$) calculated by including zero-point and thermal corrections to 298.15 K are given in kcal/mol. Importantly, differences between relative E and relative H° values are generally small enough that either set of data could be used to arrive at the conclusions. All Transition State structures were validated as first-order stationary points (i.e. a single imaginary frequency) by vibrational analysis. Single-point solvation energies in simulated toluene were calculated at the B3LYP/6-31G*/SM8 level of theory. All values are in kcal/mol or hartrees.

REFERENCES

REFERENCES

(1) Morita, K.; Suzuki, Z.; Hirose, H. *Bull. Chem. Soc. Jpn.* **1968**, *41*, 2815.

(2) Baylis, A. B. H., M. E. D. In *German Patent 2* 1972; Vol. 155.

(3) Basavaiah, D.; Rao, A. J.; Satyanarayana, T. *Chem. Rev.* **2003**, *103*, 811.

(4) Wei, Y.; Shi, M. *Chem. Rev.* **2013**, *113*, 6659.

(5) Langer, P. *Angewandte Chemie-International Edition* **2000**, *39*, 3049.

(6) Iwabuchi, Y.; Nakatani, M.; Yokoyama, N.; Hatakeyama, S. *J. Am. Chem. Soc.* **1999**, *121*, 10219.

(7) Chen, R.; Xu, S.; Wang, L.; Tang, Y.; He, Z. *Chem. Commun.* **2013**, *49*, 3543.

(8) Du, Y. S.; Lu, X. Y.; Yu, Y. H. *J. Org. Chem.* **2002**, *67*, 8901.

(9) Evans, C. A.; Miller, S. J. *J. Am. Chem. Soc.* **2003**, *125*, 12394.

(10) Cowen, B. J.; Saunders, L. B.; Miller, S. J. *J. Am. Chem. Soc.* **2009**, *131*, 6105.

(11) Guan, X. Y.; Wei, Y.; Shi, M. *J. Org. Chem.* **2009**, *74*, 6343.

(12) Meng, X. T.; Huang, Y.; Chen, R. Y. *Org. Lett.* **2009**, *11*, 137.

(13) Voituriez, A.; Panossian, A.; Fleury-Bregeot, N.; Retailleau, P.; Marinetti, A. *J. Am. Chem. Soc.* **2008**, *130*, 14030.

(14) Wallace, D. J.; Sidda, R. L.; Reamer, R. A. *J. Org. Chem.* **2007**, *72*, 1051.

(15) Zhao, G. L.; Huang, J. W.; Shi, M. *Org. Lett.* **2003**, *5*, 4737.

(16) Wang, X.; Fang, T.; Tong, X. *Angew. Chem. Int. Ed.* **2011**, *50*, 5361.

(17) Zheng, T.; Narayan, R. S.; Schomaker, J. M.; Borhan, B. *J. Am. Chem. Soc.* **2005**, *127*, 6946.

(18) Schomaker, J. M.; Borhan, B. *J. Am. Chem. Soc.* **2008**, *130*, 12228.

(19) Narayan, R. S.; Borhan, B. *J. Org. Chem.* **2006**, *71*, 1416.

(20) Schmidt, B.; Westhus, M. *Tetrahedron* **2000**, *56*, 2421.

(21) Hayakawa, H.; Miyashita, M. *Tetrahedron Lett.* **2000**, *41*, 707.

(22) Gerth, K.; Washausen, P.; Hofle, G.; Irschik, H.; Reichenbach, H. *J. Antibiot.* **1996**, *49*, 71.

(23) Coppi, L.; Ricci, A.; Taddei, M. *J. Org. Chem.* **1988**, *53*, 911.

(24) Connor, D. T.; Young, P. A.; Strandtmann, M. V. *J. Org. Chem.* **1977**, *42*, 1364.

(25) Boivin, T. L. B. *Tetrahedron* **1987**, *43*, 3309.

(26) Zhang, Y.; Panek, J. S. *Org. Lett.* **2007**, *9*, 3141.

(27) Huang, G. T.; Lankau, T.; Yu, C. H. *J. Org. Chem.* **2014**, *79*, 1700.

(28) Rho, H. S.; Oh, S. H.; Lee, J. W.; Lee, J. Y.; Chin, J.; Song, C. E. *Chem. Commun.* **2008**, 1208.

(29) Williams, T.; Pitcher, R. G.; Bommer, P.; Gutzwill.J; Uskokovi.M *J. Am. Chem. Soc.* **1969**, *91*, 1871.

(30) Chen, R. S.; Xu, S. L.; Wang, L. Y.; Tang, Y. H.; He, Z. J. *Chem. Commun.* **2013**, *49*, 3543.

(31) Du, D.; Jiang, Y.; Xu, Q.; Shi, M. *Adv. Synth. Catal.* **2013**, *355*, 2249.

(32) Feng, J. H.; Fu, X.; Chen, Z. L.; Lin, L. L.; Liu, X. H.; Feng, X. M. *Org. Lett.* **2013**, *15*, 2640.

(33) Francos, J.; Grande-Carmona, F.; Faustino, H.; Iglesias-Siguenza, J.; Diez, E.; Alonso, I.; Fernandez, R.; Lassaletta, J. M.; Lopez, F.; Mascarenas, J. L. *J. Am. Chem. Soc.* **2012**, *134*, 14322.

(34) Niu, Z. Q.; He, X. W.; Shang, Y. J. *Tetrahedron-Asymmetry* **2014**, *25*, 796.

(35) Scheffler, U.; Mahrwald, R. *Chemistry-a European Journal* **2013**, *19*, 14346.

(36) Wang, Q.; Lian, Z.; Xu, Q.; Shi, M. *Adv. Synth. Catal.* **2013**, *355*, 3344.

(37) Wang, Y.; Shi, D. Q. *Chinese Journal of Structural Chemistry* **2013**, *32*, 521.

(38) Zhang, D. H.; Shi, M. *ChemistryOpen* **2012**, *1*, 215.

(39) Lang, R. W.; Hansen, H.-J. *Org. Synth.* **1990**, *Collective Vol. 7*, p 232.

(40) Chiaradia, L. D.; Mascarello, A.; Purificacao, M.; Vernal, J.; Cordeiro, M. N. S.; Zenteno, M. E.; Villarino, A.; Nunes, R. J.; Yunes, R. A.; Terenzi, H. *Bioorg. Med. Chem. Lett.* **2008**, *18*, 6227.

(41) Batovska, D.; Parushev, S.; Slavova, A.; Bankova, V.; Tsvetkova, I.; Ninova, M.; Najdenski, H. *European Journal of Medicinal Chemistry* **2007**, *42*, 87.

(42) Gorman, A.; Killoran, J.; O'Shea, C.; Kenna, T.; Gallagher, W. M.; O'Shea, D. F. *J. Am. Chem. Soc.* **2004**, *126*, 10619.

(43) C., C. M.; Chopa, A. B. *J. Chem. Soc.-Perkin Trans. 2* **1974**, 452.

(44) Kumar, A.; Sharma, S.; Tripathi, V. D.; Srivastava, S. *Tetrahedron* **2010**, *66*, 9445.

(45) Barnes, R. P.; Goodwin, T. C.; Cotten, T. W. *J. Am. Chem. Soc.* **1947**, *69*, 3135.

(46) Mukherjee, C.; Zhang, H. M.; Biehl, E. R. *Heterocycles* **2005**, *65*, 2347.

(47) Bradsher, C. K.; Brown, F. C.; Blue, W. B. *J. Am. Chem. Soc.* **1949**, *71*, 3570.

(48) Loudet, A.; Bandichhor, R.; Wu, L. X.; Burgess, K. *Tetrahedron* **2008**, *64*, 3642.

CHAPTER II: NUCLEOPHILE ASSISTED ALKENE ACTIVATION-ELECTRONIC AND STRUCTURAL IDENTITY OF OLEFINS IN HALOFUNCTIONALIZATION REACTIONS

II.1. Introduction.

Electrophilic activation of carbon-carbon double bonds is one of the most versatile functional group transformations in organic chemistry, offering robust access to a diverse range of substructures.[1] Stereoselective alkene functionalization reactions have attracted sustained interest for the past four decades.[2,3] The results have been a number of landmark alkene functionalization reactions such as epoxidations, dihydroxylations, aminohydroxylations, hydrogenations, cyclopropanations, hydrometalations, Diels-Alder reactions and aziridinations to name a few.[4-6] Mechanistically, most of these reactions are thought to proceed *via* electrophilic activation of the alkene resulting in a cationic adduct followed by a concomitant attack of a nucleophile that intercepts the cationic intermediate. Electrophilic halofunctionalization of olefins is a sub-class of these reactions and arguably one of the most sought–after transformations in organic chemistry that allows access to a myriad of indispensible products. This field is witnessing an immense progress since the past few years, predominantly in the development of stereoselective reactions.[7-18] The key towards the success of any sought-after transformation relies on a rational approach that is substantiated by its well-established mechanistic foundations. Although halofunctionalization of olefins has seen great recent progress, the field of stereoselective alkene halogenation has mainly advanced via a trial-and-error approach and is still in its infancy when compared to other olefin functionalization reactions mentioned above.

To efficiently develop new halofunctionalization reactions, the detailed nature of attack on alkenes by halenium ion donors must be understood, along with the structural and electronic character of any resulting intermediates. Despite the enormous precedent dedicated towards understanding the mechanistic underpinnings of haliranium ions,[19-36] the factors that dictate the

Figure II-1: **a.** Catalytic asymmetric chlorolactonization of alkenoic acids. **b.** Proposed working models

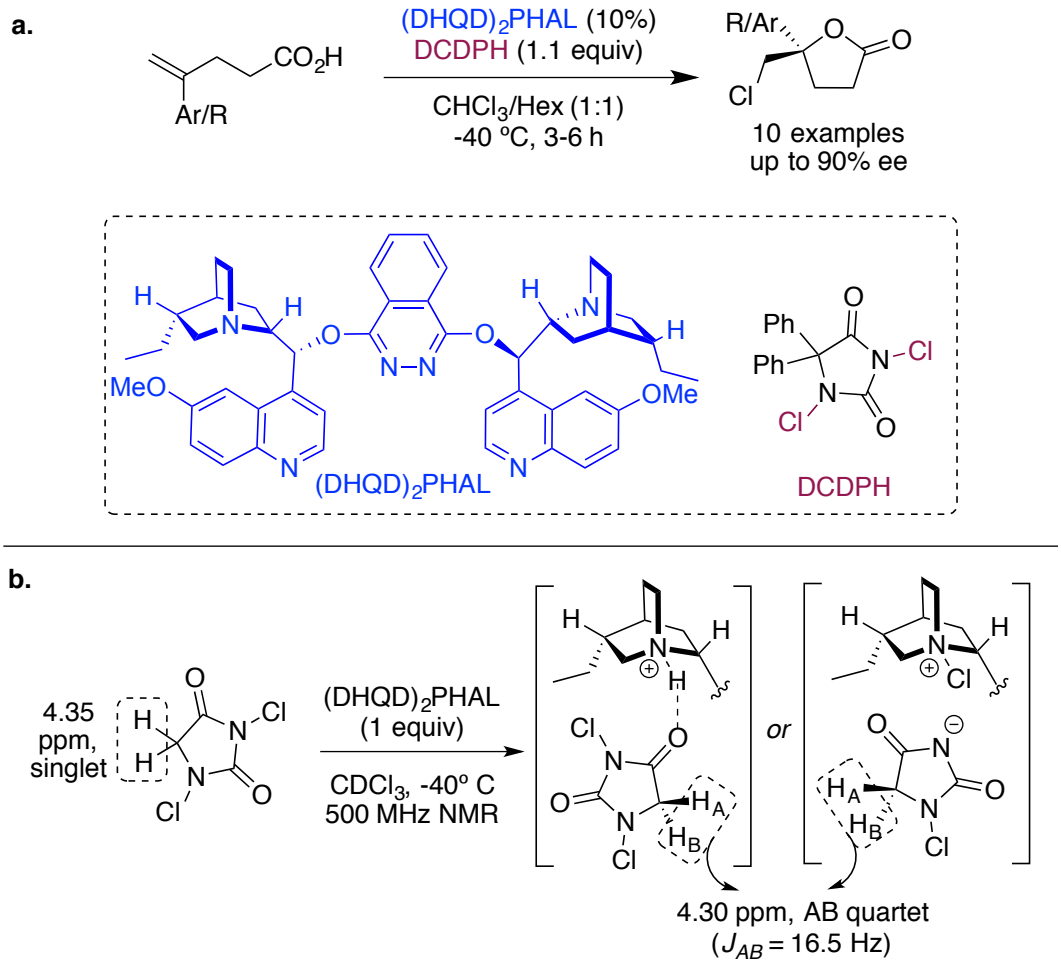

kinetic and stereochemical stability of halonium ions and their electronic and structural identity in solution still remains elusive.

II.2. Results and discussion.

II.2.1. Preliminary results and mechanistic arguments against the classical intermediates.

Over the past five years, efforts in our group have focused on developing catalytic asymmetric halofunctionalization of alkenes and on elucidation of their mechanistic underpinnings. Our early report in 2010 described the first catalytic, highly enantioselective chlorolactonization of

1,1- disubstituted alkenoic acids using $(DHQD)_2PHAL$ as a chiral amine catalyst and 1,3-dichloro-5,5-diphenylhydantoin (DCDPH) as a chlorenium source (Figure II-1a).[37] Based on initial NMR experiments, the proposed model invoked an ammonium ion (protonated or chlorinated) at the quinuclidine centered nitrogen engaging either a hydrogen bonded complex or a tight ion pair (Figure II-1b) resulting in the diastereotopic nature of the two protons on the hydantoin motif embedded within the chiral cleft of the catalyst. Proceeding studies by Dr. Roozbeh Yousefi using labeled substrate **II-1D** (Figure II-2) revealed that the addition across the 1,1-disubstituted olefin ensues under the reaction conditions to yield predominantly a *syn*-adduct. This observation is highly intriguing and at the same time, counterintuitive from a mechanistic viewpoint where, in the field of halofunctionalization of alkenes, the classical notion of cyclic-bridged haliranium ions as putative intermediates is firmly established. Kinetic studies (Reaction Progress Kinetic Analysis

Figure II-2: Deuterium labeling of 1,1-alkenoic acid **II-1D** reveal high enantiofacial selectivity of the initial chlorenium attack, and predominant formation of the *syn*-adduct.

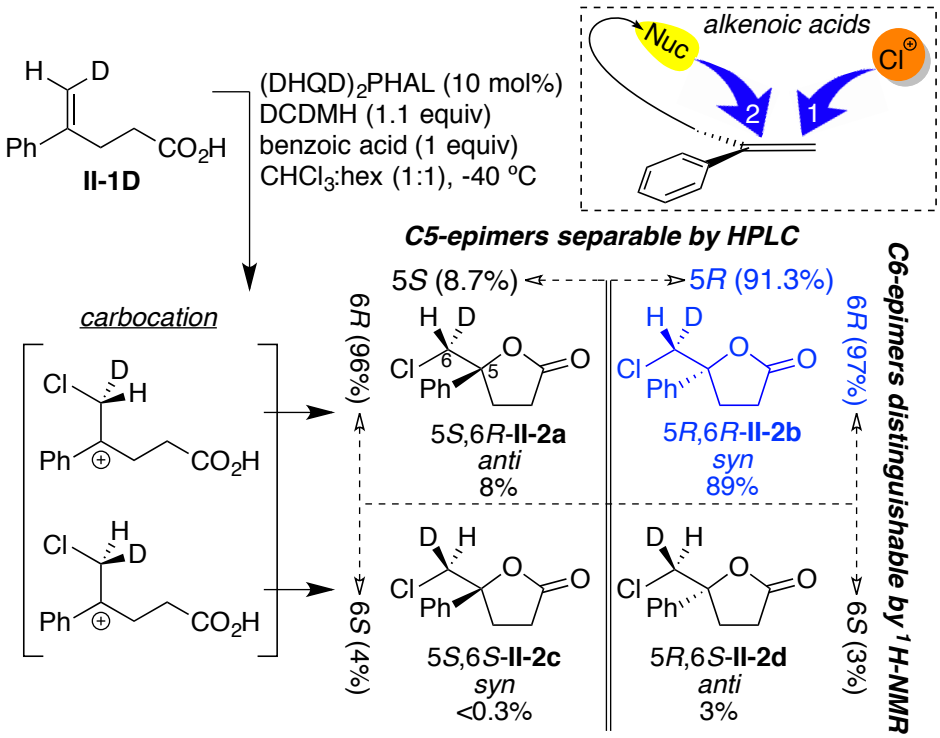

techniques-RPKA, pioneered by the Blackmond group[38]) performed by Dr. Yousefi have aided in determining the molecularity of the asymmetric chlorolactonization reaction. The reaction has zero-order dependence on the substrate concentration (suggesting saturation kinetics of the catalyst), and first order dependence on catalyst and chlorohydantoin concentrations. Taken together, these results suggest that the rate-determining step in these transformations is either the binding of the substrate to the catalyst or the transfer of the chlorine atom to the alkene in the substrate-hydantoin-catalyst ternary complex.

Nevertheless, the predominant '*syn*' addition of the halogen and the nucleophile across the alkene, as probed from **II-1D** (Figure II-2), strongly argues against the intermediacy of a bridged chloriranium ion.[19] Hence, in accordance to the studies by Fahey, Poutsma, and Sauers,[30-33,39] we postulated the intermediacy of a chloromethyl carbenium ion in the asymmetric chlorolactonization.[19]

Computational analysis to elucidate the possibility of *bridged chloronium ion intermediate* (chloriranium ion):

The possibility of participation by a bridged chloronium species was assessed using quantum chemical modeling at several levels of theory. In all cases, geometry optimization led to structures with near tetrahedral angles for the key $\angle C^{+}$-C-Cl angle at the CH_2Cl group; a bridged chloronium was never found as an energy minimum, even when calculations were started with the Cl atom centrally positioned as it is in $C_2H_4Cl^{+}$, the chloronium ion from (ethylene + Cl)$^{+}$ ion. Interestingly even in structures calculated in the "gas phase" (i.e. no solvent simulation), where the otherwise unstabilized cation would benefit most from delocalization by bridging, no such minimum was found. Figure II-3 depicts the geometry minimized model at the B3LYP/6-31G* level obtained from chlorenium addition to substrate **II-1**. As noted, several symmetrically bridged

Figure II-3: A geometry minimization of **II-1** with Cl^+ ion always reveals a chloromethyl carbenium ion with no evidence for bridging tendency of chlorine atom. The following calculations were performed at the B3LYP/6-31G* (SM8) level of theory.

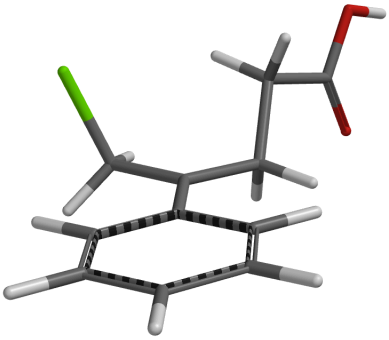

end-on view of (**II-1 + Cl**)$^+$ ion
$\angle C^+$-C-Cl = 108.8º (gas phase)
$\angle C^+$-C-Cl = 109.6º (SM8-$CHCl_3$)

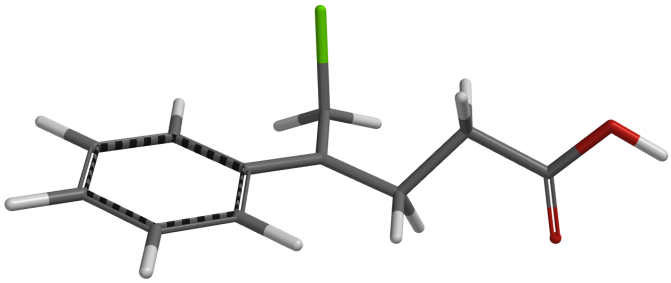

Lateral View of (**II-1 + Cl**)$^+$

chloronium starting points were explored, but the end result was always found to be the open chloromethyl carbenium ion shown above in Figure II-3.

If the chiral catalyst $(DHQD)_2PHAL$, somehow held the aryl ring in an orientation that inhibited effective conjugation with the cation center, perhaps the resulting destabilized cation would compensate by distorting to a bridging mode. To probe this possibility, the intermediate cation was geometrically minimized at the same levels of theory as described above, but now with the phenyl ring constrained at an angle of 90º with respect to the π-system under consideration (i.e. orthogonal to the 1,1-disubstituted olefin); see Figure II-4. Despite this enforced (and artificial) switch in the electronics, there was little change to the local geometry at the $–CH_2Cl$ group, or to the rotational potential energy surface. Furthermore, experimental results do show a response to donor substitution on the aryl ring, indicating that resonance is not shut off between the phenyl and the putative carbocation. These results clearly argue against the intermediacy of any bridged chloronium species (chloriranium ion).

Figure II-4: A restricted (dihedral angle) geometry minimization of **II-1** with Cl^+ ion also reveals a chloromethyl carbenium ion with no evidence for bridging tendency of chlorine atom. The following calculations were performed at the B3LYP/6-31G* (SM8) level of theory.

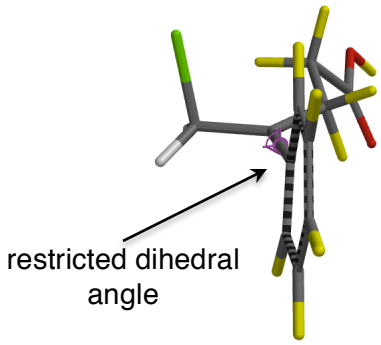

End-on view of restricted (**II-1 + Cl**)$^+$ ion
$\angle C^+$-C-Cl = 100.0º

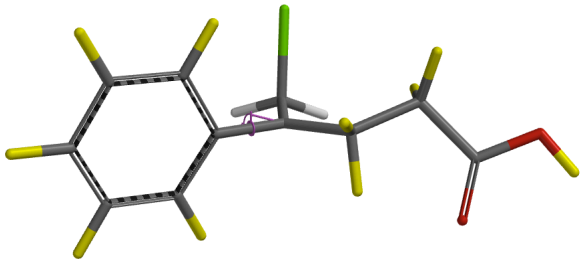

Lateral view of restricted (**II-1 + Cl**)$^+$ ion

Interestingly, the cation's structure depicted above does have the C-Cl bond aligned ideally for hyperconjugation with the cationic center. Regardless of bridging, if this structure were in a deep enough energy well, it might function like a bridged intermediate by directing nucleophilic attack to the opposite face. To probe this issue, we resorted to α-methylstyrene as a more computationally tractable system, uncomplicated by the conformational dynamics of the carboxylate side-chain. We then examined the potential energy (PE) surfaces for rotation about the C^+-CH_2Cl bond in the cation as calculated at the HF/6-31G*, MP2/6-31G*, B3LYP/6-31G*, and B3LYP/6-311++G** levels. The validity of this model was confirmed by comparing the minima from the above calculations based on the full substrate to the $C_9H_{10}Cl^+$ ion structures obtained from chlorenium addition to α-methylstyrene. As before, only open carbocation minimum energy geometries were found. For instance, the B3LYP/6-31G* optimized structure does find a minimum with the C-Cl bond aligned with the carbocation's empty 2p orbital, but it shows a $\angle C^+$-C-Cl angle of 108.8º, and the face-switching barrier to rotation of the CH_2Cl group is calculated to be only 1.6 kcal/mol in the gas phase, roughly half the value for methyl group rotation in ethane. This

calculated number is further lowered to 0.9 kcal/mol (B3LYP/6-31G*/SM8) by simulated solvation in $CHCl_3$.

Conclusions from computational analysis of **II-1** + Cl^+ ion (cationic adduct):

(a) Based on the above calculations, assuming chlorenium delivery to the alkene forms an ionic intermediate, it is an open chloromethyl benzylic carbenium ion, rather than a bridged chloronium species.

(b) Although such chloromethyl carbenium ions have energy minima with the C-Cl bond aligned with the carbocation's empty 2p orbital, and the $\angle C^+$-C-Cl angle is slightly smaller than the tetrahedral angle, the face-switching barrier to rotation of the CH_2Cl group is low as noted above. Interestingly, a second minimum in which the chlorine lies in the plane of the cation is also found. This structure, which offers no stereopreference to either face, is only 1.2 kcal/mol above the out-of-plane minimum, and $CHCl_3$ solvation lowers this difference to just 0.4 kcal/mol at the B3LYP/6-31G*/SM8 level. Overall, this ensemble of structures may be understood as conformationally free, offering no stereodirection to the lactone closure step. We note here that Haubenstock and Sauers arrived at essentially the same conclusions on their more sophisticated calculations on the simpler styrene- and butadiene-derived systems.[30,31]

(c) The preference for the open chloromethyl carbenium ion form is not isolated to styryl systems that can form stabilized benzylic cations; computational analysis of chlorenium addition to 2-methylpropene displays similar behavior. This small system is amenable to calculations at significantly more rigorous levels of theory. Rotation barriers for the resulting chloromethyl carbenium ion evaluated at different levels of theory and based on gas-phase optimized geometries are tabulated below:

Level of Theory	Barrier to rotation in gas phase (kcal/mol)	Barrier to rotation in $CHCl_3$ (kcal/mol)
B3LYP/6-31G*	3.20	3.14**
B3LYP/6-311++G**	3.16	3.07*
G3MP2//B3LYP/6-31G*	4.19	2.44*

Solvation correction computed using B3LYP/6-31G wavefunction

**Reoptimization in "solvent" lowers this barrier to 3.06 kcal/mol

Notably, even in this non-conjugated system, the calculated barriers to rotation of the C-C bond (gas phase) are too low to imply any preference for the chlorine atom to bridge over. As anticipated, an exhaustive computational analysis to probe the interaction of a *"naked"* chlorenium ion (Cl^+) and the alkenoic acid **II-1**, leads to transfer of charge from the highly electronegative halenium atom to a carbon based cation. This analysis, however, does not capture the entirety of the existing components in the reaction mixture, especially the counter anion of the halenium donor.

Furthermore, a counterintuitive result, as shown in Scheme II-1, is highlighted by substrate **II-2**. The electron donating methoxy substituent in **II-2** is expected to readily form and stabilize the proposed chloromethyl carbenium ion intermediate to a greater extent in comparison to substrate **II-1**. Hence, one would expect a greater level of stereoinduction in the corresponding chlorolactone **II-2a**. The results displayed in Scheme II-1 argue otherwise; **II-2** was observed to be the least selective substrate, yielding a nearly racemic product mixture. To probe the possibility of product racemization under reaction conditions, the racemic product **II-2a** was subjected to enantiomeric resolution via HPLC (see Scheme II-2a). The enantiomers were subjected separately to the standard reaction conditions as shown in Scheme II-2b. The lactone product

was found to be stereochemically stable under the standard reaction conditions. The possibility of olefin to olefin transfer of the chlorenium as a stereo-randomizing pathway was also probed. The results are detailed as follows (see Scheme II-2c):

Alkenoic acid **II-2** was premixed with enantiopure HPLC isolates, with (+)-**II-2a** (***R***) in the ratio 1:1 and with (-)-**II-2a** (***S***) in the ratio 5:1, respectively (ratios were confirmed by ^{1}H NMR analysis of the mixtures using appropriate delay time). In two separate experiments, these mixtures were exposed to the standard reaction conditions. Interestingly, the results reveal that the enantiopure lactone resisted racemization under the reaction conditions. It should be noted that chlorolactonization of **II-2** yields **II-2a** as a racemate under standard reaction conditions. In the first reaction where 1:1 mixture of **II-2**:(+)- **II-2a** (***R***) is employed, the racemate arising from **II-2** contributes one third of (-)-**5**(***S***) to the final product accounting for an *enantiomeric ratio* of

Scheme II-1. Stereoselectivity observed for **II-1** and **II-2**, argues against the chloromethylcarbenium ion as a putative intermediate.

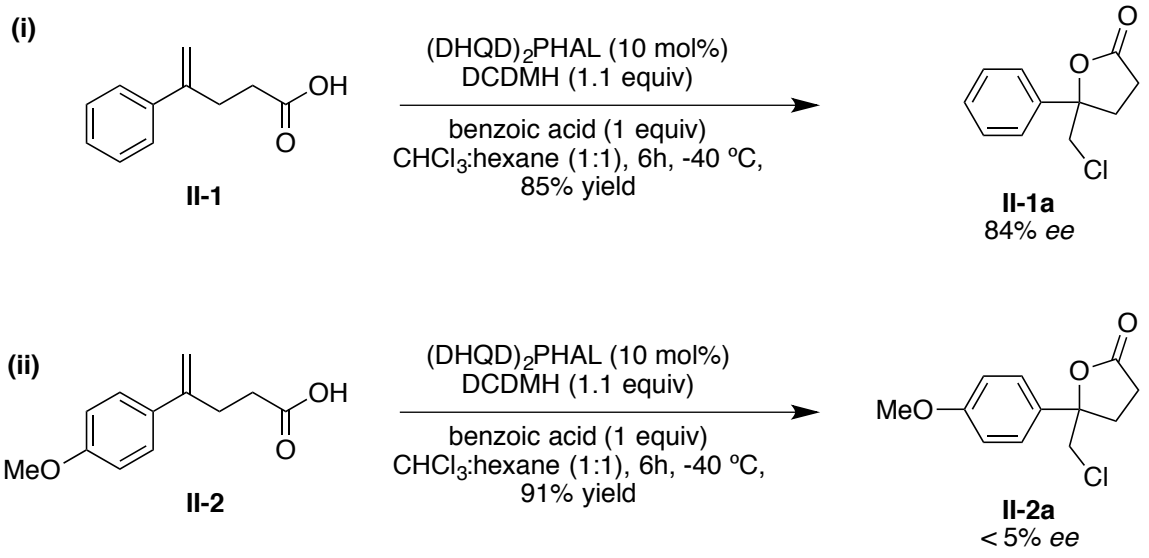

Scheme II-2. Probing the possibility of racemization of **II-2a** under standard reaction conditions employed for asymmetric chlorolactonization.

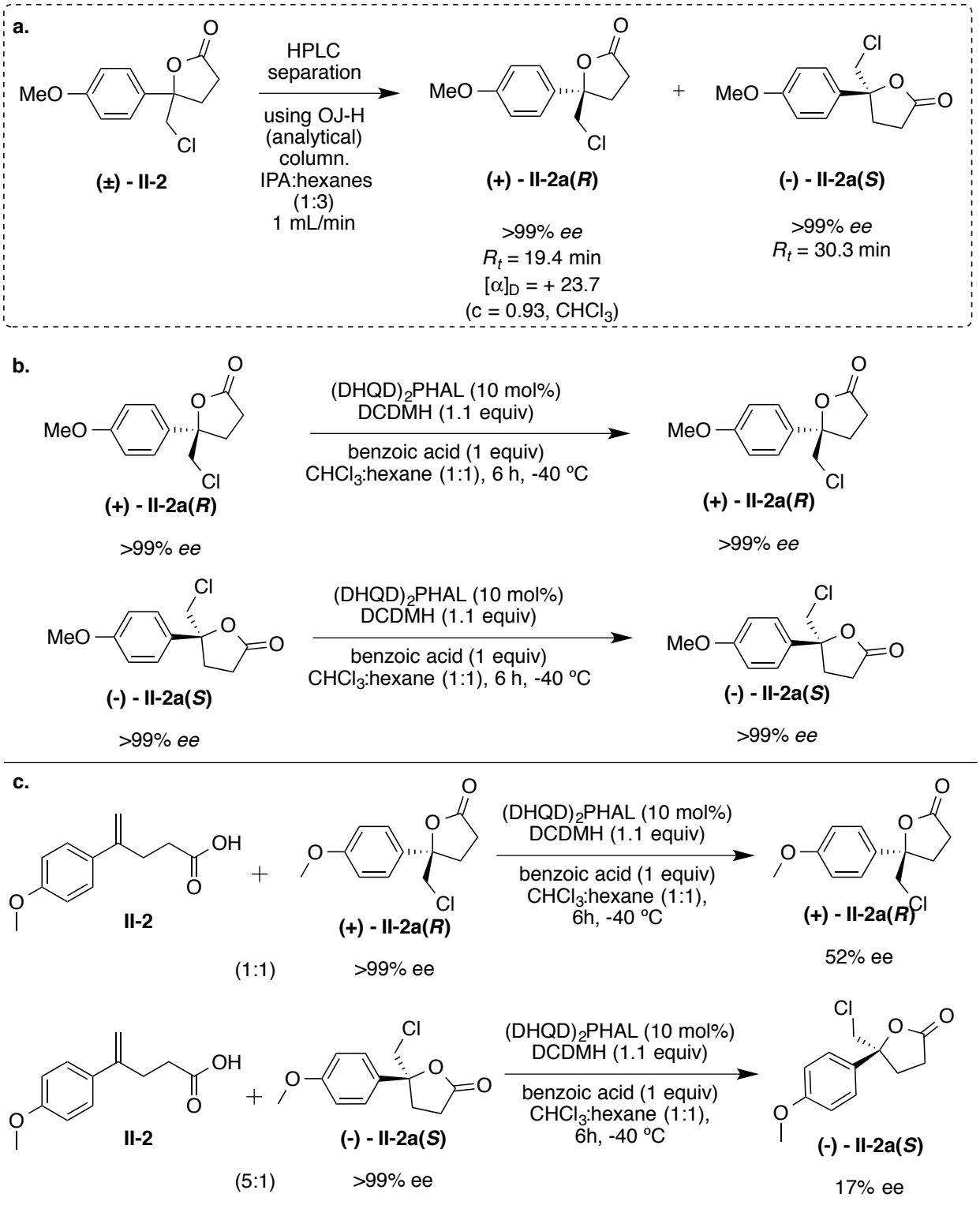

~75:25, hence the observed 52% *ee*. Similarly, the 17% *ee* observed in the latter case can be attributed to about 5/12th of the fractional contribution of (-)-**II-2a** (***S***) from **II-2**.

These results clearly demonstrates that once formed, either of the enantiomers, (+)-**II-2a** (***R***) and (-)-**II-2a** (***S***) do not undergo ring opening under the reaction conditions causing errosion of *ee*s.

Another set of data that argues against the putative halomethyl carbenium ion pathway in chlorolactonization of **II-1** is the significant differences in rates of reactions when the carboxylic acid moiety in **II-1** is substituted by different nucleophiles. As shown in Scheme II-3 below, the observed differences in rates cannot be possibly explained by considering the classical hypothesis, which limits the rate determining intermediate to the interaction of a bare "*naked*"

Scheme II-3. The rate determining-classically perceived intermediates (**A** and **B**) fail to explain the following observed rate differences.

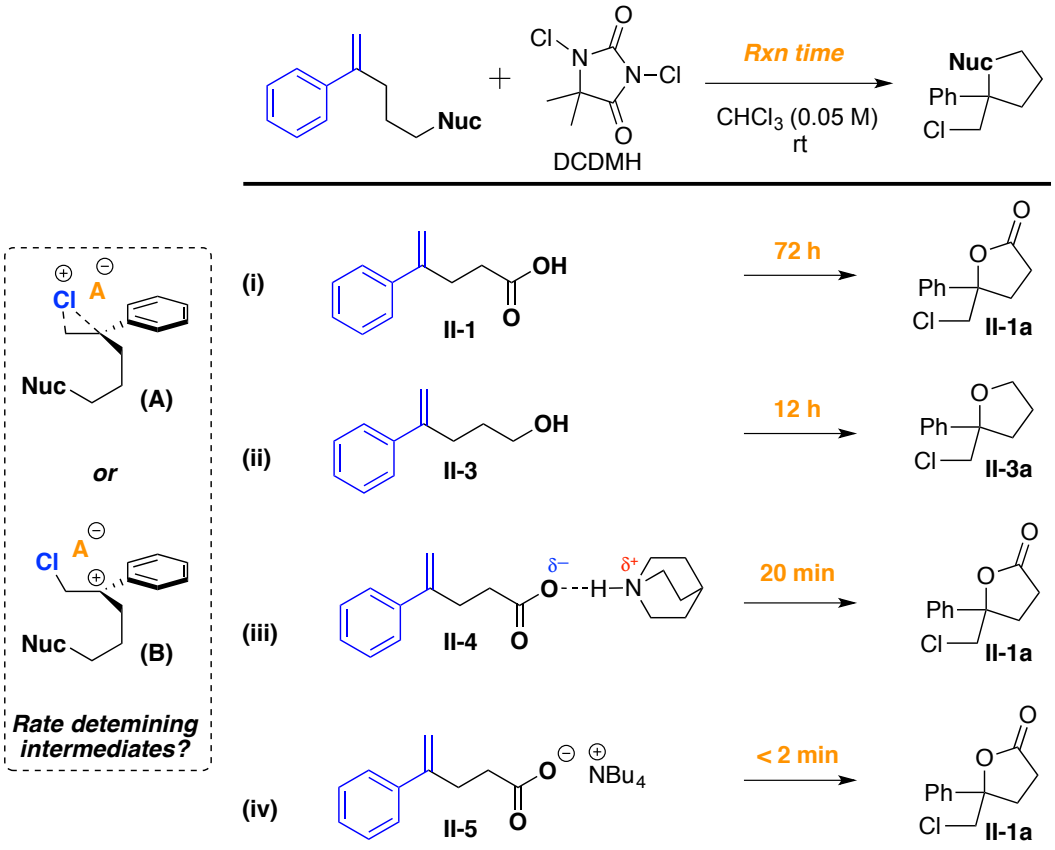

halenium ion and the olefin leading to the formation of either (**A**) or (**B**). Overall, these outcomes call for a comprehensive mechanistic probing of halofunctionalization of alkenes in general.

II.2.2. Mechanistic background.

Mechanistically, halofunctionalization of alkenes has been extensively studied since their discovery. The exclusive formation of *anti*-adducts during halogenation of olefins let to the first proposal by Kimball in 1937 for the intermediacy of symmetrically bridged haliranium ions (three membered cyclic intermediates; see Figure II-5, intermediate I).[10,40,41] As described above, studies from our own lab as well as those of Fahey, Sauers and others, have reported firm evidence against the intermediacy of haliranium ions in halofunctionalization reactions.[19,30-32,42-44] The observation of both *syn* and *anti*-adducts from halofunctionalizations of styrylic substrates suggest instead halomethyl carbenium ions intermediates (Figure II-5, intermediate II).[32] Furthermore, the seminal work by Fahey, Poutsma, Williams and several others have demonstrated cases where either of these classically perceived halonium ion intermediates (**I** or **II**) fail to provide an

Figure II-5. Path A and path B represent the rate determining-classically perceived intermediates (**I** and **II**) involved in electrophilic addition to alkenes.

Classical Perception of Electrophilic Addition to Alkenes:

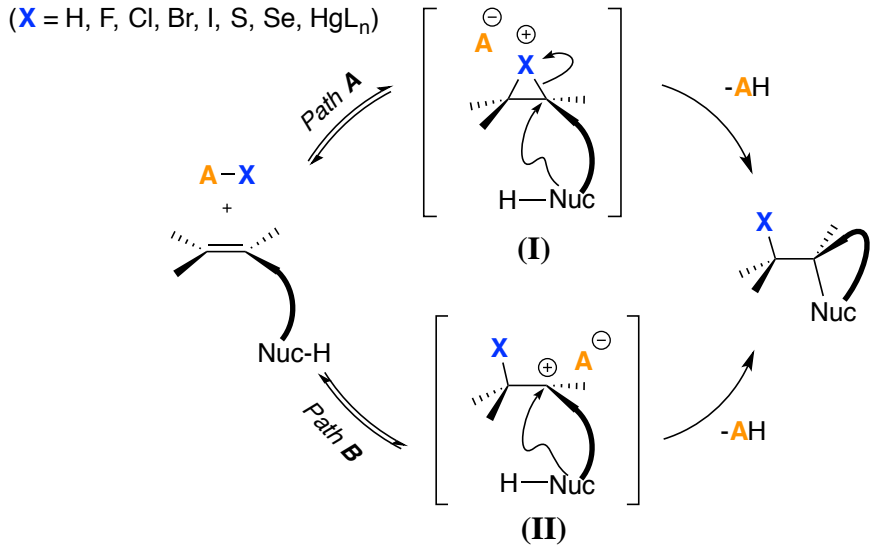

explanation of the observed experimental outcomes. For instance, a.) *trans*-2-butene and isobutylene exhibit similar rates for dichlorination even though the latter can form a more stable 3° carbenium ion,[22]; b.) for dichlorination of a given alkene, a change in solvent polarity displays a counterintuitive switch in the stereoselectivity where non-polar solvents strongly favor *syn*-addition,[19,22,32]; c.) stereoselectivity of dichlorination is markedly different for stilbene, acenaphthylene and phenanthrene where all three substrates have the ability to form a stabilized benzylic cation,[32,45]; d.) dichlorination of *trans* di-*tert*-butylethylene gives products of methyl migration (suggesting carbocationic intermediates) along with the desired dichloride adduct whereas, the highly sterically encumbered *cis* analogue (anticipated to form a carbenium ion more likely than its *trans* isomer as this event would relieve about 12 kcal/mol of steric strain) yields exclusive *anti*-adducts with no trace of rearrangement products,[34]; and, e.) most strikingly, addition of catalytic amounts of halide anions accelerates dihalogenation of olefins, establishing a crucial role for a nucleophile in the rate determining step.[20,46]

II.2.3. Computational analysis for probing alternative mechanistic pathways.

Mechanistically, halofunctionalization of π-systems are thought to be well-understood reactions; in Sophomore Organic chemistry texts show these as two-step processes: (1) electrophilic attack on the alkene functionality to form a cationic adduct, and (2) interception of this adduct by a nucleophile (Figure II-5, paths A and B) to yield the addition product. Olefins that benefit from extended conjugation with aromatic substituents do not have any preference to form the bridged haliranium ion intermediates; instead they may form the halocarbenium intermediate as shown in path B. To probe the validity of this pathway in the asymmetric chlorolactonization of **II-1** initiated by $(DHQD)_2PHAL$ as a chiral amine catalyst and 1,3-dichloro-5,5-dimethylhydantoin (DCDMH) as the terminal chlorenium source, we resorted to transition state analysis at the B3LYP/6-31G*/SM8 ($CHCl_3$) level of theory. Several starting points (geometries) were considered

to obtain a transition state structure for the formation of the proposed chloromethyl carbenium ion. However, none of the geometries led to a defined transition state towards formation of the carbenium ion. In presence of the donor anion, the chlorenium atom could not be transferred to olefin.

This observation led to an important question in halogenation chemistry: energetically, what is the cost of transferring a halenium ion from its donor to an olefin? In other words, what are the relative "*Halenium Affinities*" of the olefin and the donor anion and, can we quantify the propensity of an alkene towards capture of a halenium ion from its donor? To address these questions, we introduce a previously unexplored parameter -Halenium Affinity (*HalA*)- as a quantitative descriptor of the bond strengths of various functional groups to halenium ions.[47] The *HalA* scale ranks potential halenium ion acceptors based on their ability to stabilize a '*free halenium ion*'. Alkenes in particular but other Lewis bases as well, such as amines, amides, carbonyls and ether oxygens, etc. have been classified on the *HalA* scale. The influences of subtle electronic and steric variations, as well as the less predictable anchimeric and stereoelectronic effects, are intrinsically accounted for by *HalA* computations, providing quantitative assessments beyond simple 'chemical intuition'. Specifically, we define the *HalA* value for a given Lewis base (:LB) as the DFT calculated (gas phase) energy change upon attachment of a halenium ion (X^+), as shown in the dashed box below. The acceptor fragment may be neutral or anionic (*i.e.* the X-LB complex is cationic or neutral), leading to two distinct cases:

$$\textit{neutral acceptor}\text{: } \Delta H_{rxn}\ (X^+ + :LB \rightarrow X{-}LB^+)$$

$$\textit{anionic acceptor}\text{: } \Delta H_{rxn}\ (X^+ + :LB^- \rightarrow X{-}LB)$$

The ***HalA*** values in kcal/mol are derived at T = 298.15 K (unless noted otherwise) as in equation (1) and (2):

$$\boldsymbol{HalA} = -\Delta E_{elec} - \Delta ZPE - \Delta E'_{vib} + \frac{5}{2}RT \qquad (1)$$

$$E'_{vib}(T) = \sum_{i=1}^{3n-6} \frac{Nhv_i}{e^{Nhv_i/RT} - 1} \qquad (2)$$

where; $\Delta E_{(elec)} = E_{(electronic)}$(X-LB adduct) – [$E_{(electronic)}$(:LB) + $E_{(electronic)}$ (X^+)]; zero point energy change ΔZPE = ZPE(X-LB adduct) – ZPE(:LB); $\Delta E'_{(vib)} = E'_{(vib)}$(X-LB adduct) – $E'_{(vib)}$(:LB) i.e. difference in temperature dependence of vibrational energy; N is Avogadro's number: 6.022×10^{23} mol^{-1}, *h* is Planck's constant: $6.62606957(29)\times10^{-34}$ J·s, and n_i is the i^{th} vibrational frequency. Finally, the 5/2 RT quantity accounts for translational degrees of freedom and the ideal gas value for the change from two particles to one. The ground state energy of the halenium ion is calculated for its triplet state.

Qualitative reactivity ranking of potential halogen attack sites using *HalA* computations can be made using the *HalA* table (see Figure II-6) whereas quantitative comparison of affinities can be established by computing the full structures using optimum solvation models. Figure II-6 provides the *HalA* (Cl) scale for various functional groups to allow a qualitative comparison. As shown, functional groups (acceptors) undergoing extended conjugation with the substituents attached, span a larger range of *HalA*. For instance, alkenes, alkynes, amines, aromatic compounds etc. whose HOMO can be easily altered based on the electronics of the substituents, display a wider range of *HalA* values in comparison to epoxides or alcohols where the attached substituents can only exert a weaker inductive effect. The *HalA* scale has been experimentally verified by analysis of the equilibrium ratios of various chloropyridinium salts. Ms. Nastaran Marzijarani performed an exhaustive survey of experiments on chloropyridinium salts and

Figure II-6. The *HalA* (Cl) scale based on theoretical estimates of over 500 chlorenium ion acceptors.

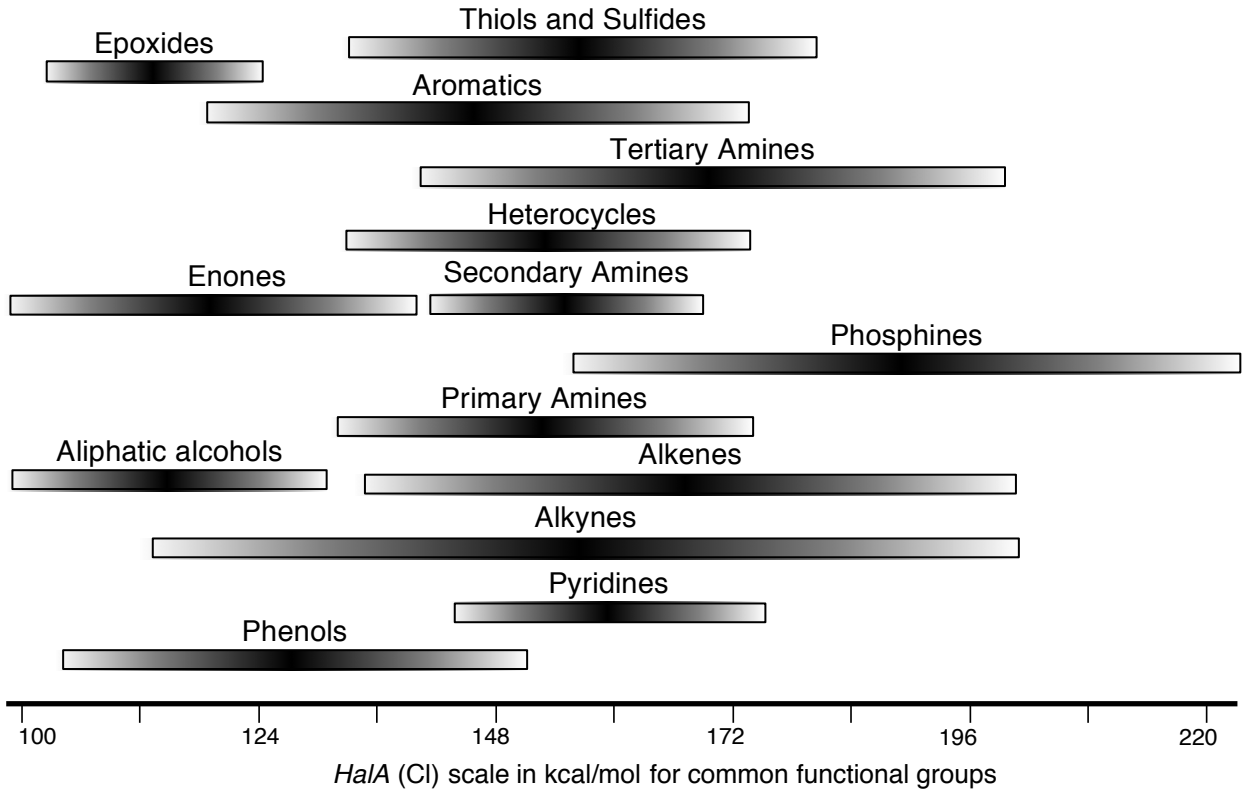

displayed that the predicted *HalA* values are in excellent agreement with the experimentally determined ratios.

A relative comparison of halenium affinities can facilitate (a) a rational approach towards choice of compatible nucleophiles (especially when the nucleophilic atom is embedded within motifs that have similar steric/electronic profiles) (b) it can account for the modulation of *HalA* values of alkenes by the anchimeric assistance of neighboring functionalities; this aspect underscores the importance of quantitatively evaluating *HalA* values on full structures rather than on truncated models. Furthermore, subtle electronic perturbations leading to modulations of *HalA* values are also accounted for in the calculations, (c) accurate predictions of chemoselectivity towards development of halenium initiated cascade/Domino reactions, and (d) most importantly,

Figure II-7. *HalA* (Cl) predictions at the B3LYP/6-31G*/SM8($CHCl_3$) level of theory predicts the alkenoic acid **II-1** to be inefficient to capture the chlorenium atom from DCDMH.

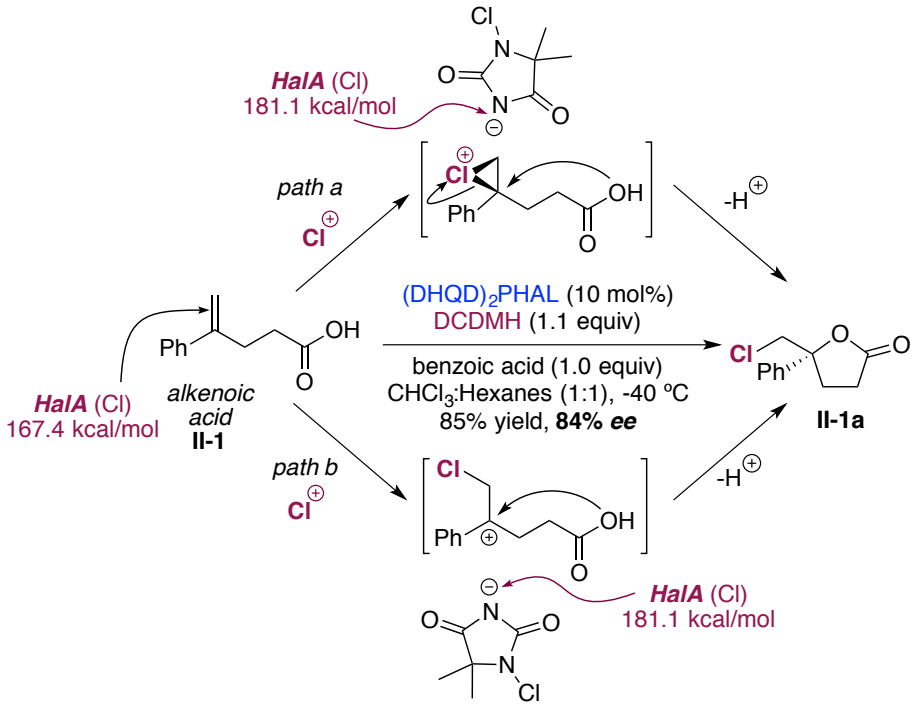

this tool can be employed as an indirect probe to verify the possibility of halenium ion transfer between two acceptors.

Application of *HalA* computation to cholorolactonization reveals that the alkenoic acid **II-1** cannot compete in terms of its halenium affinity to capture a chlorenium atom from DCDMH. The olefin has a 13.7 kcal/mol lower *HalA* (Cl) in comparison to the anion of the chlorenium donor. However, the reaction does proceed in practice and goes to completion at -40 ºC in about 6 h. This raises an imperative question as to what phenomenon allows compensation for the 13.7 kcal/mol difference in *HalA* values? An exhaustive search for transition state structure led us to an interesting finding wherein, the nucleophile plays a key role by interacting with the olefin and eventually exalts its HOMO energy, allowing it to capture the halenium ion. Figure II-8 depicts the calculated transition state for the above chlorolactonization where two molecules of the alkenoic acid are involved in strong H-bonding interactions with the two most basic sites on the catalyst (the quinuclidine nitrogens). This interaction serves benefits the reaction in multiple ways: a. the

Figure II-8. Calculated transition state structure for the asymmetric chlorolactonization of **II-1** catalyzed by $(DHQD)_2PHAL$ at the B3LYP/6-31G*/SM8($CHCl_3$) level of theory.

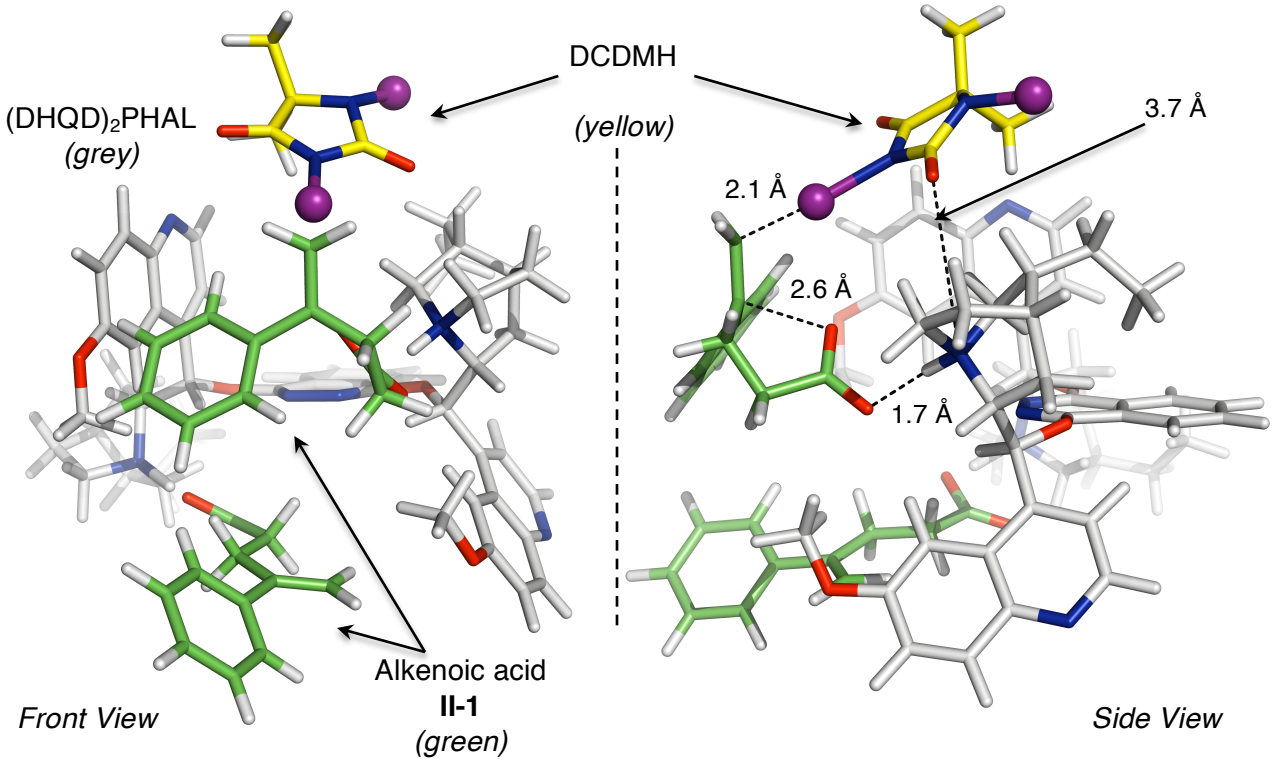

substrate based olefin is occluded within the chiral cleft of $(DHQD)_2PHAL$, b. the H-bonded complex enhances the nucleophilic character of the carboxyl moiety promoting a stronger pre-polarization of the olefin via nucleophile-olefin interaction (enhancing its HOMO energy) and, c. the C2-carbonyl of DCDMH is electrostatically attracted to the ammonium center, allowing a pre-disposition of the reactants in a spatial setting, enhancing the rate of the reaction as well as imparting the observed enantioinduction.

Among all the features, the assistance of nucleophile is of utmost importance towards initiating the chlorenium atom transfer. To further probe this hypothesis, which we dub as "Nucleophile Assisted Alkene Activation" (*NAAA*), the following theoretical and experimental studies are presented.

II.3. Nucleophile Assisted Alkene Activation (NAAA)

II.3.1. The classical perception of halonium ions.

In path A or B in Figure II-5, the conventional mechanism would view the electrophilic halenium attack to form bridged halonium or an open halo-carbenium ion as the rate-determining step. This allows the electronic nature of substituents directly attached to the olefin to influence the formation of intermediate **I** (either symmetrically or asymmetrically bridged) and/or intermediate **II**. Three inferences arise from this picture: (i) The reaction rate should be governed by the first step, forming intermediates **I** or **II**; (ii) the stereo-preference and regioselectivity of the nucleophilic attack should be dictated by the stereoelectronic identity of **I** and **II**; and, (iii) nucleophilic attack (step 2) should have no significant bearing on the rate of the overall addition. Despite these well-defined features, numerous previously reported experimental outcomes are not well explained by this classical scenario. The major drawback in this analysis is the uncharted role of the nucleophile and the counter anion of the halenium donor.

II.3.2. Halenium affinity (*HalA*) as a mechanistic probe.

As described earlier, the *HalA* scale ranks potential halenium ion acceptors based on their ability to stabilize a *free halenium ion*. Although this is an indirect approach, the *HalA* values serve as quantitative descriptors of the bond strengths of various functional groups to halenium ions. To probe the classical approach, wherein a donor transfers a halenium ion onto an olefin leading to a haliranium ion (or halocarbenium ion) in proximity with its donor counter anion, we resorted to comparison of their relative *HalA* values (Figure II-9). The SM8 model for simulated chloroform (a typical solvent for halogenation reactions) was employed for this *HalA* assessment. The role of the byproduct anion after halenium ion delivery has received relatively little attention in mechanistic descriptions of electrophilic halogenations. A handful of reports have explored bridged halonium ions with counterions such as trifluoromethylsulfonate, BF_4^-

Figure II-9. a. Relative *HalA* values (B3LYP/6-31G*/SM8-$CHCl_3$)for some prototypical alkenes in comparison to 1-methylcyclohexene. b. Relative *HalA* values of anions of commonly used halenium ion donors in comparison to 1-methylcyclohexene. Values in parenthesis are absolute *HalA* values. c. Classical mechanistic perception leading to charged intermediates. d. Competition between neutral and anionic acceptors for capture of chlorenium ion (complex-**A**) and competition between two neutral acceptors (complex-**B**).

a.

Neutral Acceptors	ΔHalA1[a] (F) Kcal/mol	ΔHalA1[a] (Cl) Kcal/mol	ΔHalA1[a] (Br) Kcal/mol	ΔHalA1[b] (I) Kcal/mol
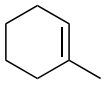	**0.0** (369.2)	**0.0** (152.1)	**0.0** (125.5)	**0.0** (93.8)
	1.3	4.4	4.0	3.9
	7.7	8.7	7.3	8.4
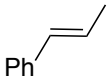	1.2	3.4	3.1	4.9
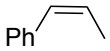	4.2	2.2	1.7	4.0
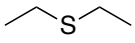	-6.9	-3.2	0.6	2.8

b.

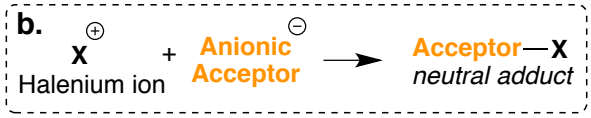

Anionic Acceptors	ΔHalA1[a] (F) Kcal/mol	ΔHalA1[a] (Cl) Kcal/mol	ΔHalA1[a] (Br) Kcal/mol	ΔHalA1[b] (I) Kcal/mol
F^-	15.6	---	---	---
Cl^-	---	15.4	---	---
Br^-	---	---	28.3	---
I^-	---	---	---	124.2
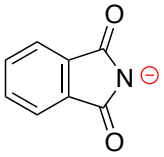	---	39.0	42.3	---
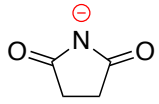	---	41.9	45.1	133.0
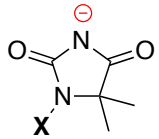	---	29.0 (X=Cl)	33.4 (X=Br)	---
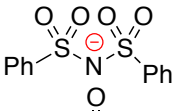	-4.9	---	---	---
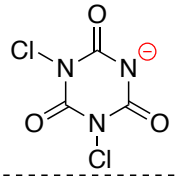	---	8.0	---	---

c.

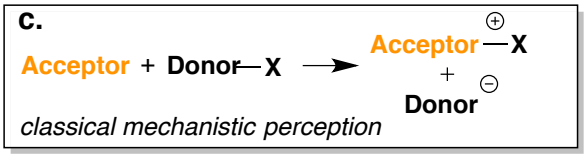

[a] B3LYP/6-31G*/SM8 ($CHCl_3$)
[b] B3LYP/6-31G*/LANL2DZ (gas phase)

d.

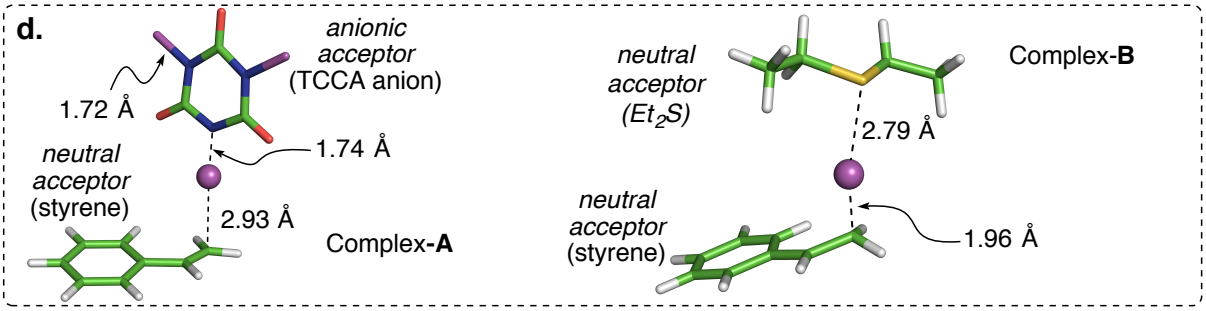

and antimony (VI) halides, anions with extremely low *halenium affinity*.[35,48-52] In contrast, the most commonly employed halenium donors in halo-functionalization of olefins are imide-based reagents or dihalogens themselves, whose counter anions have higher halenium affinities (compare *HalA* values in Figure II-9 a and b).

To validate the *HalA* assessments, a theoretical competition for a chlorenium ion was set up between dichloroisocyanurate anion (with the lowest *HalA*-Cl value among imide based donors studied to date) and styrene as the alkene acceptor (Figure II-9 d, complex **A**). The B3LYP/6-31G*/SM8 ($CHCl_3$) level of theory reveals only a weak Van der Waals interaction between styrene and the chlorine in this complex, without a trace of olefin re-hybridization. The TCCA imide nitrogen, on the other hand, retains its N-Cl bonding at a distance (1.74 Å) almost equidistant to the other two N-Cl bonds (1.72 Å). A similar competition between diethylsulfide (mimicking the chlorenium ion donor-chlorodiethylsulfonium hexachloroantimonate)[53] and styrene finds the chlorenium ion again shared unequally between the two 'neutral' acceptors. However; in this case the styrene is the stronger acceptor, pulling the chlorine close (1.96 Å; see complex **B**). Since reaction of neutral species to form ionic products in general is energetically uphill in organic solvents, transfer of chlorenium ion to olefins by expulsion of an anionic donor is not an optimum choice for a reaction pathway (Figure II-9 c). Due to the high electronegativity of halogens, during a halofunctionalization reaction, the halenium atom will break the bond to the donor atom only after it has acquired enough electron density from the acceptor. Hence, to ensure complete transfer of halenium ion from a donor haloimide to an acceptor alkene, the *HalA* of the anionic imidate (after the N-X bond is severed) should be less than the corresponding alkene. In essence, anionic species will always outcompete a neutral acceptor to capture a halenium ion (Figure II-9 b and d). Yet reagents such as TCCA are not only successful but also highly reactive in electrophilic halofunctionalizations of alkenes. What enables olefins to react with these imide based halenium

ion donors? The following series of experiments provides evidence for activation by the nucleophilic partner, presumably by exalting the HOMO of the π-system and thereby increasing its nucleophilicity. This hypothesis accords with the Salem-Klopman equation that quantifies the degree of perturbation of molecular orbitals upon interaction of electrophiles and nucleophiles with a π-system.[54,55] The following set of experimetnal results validate the *HalA* predictions.

As represented in Figure II-10, the classical mechanistic perception of halofunctionalization of olefins predicts the transfer of a halenium ion from a donor to an olefin leading to a bridged haliranium ion (or halocarbenium ion) in proximity with its donor counter anion. To elucidate the thermodynamics of this process, we resorted to comparison of *HalA* values. The SM8 model for simulated chloroform (a typical solvent for halogenation reactions) was employed for this *HalA* assessment.

A competition reaction was set up between tetra-n-butylammonium succinimidate (anionic

Figure II-10. Classical perception of halofunctionalization of olefins.

Application of HalA to address the energy cost for formation of charged intermediates

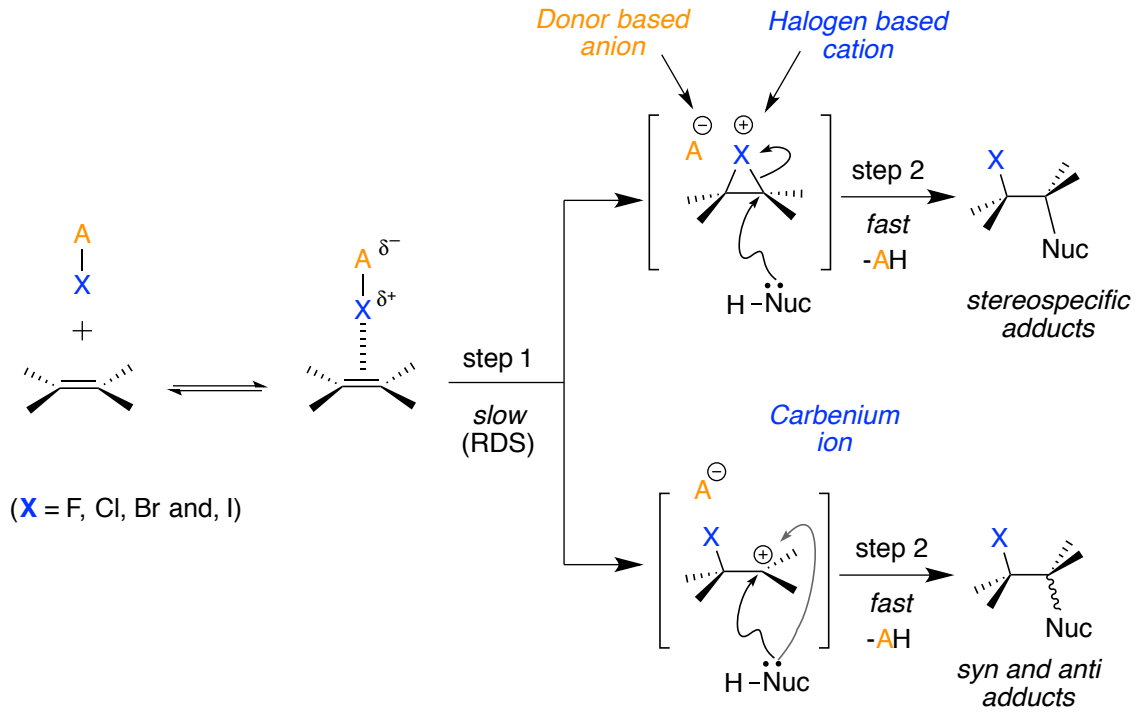

Figure II-11. ^{1}H NMR spectra, ($CDCl_3$, rt, dark): a. *N*-chlorosuccinimide (NCS), b. tetra-n-butylammonium succinimidate, c. 1,3-dichloro-5,5-dimethylhydantoin (DCDMH), d. a 1:1 mixture of succinimide anion and DCDMH, the ^{1}H NMR resonances depict the succinimide anion abstracts the chlorenium ion completely from DCDMH owing to the higher *HalA* value of succinimide anion (Δ*HalA* = 8.9 kcal/mol).

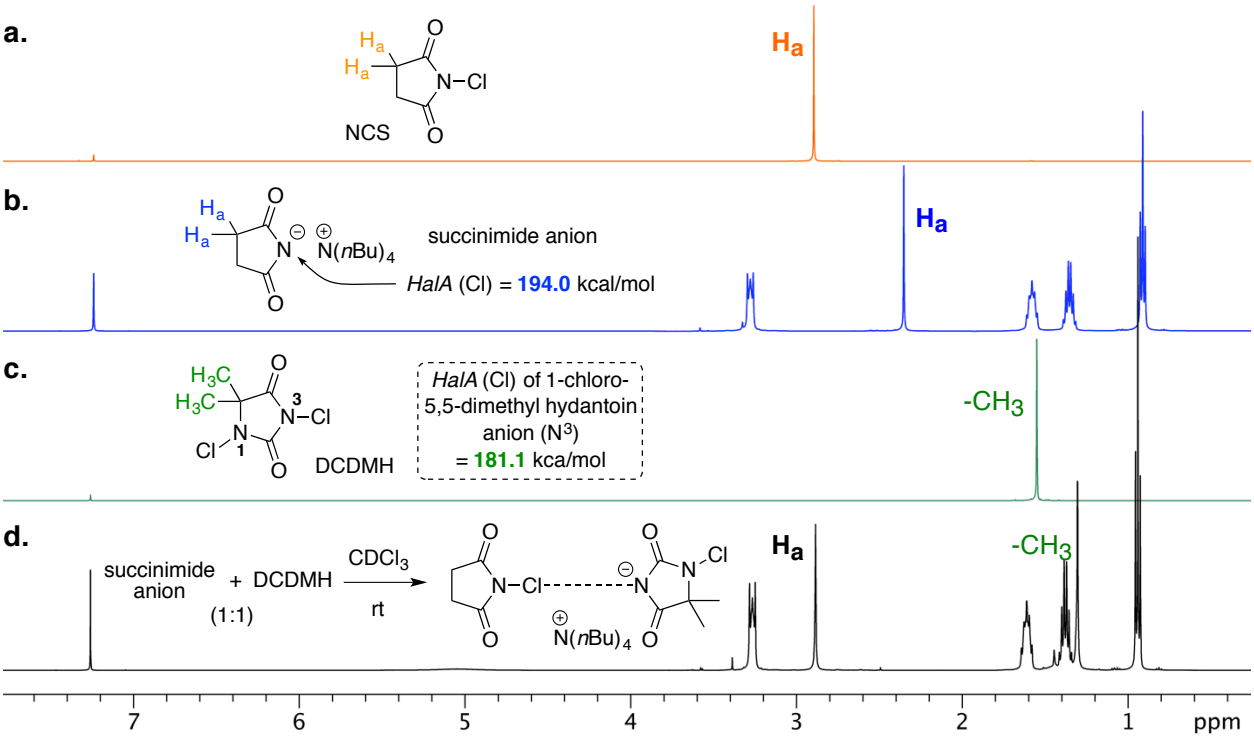

acceptor) and 1,3-dichloro-5,5-dimethylhydantoin-DCDMH (neutral donor) to study the possible transfer of chlorenium atom, see Figure II-11. The succinimidate anion (spectrum b) has a 8.9 kcal/mol higher *HalA* (Cl) value than the N3 anion of monochlorohydantoin, hence for the above competition reaction, we can predict the succinimidate anion to abstract a chlorine atom from the N3-Cl bond of DCDMH to produce *N*-chlorosuccinimide and a N3 anion of monochlorohydantoin. As anticipated, the exclusive formation of *N*-chlorosuccinimide (NCS) is observed (spectrum d) upon reaction of an equimolar ratio of succinimidate anion and DCDMH.

On the contrary, a similar competition reaction between NCS and tetra-n-butylammonium salt of 1,5,5-trimethylhydantoin N3 anion (TMH anion) does not lead to transfer of chlorine atom (spectrum d, Figure II-12). TMH anion has a 2.9 kcal/mol lower *HalA* (Cl) value than succinimidate anion and hence, it is inefficient to capture the chlorenium atom from NCS. Instead, it engages a

Figure II-12. ^{1}H NMR spectra, ($CDCl_3$, rt, dark): a. *N*-chlorosuccinimide (NCS), b. tetra-n-butylammonium succinimidate, c. tetra-n-butylammonium 1,5,5-trimethylhydantoin-1-ide (TMH anion), d. a 1:1 mixture of NCS and TMH anion, the ^{1}H NMR resonances depict the TMH anion being inefficient to abstract the chlorenium ion from NCS owing to the lower *HalA* value of TMH anion (Δ*HalA* = 2.9 kcal/mol).

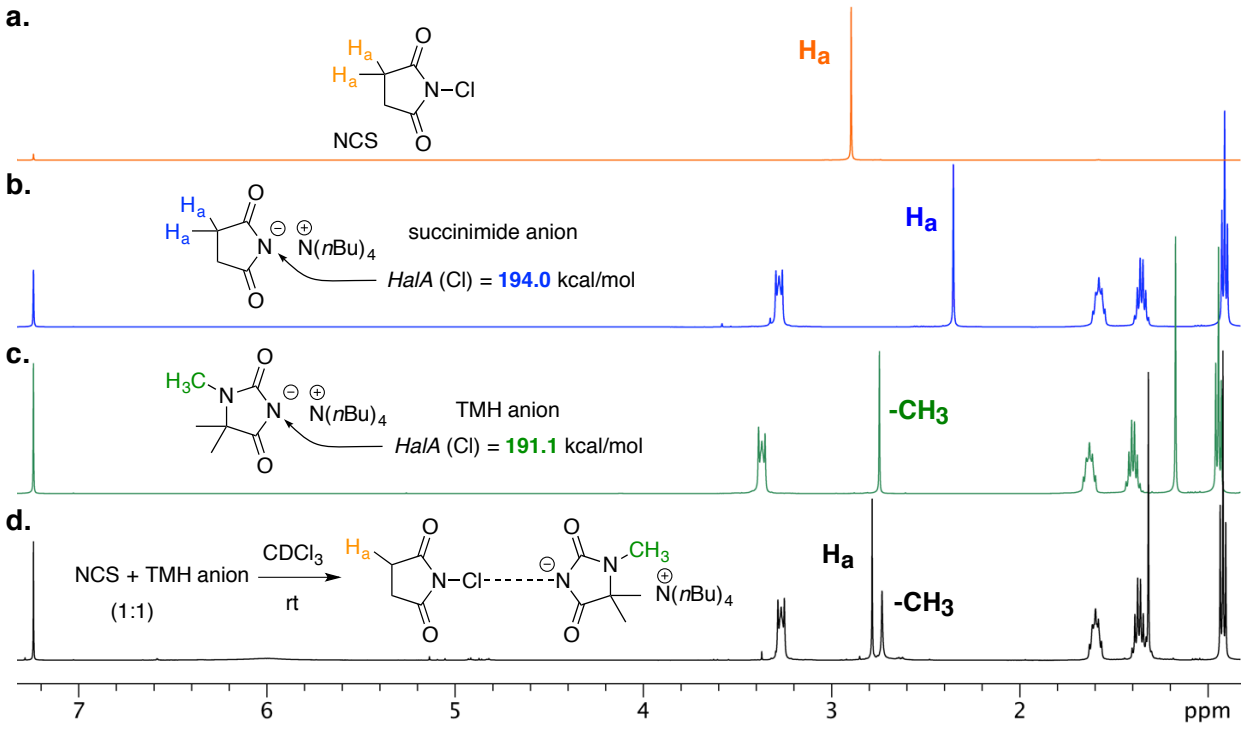

weak halogen bonding with the chlorenium atom as indicated by the minuscule downfield shift (0.02 ppm) of N1-CH_3 resonance and a 0.1 ppm upfield shift of the NCS methylene proton resonance.

Following the validation of *HalA* predictions, we studied the possibility of halenium ion transfer to α-methylstyrene using different chlorenium ion sources in the absence of a nucleophile. Trichloroisocyanuric acid (TCCA), inheriting an excellent leaving group attached to the chlorenium atom (*HalA* of dichloroisocyanurate anion = 160.1 kcal/mol), is predicted by *HalA* computations to deliver a chlorenium ion to electron rich alkenes such as α-methylstyrene (*HalA* = 160.8). This stands out to be an exceptional case as the alkene by itself has a higher *HalA* (Cl) than the donor anion by 0.7 kcal/mol.

To verify this prediction, we studied the ^{1}H NMR resonance of α-methylstyrene in presence of several chlorenium sources. As shown in Figure II-13, chlorenium sources such as NCS and DCDMH, whose imidate anion (formed after Cl^+ delivery) has higher *HalA* (Cl) value than α-methylstyrene are inefficient to effect chlorination of the olefin. The olefinic ^{1}H NMR

Figure II-13. ^{1}H NMR spectra, ($CDCl_3$, rt, dark): a. α-methylstyrene, b. *N*-chlorosuccinimide (NCS), c. equimolar ratio of α-methylstyrene and NCS, d. 1,3-dichloro-5,5-dimethylhydantoin (DCDMH), e. a 1:1 mixture of α-methylstyrene and DCDMH. The unchanged ^{1}H NMR resonances of NCS and DCDMH in spectra c and e illustrate the fact that α-methylstyrene, owing to its lower *HalA* (Cl) value, is inefficient to capture the Cl^+ atom from either donors to form charged products. f. Chlorination of α-methylstyrene using TCCA.

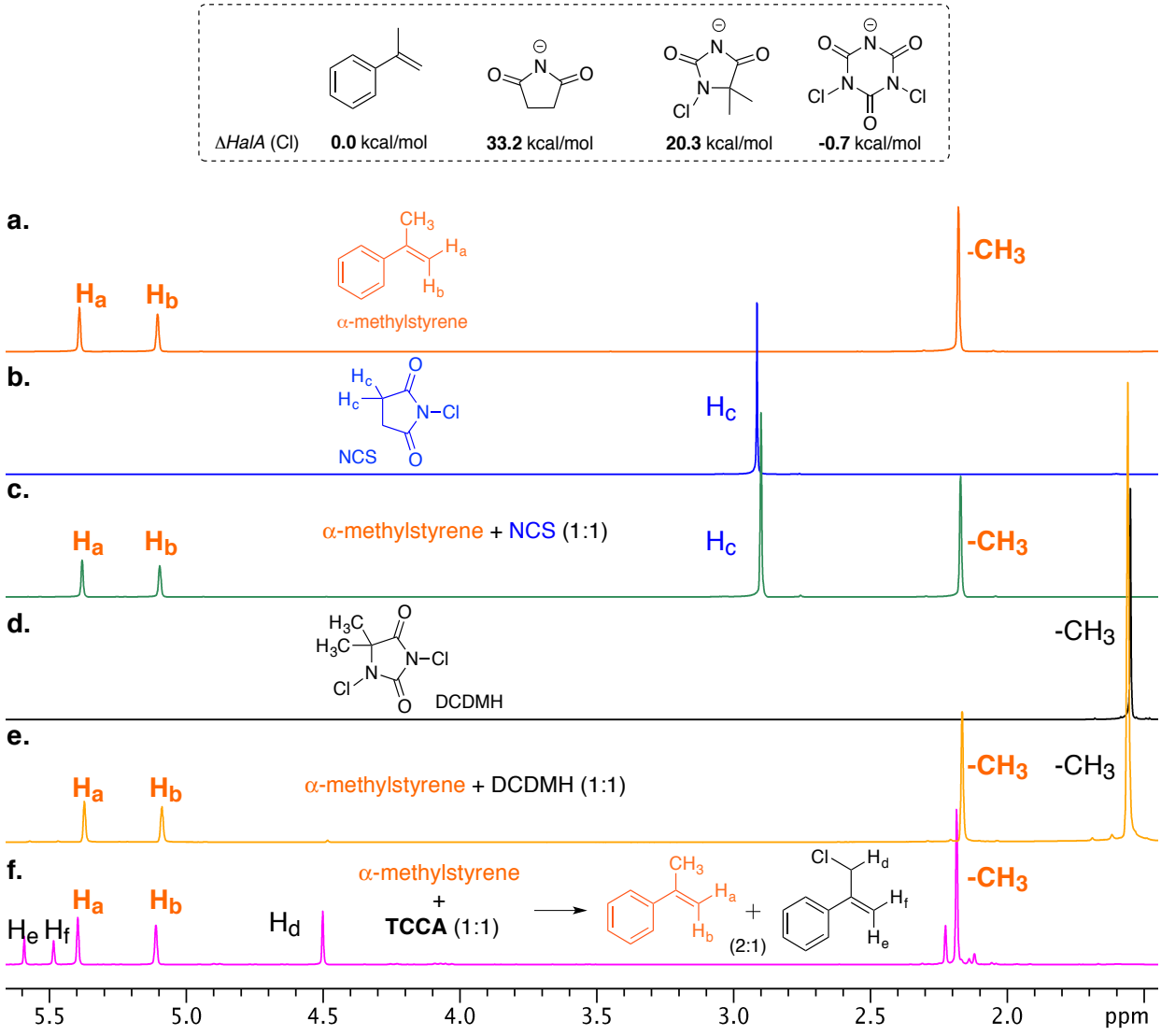

resonances (Figure II-13, spectrum c and e) of α-methylstyrene do not indicate any strong halogen bonding interactions between the olefin and the chlorenium source. However, TCCA, whose counter anion has a 0.7 kcal/mol lower *HalA* than α-methylstyrene, is effective to yield α-chloromethylstyrene as shown in spectrum f.

These examples underscore the importance of *HalA* as a mechanistic probe towards accurately predicting halenium ion transfers. Due to the high electronegativity of halogens, during a halofunctionalization reaction, the halenium atom will break the bond to the donor atom only after it has acquired enough electron density from the acceptor. Hence, to ensure a complete transfer of halenium ion from a donor haloimide to an acceptor alkene, the *HalA* of the anionic imidate (after the N-X bond is severed) should be less than the corresponding alkene, which is not a common instance as seen from the experiments described above. In essence, anionic species will always outcompete a neutral acceptor to capture a halenium ion. All the above results taken together with the detailed and exhaustive studies from other labs[30,31,42,44] demonstrates that formation of charged intermediates, such as the haliranium ion (bridged halonium ion) bearing a cationic halonium is unlikely under prototypical halofunctionalization reactions involving imide based reagents or dihalogens in general.

Note: Unless otherwise mentioned, all NMR experiments shown above, were performed in $CDCl_3$ at 0.05 M substrate concentration, at room temperature. Experiments involving halenium ion sources were performed in absence of light to avoid radical halogenation. In case of treatment of α-methylstyrene with DCDMH and TCCA, mixing of the reactants in $CDCl_3$ was performed at 0 ºC in the absence of light and the mixture was eventually warmed to room temperature over a course of 3 min (in an amber glass NMR tube). All spectra were acquired within 5 min of mixing reactants.

Now, we can apply the *HalA* values towards probing the ***non-catalytic*** chlorolactonization of **II-1**. Comparing the *HalA*(Cl) values for an unactivated olefin (~165 kcal/mol) with a common Cl^+ donor such as the monochlorohydantoin anion (181.1 kcal/mol) in chloroform, one predicts no chlorenium transfer, a result of the much higher *HalA* value of the donor anion compared to the olefin (Figure II-14b). Naked Cl^+ to **II-1** would be expected to attack without barrier to form a

Figure II-14. Computational predictions for possible chlorenium atom transfer (B3LYP/6-31G*/SM8-$CHCl_3$).

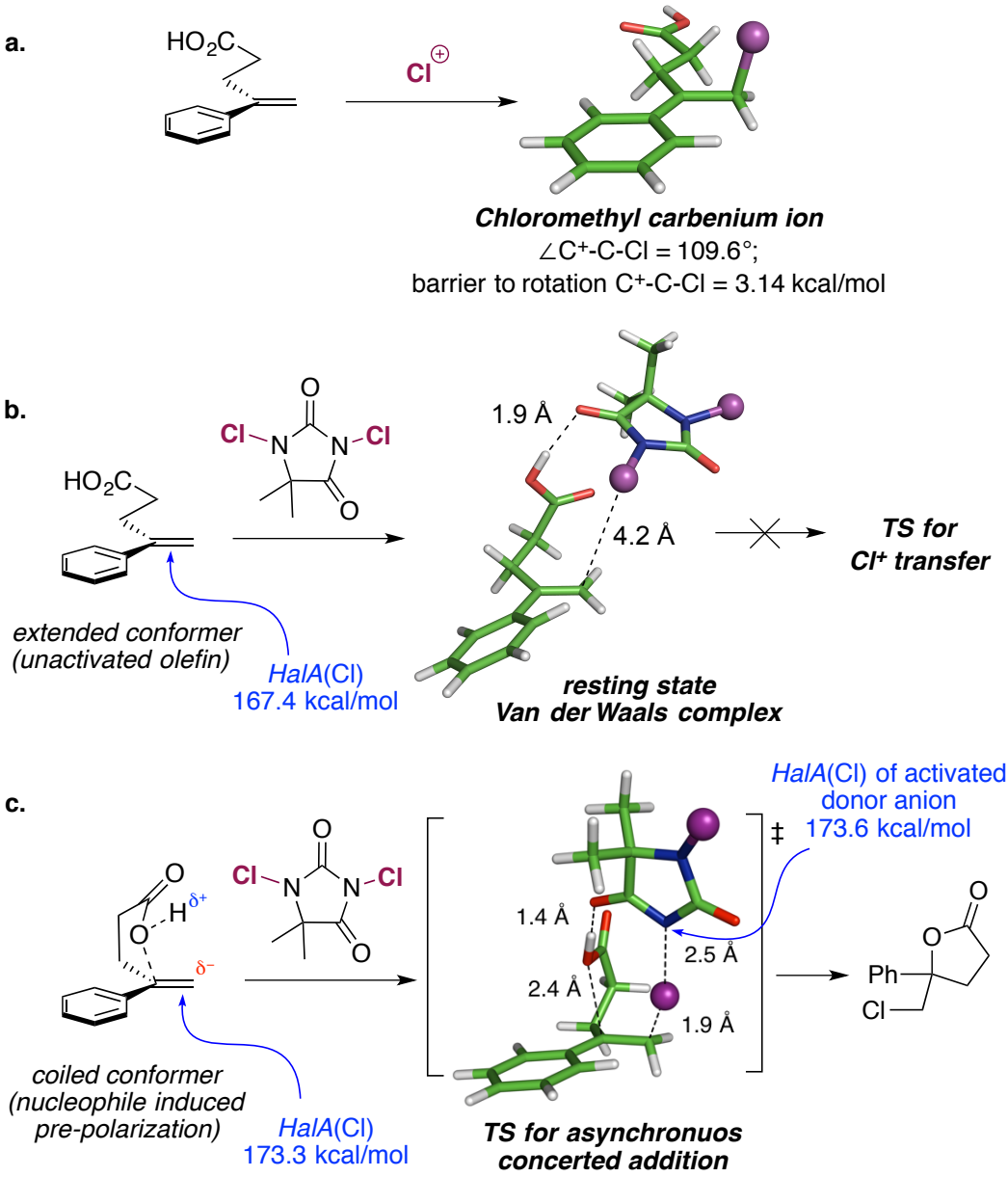

Scheme II-4: The rate determining-classically perceived intermediates (**A** and **B**) fail to explain the observed rate differences, whereas the nucleophile assisted activation pathway predicts the barriers (B3LYP/6-31G*/SM8-$CHCl_3$) for halofunctionalization, which are in accordance to the observed rates.

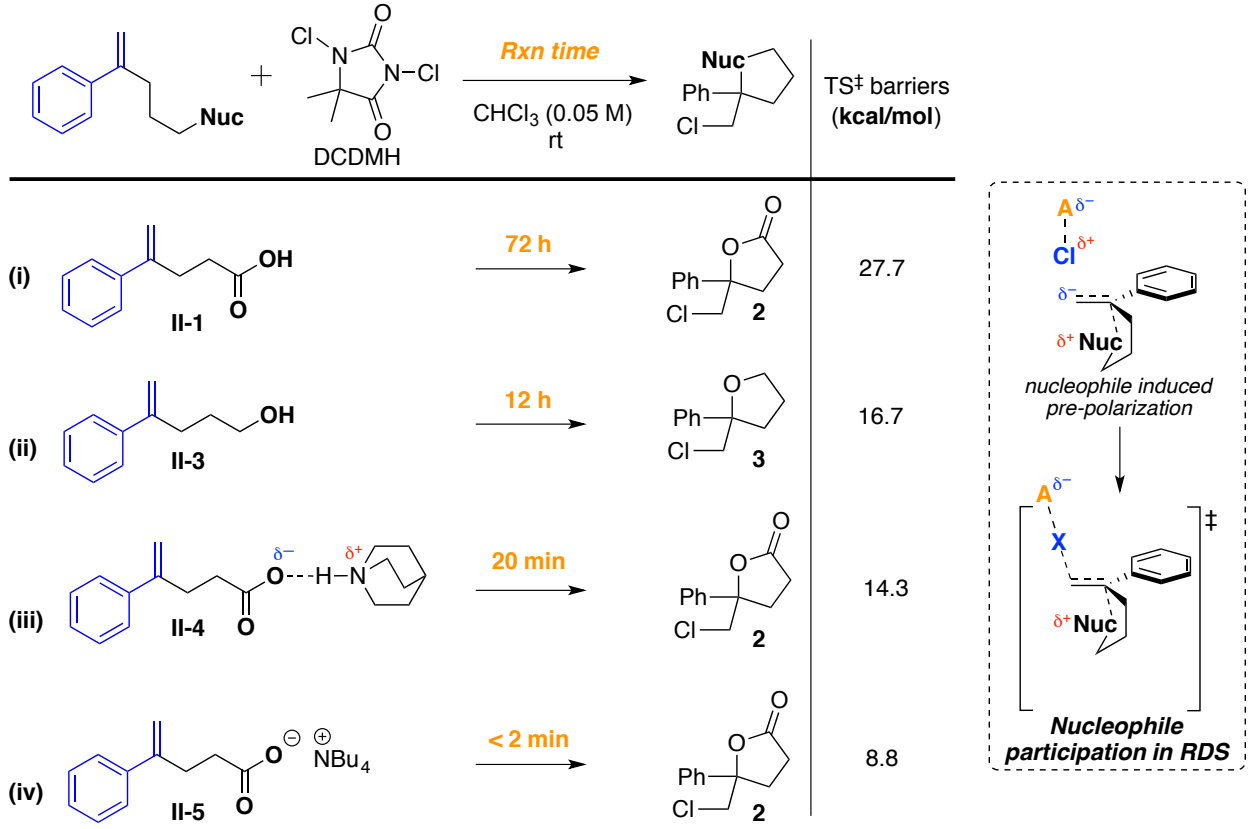

chloromethyl carbenium ion (Figure II-14a) but the actual reagent- 1,3-dichloro-5,5-dimethylhydantoin (DCDMH) can only transfer Cl^+ to one conformation of the olefin where the nucleophile is able to interact with the π-system. This geometry positions the carboxylic acid in close proximity to the C2 of the olefin (Figure II-14c). Calculations show that this nucleophilic interaction with the olefin raises the energy of its π bonding orbital (the HOMO) by 0.10 eV, enabling it to compete with the donor anion for the chlorenium atom, and in effect increasing the *HalA* of the now activated olefin. Upon DCDMH association, this conformation shows N-Cl bond elongation and leads to a transition state for chlorolactonization. This detailed scenario predicts that the reaction precedes via nucleophile assisted alkene activation (*NAAA*), which depends not

only on the nucleophilicity of the olefin (as measured by *HalA*), but also on the source of the chlorenium. The *HalA* of the olefin, a composite of the olefin with all its interactions including the suggested nucleophilic activation, is higher as compared to the isolated, unperturbed olefin moiety. The transition state calculations on the reactions depicted in Scheme II-4 with conformations favorable to *NAAA* yield activation energies consistent with the observed reaction rates. In other words, the ordering of reaction times, **II-1** > **II-3** > **II-5** (carboxylate, the most nucleophilic substrate in the list) is consistent with the ordering of the calculated reaction barriers 27.7 > 16.7 > 8.8 kcal/mol, respectively.

II.3.3. Kinetic isotope studies in chlorocyclization of II-1, II-2 and II-3.

Scheme II-5 displays a sampling of experimental and theoretical methods used to investigate the concerted (albeit asynchronous) nucleophilic activation of olefin/halenium capture en route to halocyclizations. Chlorolactonization (more than bromo- or iodolactonization) provides ample opportunity to substrate **II-1** to proceed via a tertiary benzylic carbenium ion. To probe whether *NAAA* competes with this stepwise pathway, we have used natural abundance KIE measurements and heavy atom labeling studies to probe the transition states of halofunctionalization reactions. Using a blend of theoretical predictions (from calculated transition structures) and experimental results of ^{13}C KIE experiments, the hybridization states of the olefinic carbons at the transition state during halofunctionalization reactions can be probed. To interpret ^{13}C KIE values, we considered the three possible alternative pathways depicted in Figure II-15. (i) Path A involves the classic bridged haliranium ion wherein both olefinic carbons undergo modest rehybridization during formation of intermediate (**I**). However, the benzylic stabilization in **II-1**, will render the haliranium ion asymmetric ($C_{(benzylic)}$-Cl bond longer than $C_{(homobenzylic)}$-Cl bond). If formation of this haliranium intermediate is the RDS, the benzylic

carbon should be least affected by isotope substitution and hence, the magnitude of ^{13}C KIE at the benzylic carbon should be lower than that on the chloromethylene carbon. (ii) For Path B-intermediate (**II**), the benzylic carbon would experience no hybridization change (sp^2 to sp^2), yielding an isotope effect near unity, whereas the fully rehybridized carbon β to phenyl should show a substantial KIE. (iii) Finally, the new proposed Path C entails nucleophile involvement in the RDS, with the magnitude of the isotope effect reflecting the electronic nature of the

Figure II-15. Path A and path B represent the rate determining-classically perceived intermediates (**I** and **II**) involved in electrophilic addition to alkenes. Path C represents the nucleophile assisted activation pathway.

Classical Perception of Electrophilic Addition to Alkenes:

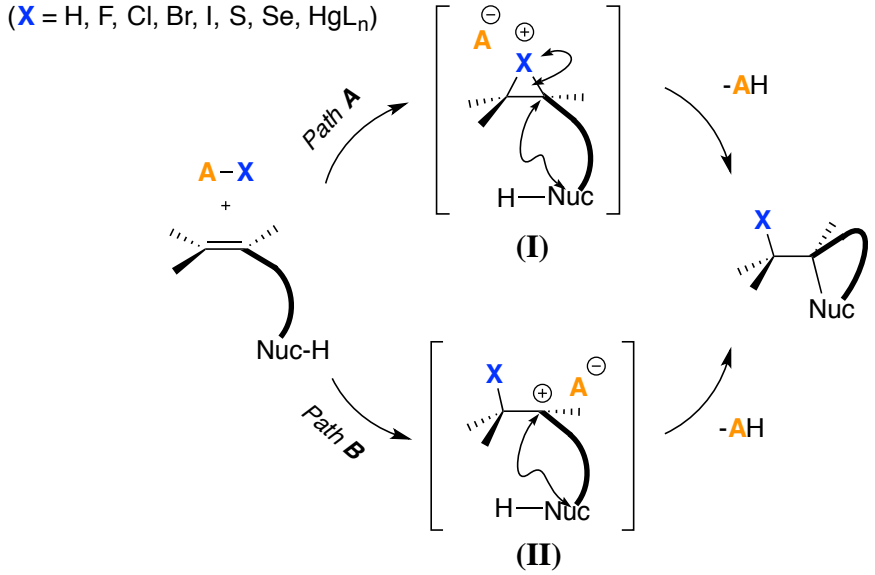

Nucleophile Assisted Alkene Activation: NAAA

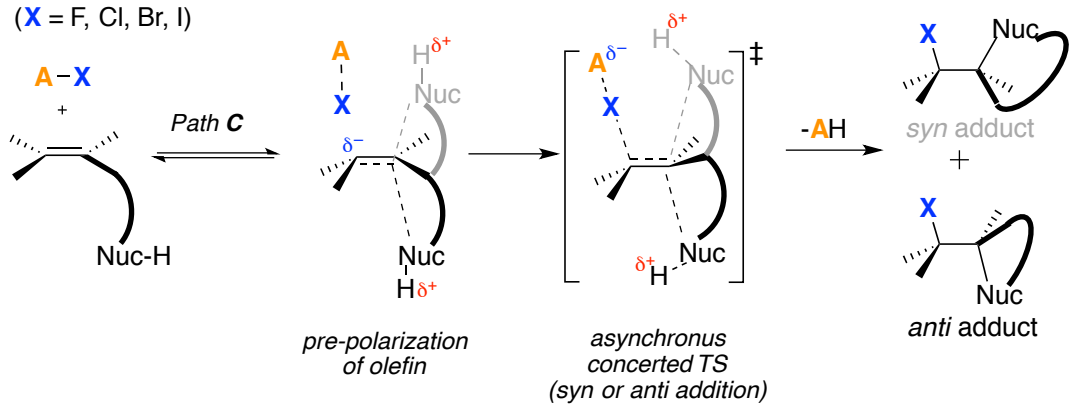

nucleophile as well as the substitution pattern of the olefin. Since, the nucleophile assists the pre-polarization of the alkene, the benzylic carbon should display a higher magnitude of ^{13}C KIE in comparison to the chloromethyl carbon. The experimental KIEs may also be compared with those from theoretically calculated transition states for these three paths.

Scheme II-5 illustrates the use of isotopic tools to decipher transition state characteristics in the chlorolactonization of **II-1**. Here, a clear case can be made for the nucleophile playing a role in activating the olefin. The relative magnitude of ^{13}C KIE on the benzylic vs the homo benzylic carbon clearly argues against Path A (Figure II-15) and hence, it can be excluded (Scheme II-5a). Similar but more thorough studies by the Sauers group[30] and from our own lab agree in reasoning against bridging haliranium ions. Based on these studies (where the donor anion is not invoked), upon capture of a halenium ion, **II-1** can be envisioned to undergo formation of a tertiary benzylic halomethyl carbenium ion (Path B, Figure II-15). This provides an excellent opportunity to probe for the existence of the putative halocarbenium ion by ^{2}H as well as ^{13}C KIEs. A series of labeled substrates were synthesized and tested to probe the possible role of intermediate **III**. The C-H bonds *alpha* to the carbenium center would be expected to contribute to the cation's stabilization *via* hyperconjugation and hence, the secondary ^{2}H KIE at that site should be a sensitive probe for the cation's intermediacy. Since it would be less stabilized by neighboring D than by H atoms, halocarbenium ion formation should be slower in the labeled substrate **II-1**-D_2 and **II-2**-D_2 than in the parent.

Furthermore, ^{13}C KIE experiments (natural abundance measurements pioneered by Singleton and coworkers), in conjunction with quantum chemical transition state predictions can also probe the changes in hybridization state of the benzylic carbon in the RDS.[56,57]

Scheme II-5. a, b. ^{13}C KIE results predicted at the B3LYP/6-31G* level of theory and its validation by experimental results. c, d. Secondary KIE (^{2}H) for halolactonization of **II-1** and **II-2**. e, f. Primary ^{18}O KIE experimental results for **II-1** and **II-2**.

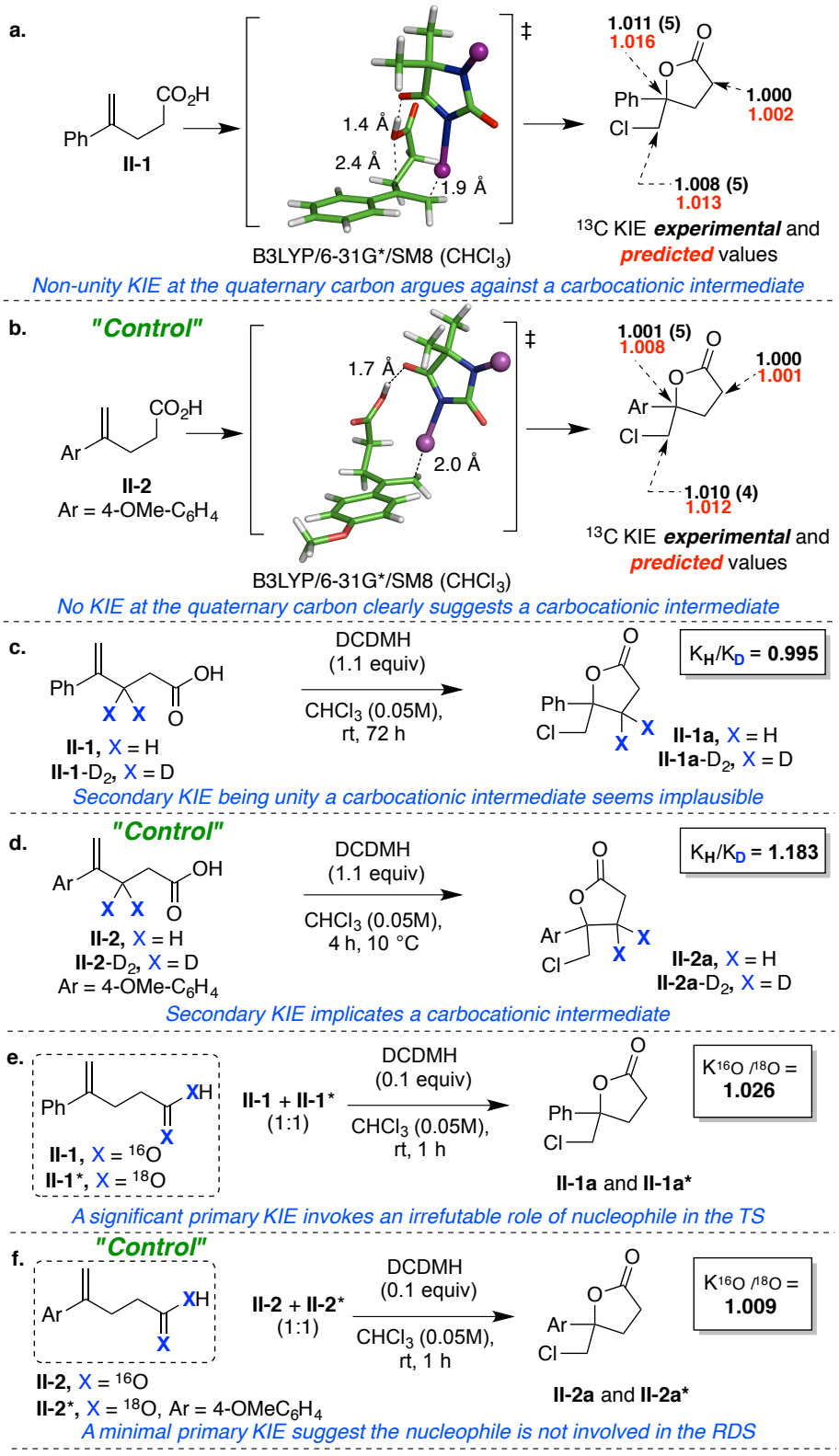

The results observed under prototypical conditions for halocyclization are summarized in Scheme II-5a. Surprisingly, substrate **II-1** (certainly capable of forming a tertiary benzylic carbenium ion) exhibit no evidence for a chlorocarbenium intermediate. The benzylic carbon shows a non-unity ^{13}C isotope effect of 1.011 (Scheme II-5a), while the near-unity ^{2}H KIE for **II-1**-D_2 (Scheme II-5c) argues against carbenium ion development at that site, at least in the RDS. A quantum chemically evaluated transition state for chlorolactonization of **II-1** explicitly supports this idea, showing instead an asynchronous concerted addition of the carboxylic acid and the chlorenium atom across the styrylic moiety (Scheme II-5a). This process avoids charge buildup on any of the reactants. The transition state calculations also reveal a concomitant proton transfer from the carboxylic acid moiety to the carbonyl oxygen of the hydantoin (H-O distance of 1.4 Å) during the addition reaction (see Figure II-16). Proton transfer in the transition state should lead to a non-zero KIE for chlorolactonization of **II-1**-OD. In fact cyclization of **II-1** vs **II-1**-OD does show a substantial KIE, *a strong corroboration of the notion that the remote nucleophile is involved in accelerating the reaction.* These interpretations were confirmed by findings for substrates **II-2** and **II-2**-D_2 (employed as a 'control'), in which a resonance-stabilized carbenium ion can form. There, the unity ^{13}C KIE at the quaternary carbon and ^{2}H secondary KIE of 1.183 support the intermediacy of a halomethyl carbenium ion (Scheme II-5b and II-5d) with hyperconjugative stabilization from the neighboring C-H bonds. Furthermore, in comparison to the classical mechanisms, *NAAA* invokes a strong and obligatory role for the nucleophile during the course of the reaction. To probe the influence of the nucleophile directly, KIE of the carboxylic acid oxygen atoms was investigated. Clearly one would not expect an ^{18}O KIE if the carboxylic acid was not involved in the RDS or as a player in determining the course of the reaction. This, in fact, is the case with the 'control' substrate **II-2**, which proceeds mainly via the benyzlic carbocation, with

Figure II-16. Predicted transition state for chlorolactoniaztion of **II-1** depicting the proton transfer from the carboxylic acid moiety to the carbonyl of chlorohydantoin.

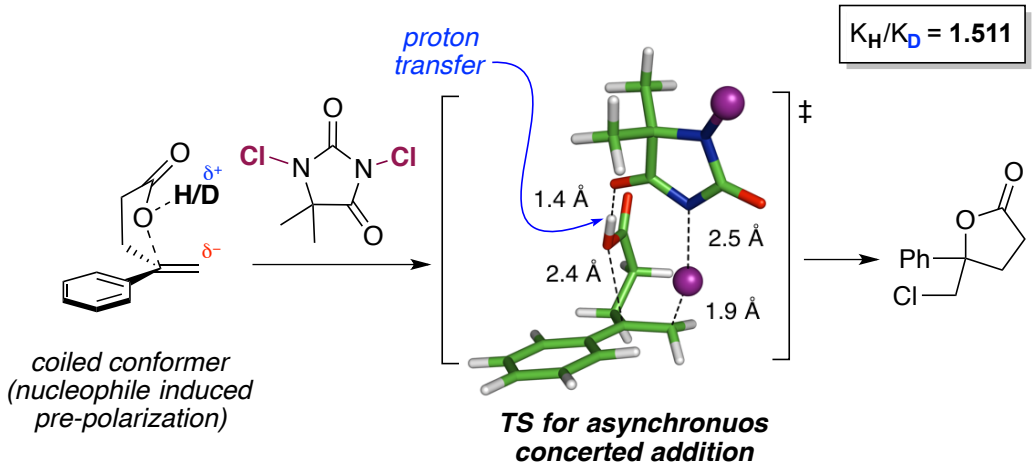

K_{16O}/K_{18O} = 1.009 (Scheme II-5f). In stark contrast, a substantial ^{18}O KIE is observed for the chlorocyclization of **II-1** (K_{16O}/K_{18O} = 1.026). The latter data clearly shows the direct involvement of the nucleophile, as preselection of ^{16}O in favor of ^{18}O must have been determined prior to capture of the chlorenium ion. This data paints a scenario that is in agreement with the transition state calculations described above (Scheme II-5a), highlighting the crucial role of the nucleophile in activating the olefin.

Kinetics of chlorolactonization of **II-1** (*syn* vs *anti* addition):

Although the experimental KIE of 1.511 for **II-1** vs **II-1**-OD corroborates the theoretically predicted value of 2.2, the computational analysis is based on the TS for *syn*-addition (Figure II-16). Experimentally, the reaction also yields an *anti*-adduct. Interestingly, the value for *syn*:*anti* addition varies based on the concentration of the reagent. The following set of experiments demonstrates the effect of concentration on chlorolactonization of **II-1a**.

The vinylidene group of the styryl substrates (**II-1**-D and **II-2**-D) offers an additional handle to probe the nature of intermediates in these reactions. Our recently reported synthesis of substrate **II-1**-D enabled us to probe the relative stereochemistry of the overall addition.[19] Using

Table II-1. *anti*:*syn* ratios for the deuterium labeled styryl substrates. The plot of ratios *vs.* concentration suggest a bimolecularity for chlorolactonization of **II-2**-D whereas a more complex scenario in case of **II-1**-D. For entries 1-6, the reagent concentration equals that of the substrate.

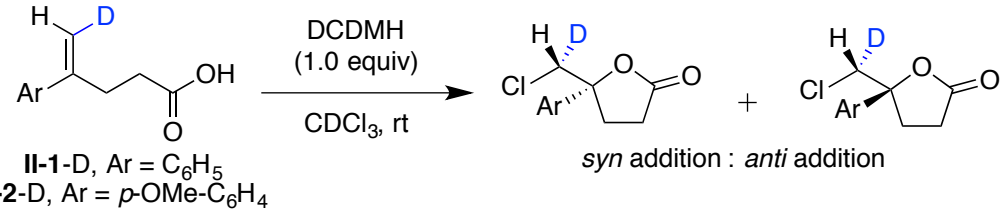

II-1-D, Ar = C_6H_5
II-2-D, Ar = *p*-OMe-C_6H_4

Entry	Sunstrate conc. (M)	ratio (*anti*:*syn*) from **II-1**-D	ratio (*anti*:*syn*) from **II-2**-D
1	1.0	2.30	1.20
2	0.5	2.05	0.70
3	0.1	1.13	0.46
4	0.05	0.90	0.43
5	0.025	0.73	--
6	0.0125	0.67	0.35
7	0.0125 (0.1 M DCDMH)	1.03	--

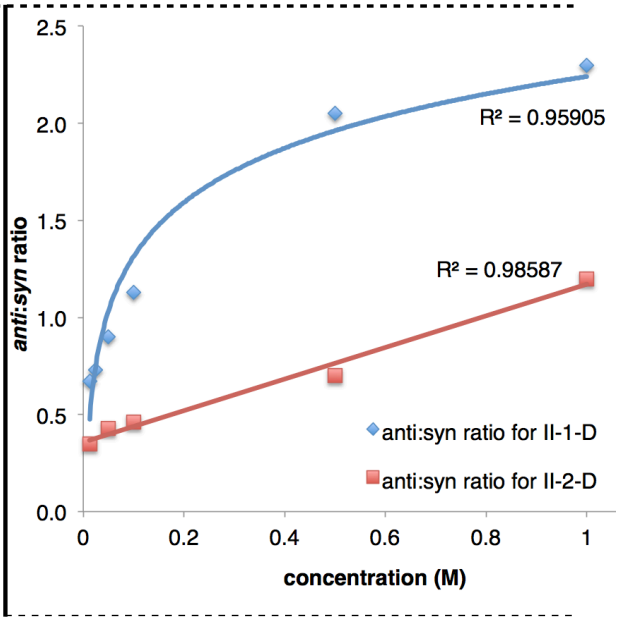

the same probe we elucidated the effects of reactant concentration on the overall addition. Interestingly, the *non-catalyzed* reaction displayed a significant concentration effect onthe ratio of *syn*:*anti* adducts (Table II-1). The *anti*-adduct was predominant at higher concentrations while the *syn*-adduct dominated at lower concentrations. The effective concentration of the chlorenium donor was elucidated to be the key factor in controlling the *syn*:*anti* ratio (entry 7, Table II-1). The concentration of the reagent (or any basic moiety) is the key feature that determines the stereochemical course of halofunctionalization of olefins. Furthermore, substrate **II-1**-D showed non-linear effects of concentration on *syn*:*anti* ratios whereas a linear trend was seen with substrate **II-2**-D. If the RDS of the reaction involves a 1:1 (substrate : reagent) complex, then the bimolecular reaction should display a linear trend as seen for **II-2**-D. These studies highlight the

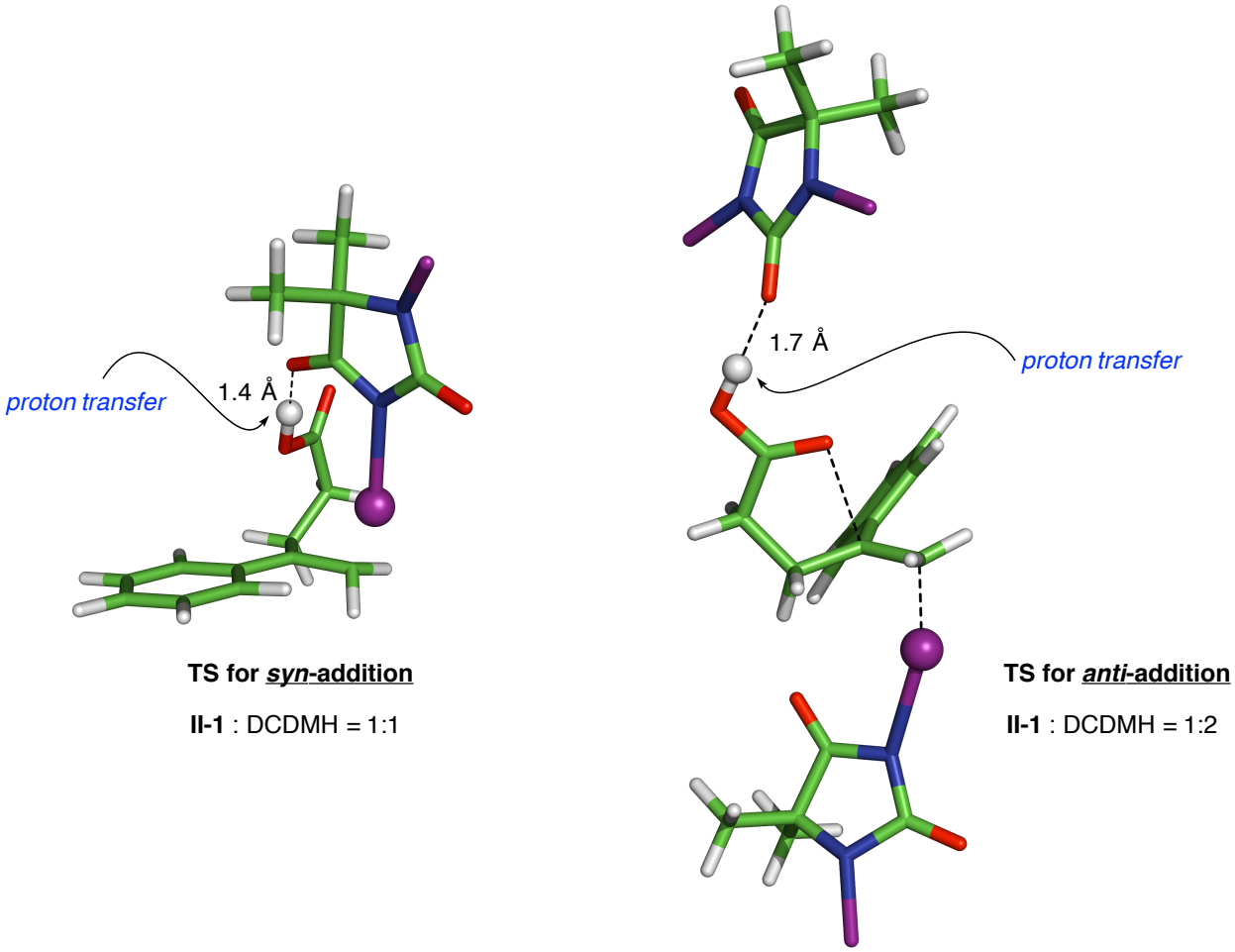

Figure II-17. Predicted molecularity from computational analysis for *syn* and *anti* addition during the chlorolactonization of **II-1**. The concomitant proton transfer stabilizes the TS for chlorolactonization as the nucleophile polarizes the π-system of the olefin. These predictions are corroborated by experimental RPKA analysis.

idea that during the RDS of chlorolactonization of **II-1**-D, more than one molecule of the chlorenium source is involved. To verify this hypothesis, we initiated transition state analysis for *syn* and *anti* addition, the summary of which is depicted in Figure II-17. The *syn*-addtion (a cyclic TS with minimal separation of charge) requires one molecule each of **II-1** and DCDMH, whereas, the *anti*-addition commences only when a basic moiety (such as one more molecule of DCDMH) is involved in accepting the proton from the carboxylic acid moiety. The concomitant proton transfer serves to stabilize the TS structure as the nucleophilic oxygen polarizes the olefin's π-system. In essence, either DCDMH (during the initial stages of conversion) or 1-chloro-5,5-

Table II-2. *anti*:*syn* ratios for the deuterium labeled styryl substrates. The carboxylate in **II-5**-D displays a high preference for *anti*-addition as well as a linear trend of *anti*/*syn* with concentration in contrast to **II-1**-D.

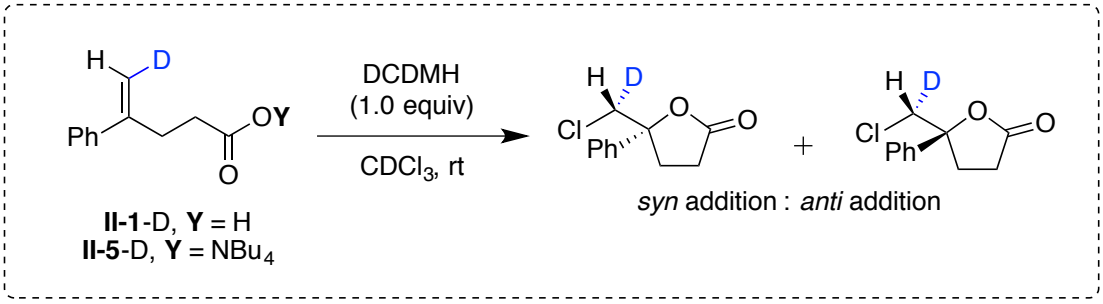

II-1-D, **Y** = H
II-5-D, **Y** = NBu_4

Conc. (M) of alkenoic acid (and DCDMH)	*anti*/*syn* from **II-1**-D	*anti*/*syn* from **II-5**-D
1.2	2.4	16.5
1	2.3	15.7
0.5	2.1	13.4
0.1	1.1	11.5
0.05	0.9	--
0.025	0.7	--
0.0125	0.7	10.1

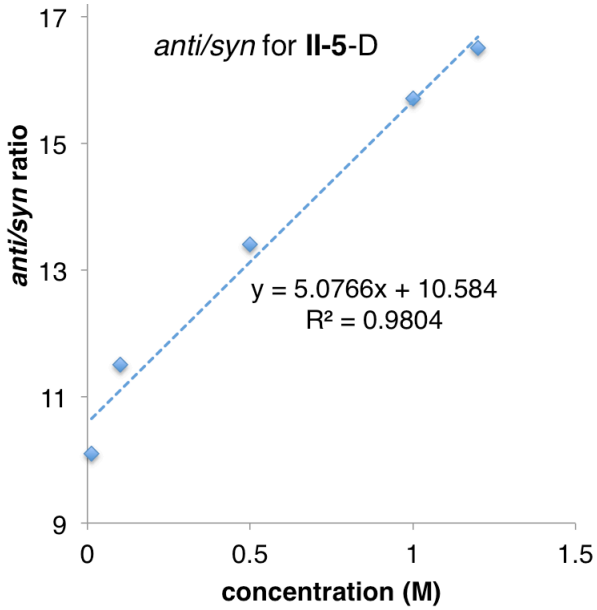

dimethylhydantoin (towards the latter stages as the reaction progresses) can serve as a potential base to favor the trimolecular transition state leading to the formation of *anti*-product. Hence, at higher reagent concentration (favoring the trimolecularity) the *anti*-adduct dominates while, at lower reagent concentration (lower *local* concentration reduces the probability for trimolecularity) the *syn*-adduct is preferentially formed. To corroborate the results from computational analysis, we performed a detailed study using '*RPKA*' analysis, pioneered by Blackmond and co-workers.[38] The kinetic studies revealed a reaction that is first order in the alkenoic acid and 3/2 order in DCDMH. This result supports the fact that more than one molecule of the reagent (DCDMH) is

involved in the RDS of this chlorolactonization. Analyses of the kinetic complexities of these processes are in progress.

Furthermore, to highlight the fact that *anti*-addition on **II-1** requires trimolecularity, we measured the *anti/syn* ratios in halolactonization of **II-5**-D (seeTable II-2). The carboxylate in **II-5**-D does not require assistance of a third component to serve as base, hence, as in **II-2**, the carboxylate **II-5**-D also displays a linear trend and an enhanced preferenced towards *anti*-addition. A similar behaviour is observed when halolactonization of **II-1**-D was performed in presence of 20 mol% base (quinuclidine or DABCO).[19] Finally, the dependence for *anti:syn* addition in the halolactonization of **II-1**-D has been catagorized as follows:

a. Halenium ion dependence:

As anticipated, with increasing size of the halenium ion, the sterically congested TS leading to *syn* adduct becomes more energetic in comparison to the TS for *anti*-addition. This leads to a higher *anti:syn* ratio in the halolactonization of **II-1**-D. As shown in Table II-3, the preference for *anti* adduct increases in the expected order: Cl < Br < I.

Table II-3. *anti*:*syn* ratios for halolactonization of **II-1**-D. The halolactonization displays a high preference for *anti*-addition with increasing size of the halenium ion.

Concentration (M) of **II-1**-D (and halenium source)	*anti*/*syn* for *chlorolactonization*	*anti*/*syn* for *bromolactonization*	*anti*/*syn* for *iodolactonization*
1.0	2.3	19	>20
0.5	2.1	--	--
0.1	1.1	9.5	>20
0.05	0.9	9.05	--
0.025	0.7	--	--
0.0125	0.7	8.3	>20

b. Solvent dependence:

Although the observed results cannot be generalized to known solvent effects, non-polar solvents seem to promote the *anti*-adduct in chlorolactonization of **II-1**-D with acetone being an exception (Table II-4).

c. Dependence of *anti:syn* ratio on the acidity of DCDMH vs monochlorohydantoin:

As described above, the TS leading to the formation of *anti*-adduct from **II-1** requires a third component (apart from **II-1** and DCDMH) that can engage H-bonding interaction with the carboxylic acid while it is activating the olefin (see Figure II-17). During the early stages of the reaction, this role can be fulfilled by DCDMH. However, with the depletion of DCDMH (as the reaction progresses), the byproduct monochlorohydantoin has to engage the H-bonding interaction (with -COOH of **II-1**) to stabilize the TS for *anti*-addition. Since, the N-H in monochlorohydantoin, by itself is relatively acidic (pKa = 7.17),[58] the TS leading to *anti*-addition should be less favored, especially towards the later stages of the reaction. Our ^{1}H NMR analysis display a slight decrease in the *anti*-addition during the latter stages of chlorolactonization of **II-1**-D

Table II-4. Solvent effect on *anti*:*syn* ratio for halolactonization of **II-1**.

Solvent (*conc. of **II-1**-D = 0.05M*)	*anti*/*syn* from **II-1**-D
Acetone	10
Hexanes	4.5
Carbon Tetrachloride	3.5
Acetonitrile	3.5
HFIP	1.9
DMF	1.7

Table II-5: Dependence of *anti*:*syn* ratio on the acidity of DCDMH vs monochlorohydantoin. The following chlorolactionization of **II-1**-D was performed at 0.05 M substrate concentration.

time (h)	*anti*/*syn* from **1a**-D
1	1.03
10	0.90
20	0.85
70	0.85

(Table II-5).

Most importantly, these studies highlight the enabling role of nucleophile and corroborate the computationally derived hypothesis for the molecularity of *syn* and *anti* addition processes in halofunctionalization of **II-1**. This hypothesis is further validated by the following K^{16}_{O}/K^{18}_{O} studies using ^{18}O enriched **II-1** to provide a definitive evidence towards the participation of nucleophile in electrohilic addition to olefins.

The isotope effects and variable *syn*:*anti* ratio results above firmly argue against an open carbenium ion intermediate in cyclization of **II-1**. Our own previous studies and reports from other groups as well have questioned the generality of the bridged haliranium ions in halofunctionalizations. The subtleties encountered just in investigating the halofunctionalization of olefins call for further comprehensive analysis in order to understand the continuum of possible mechanistic pathways operating in several electrophilic addition reactions. The following studies with several aliphatic and aromatic probes validate the generality of *NAAA* hypothesis.

II.3.4. Imperative role of nucleophile.

In their halofunctionalization studies, Williams, Dangat and Wirth made the intriguing observation that catalytic amounts of nucleophilic anions substantially enhance reaction rates.[20,46,59] Furthermore, in chlorofunctionalizations of 1-phenylpropenes, Fahey reported significant variations in product distribution merely by varying the choice of nucleophile. These experimental results point to nucleophile participation in determining reaction rates and stereoselectivities.[20,32,46] Moreover, based on *HalA* predictions, the π-systems of the olefins shown in Figure II-9 are incapable of abstracting the chlorenium ion by themselves, from any of the commonly used imide-based halenium donors. The NAAA hypothesis entails interaction of a nucleophile with the olefin's π-system (to raise its HOMO energy) leading to capture of an electrophile. To probe the *NAAA* hypothesis, we selected the intramolecular halolactonization of the dienoic acid **II-6** as a model reaction (Figure II-18). The nucleophilicity of the carboxylic acid moiety's is easily altered by addition of basic additives, while the rigidity of the cyclic framework restricts the conformational freedom of the carboxylate nucleophile. The intramolecular halolactonization of substrate **II-6** and its tetra *n*-butylammonium (TBA) salt **II-7** were therefore studied in detail. Based on classical hypothesis, the olefin-halenium adduct can be defined by either intermediates **A** or **B** (Figure II-18). If initial attack on the π-bond forms the haliranium ion, the tertiary carbon would be expected to bear the greatest positive character or even exist as an open carbenium ion. [22,60] The nucleophile would then close the ring by attack on the most electrophilic site, the tertiary carbon, to form product II-**6a**. Given that chlorenium ions do not exchange between halogenated alkenes,[35] intermediates **A** and **B** (Figure II-18a) should be both rate and product-determining. Therefore, altering the nucleophilicity should not significantly alter the overall regioselectivity or rate.

Figure II-18. a. Classical prediction for the outcome of halolactonization of **II-6** b. NAAA prediction for regioselectivity of halolactonization of **II-6** and **II-7** based on enhanced nucleophile strength.

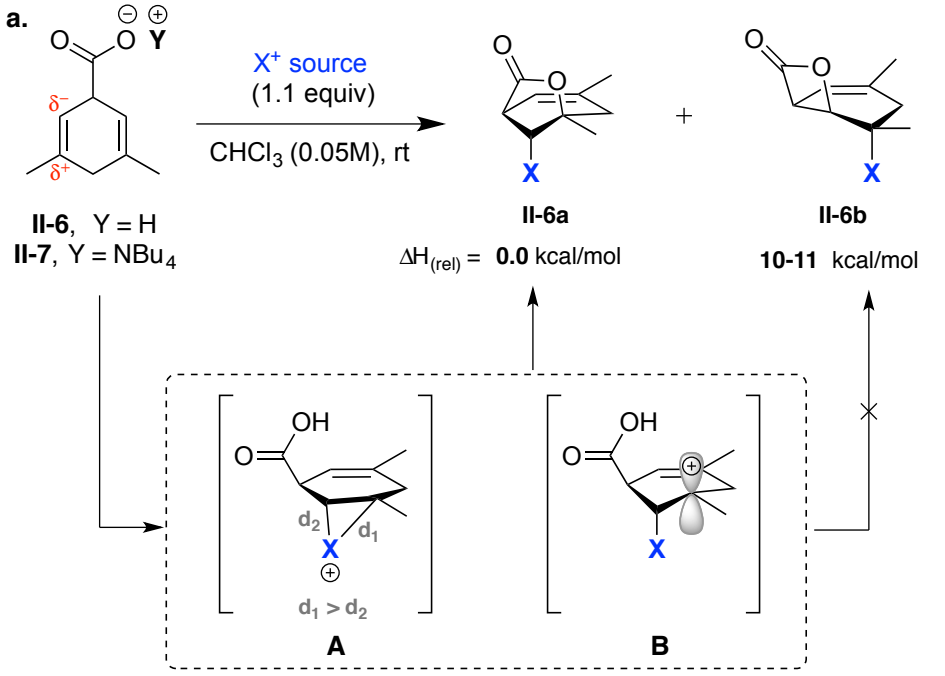

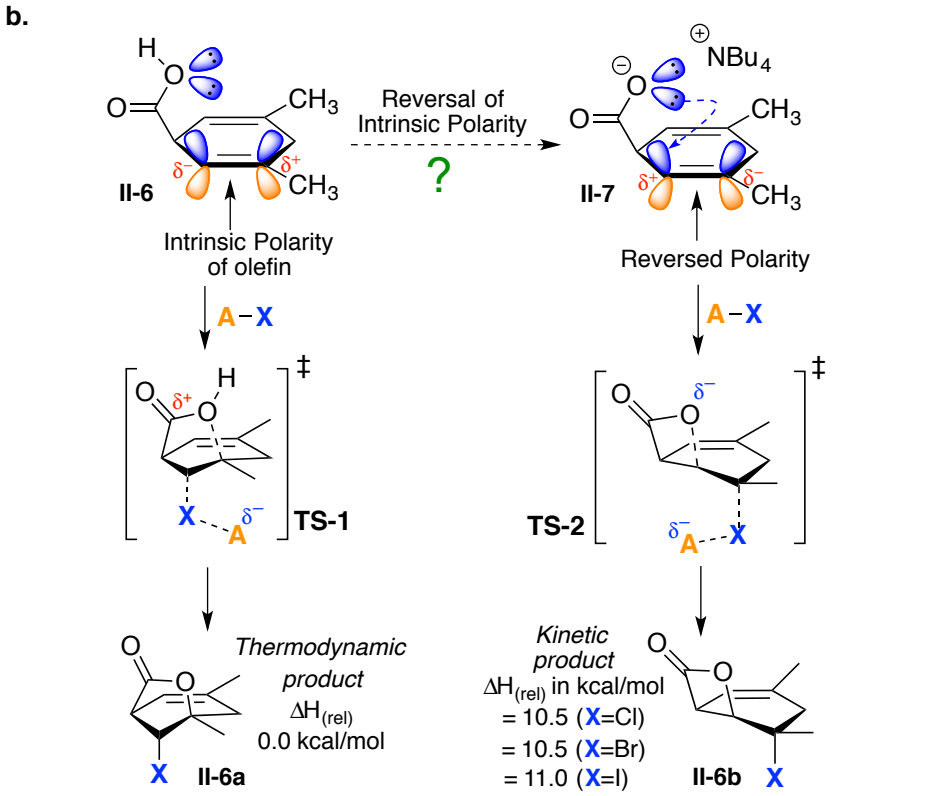

On the contrary, if the reaction proceeds through a nucleophile assisted pathway, substrate **II-6** bearing a weakly nucleophilic carboxylic acid moiety should give the same product (**II-6a**) via a asynchronous concerted pathway (Figure II-18b). Furthermore, enhancing the nucleophilic character of the carboxyl group in **II-6** may cause a reversal in the intrinsic polarity of the olefin leading to a contemporaneous capture of the halenium atom at the tertiary carbon yielding the 4-*exo*-halolactones- **II-6b**. The regioselectivity of these strained products will be governed by the conformation preference of the "activated" nucleophile. Moreover, the rate of the

Table II-6. Halolactonization of **II-6** and **II-7**. 1,3-dichloro-5,5-dimethylhydantoin (DCDMH), *N*-bromosuccinimide (NBS), *N*-iodosuccinimide (NIS). [a]Isolated yields. [b]Ratios were determined by ^{1}H NMR analysis (500 MHz). Values in parenthesis are for reactions that were catalyzed using 20 mol% quinuclidine as an amine base.

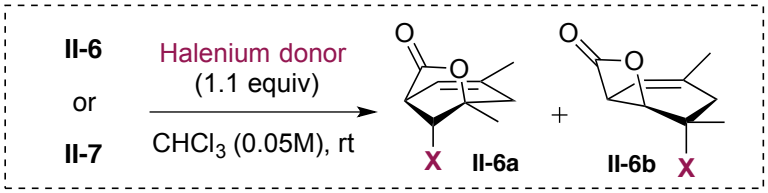

Entry	Substrate	Halenium donor	Time (min)	Overall yield[a]	ratio[b] **II-6a** :**II-6b**
1	**II-6**	DCDMH	240 (30)	84% (88%)	>98:2 (10:1)
2	**II-6**	NBS	180 (30)	97% (>99%)	>98:2 (11:1)
3	**II-6**	NIS	180 (30)	89% (90%)	>98:2 (>98:2)
4	**II-7**	DCDMH	>2	95%	2:1
5	**II-7**	NBS	>2	>99%	2.5:1
6	**II-7**	NIS	>2	93%	>98:2

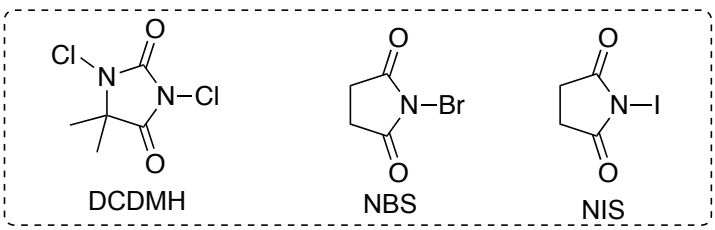

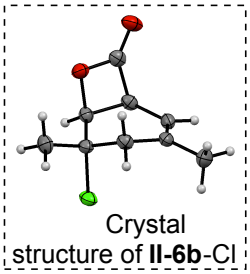
Crystal structure of **II-6b**-Cl

reaction will be dictated by the *strength* of the nucleophile; stronger the nucleophilicilty-faster the rate. As anticipated, the weak nucleophile in **II-6** under non-catalyzed halolactonization conditions (Table II-6, entry 1) did proceed as anticipated to furnish regioselectively, the 5-*endo*-halolactones **II-6a**. Screening of achiral amine catalysts revealed that addition of 20 mol% of quinuclidine gave an 8-fold rate enhancement (values in parenthesis under entry 1). Interestingly, in this case, about 9% of the thermodynamically disfavored chlorolactone **II-6b-**Cl was also isolated. Formation of this 4-*exo* cyclization product under prototypical halolactonization conditions raises the following questions: a.) Why would the classically expected, bridged chloronium ion (more appropriately 'chloriranium ion') furnish the strained-ring product **II-6b**-Cl under base catalyzed conditions?; and b.) is it the nature of the base used or the presence of the internal nucleophile that enables formation of such a strained product (a β-lactone and a quaternary chloride fused to a cyclohexene framework)? To address the latter question, the tetra-n-butylammonium salt (**II-7**) was subjected to chlorolactonization under the same conditions (entry 4), yielding 33% of product **II-6b**-Cl and displaying another 15-fold rate enhancement.

Halolactonization of the free acid **II-6** gave the corresponding 5-*endo* halolactones **II-6a** (Table II-6) with all halogenating agents. On the other hand, addition of 20 mol% basic amine (quinuclidine) as a catalyst, or the use of salt **II-7** resulted not only in significant rate acceleration, but also in formation of the 4-*exo*-lactones **II-6b**. This regiochemical switch clearly suggests a central role for the nucleophilic partner in the addition. Reaction of the substrate with enhanced nucleophilicity forms a kinetic product that is not only at odds with the intrinsic polarity of the π-system, but also strained, and thus thermodynamically disfavored by over 10.0 kcal/mol over the 5-*endo* lactone. The exclusive *anti*-addition observed for the overall addition (confirmed by ^{1}H NMR and X-ray structure) in products **II-6a** and **II-6b** rules out the formation of a carboxyl hypohalide (-CO_2-X) as an intermediate, due to its tendency to undergo *syn* addition.

To test the validity of increased nucleophilicity as the defining influence for regioselectivity, we resorted to haloetherification of the same core. Substrate **II-8** incorporates an alcohol moiety, more nucleophilic than the carboxylic acid in **II-6**, but neutral, unlike the carboxylate in **II-7**. As anticipated, the non-catalyzed bromoetherification of **II-8** gave a higher 4- *exo*:5-*endo* product

Table II-7. a. Halolactonization of **II-8** b. Halolactonization of **II-9**. 1,3-dichloro-5,5-dimethylhydantoin (DCDMH), *N*-bromosuccinimide (NBS), *N*-iodosuccinimide (NIS). [a]Isolated yields. [b]Ratios were determined by ^{1}H NMR analysis (500 MHz). [c]Ratios could not be determined by crude ^{1}H NMR analysis. Values in parenthesis are for reactions that were catalyzed using 20 mol% quinuclidine as an amine base.

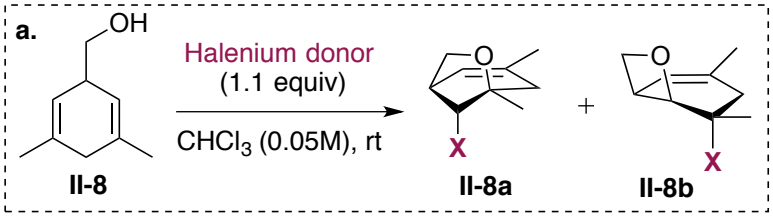

Entry	Substrate	Halenium donor	Time (min)	Overall yield[a]	ratio[b] **II-8a** : **II-8b**
1	**II-8**	DCDMH	40 (15)	64% (75%)	n.a[c]
2	**II-8**	NBS	30 (10)	81% (92%)	5:1 (5:1)
3	**II-8**	NIS	30 (10)	86% (89%)	>98:2 (>98:2)

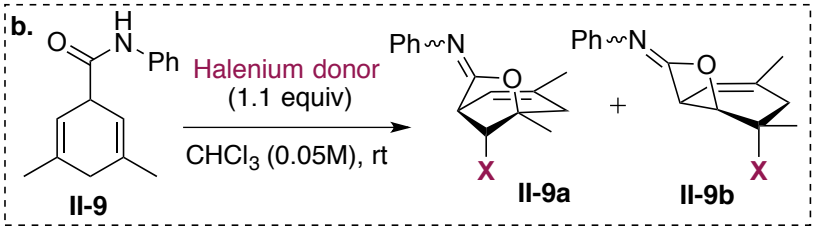

Entry	Substrate	Halenium donor	Time (min)	Overall yield[a]	ratio[b] **II-9a** : **II-9b**
1	**II-9**	DCDMH	600	78%	>98:2 (*E*:*Z* = 1:1)
2	**II-9**	NBS	8400	88%	>98:2 (*E*:*Z* = 1:1)
3	**II-9**	NIS	10800	76%	>98:2 (*E*:*Z* = 1:1)

ratio (**II-8b**-Br: **II-8b**-Br) than the corresponding bromolactonization of **II-6**, see Table II-7. Furthermore, addition of quinuclidine as a base additive did not make any difference to the regioselectivity of this reaction. This result is consistent with the fact that an amine base cannot deprotonate the alcohol before it has engaged the nucleophilic attack; however, the base does help to stabilize the TS for haloetherification (H-bonding interactions) and hence, an enhancement in the observed rate. On the other hand, lowering the nucleophilicity by incorporating amide

Table II-8. Halolactonization of **II-10** and **II-11** displaying the role of a conformationally rigidified nucleophile in determining the regioselectivity of the overall addition. [a]Isolated yields. [b]Ratios were determined by ^{1}H NMR analysis (500 MHz).

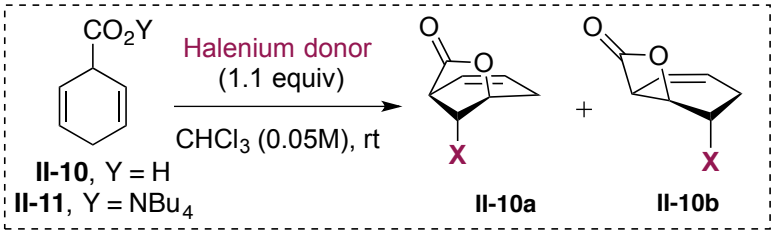

Substrate	Halenium donor	Time (min)	Overall yield[a]	ratio[b] **II-10a** : **II-10b**
II-10	DCDMH	480	73%	<2:98
II-10	NBS	840	86%	<2:98
II-10	NIS	840	75%	1:20
II-11	DCDMH	>2	91%	<2:98
II-11	NBS	>2	>99%	<2:98
II-11	NIS	>2	80%	<2:98

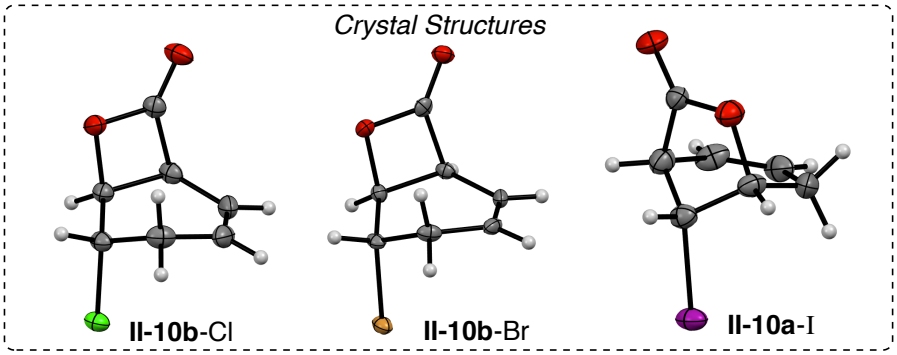

functionality in substrate **II-9** furnished solely the 5-*endo* cyclized products **II-9a**, and only after a relatively longer reaction time. Iodofunctionalization of either of these substrates failed to form the 4-*exo* products. This could be due to the overriding steric cost of bearing an iodo-substituent on a quaternary carbon.

Dihydrobenzoic acid (**II-10**), in which the olefin sites have unbiased intrinsic polarities, favored the 4-*exo* products almost exclusively when its tetra-*n*-butylammonium (TBA) salt (**II-11**) was the alkene substrate (Table II-8). As an important note, based on electron withdrawing inductive effect of the carbonyl group in **II-10** and **II-11**, the classical pathway will predict an opposite sense of regioselectivity towards formation of halolactones **II-10b**.

The findings above reveal the nucleophile's key role in directing halofunctionalization reactions. The increased nucleophilicity not only accelerates rates by orders of magnitude but also overrides the intrinsic polarity of the olefin towards electrophilic halenium attack. These results, however, are not sufficient to rule out the existence of haliranium ions as possible intermediates. To probe further, open-chain substrates and their corresponding TBA salts were examined for regioselectivity and rate enhancement as follows.

II.3.5. Regiospecificity of a conformationally constrained nucleophile.

Substrate **II-12** (Figure II-19) incorporates a *cis*-olefin in conjugation with a phenyl ring. The aliphatic side chain incorporating the carboxylic acid at its terminus is conformationally contrained by allylic strain due to the *cis*-geometry of the olefin. Considering the classical mechanism (paths A or B, Figure II-19), the carboxylic acid side chain in intermediate-**I** from path A should be conformationally free as the olefinic carbons are now re-hybridized to a non-planar geometry, alleviating the allylic strain. Benzylic stabilization then would render the haliranium ion asymmetric, guiding the regioselectivity of the overall addition to favor the 6-*endo* product ($d_1 > d_2$, intermediate-**I**, Figure II-19). Stereodefined products, with *syn*-orientation of the phenyl and

Figure II-19. Comparison of classical approach (path A and B) vs the regio-defined capture of the halenium by nucleophile pre-polarized π-system (path C).

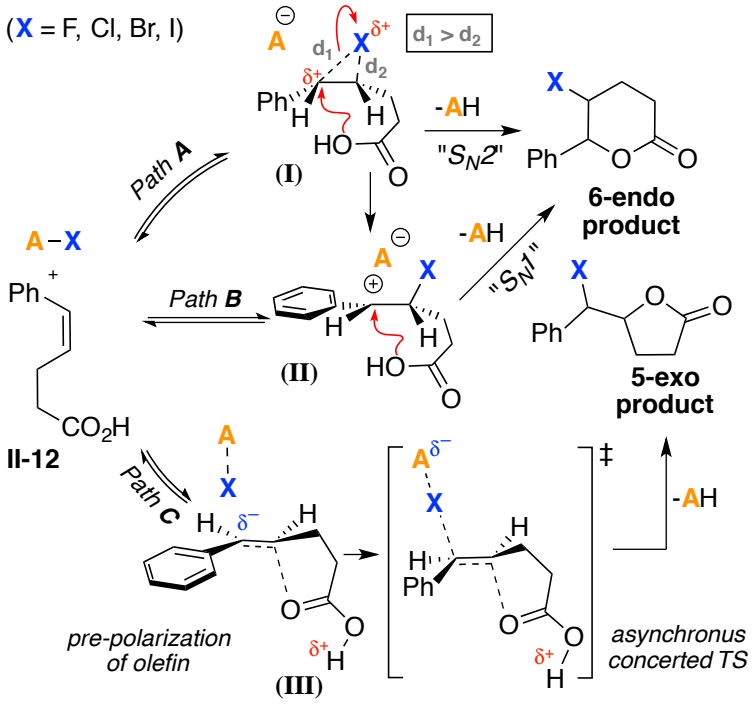

halogen, would thus be expected from intermediate-**I**. However, based on reports from Sauers and from our lab (based on *ab initio* estimations of styrylic systems with '*naked halenium ions*' in the absence of donor counter anions), path B is more likely; intermediate-**II** should have low rotational barrier (<3.5 kcal/mol) along the C^{+}-C-X bond.[19,30,31] Again, the 6-endo regioselectivity would be expected, but relative stereospecificity would be governed thermodynamically, favoring *anti*-products with both phenyl and halogen moieties in *equatorial* orientation.

In the case of Path C, the nucleophile donates into the alkene, raising the HOMO energy of its π-system. The conformational constraints imposed by the *cis*-olefin's allylic strain bias its reach to the homobenzylic carbon (intermediate-**III**). This pre-activated olefin then undergoes contemporaneous attack by the electrophilic halenium at the benzylic carbon and the carboxylate nucleophile at the neighboring site, ultimately furnishing 5-*exo* products, opposite to the sense of regioselectivity predicted for paths A or B. As seen in Table II-9, the experimental outcomes

Table II-9. a. Halolactonization of alkenoic acid **II-12** and **II-13**. b. Halolactonization of alkenoic acid **II-14** and **II-15**. [a]Isolated yields. [b]Ratios were determined by ^{1}H NMR analysis (500 MHz). [c]No isomerization observed for the recovered olefinic substrate. [d]No isomerization of the olefinic substrate was observed during the course of the reaction. [e]52% conversion. [f]19% conversion.

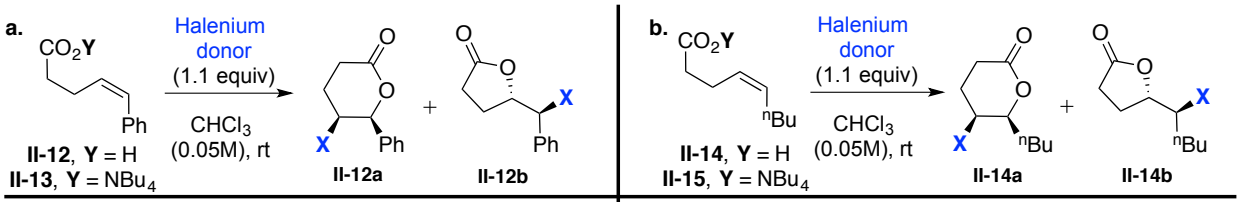

Substrate	Halenium donor	Time (h)	Overall yield[a]	ratio[b] **II-12a** : **II-12b**
II-12	DCDMH	144	no reaction	--[c]
II-12	NBS	28	89%	<2:98
II-12	NIS	30	86%	<2:98
II-13	DCDMH	12	78%	<2:98[d]
II-13	NBS	1	96%	<2:98
II-13	NIS	1	93%	<2:98

Substrate	Halenium donor	Time (h)	Overall yield[a]	ratio[b] **II-14a** : **II-14b**
II-14	DCDMH	96	35%[e,c]	<2:98
II-14	NBS	96	15%[f,c]	<2:98
II-14	NIS	72	85%	<2:98
II-15	DCDMH	1	90%	<2:98
II-15	NBS	1	94%	<2:98
II-15	NIS	1	87%	<2:98

support the mechanism of path C. Substrate **II-12** exclusively yields the 5-*exo* halolactones (**II-12b**). Boosting the nucleophilicity (substrate **II-13**) does not make any difference to the observed regioselectivity, but the reaction rate is significantly higher. Thus, the putative Van der Waals complex A (Figure II-9d) of the olefin and the halenium donor reagent requires the nucleophile's assistance to re-hybridize the olefin's sp^2 carbons. Path C (Figure II-19) thus bypasses the benzylic stabilization invoked in paths A and B, explaining the observed regiochemistry. Moreover, the recovered staring material from the chlorolactonization of **II-12** and **II-14** did not undergo isomerization, suggesting that mechanistic pathways (such as path A or B) that caould lead to stereorandomization are not operational. Substrates **II-14** and **II-15**, lacking the possibility of benzylic stabilization, show a similar effect where the kinetically favored 5-*exo* products (**II-14b**) are formed exclusively. Furthermore, as reported by Denmark et al. the *Z*-alkenoic alcohols

display similar regiopreferences with enhanced reaction rates in comparison to the corresponding alkenoic acids.[61]

II.3.6. Interaction of nucleophile with olefin π-system in absence of halenium ion donor.

If a nucleophile interacts with the π* of C=C to alter its HOMO energy, then such an interaction should exist even in the absence of an electrophile. To probe this possibility, we resorted to NMR studies in $CDCl_3$ as a solvent. The NMR shifts of the olefinic protons and carbons in $CDCl_3$ should show effects when the electronics of a remotely tethered nucleophile are modified. As shown in Figure II-20, our NMR studies clearly demonstrate the '*through-space*' interaction of a remotely tethered nucleophile with the π–system of olefins. The olefinic components (H and C) in free acid **II-12** display proton resonances at 6.50 ppm for H_a and 5.62 ppm for H_b while the corresponding ^{13}C resonances appear at 130.4 and 129.8 ppm. Changing the tethered nucleophile to a primary alcohol (more nucleophilic than carboxylic acid) in **II-12**-OH leads to upfield shifts of the distal olefinic H_a's and corresponding carbons (C-H_a) whereas the more proximal H_b and C(-H_b) experience de-shielding (downfield shift) relative to their parent acid. It is important to note that inductive effects will not result in a shielding effect of an atom (C-H_a) located five bonds away and a de-shielding effect on an atom (C-H_b) that is four bonds away. This differential effect can be attributed to the interaction between the non-bonding electrons of the nucleophile and the π* orbitals of olefin. The extended conjugation as a result of a '*through-space*' interaction leads to a kinetically governed conformational preference of the side chain such that the electron density increases at C-H_a (shielding effect), see Figure II-20, dashed box. Consistent with the reactivity patterns, increasing the nucleophilicity extends and magnifies this polarization; carboxylic acid **II-12** treated with 1.0 equiv of an organic base (quinuclidine), and the tetra-n-butyl ammonium salt **II-13** display the same trend with enhanced effect.

Furthermore, treatment of **II-13** with substituted pyridines display an enhanced polarization of the olefin with increasing pK_a of the pyridine derivative. Table II-10 represents the effects on ^1H and ^{13}C resonances of the olefin upon altering the nucleophile strength of a functionality tethered remotely on the alkene. To *fine-tune* these effects we resorted to NMR studies of substrate **II-12** upon its treatment with bases exhibiting a range of pK_a values. Table II-10 displays an ascending trend of nucleophile assisted olefin activation as the basicity of the added base increases. Weak bases such as 4-cyanopyridine, 2,6-di-tert-butylpyridine and pyridine (entries 1-3) whose conjugate acid has a pK_a similar to the carboxylic acid (pK_a assumed to be approximately 4.5),[62] do not affect the ^1H and ^{13}C resonances of the olefin to any observable extent. In contrast, stronger Lewis bases, 2,4,6-lutidine, DABCO and quinuclidine result in an upfield shift of the distal carbon C5(-H_a) and the corresponding proton H_a whereas, the de-shielding (downfield shift) is observed for the more proximal C4(-H_b) and H_b. The magnitude of this effect depends on the pK_a of the base employed. It is important to note that the ability to modulate nucleophilic character of a carboxylic acid by varying the basicity of the Lewis base provides with a handle to guide the course of the reaction; thermodynamic or kinetic.

Figure II-20. NMR resonances of olefinic C and H (at room temperature in $CDCl_3$) displaying the interaction of a remotely tethered nucleophile with the π-system upon modulation of the nucleophilic strength.

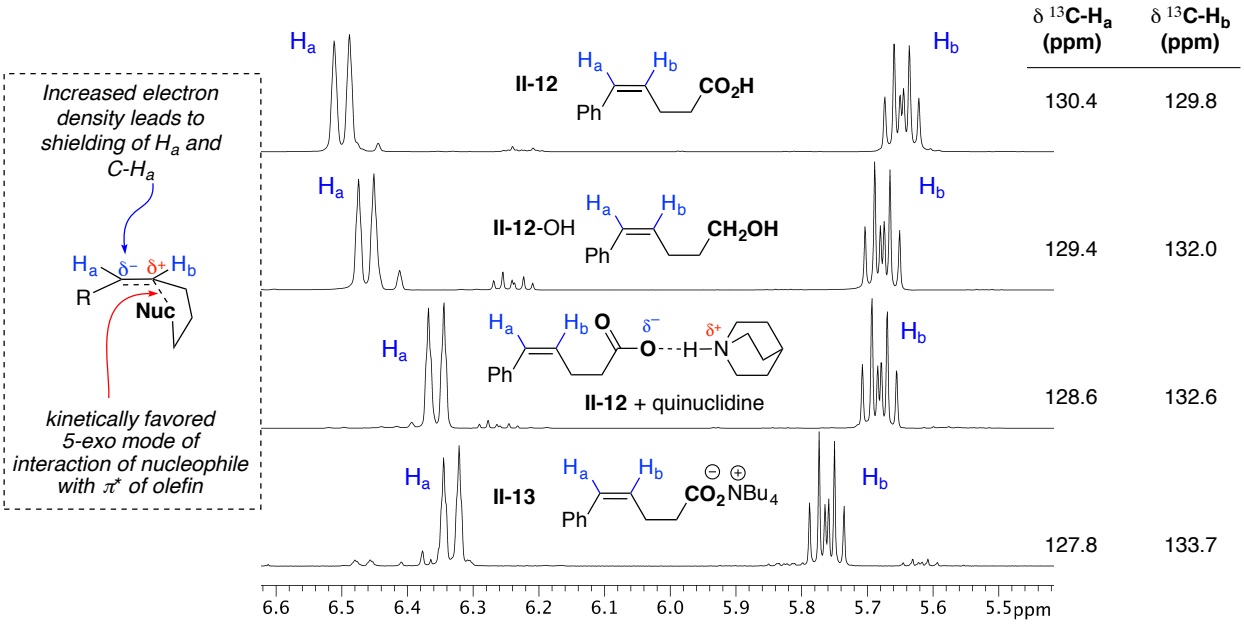

Entry	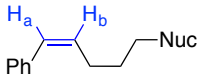	δHa (ppm)	δHb (ppm)	δ13C-Ha (ppm)	δ13C-Hb (ppm)
1	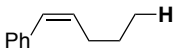	6.41	5.68	133.0	128.8
2	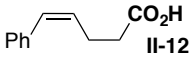 **II-12**	6.48	5.62	130.4	129.8
3	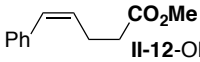 **II-12**-OMe	6.49	5.64	130.3	130.2
4	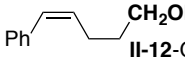 **II-12**-OH	6.44	5.66	129.4	132.0
5	**II-12** + 1.0 equiv. quinuclidine	6.34	5.66	128.6	132.6
6	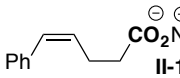 **II-13**	6.30	5.73	127.8	133.7

Table II-10. Correlation of *basicity* to *nucleophilic activation* of an olefin by carboxylic acid. Effect on ^{1}H and ^{13}C resonances of **II-12** (at room temperature in $CDCl_3$) upon treatment with bases.

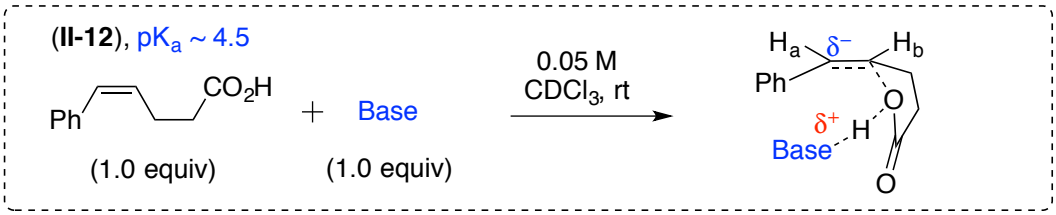

Entry	Base	pK_a of conjugate acid (in H_2O)	δH_a (ppm)	δH_b (ppm)	$\delta^{13}C$-H_a (ppm)	$\delta^{13}C$-H_b (ppm)
1	*none*	---	6.48	5.62	130.4	129.8
2	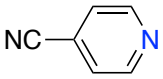	1.90	6.48	5.63	130.2	130.0
3	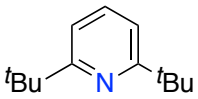	4.95	6.48	5.63	130.4	129.9
4	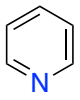	5.21	6.45	5.66	130.5	129.5
5	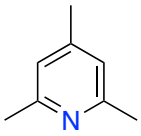	7.43	6.43	5.66	129.7	130.9
6	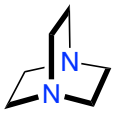	8.82	6.39	5.64	129.2	131.6
7	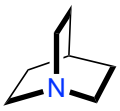	11.0	6.34	5.66	128.6	132.6
8	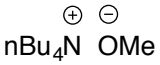	15.5	6.30	5.73	127.8	133.7

Increasing Basicity / *Enhanced activation of olefin*

Figure II-21. ^{1}H and ^{13}C resonances of **II-13** (at room temperature in $CDCl_3$) over a range of concentration (1.0 M to 0.001 M)

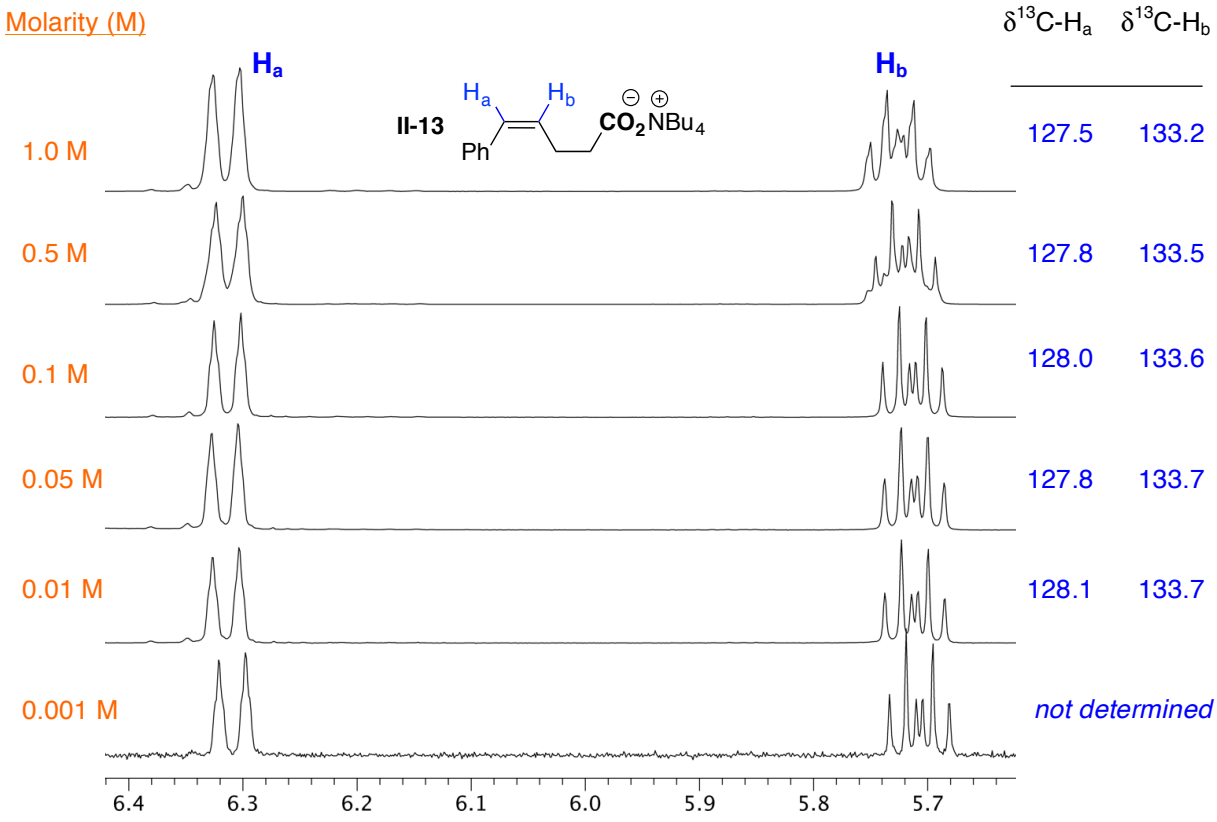

The ^{1}H and ^{13}C resonances observed are concentration independent. To verify whether the change in ^{1}H and ^{13}C resonances of the olefinic moiety were due the proposed '*through-space*' interaction and not because any aggregation effect, we studied the NMR of **II-13** under different concentrations. Figure II-21 depicts the ^{1}H and ^{13}C resonances of **II-13** in $CDCl_3$ at room temperature at different concentrations ranging from 1.0 M to 0.001 M. The unchanged ^{1}H and ^{13}C resonances over a wide range of concentration imply absence of aggregation or any concentration dependent phenomenon that can potentially affect the observed chemical shifts. Similarly, **II-12**, **II-12**-OH and the acid-base complex **II-12** with quinuclidine (Figure II-20, entries, 2, 4 and 5) did not show any effect of concentration of their corresponding chemical shifts.

These observations are consistent with quantum chemical NMR shift calculations on the lowest energy conformations of **II-12**, **II-12**-OH and **II-13** at the B3LYP/EDF2 level of theory. The additional examples shown below substantiate the same hypothesis of '*through-space*' interaction. The carboxylate salts display an enhanced activation of the olefin in comparison to the corresponding free acids.

Alkenoic acids and the corresponding carboxylates were then subjected to conformational search at the B3LYP/6-31G* (gas phase) level of theory. Geometry optimization was performed

Figure II-22. a. ^{1}H and ^{13}C resonances of alkenoic acid **II-12** predicted at the B3LYP/EDF2 level of theory. The conformers were initially subjected to geometry optimization at the B3LYP/6-31G*/SM8 ($CHCl_3$) level. b. Orbital energies of **II-12** and **II-13** at HF/6-31G*.

a.

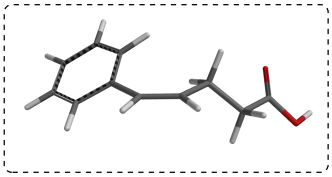

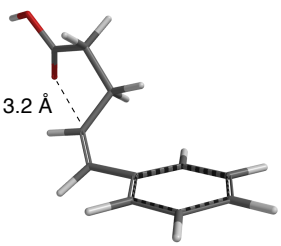

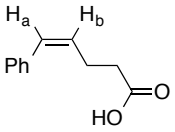

extended chain staggered conformer

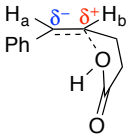

conformer exhibiting 'through-space' interaction

	$\Delta H_{(rel)}$ in kcal/mol B3LYP/6-31G*/ SM8 ($CHCl_3$)	Predicted ^{1}H and ^{13}C resonances (B3LYP/EDF2)			
		δH_a (ppm)	δH_b (ppm)	$\delta^{13}C$-H_a (ppm)	$\delta^{13}C$-H_b (ppm)
	0.0	6.50	5.80	131.9	130.7
	0.2	6.49	6.16	130.9	131.9
Boltzman gated average-predicted vs (experimental)					
		6.48	5.80	132.0	130.8
		(6.48)	(5.63)	(130.4)	(129.8)

b. Orbital energies (eV) evaluated at HF/6-31G*/SM8 ($CHCl_3$)

HOMO (eV)	LUMO (eV)	$\Delta E_{(LUMO-HOMO)}$ (eV)
-8.2	3.2	11.3

II-12

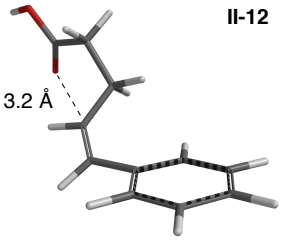

$\Delta\Delta E_{(LUMO-HOMO)}$ = 0.1 eV
= 2.3 kcal/mol

HOMO (eV)	LUMO (eV)	$\Delta E_{(LUMO-HOMO)}$ (eV)
-7.6	3.6	11.2

II-13

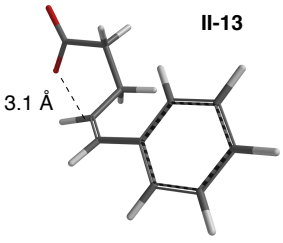

on these conformers at the B3LYP/6-31G*/SM8 ($CHCl_3$) level of theory. To confirm that each structure was a true minimum, vibrational analyses were performed. These optimized structures were evaluated for a.) orbital energies at the HF/6-31G*/ SM8 ($CHCl_3$) level of theory and, b.) NMR prediction at the B3LYP/EDF2 level of theory.

Substrate **II-12** and **II-13** were subjected to the above quantum chemical computational analysis. As shown in Figure II-22a, the two conformers of **II-12**, extended and coiled, although have similar energies (ΔH = 0.2 kcal/mol), their NMR resonances are quite different. As one would

Figure II-23. a. Modulation of HOMO energy of olefin in **II-1** upon its interaction with a nucleophile. b. Experimental evidence by ^{1}H NMR.

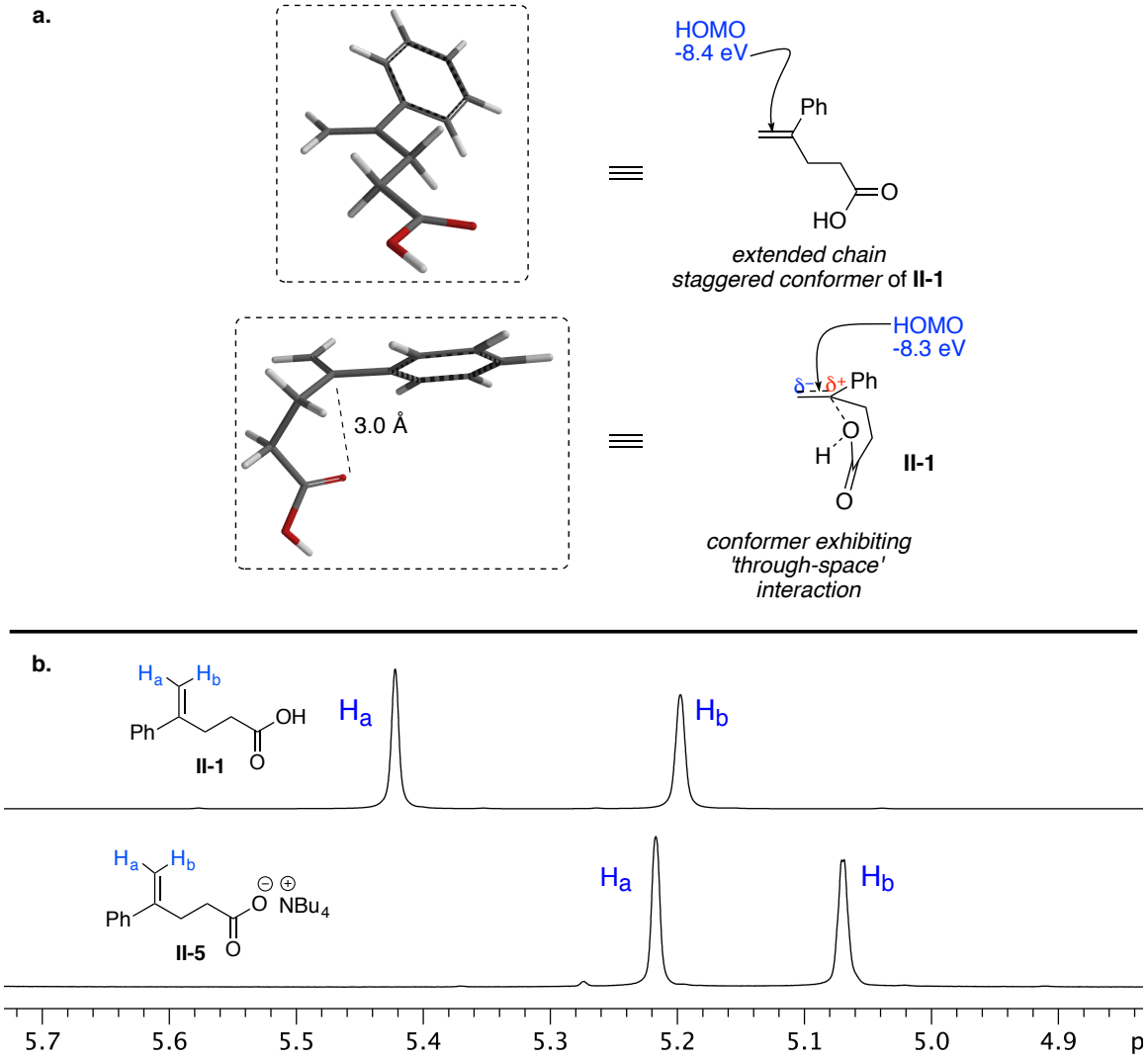

predict, the extended chain conformer exhibits downfield resonances (^{1}H and ^{13}C) at the benzylic position relative to the homobenzylic position. In contrast the coiled conformer displays a switch in the ^{13}C resonances as the nucleophile engages a '*through-space*' interaction with the homobenzylic carbon. In this conformer, the C5=C4$^{\cdots}$O=C interaction causes de-shielding (downfield shift) of the homobenzylic carbon (C4) whereas the distal C5 carbon experiences shielding effect as a result of accumulation of electron density. This effect is also evident by an increase of 0.1 eV in the HOMO energy of the olefin in the coiled conformer of **II-12**. As with any carboxylic acid, **II-12** will also tend to engage itself in the stronger intermolecular H-bonding interactions forming the carboxylic acid 'dimers', thus favoring the extended conformer over the coiled one. A Boltzmann gated NMR prediction at the B3LYP/EDF2 level of theory leads to the same conclusion as the Boltzmann averaged NMR resonances of the conformers of **1f** have more contribution from the extended conformer.

The computational analysis of **II-13** also validate the Nucleophile Assisted Alkene Activation (*NAAA*) hypothesis. In this case, the lowest energy conformer was found to be the coiled conformer (see Figure II-22b), as estimated at the B3LYP/6-31G*/SM8 ($CHCl_3$) level of theory. It is energetically favored over the extended conformer by 0.3 kcal/mol. Furthermore, as shown in Figure II-22b, the HOMO energy of the π-system in **II-13** is elevated by 0.5 eV (11.5 kcal/mol) in comparison to **II-12**, thus, predicting the carboxylate in **II-13** to be a stronger olefin activator. Similarly, as shown in Figure II-23, interaction of the carboxylic acid with the π-system of the olefin in **II-1** raises the olefin HOMO energy by 0.1 eV. This effect is more pronounced in substrates **II-6** and **II-7**, which incorporate a conformationally rigid framework (Figure II-24). The conformational rigidity of the cyclohex-1,4-diene framework is manifested in the extent of olefin activation by the nucleophile. The HOMO-LUMO energy gap in the parent alkene is attenuated by 0.3 eV upon incorporating the weakly activating carboxylic acid in **II-6**. The salt **II-7** further

Figure II-24. Orbital energies of **II-6** and **II-7** in comparison to 1,5-dimethylcyclohexa-1,4-diene.

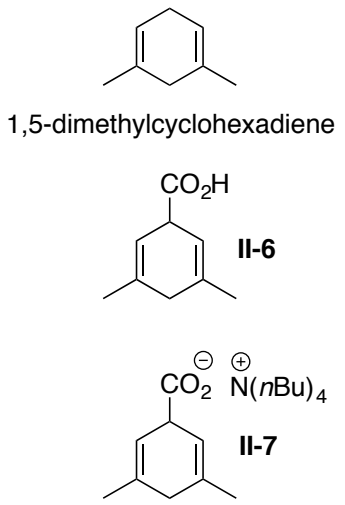

	HOMO (eV)	LUMO (eV)	$\Delta E_{(LUMO-HOMO)}$ (eV)	$\Delta\Delta E$ (eV)
1,5-dimethylcyclohexadiene	-8.8	5.1	13.9	
				0.3
II-6	-9.1	4.5	13.6	
				1.4
II-7	-7.5	4.7	12.2	

mitigates the energy gap by another 1.4 eV. Overall, the interaction of nucleophile with the π-system not only raises the HOMO energy, but also attenuates the HOMO-LUMO energy gap.

More importantly, these studies imply that the interaction between the nucleophile and the olefin may be a key mechanistic feature of electrophilic addition reactions in general. For instance, the thiourea catalyzed hydroamination reported by Jacobsen's lab involves activation of an alkene by a tethered hydroxylamine where the intrinsic α-effect leads to enhanced nucleophilicity of the amine nitrogen that allows polarization of the alkene without assistance of any metal ion.[63] Similarly, the exquisite regioselectivity reported by Sigman et. al. in the Pd(II) catalyzed functionalization of alkenes indicates a key role of the tethered alcohol nucleophile. [64] Finally, the inverse electron demand Diels-Alder reaction mediated tetrazine ligation with *trans* cyclo-octene reported by Fox et. al. displays several fold rate enhancement upon placement of a remotely tethered nucleophilic alcohol moiety on the *trans* cyclo-octene, capable of polarizing the oleffin by exalting its HOMO energy.[65,66] As a class, olefins have similar HOMO energies, *NAAA* (in general)

attenuates the HOMO-LUMO gap allowing them to react with a variety of electrophiles (with a wide range of LUMO energies).

Finally, the examples in Figure II-25 display the same interaction between a nucleophile and an olefin regardless of the substitution pattern on the olefin. The conformation preference of the nucleophile dictates which of the olefinic carbons it interacts with. The proximal carbon displays a downfield shift in NMR as this interaction leads to a partially formed C-O bond. The distal olefinic carbon on the other hand displays upfield shift in NMR as the π-system is polarized by the nucleophilic moiety. This effect becomes more pronounced as the nucleophilicity is enhanced.

Figure II-25 ^{1}H NMR resonances of alkenoic acids and their corresponding salts

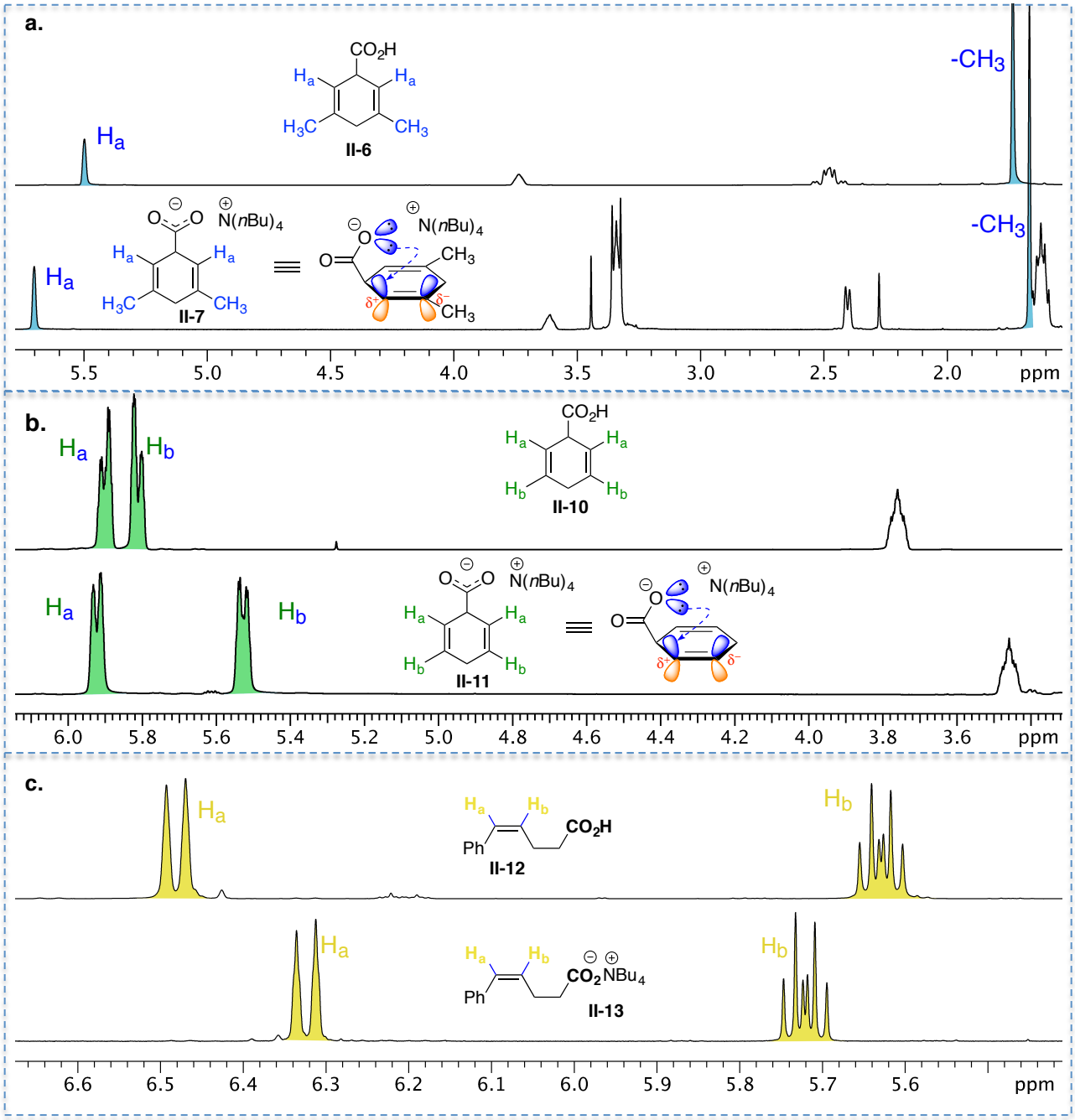

Figure II-25. (cont'd)

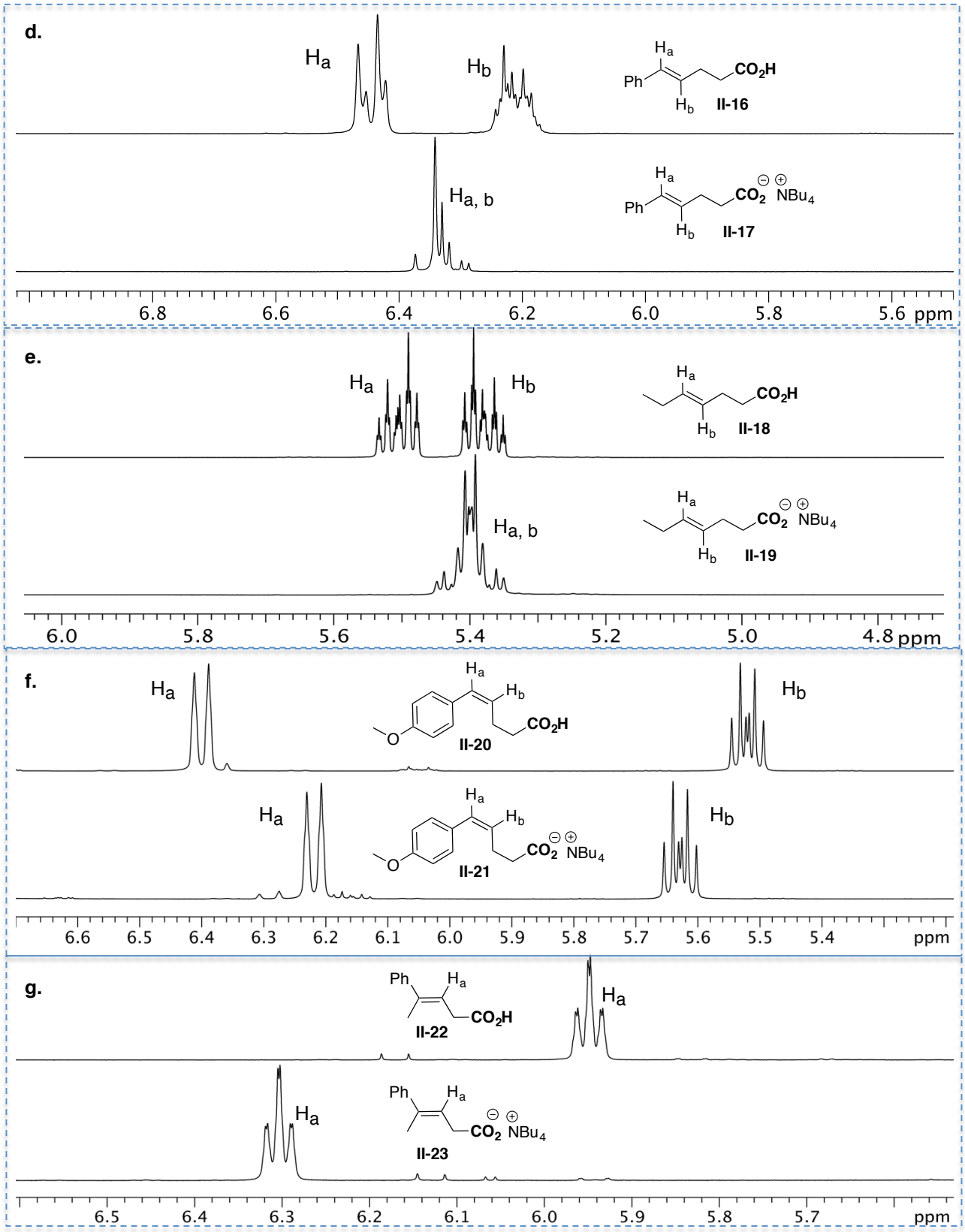

II.3.7. Unconstrained nucleophilic reach: Insinuation of '*early*' or '*late*' transition states.

For substrate **II-12**, the regiospecificity is governed by the conformational preference of the nucleophile tethered on the side chain of a *cis*-olefin. Conversely, for a *trans*-alkenoic acid, the stereoisomeric *trans* olefin, bears no restriction on the reach of the nucleophile to either of the olefinic carbons. Although kinetically, a 5-*exo* ring closure would be favored, modulation of the electronics on the nucleophile may enable access to the thermodynamically favored 6-*endo* product as well. Based on the electronegativity of the halenium atom and the strength of the nucleophile, the reaction path for halofunctionalization of a *trans* alkenoic acid can be directed either though a '*late*' or an '*early*' transition state (Figure II-26). For instance, given the order of electronegativity of halogens, (I < Br < Cl < F) the acceptor-halogen bond strength for a given acceptor also increases in the same order. Hence, by virtue of its relatively high electronegativity, a chlorenium atom in a halofunctionalization reaction will break the bond to its donor only after it has acquired enough electron density from its acceptor (and '*later*' than would an ionium atom), in a process analogous to the familiar S_N2 reaction at carbon. The lower the *HalA* value of a generic olefin, the more contribution from the nucleophile is required to complete the departure of the

Figure II-26. Accessing '*late*' vs '*early*' transition state based on *NAAA* hypothesis.

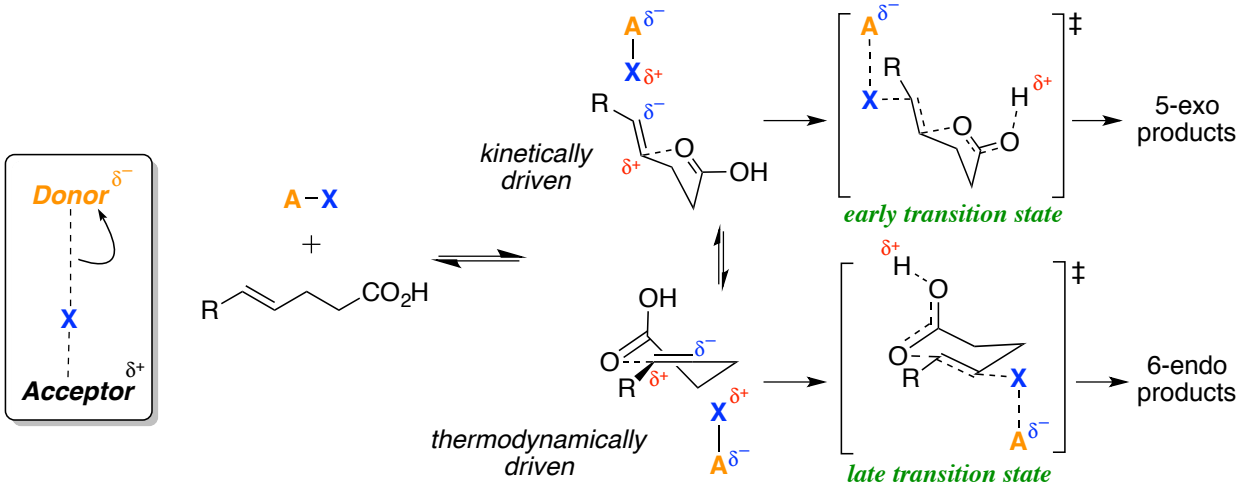

donor, pushing the transition state later. In turn, the later the resulting transition states, the more sensitive they are to thermodynamic parameters. In accord with the trend of electronegativity among halogens, a donor bearing a chlorine atom should lead to a late transition state as compared to the same donor bearing a bromine or iodine atom. Hence, for substrate **II-16** (Table II-11a), where the nucleophile has easy access to both the olefinic carbons, a *late* transition state (involving a chair conformation) will be more likely in chlorofunctionalization vs. bromo- or iodofunctionalization.

As anticipated, the chlorolactonization of **II-16** as well as its more nucleophilic counterpart **II-17**, favors the thermodynamic lactone **II-16a**-Cl, whereas, enhancing the nucleophilicity reverses the regioselectivity for bromo- and iodolactonization of substrate **II-17** (Table II-11a) towards the kinetic products **II-16b**. Substrates **II-16** and **II-17** are excellent probes, revealing the fact that regioselectivity in electrophilic addition reactions can be switched simply by modulating

Table II-11. Halolactonization of substrates **II-16** to **II-19**. [a]Isolated yields. [b]Ratios were determined by ^{1}H NMR analysis (500 MHz). [c]No isomerization observed for the recovered olefinic substrate. [d]No isomerization of the olefinic substrate was observed during the course of the reaction.

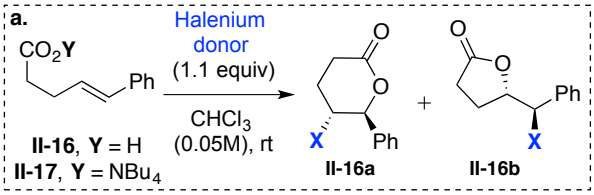

Substrate	Halenium donor	Time (h)	Overall yield[a]	ratio[b] **II-16a** : **II-16b**
II-16	DCDMH	144	20%[c]	>98:2
II-16	NBS	120	74%	>98:2
II-16	NIS	30	80%	7.7:1
II-17	DCDMH	18	79%	4.8:1
II-17	NBS	4	87%	1:13.5
II-17	NIS	2.5	78%	1:7.4

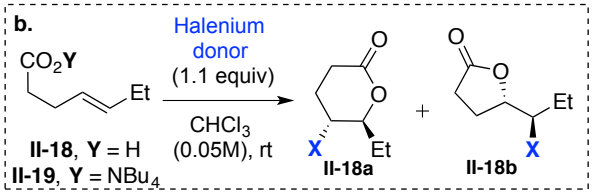

Substrate	Halenium donor	Time (h)	Overall yield[a]	ratio[b] **II-18a** : **II-18b**
II-18	DCDMH	96	70%	1:1.8
II-18	NBS	96	85%	1:4.3
II-18	NIS	2	85%	1:5.0
II-19	DCDMH	0.5	70%	1:2.1
II-19	NBS	0.5	89%	1:41
II-19	NIS	0.5	81%	1:45

the nucleophilicity of a given nucleophile and the electron deficiency of the electrophile involved. Substrate **II-18** on the other hand lacks the benzylic stabilization and hence the conformational preference of the nucleophile dominates in deciding the regioselectivity. Comparably, bromo- and iodolactonizations of **II-19** promote the kinetic products *via* early transition states, as boosting the nucleophilicity enhances the regiopreference towards formation of products **II-18b** (Table II-11b).

II.3.8. Effect of electrophilicity of halenium ion and nucleophlicity of olefin in halocyclization reactions.

The interplay of these effects have been discussed as follows:

(i) Leaving group ability (*HalA*) of halenium ion donor:

For substrate **II-12**, the regiospecificity is governed by the conformational preference of the nucleophile tethered on the side chain of a *cis*-olefin (Table II-12a, path C). Conversely, involvement of a relatively more electrophilic halenium ion source may lead to formation of a tight Van der Waals complex causing re-hybridization of the olefinic carbons thus, channeling the reaction *via* path B. Hence, modulation of the electronics on the halenium donor may allow us to

Table II-12. Effect of electrophilicity of halenium ion source on regioselectivity of halofunctionalization reaction.

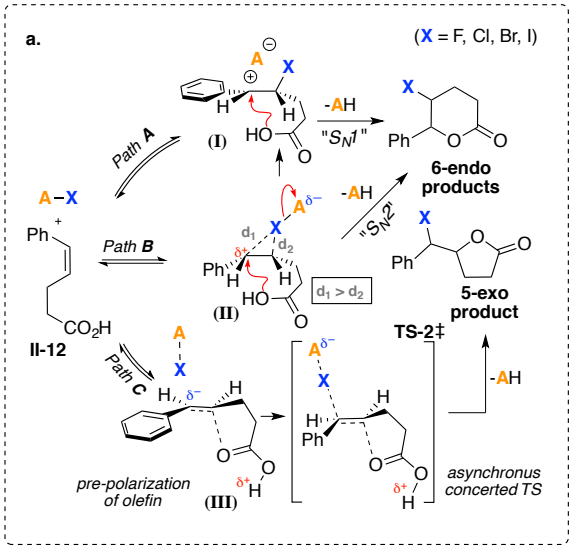

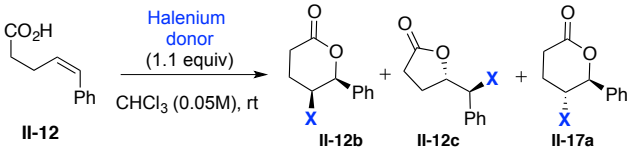

Entry	Halenium donor	ΔHalA[a]	Time (h)	Overall yield[b]	ratio[c] 12a :12b :17a
1	NCS	**0.0** (194.0)	180	no reaction	--
2	DCDMH	-12.9	144	no reaction	--
3	Dichloramine-T	-13.7	48	70%	1.0 : 1.1 : 1.4
4	NBS	**0.0** (170.6)	28	89%	>98 : <1.0 : <1.0
5	DBDMH	-11.7	5	58%	4.4 : 1.0 : 5.0
6	Br_2	-16.8	0.5	96%	<1.0 : 4.3 : 1.0

direct the reaction path though a '*late*' or an '*early*' transition state. Although the olefin moiety can engage itself in a weak Van der Waals interaction with a halenium ion (attached to its donor), the addition across the π–system will occur only with the aid of nucleophile participation *via* an asynchronous concerted pathway. The extent of re-hybridization of the olefinic carbons in the halenium ion-olefin complex, will depend on the leaving group ability of the donor anion and the electronic nature of the olefin. Hence, a tight Van der Waals complex that can re-hybridize the olefinic carbons to an extent that involves the resonance of the phenyl ring, will certainly direct the regioselectivity of addition to favor the 6-endo products. Table II-12 displays this switch in regioselectivity as the *HalA* value of the donor anion drops (i.e. the leaving group ability of the halenium ion donor increases).

(ii) Nucleophilicity of olefin:

On the contrary, substrate **II-20** with enhanced electron density on the olefin yields a mixture of *syn* and *anti* δ-lactones **II-20a** and **II-20b**, respectively (Table II-13). The pre-activated olefin due to the enhanced electron donating resonance effect of the p-methoxyphenyl moiety, does not require assistance of the nucleophile to exalt its HOMO energy. The formation of isomeric products imply multiple pathways being operational under the reaction conditions. Product **II-20a** arises from a halomethyl cabenium ion, **II-20b** might result from the same carbenium intermediate or it may be the result of *NAAA* pathway. Finally, product **II-20c** (not formed using the free acid **II-20**) is the outcome of *NAAA* pathway. Furthermore, employment of the salt **II-21** yields the 5-endo bromo and iodo-lactones **II-20c**-Br and **II-20c**-I, demonstrating the effect of enhanced nucleophilicity that outcompetes the intrinsic polarization of the olefin by the electron-rich aromatic nucleus.

Table II-13. Effect of nucleophilicity of olefin on regio- and stereoselectivity of halofunctionalization reaction.

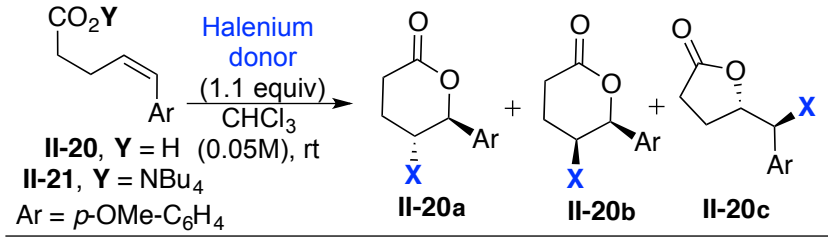

Substrate	Halenium donor	Time (h)	Overall yield[a]	ratio[b] **a** : **b** : **c**
II-20	DCDMH	12	80%	2.3 : 1.0 : <1.0
II-20	NBS	48	73%	1.3 : 1.0 : <1.0
II-20	NIS	5	66%	1.0 : 4.0 : <1.0
II-21	DCDMH	1	67%	1.0 : 1.3 : <1.0
II-21	NBS	0.7	32%	2.0 :1.0 : 46.0
II-21	NIS	1	--	<1.0 : <1.0 : >98.0

(iii) Strength of nucleophile vs nucleophilicity of olefin:

Substrate **II-22** and its salt **II-23**, incorporates a trisubstituted *E*-olefin in conjugation with a phenyl ring (Table II-14). Hence, it has ample opportunity to form a tertiary benzylic cation to yield a γ-lactone with scrambling of stereochemical information of the starting olefin. Furthermore, the conformation of the nucleophile being unconstrained, it can access either of the olefinic carbons to channel the reaction via *NAAA* pathway. Although kinetically, the 4-exo cyclization mode will be favored, the nucleophile will have to work against the intrinsic polarity of the olefin. Therefore, the free acid **II-22** (weak nucleophile) predominantly yields product **II-22b**. Substrate **II-23**, incorporating a strong nucleophile also favors the same 5-endo products, however it does yield

Table II-14. Effect of enhanced nucleophilicity of the nucleophile on regio- and stereoselectivity of halofunctionalization reaction.

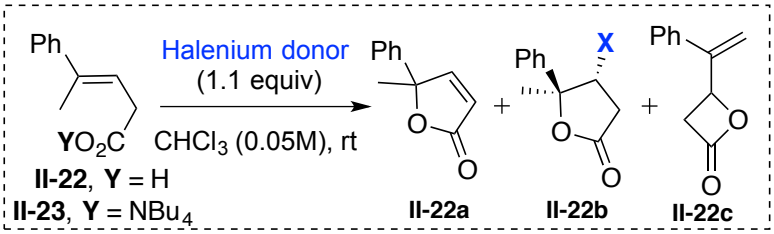

Substrate	Halenium donor	Time (h)	Overall yield[a]	ratio[b] **a:b:c**
II-22	DCDMH	96	71%	1.0 : 20.0 : <1.0
II-22	NBS	10	69%	<1.0 : 49.0 : <1.0
II-22	NIS	3	82%	<1.0 : 49.0 : <1.0
II-23	DCDMH	0.5	76%	3.8 : 1.3 : 1.0
II-23	NBS	0.5	88%	6.4 : 7.6 : 1.0
II-23	NIS	0.5	81%	>49.0 : <1.0 : <1.0

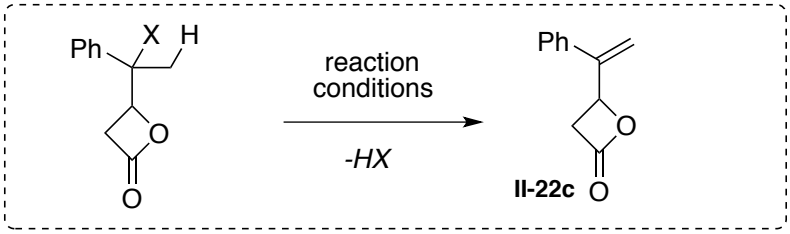

about 10-20% of the 4-exo products suggesting a central role for the nucleophilic partner in the addition reaction.

1.4. Summary.

Electrophilic addition to alkenes is certainly not as simple as it is perceived through classical mechanistic pathways. We have probed every facet of this reaction using halofunctionalization as a prototypical reaction and elucidated the key role played by every component that partakes in this reaction. Following is a brief account of the above studies:

a. Halofunctionalization reactions begin with a S_N2 attack of a Lewis base acceptor on a halenium atom (attached to its donor), displacing the donor anion as shown in equation (1):

$$LB: + X–D \rightarrow LB^{+}–X + D^{-} \text{.....(1)}$$

As in every S_N2 reaction, the forward reaction will be feasible only if the Lewis base (LB:) is a stronger nucleophile in comparison to the donor anion (D^{-}).

b. A hypothetical delivery of halenium atom to an alkene *via* commonly employed imide-based reagents or dihalogens, yield anions that have higher *HalA* values compared to weak Lewis base acceptors such as olefins.[47] Hence, in accordance to equation (1), halo-imides or dihalogens are inefficient towards transfer of halenium atoms to olefins without any external aid from nucleophiles. Experiments probed by *HalA* values validate this conclusion.

c. Although, there is precedence for existence of bridged halonium ions,[23-27,35,48,50] the conditions under which they are generated are however, very specific (not prototypical). Attachment of a halenium ion on an alkene as a bridged halonium ion requires counter anions such as trifluoromethanesulfonate, *p*-toluenesulfonate, tetrafluoroborate or antimony (VI) halides that are extremely weak nucleophiles, inheriting very low *HalA* values.

d. For olefins that enjoy extended conjugation from aromatic rings (e.g. **II-1-5**), the bridged halonium ion does not exist even with a '*naked*' halenium ion. Several groups[30,31,42-44] including ours[19,47] have reported this fact by thorough computational analysis and ^{13}C perturbation experiments for aliphatic as well as aromatic substituted olefins.

e. The aliphatic and aromatic substituted olefins employed as a probe for stereo- and regioselectivity in halofunctionalization reactions (**II-1-23**) clearly demonstrate the enabling role of nucleophile. The ground state kinetic conformational preference of a tethered

nucleophile dictates the direction of polarization, which eventually decides the regio- and stereoselectivity for the overall addition. The nucleophilic strength on the other hand governs the rate of the reaction. This effect of nucleophile on the π-system of alkenes (raising HOMO energy) is observed *via* NMR analysis, even in the absence of any external electrophile.

f. Electron rich olefins such as **II-2** (or enol ethers, enamines etc.) that have *HalA* value greater than the donor anion, may not require the assistance of nucleophile and the reaction then proceeds through a β-halocarbenium intermediate.

All the above results taken together with the detailed and exhaustive studies from other labs[30,31,42,44] demonstrates that formation of charged intermediates, such as the haliranium ion (bridged halonium ion) bearing a cationic halonium is unlikely under classical halofunctionalization reactions involving imide based reagents or dihalogens in general. As a class, olefins have similar HOMO energies, the assistance of nucleophile (in general) attenuates the HOMO-LUMO gap allowing them to react with a variety of electrophiles (with a wide range of LUMO energies). Currently, the efforts in our lab are focused on probing the validation of this hypothesis in several electrophilic addition reactions of olefins other than halofunctionalization of olefins and applying this mechanistic finding in conjunction with *HalA* to develop new stereoselective reactions of olefins. The shift in paradigm of the mechanistic picture now provides us with a handle to control the path of addition reactions; thermodynamic or kinetic.

II.5. Experimental section.

II.5.1. General information.

Molecular sieves (4Å) were dried at 160 °C under 0.25 mtorr pressure prior to use. Unless otherwise mentioned, solvents were purified as follows. $CHCl_3$ (amylene stabilized) was purchased from Sigma Aldrich and incubated over 4Å MS for 48 h prior to use. Toluene and CH_2Cl_2 were dried over CaH_2 whereas THF and Et_2O were dried over sodium (dryness was monitored by colorization of benzophenone ketyl radical); they were freshly distilled prior to use. NMR spectra were obtained using a 500 MHz and 600 MHz Varian NMR spectrometers and referenced using the residual ^1H peak from the deuterated solvent. Infrared spectra were measured on a Nicolet IR/42 spectrometer FT-IR (thin film, NaCl cells). Waters 2795 (Alliance HT) instrument was used for HRMS (ESI) analysis with polyethylene glycol (PEG-400-600) as a reference.

Column chromatography was performed using Silicycle 60Å, 35-75 μm silica gel. Pre-coated 0.25 mm thick silica gel 60 F254 plates were used for analytical TLC and visualized using UV light, iodine, potassium permanganate stain, *p*-anisaldehyde stain or phosphomolybdic acid in EtOH stain.

Halofunctionalization reactions were performed in the absence of light. *N*-chlorosuccinimide (NCS), *N*-bromosuccinimide (NBS), *N*-iodosuccinimide (NIS), 1,3-dichloro-5,5-dimethylhydantoin (DCDMH), 1,3-dibromo-5,5-dimethylhydantoin (DBDMH) and *N*-chlorophthalimide (NCP) were re-crystallized prior to use. All other commercially available reagents and solvents were used as received unless otherwise mentioned.

II.5.2. Kinetic isotope effects and rate studies.

General considerations for ^{13}C KIE measurements:

For each set of ^{13}C KIE experiment, two reactions were performed: 1. the first reaction that led to 100% conversion of the starting alkenoic acid/alcohol and, b. a second reaction, that was allowed to proceed to ~20% conversion of the starting material by adding about 20 mol% of the halogenating reagent.

The scale for each reaction in a set was adjusted such that 1.0-1.5 mmol of the product can be isolated in each case. For instance, the reaction that led to 100% conversion to produce the chlorolactone **II-1a** was performed using 1.5 mmol of **II-1**, whereas the second reaction which was allowed to proceed to ~20% conversion was performed using 7.0 mmol of **II-1**. In each of these reactions, ~1.3 mmol of the product was isolated (>95% yield b.r.s.m). For ^{13}C KIE measurements on the chloroether **II-3a**, reactions were typically performed on 12.0-15.0 mmol scale. The product **II-3a** being volatile, the isolated yields were low (30-50%). Furthermore, for every substrate, two sets of ^{13}C KIE measurements were performed (each set comprising the 100% and 20% conversion reactions).

II.5.2.1. ^{13}C KIEs for halocyclization of II-1, II-2 and II-3:

^{13}C KIE determination for **II-1a**:

The ^{13}C KIEs for **II-1a** were determined by product analysis. Two independent reactions were run to 22 ± 2 % and 22 ± 2 % conversion and the product isolated. The ^{13}C isotopic compositions of these samples were compared to samples of product isolated from 100% conversion reactions (no isotopic fractionations). The ^{13}C KIEs were determined in a standard way from the isotopic enhancements and fractional conversions. All samples were prepared using a constant 1.2 mmol of **II-1a** in 5 mm NMR tubes filled with $CDCl_3$ to a constant height of 5 cm. All ^{13}C spectra were recorded at 125 MHz using inverse gated decoupling, 53 s (5 times T1) delays between calibrated $\pi/2$ pulses, and a 7.0 s acquisition time. Six spectra each with 128 transients were obtained for each four samples of **II-1a** (two samples per experiment). Integrations were determined numerically using a constant integration region for each peak (10 times the peak width at half height). A zero-order baseline correction was generally applied, but in no case was a first-order (tilt) correction applied. The integration of one of the methylene peaks was set to 1.000 since the KIE at this position is expected to be negligible. The results for the two individual sets are displayed below (values in black are experimental and values in red are predicted for the TS calculated at the B3LYP/6-31G*/SM8-$CHCl_3$).

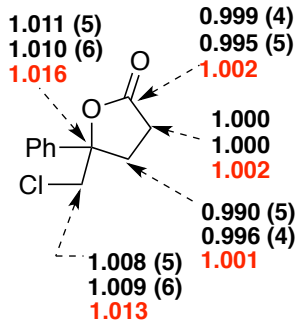

^{13}C KIE ***experimental*** and ***predicted*** values

The ^{13}C KIE determined for the chlorolactone **II-1a** qualitatively corroborates the *NAAA* hypothesis. The quaternary carbon displays a larger KIE than the chloromethylene carbon. The trend implies a higher degree of re-hybridization at the benzylic carbon in comparison to the chloromethylene carbon during the transition state. Most importantly, when the nucleophilicity of the carboxylic acid was enhanced by addition of catalytic amounts of base (20% DABCO), the KIE at the quaternary carbon displayed a significant drop in comparison to the halomethylene carbon. The DABCO (base) activated carboxylic acid is a better nucleophile in comparison to the free acid (see Figure II-27). This activation allows the nucleophile to polarize the olefin (raise the HOMO energy) from a longer distance (1.92 Å) to initiate the desired halofunctionalization *via* an early transition state. On the other hand, to polarize the olefin to a similar extent in order to achieve the desired halofunctionalization, the free acid (in an uncatalyzed reaction) has to rely on the weak activation provided by another molecule of halenium ion donor (weak base). Hence, the desired level of polarization can be achieved *via* a late transition state with a shorter C=O·····C=C distance (1.78 Å). The magnitude of ^{13}C KIE being proportional to the extent of re-hybridization during the TS, hence, we observed a lower KIE for the quaternary carbon for a catalyzed reaction (early TS) in comparison to the uncatalyzed halofunctionalization (late TS). Conversely, the extent of re-hybridization of the halomethylene carbon (in the transition state) is influenced more by the halenium ion source, which remains unchanged in the catalyzed as well as the uncatalyzed process.

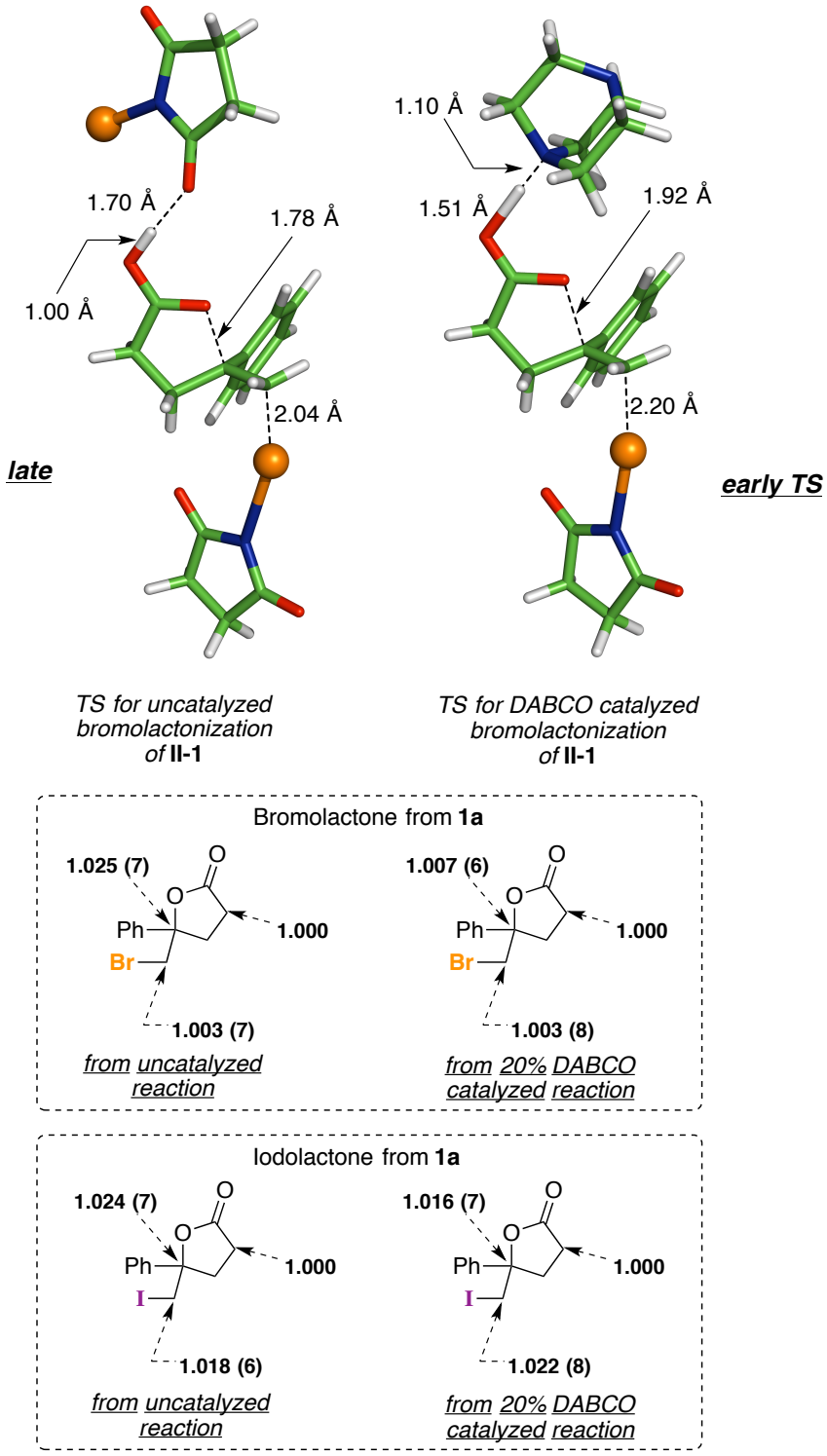

Figure II-27. Comparison of TS for catalyzed and uncatalyzed bromolactonization of **II-1**. For clarity, the TS only for *anti*-addition (predominant stereoisomer formed during bromo and iodolactonization of **II-1**) in bromolactonization is shown. The dashed boxes below represent the experimental ^{13}C KIEs for the catalyzed and uncatalyzed bromo and iodo-lactonization.

^{13}C KIE determination for **II-2a**:

The ^{13}C KIEs for **II-2a** were determined by product analysis. Two independent reactions were run to 18 ± 2 % and 20 ± 2 % conversion and the product isolated. The ^{13}C isotopic compositions of these samples were compared to samples of product isolated from 100% conversion reactions (no isotopic fractionations). The ^{13}C KIEs were determined in a standard way from the isotopic enhancements and fractional conversions. The samples for the first experiment, 18 ± 2 % and 100% conversion samples were prepared using a constant 1.3 mmol and the samples for the second experiment, 20 ± 2 % and 100% conversion samples were prepared using a constant 1.2 mmol of the chlorolactone **II-2a** in 5 mm NMR tubes filled with $CDCl_3$ to a constant height of 5 cm. All ^{13}C spectra were recorded at 125 MHz using inverse gated decoupling, 64 s (5 times T1) delays between calibrated $\pi/2$ pulses, and a 7.0 s acquisition time. Six spectra each with 256 transients were obtained for each four samples of **II-2a** (two samples per experiment). Integrations were determined numerically using a constant integration region for each peak (10 times the peak width at half height). A zero-order baseline correction was generally applied, but in no case was a first-order (tilt) correction applied. The integration of one of the methylene peaks was set to 1.000 since the KIE at this position is expected to be negligible. The results for the two individual sets are displayed below (values in black are experimental and values in red are

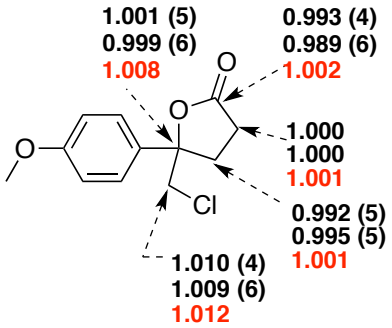

^{13}C KIE ***experimental*** and
predicted values

predicted for the TS calculated at the B3LYP/6-31G*/SM8-$CHCl_3$).

^{13}C KIE determination for **II-3a**:

The ^{13}C KIEs for **II-3a** was determined by product analysis. Two independent reactions were run to 33 ± 2 % and 22 ± 2 % conversion and the product isolated. The ^{13}C isotopic compositions of these samples were compared to samples of product isolated from 100% conversion reactions (no isotopic fractionations). The ^{13}C KIEs were determined in a standard way from the isotopic enhancements and fractional conversions. The samples for the first experiment, 33 ± 2 % and 100% conversion samples were prepared using a constant 0.95 mmol and the samples for the second experiment, 22 ± 2 % and 100% conversion samples were prepared using a constant 1.0 mmol of **II-3a** in 5 mm NMR tubes filled with $CDCl_3$ to a constant height of 5 cm. All ^{13}C spectra were recorded at 125 MHz using inverse gated decoupling, ~120 s (5 times T1) delays between calibrated π/2 pulses, and a 7.0 s acquisition time. Six spectra each with 64 transients were obtained for each four samples of **II-3a** (two samples per experiment). Integrations were determined numerically using a constant integration region for each peak (10 times the peak width at half height). A zero-order baseline correction was generally applied, but in no case was a first-order (tilt) correction applied. The integration of one of the methylene peaks was set to 1.000 since the KIE at this position is expected to be negligible.

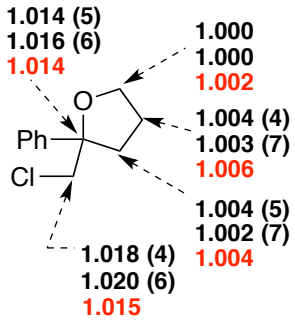

^{13}C KIE ***experimental*** and ***predicted*** values

General considerations for K_H/K_D measurements:

For following the kinetics of halofunctionalization reactions, Agilent 6850 series II GC and Agilent 7890A GC-MS instruments equipped with an auto-sampler were used. Halofunctionalization reactions were performed in 1.5 mL amber colored glass vials using amylene stabilized dry chloroform at 0.05 M substrate concentration. The vials were placed in a water bath (charging water in the auto-sampler bed) to avoid heat transfer from the instrument to the reaction mixture in the vial. Undecane (0.05 M in $CHCl_3$) was used as an internal standard. Prior to every reaction, a standard curve was obtained for the starting compound and the corresponding product using standard solutions. The slope and intercept involved in these standard curves were accounted for during evaluation of the substrate and product concentration before and during the course of the reaction.

Note: For every substrate/product, an initial injection was followed up by a blank injection (amylene stabilized $CHCl_3$) to verify presence of any residual compound. Based on this analysis the sequence of auto-sampler can be adjusted to include appropriate number of blank injections to remove the residual component, if any.

II.5.2.2. Kinetics of II-1 vs II-1-D_2:

The kinetics for chlorolactonization of **II-1** and **II-1**-D_2 were followed using Aglient 6850 Series II GC instrument equipped with a Agilent DB-5ms column (30m x 0.32 mm x 0.25 μm). The reactions were performed in a 1.5 mL amber colored vial using 0.03 mmol of substrate in 0.6 mL of amylene stabilized chloroform (0.05 M) containing undecane as an internal standard. The temperature ramp used for analysis is as follows: DB-5ms; 60 ºC to 250 ºC - start temperature 60 ºC (hold time = 0.0 min) with increments of 20 ºC/min upto 250 ºC (hold time at 250 ºC = 12.0 min). Total time = 28.5 min.

Initially a standard curve was obtained for the alkenoic acid **II-1** as shown in Table II-15 above. Using this data from standard curve, mmol of alkenoic acid were plotted against the ratio of areas (sample:std) and a linear fit (y=mx+c) was employed to obtain the slope and intercept. Similarly, standard curves for **II-1**-D_2 and the products **II-1a** and **II-1a**-D_2 were obtained and the corresponding slopes and intercepts were used to calculate the reactant and product concentration during the course of the reaction. The GC measurements were performed in intervals of 30 min to follow the consumption of the starting alkenoic acid. As shown in Figure II-28, the time (min) of the reaction was plotted against concentration (mmol) of the starting material

Table II-15. Standard curve for alkenoic acid **1a**. Slope = 0.0626, Intercept = -0.00038, R^2 = 0.9996

Solution	Concentration (mmol)	Area under internal standard (R_t = 3.6 min)	Area under II-1 (R_t = 6.7 min)	Ratio of Sample:Std
1	0.0500	2223.3	1783.2	0.8021
2	0.0250	4244.9	1739.4	0.4098
3	0.0125	5024.4	1047.9	0.2086
4	0.0063	5639.2	638.2	0.1132
5	0.0031	5833.1	304.0	0.0521
6	0.0016	6152.4	148.9	0.0242

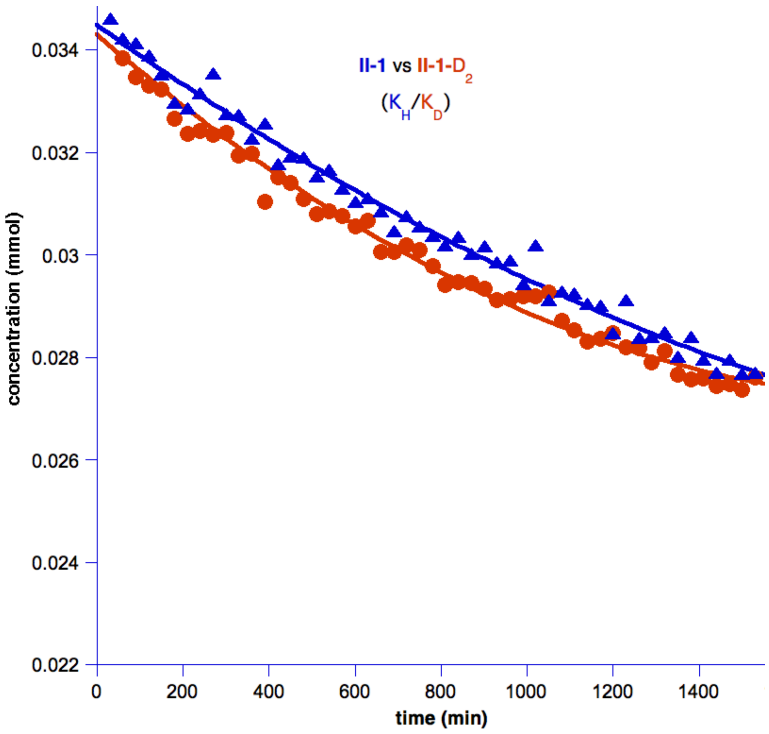

Figure II-28. Plot of concentration (mmol) against time (min) comparing rates of chlorolactonization of **II-1** and **II-1**-D_2 (Set I). The plot displays a second order polynomial fit (R^2=0.98 for **II-1** and, R^2=0.96 for **II-1**-D_2).

and K_H/K_D was then evaluated.

Data for three individual sets of reactions was acquired as described above.

Set I: K_H/K_D = 0.996, Set II: K_H/K_D = 0.995, Set III: K_H/K_D = 0.995

Mean **K_H/K_D = 0.995**, Standard deviation = 0.001

II.5.2.3. Kinetics of II-3 vs II-3-D_2:

The K_H/K_D estimations for **II-3** and **II-3**-D_2 was performed in a similar fashion to the procedure explained above for chlorolactonization of **II-1** and **II-1**-D_2. The temperature ramp used for analysis is as follows: DB-5ms; 60 ºC to 250 ºC - start temperature 60 ºC (hold time = 0.0 min)

with increments of 20 ºC/min upto 250 ºC (hold time at 250 ºC = 12.0 min). Total time = 28.5 min. Rt $_{(\text{internal standard-undecane})}$ = 3.6 min, Rt $_{(\textbf{II-3} \text{ or } \textbf{II-3}\text{-D2})}$ = 6.0 min, Rt $_{(\textbf{II-3a} \text{ or } \textbf{II-3a}\text{-D2})}$ = 6.5 min.

Data for three individual sets of reactions is as follows:

Set I: K_H/K_D = 1.000, Set II: K_H/K_D = 0.996, Set III: K_H/K_D = 0.991

Mean **K_H/K_D = 0.996**, Standard deviation = 0.005

II.5.2.4. Competitive halocyclization of II-1 vs II-3:

The competitive halocyclization of **II-1** and **II-3** were followed using a Aglient 6850 Series II GC instrument equipped with a Agilent DB-5ms column (30m x 0.32 mm x 0.25 μm). The reactions were performed in a 1.5 mL amber colored vial containing 0.03 mmol of each substrate (1:1) in 0.6 mL of amylene stabilized chloroform (0.05 M) containing undecane as an internal standard. To this mixture, 1.0 equiv of DCDMH was added and the measurements were initiated. The temperature ramp used for analysis is as follows: DB-5ms; 60 ºC to 250 ºC - start temperature 60 ºC (hold time = 0.0 min) with increments of 20 ºC/min upto 250 ºC (hold time at 250 ºC = 12.0 min). Total time = 28.5 min. The ratio $K_{(\textbf{II-3})}/K_{(\textbf{II-1})}$ was estimated by taking a ratio of individual slopes.

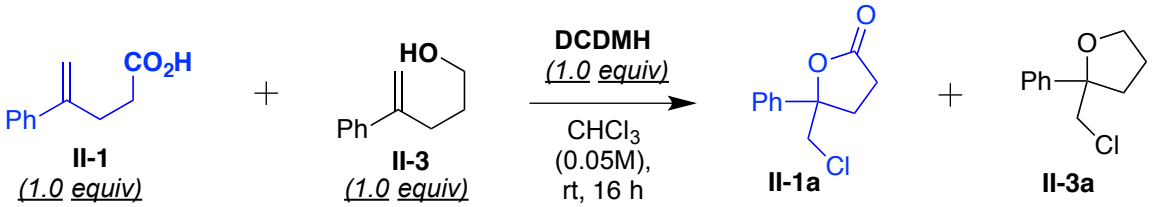

$k_{(\text{ene-alcohol})}/k_{(\text{ene-acid})}$ = **4.7**

The alkenoic alcohol **II-3** was found to react about 5 times faster than the alkenoic acid **II-1**. Although, both substrates incorporate the same 1,1-disubstituted olefin moiety, the fact that alcohol **II-3** (more nucleophilic) consumes the halogenating reagent about five times faster than the acid **II-1** (less nucleophilic), unequivocally establishes an imperative role of nucleophile in halofunctionalization reactions.

II.5.2.5. Kinetics of II-2 vs II-2-D_2:

The kinetics for chlorolactonization of **II-2** and **II-2**-D_2 were followed using a 500 MHz Varian NMR instrument equipped with a cryogenic probe. The chlorolactonization of **II-2** was faster at room temperature (~50% conversion in 5 min). Hence, the chlorolactonization of **II-2** and **II-2**-D_2 were performed at -10 ºC in a 5 mm diameter Wilmad NMR tube. The reactions were performed in amber colored NMR tubes using 0.03 mmol of substrate in 0.6 mL of amylene stabilized chloroform (0.05 M) containing undecane as an internal standard. The NMR instrument was shimmed and equilibrated with the sample containing the alkenoic acid and internal standard. The acquisition was started within 3 min after the addition of 1.0 equiv of DCDMH.

The NMR spectra were acquired in intervals of 5 min to follow the consumption of the starting alkenoic acid. As explained for alkenoic acid **II-1** above, the time (min) of the reaction was plotted against concentration (mmol) of the starting material (see Figure II-29) and K_H/K_D was then evaluated.

Data for three individual sets of reactions was acquired as described above.

Set I: K_H/K_D = 1.179, Set II: K_H/K_D = 1.187, Set III: K_H/K_D = 1.183

Mean $\mathbf{K_H/K_D = 1.183}$, Standard deviation = 0.004

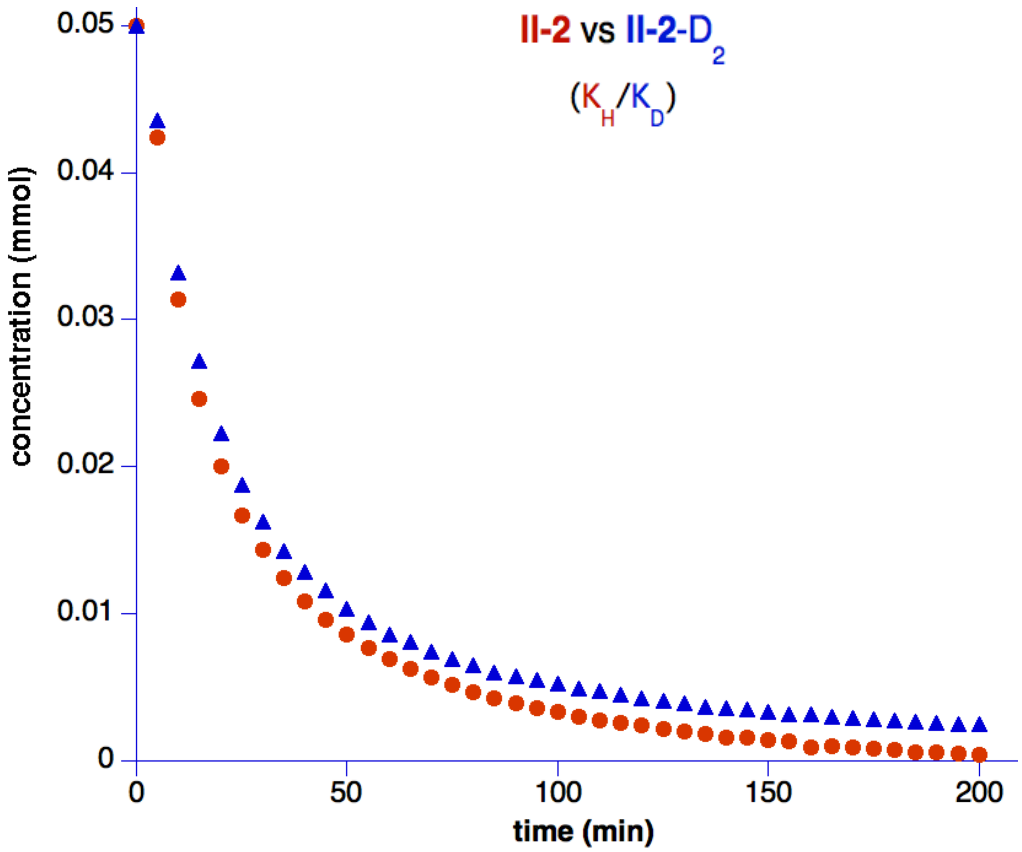

Figure II-29. Plot of concentration (mmol) against time (min) comparing rates of chlorolactonization of **II-2** and **II-2**-D_2 (Set I). Second order polynomial fit (R^2=0.99 for **II-2** and, R^2=0.97 for **II-2**-D_2).

II.5.2.6. Kinetics of II-1 vs II-1-OD:

This KIE experiment was performed to validate the transition state for chlorolactonization of **II-1** (Figure II-30) estimated at the B3LYP/6-31G*/SM8 ($CHCl_3$) level of theory. Based on the predictions, the TS involves a concomitant proton transfer (from the carboxylic acid to the carbonyl of hydantoin) during the chlorocyclization. Since the proton transfer event is associated with the rate-determining step, the predicted K_H/K_D is 2.2. To corroborate the predictions, the chlorolactonization of **II-1** and **II-1**-OD was performed in $CHCl_3$, similar to the procedure explained

above for chlorolactonization of **II-1** and **II-1**-D_2. The temperature ramp used for analysis is as follows: DB-5ms; 60 ºC to 250 ºC - start temperature 60 ºC (hold time = 0.0 min) with increments of 20 ºC/min upto 250 ºC (hold time at 250 ºC = 12.0 min). Total time = 28.5 min.

Data for three individual sets of reactions is as follows:

Set I: K_H/K_D = 1.514, Set II: K_H/K_D = 1.498, Set III: K_H/K_D = 1.521

Mean **K_H/K_D = 1.511**, Standard deviation = 0.012

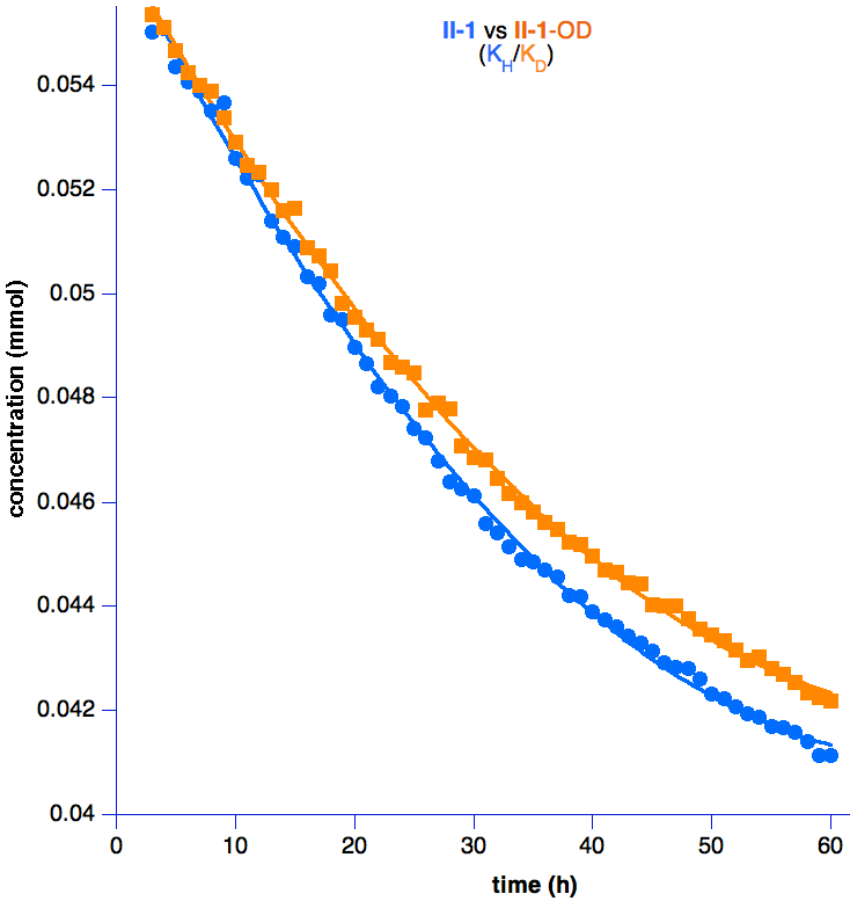

Figure II-30. Plot of concentration (mmol) against time (min) comparing rates of chloroetherification of **II-1** and **II-1**-OD. Second order polynomial fit (R^2=0.999 for **II-1** and, R^2=0.999 for **II-1**-OD).

Although the experimental KIE of 1.511 for **II-1** vs **II-1**-OD corroborates the theoretically predicted value of 2.2, the computational analysis is based on the TS for *syn*-addition (Figure II-17). Experimentally, the reaction also yields an *anti*-adduct. As explained above, the value for *syn*:*anti* addition depends on several factors, most importantly, the concentration of the reagent.

Albeit, the enabling role of nucleophile is highlighted in these studies, corroborating the computationally predicted TS for *syn* and *anti* addition in halofunctionalization of **1a**. This hypothesis is further validated by the following $K^{16}{}_O/K^{18}{}_O$ studies using ^{18}O enriched **1a** to provide a definitive evidence towards the participation of nucleophile in electrohilic addition to olefins.

II.5.2.7. Kinetics of II-1 vs II-1*:

The ^{18}O KIE for chlorolactonization of **II-1** and **II-1*** was elucidated using a Aglient 7890A GC instrument coupled to a Agilent 5975C EI-MS with triple axis detector. The GC was equipped with a Agilent DB-5ms column (30m x 0.32 mm x 0.25 μm). The reactions were performed in a 1.5 mL amber colored vial using approximately 1:1 ratio of substrate **II-1** and **II-1*** (0.015 mmol each) in 0.6 mL of amylene stabilized chloroform (0.05 M). The temperature ramp used for analysis is as follows: DB-5ms; 60 ºC to 320 ºC - start temperature 60 ºC (hold time = 0.0 min) with increments of 20 ºC/min upto 320 ºC (hold time at 320 ºC = 1.0 min). Total time = 14.0 min.

The following steps were taken to elucidate the ^{18}O KIE for chlorolactonization of **II-1** and **II-1***:

1. The spectrometer was modified to perform SIM (Selected Ion Monitoring) analysis. For analysis of **II-1** and **II-1***, only three molecular ions corresponding to the alkenoic acids: 176.1 (2 x ^{16}O), 178.1 (^{16}O and ^{18}O) and 180.1 (2 x ^{18}O) were selected for analysis. For the related chlorolactone products, the molecular ions (210, 212 and 214) displayed very low intensities and the observed base peaks were 161, 163 and 165 resulting *via* loss of

chloromethylene radical $^{\bullet}(CH_2Cl)$. Hence, to avoid the possible kinetic isotope effects involved in this primary fragmentation, analysis of the product was excluded.

2. After the initial set up, 1.0 μL of the reaction mixture containing approximately 1:1 ratio of **II-1** : **II-1*** was injected to identify the ^{16}O:^{18}O ratio. This injection was followed by a blank injection (2.0 μL of amylene stabilized $CHCl_3$). The blank run was anaylized for presence of any residual **II-1** or **II-1***. If traces of the starting compunds were detected in the spectrum, another blank injection of the same volume was performed and the corresponding spectrum was analyzed for traces of any residual stating compound. This analysis is essential for accurate determination of ^{16}O:^{18}O ratio as one isotope serves as an internal standard for the other. For the mixture of **II-1** and **II-1***, 2 blank runs were followed after every injection.
3. The instrument was tuned prior to the KIE measurements and after the measurements. Based on the level of H_2O content (as displayed in the auto-generated tune report), we observed differences in the ratio of 178.1 (^{16}O and ^{18}O) and 180.1 (2 x ^{18}O) masses. This is the most crucial factor in measurement of ^{18}O KIE. Although, the differential content of unavoidable moisture resulted in different extent of ^{16}O-^{18}O exchange in the starting alkenoic acid, the overall ratio was observed to be constant. Hence, for elucidating the KIE (K^{16}_O/K^{18}_O), a ratio of area under mass 176.1 : (178.1+180.1) was considered. Furthermore, to ensure minimum change in the H_2O content in one set of experiment, an auto-tune report was generated prior to, and after all the measurements were made. If the levels of H_2O content were significantly different prior to and after the measurements, a new experiment must be started over.
4. After adjusting all the parameters describe in step 1-3, three individual measurements (each measurement being followed by two blank runs) were made to observe the

consistency in measurement of ^{16}O:^{18}O ratio in the mixture of labeled and unlabeled alkenoic acid. A mean value was recorded with the associated standard deviation.

5. To this mixture of alkenoic acids, ~10 mol% of 1,3-dichloro-5,5-dimethylhydantoin (DCDMH) was added and the reaction mixture was stirred for 3-4 h. The conversion of the starting material was monitored by GC analysis every hour as described above.
6. Upon achievement of a steady measurement on starting compound consumption, the reaction mixture was then subjected to step 4 and three more readings were acquired. The mean reading and the standard deviation were recorded.
7. Finally, the KIE (K^{16}_O/K^{18}_O) was obtained as a ratio of area under mass 176.1 : (178.1+180.1), see step 3 for details.
8. Steps 1-7 were repeated for 3 more times and the mean value for K^{16}_O/K^{18}_O was recorded with the associated standard deviation..

Data for three individual sets of reactions is as follows:

Set I:

^{16}O:^{18}O (before reaction): a.) 1.201 b.) 1.201 and, c.) 1.201

mean value =1.201, standard deviation = 0.000

^{16}O:^{18}O (12% conversion): a.) 1.176 b.) 1.177 and, c.) 1.171

mean value =1.175, standard deviation = 0.003

K^{16}_{O}/K^{18}_{O} (set I) = 1.022

Set II:

^{16}O:^{18}O (before reaction): a.) 1.147 b.) 1.145 and, c.) 1.147

mean value =1.146, standard deviation = 0.001

^{16}O:^{18}O (10% conversion): a.) 1.115 b.) 1.114 and, c.) 1.114

mean value =1.114, standard deviation = 0.001

K^{16}_{O}/K^{18}_{O} (set I) = 1.029

Set III:

^{16}O:^{18}O (before reaction): a.) 1.135 b.) 1.135 and, c.) 1.136

mean value =1.135, standard deviation = 0.001

^{16}O:^{18}O (10% conversion): a.) 1.104 b.) 1.108 and, c.) 1.103

mean value =1.105, standard deviation = 0.003

K^{16}_O/K^{18}_O (set I) = 1.027

Mean K^{16}_O/K^{18}_O = 1.026, Standard deviation = 0.004

II.5.2.8. Kinetics of II-2 vs II-2*:

The ^{18}O KIE for chlorolactonization of **II-2** and **II-2*** was elucidated as described above for substrate **II-1** and **II-1***. These reactions were also performed in a 1.5 mL amber colored vial using approximately 1:1 ratio of substrate **II-2** and **II-2*** (0.015 mmol each) in 0.6 mL of amylene stabilized chloroform (0.05 M). The temperature ramp used for analysis is as follows: DB-5ms column; 60 ºC to 320 ºC - start temperature 60 ºC (hold time = 0.0 min) with increments of 20 ºC/min upto 320 ºC (hold time at 320 ºC = 10.0 min). Total time = 23.0 min.

Data for three individual sets of reactions is as follows:

Set I:

^{16}O:^{18}O (before reaction): a.) 1.061 b.) 1.160 and, c.) 1.160

mean value =1.060, standard deviation = 0.001

^{16}O:^{18}O (9% conversion): a.) 1.050 b.) 1.050 and, c.) 1.052

mean value =1.051, standard deviation = 0.001

K^{16}_{O}/K^{18}_{O} (set I) = 1.0086

Set II:

^{16}O:^{18}O (before reaction): a.) 1.192 b.) 1.196 and, c.) 1.200

mean value =1.196, standard deviation = 0.004

^{16}O:^{18}O (10% conversion): a.) 1.189 b.) 1.186 and, c.) 1.183

mean value =1.186, standard deviation = 0.003

K^{16}_{O}/K^{18}_{O} (set I) = 1.0084

Set III:

^{16}O:^{18}O (before reaction): a.) 1.158 b.) 1.152 and, c.) 1.156

mean value =1.155, standard deviation = 0.003

^{16}O:^{18}O (9% conversion): a.) 1.147 b.) 1.144 and, c.) 1.144

mean value =1.145, standard deviation = 0.002

K^{16}_O/K^{18}_O (set I) = 1.0087

Mean K^{16}_O/K^{18}_O = 1.009, Standard deviation = 0.0002

II.5.3. Synthesis of substrates and intramolecular halocyclization of alkenes.

i. Synthesis of substrates II-6, II-7, II-10 and II-11:

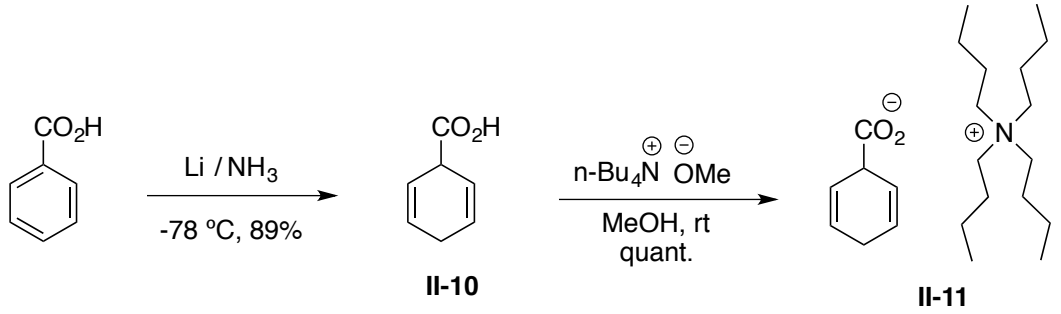

Dihydrobenzoic acid (II-10):

Compound **II-10** was synthesized by Birch reduction as reported previously.[67] Benzoic acid (7.0 g, 57.3 mmol) was charged in a flame dried 250 mL three neck flask. One of the necks was connected to nitrogen inlet at atmospheric pressure while a condenser was attached to the center neck. The flask was purged with nitrogen for 1-2 min while rested in a -78 ºC bath (acetone/dry ice). The third neck of the flask was then closed with a glass adapter and ammonia gas was condensed until the total volume was 100 mL. To a vigorously stirred solution of benzoic acid in liquid ammonia was added lithium (1.19 g 172.0 mmol, 3.0 equiv, cut into small pieces prior to addition) in portions over a period of 30 min. After the addition was complete, the solution was stirred for another 30 min and quenched carefully by addition of solid ammonium chloride (~15 g) until the solution turned into a white gel. The flask was gradually warmed to room temperature over 20 min while the ammonia was removed under a stream of nitrogen gas. The resulting solid residue (free of ammonia) was dissolved in distilled water (30 mL) and cooled on an ice-water bath. The solution was acidified to pH 2 using concentrated HCl (12 M). The product was extracted in dichloromethane (3 x 20 mL). The organics were separated, dried over anhydrous

Na_2SO_4, filtered, concentrated. Pure **II-10** was obtained as colorless oil in 98% yield (8.1 g). It was used immediately for further steps without prolonged storage.

Note: Compound **II-10** undergoes rapid oxidation at room temperature. It can be stored as a frozen solution in argon purged benzene at -80 ºC for about 2-3 weeks.

Analytical data for **II-10**:[67] pale yellow oil; ^{1}H NMR (500 MHz, $CDCl_3$) δ 11.73 (1H, br s), 5.90 (2H, m), 5.80 (2H, m), 3.76 (1H, m), 2.68 (2H, m) ppm; ^{13}C NMR (125 MHz, $CDCl_3$) δ 178.9, 126.9, 121.5, 41.5, 25.8 ppm.

Tetrabutylammonium cyclohexa-2,5-diene-1-carboxylate (II-11):

A 50 mL flame dried round flask was charged with **II-10** (2 g, 13.14 mmol) under nitrogen atmosphere. To this solid was added was added commercially available ~20% tetra-n-butylammonium methoxide in methanol (20.0 mL) at room temperature. The resulting mixture was concentrated using rotary evaporator and then subjected to 250 mtorr of pressure using a vacuum pump. Since the commercially available solution is approximately 20% of n-Bu_4NOMe in MeOH by weight, the corresponding translucent gel obtained after concentration was evaluated by ^{1}H NMR to ensure 1:1 ratio of **II-10** to the added base. The delay time (d_1) for NMR analysis was adjusted to 10 s to obtain accurate integration data. The resulting salt **II-11** was then stored in a freezer at -20 ºC or used immediately for further reactions.

Analytical data for **II-11**: White gel; ^{1}H NMR (500 MHz, $CDCl_3$) δ 5.92 (2H, m), 5.53 (2H, m), 3.46 (1H, m), 3.18 (8H, AB quartet, J = 8.5 Hz), 2.51 (1H, m), 1.50 (8H, m), 1.30 (8H, sextet, J = 7.5 Hz), 0.86 (12H, t, J = 7.5 Hz) ppm; ^{13}C NMR (125 MHz, $CDCl_3$) δ 177.7, 129.5, 121.4, 58.7, 50.1, 47.8, 35.9, 24.0, 23.2, 19.7, 13.6 ppm. IR (film) 3181, 2960 (s), 2874, 1678, 1633, 1580, 1435, 1314, 1117, 880, 793 cm^{-1}.

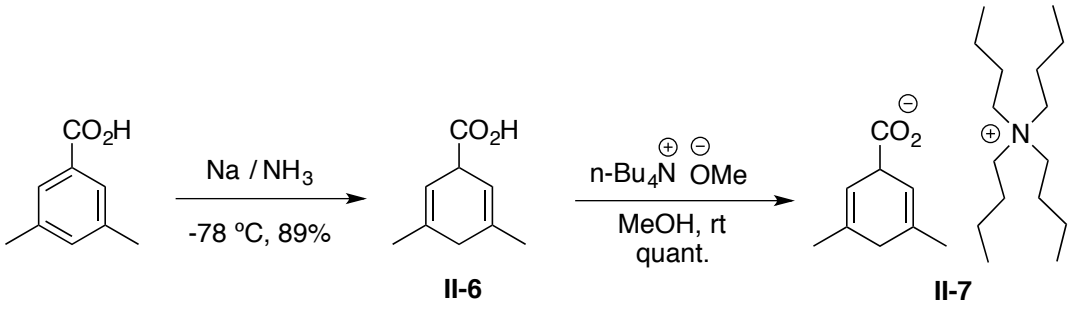

II-6 **II-7**

3,5-dimethyldihydrobenzoic acid (II-6):

II-6 was synthesized as reported previously.[68] Commercially available 3,5-dimethylbenzoic acid was recrystallized from hot ethyl acetate and dried prior to use. 3,5-Dimethylbenzoic acid (5.0 g, 33.0 mmol) was charged in a flame dried 250 mL three neck flask. One of the necks was connected to nitrogen inlet at atmospheric pressure while a condenser was attached to the center neck. The flask was purged with nitrogen for 1-2 min while rested in a -78 ºC bath (acetone/dry ice). The third neck of the flask was then closed with a glass adapter and ammonia gas was condensed until the total volume was 150 mL. To a vigorously stirred suspension of 3,5-dimethylbenzoic acid in liquid ammonia was added sodium (3.0 g, 130.4 mmol, 4.0 equiv), in portions over a period of 30 min (part of the sodium clumps were cut into smaller pieces and immediately added). After the addition was complete, the solution was stirred for another 30 min and quenched carefully by addition of solid ammonium chloride (~12 g) at -78 ºC until the solution turned into a white gel. The flask was gradually warmed to room temperature over 20 min while the ammonia was removed under a stream of nitrogen gas. The resulting solid residue (free of ammonia) was dissolved in distilled water (30 mL) and cooled on an ice-water bath. The solution was acidified to pH 2 using concentrated HCl (12 M). The product was extracted in dichloromethane (3 x 20 mL). The organics were separated, dried over anhydrous Na_2SO_4, filtered, and concentrated. The crude white solid was recrystallized from hot ethyl acetate to yield

4.51 g of pure **II-6** as a crystalline white solid (89% yield). Crystalline **II-6** (devoid of impurities) can be stored in a freezer at -20 ºC under argon atmosphere for over a year without any traces of re-aromatization.

Note: If the commercially available 3,5-dimethylbenzoic acid is not purified prior to use, **II-6** is obtained as a yellowish solid. The resulting impurities can then be removed by multiple recrystallizations from hot ethyl acetate, however with a significant drop in isolated yield.

Analytical data for **II-6**: White solid, m.p. 117 °C (lit.[68] 105 °C); ^{1}H NMR (500 MHz, $CDCl_3$) δ 12.20-11.20 (1H, br s), 5.50 (2H, m), 3.74 (1H, m), 2.48 (2H, dddd, *J* = 7.5, 8.5, 22.0, 30.0 Hz), 1.73 (6H, s) ppm; ^{13}C NMR (125 MHz, $CDCl_3$) δ 179.6, 134.4, 115.6, 43.9, 35.6, 23.0 ppm.

Tetra-n-butylammonium-3,5-dimethylcyclohexa-2,5-diene-1-carboxylate (II-7):

Compound **II-7** was synthesized using the procedure described above for **II-11**. The resulting salt **II-7** was used immediately for further reactions. It can be stored in a freezer at -20 ºC under argon atmosphere for a month, after which the product begins to turn yellow.

Analytical data for **II-7**: White gel; ^{1}H NMR (500 MHz, $CDCl_3$) δ 5.69 (2H, m), 3.61-3.57 (1H, s), 3.32 (8H, AB quartet, *J* = 8.5 Hz), 2.39 (1H, m), 1.65 (6H, s), 1.64-1.57 (8H, m), 1.39 (8H, sextet, *J* = 7.5 Hz), 0.95 (12H, t, *J* = 7.0 Hz) ppm; ^{13}C NMR (125 MHz, $CDCl_3$) δ 177.7, 129.5, 121.4, 58.7, 50.1, 47.8, 35.9, 24.0, 23.2, 19.7, 13.6 ppm. IR (film) 3180, 2963 (s), 2876, 1698, 1653, 1584, 1465, 1385, 1109, 883, 790 cm^{-1}.

ii. Synthesis of substrates 1a-q:

Substrates **II-1**,[69] **II-2**,[70] **II-3**,[70] **II-2**-OH,[70] **II-12**,[71] **II-12**-OH,[72] **II-14**,[73] **II-16**,[74] **II-18**,[75] **II-18**-OH,[76] **II-20**,[77] and **II-22**[78,79] were synthesized as reported previously. The corresponding tetra-n-butylammonium salts **II-5**, **II-13**, **II-15**, **II-17**, **II-19**, **II-21** and **II-23** were prepared as described above for **II-11**.

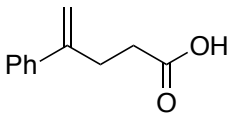

II-1

Analytical data for **4-phenylpent-4-enoic acid** (**II-1**):[69] White solid, m.p. 95 ºC; ^{1}H NMR (500 MHz, $CDCl_3$) δ 12.31 (1H, br. s), 7.49 (2H, d, *J* = 7.0 Hz), 7.41 (2H, t, *J* = 7.5 Hz), 7.36 (1H, t, *J* = 7.0 Hz), 5.42 (1H, br. s), 5.20 (1H, br. s), 2.94 (2H, t, *J* = 7.5 Hz), 2.62 (2H, t, *J* = 8.0 Hz); ^{13}C NMR (125 MHz, $CDCl_3$) δ 179.9, 146.5, 140.3, 128.4, 127.6, 126.0, 112.9, 33.0, 30.0 ppm.

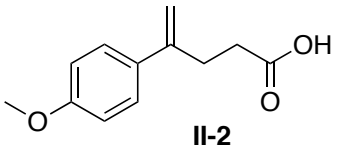

II-2

Analytical data for **4-(4-methoxyphenyl)pent-4-enoic acid** (**II-2**):[70] White solid, m.p. 95 ºC; ^{1}H NMR (500 MHz, $CDCl_3$) δ 11.11 (1H, br. s), 7.33 (2H, m), 6.85 (2H, m), 5.23 (1H, br. s), 5.00 (1H, br. s), 3.80 (3H, s), 2.80 (2H, t, *J* = 7.5 Hz), 2.51 (2H, t, *J* = 8.0 Hz); ^{13}C NMR (125 MHz, $CDCl_3$) δ 178.7, 159.3, 145.8, 132.8, 127.2, 113.8, 111.4, 55.3, 32.9, 30.2 ppm.

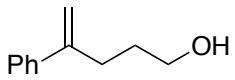

II-3

Analytical data for **4-phenylpent-4-en-1-ol** (**II-3**):[70] colorless oil; ^{1}H NMR (500 MHz, $CDCl_3$) δ 7.43- 7.26 (5H, m), 5.33 (1H, s), 5.11(1H, s), 3.67 (2H, t, *J* = 6.5 Hz), 2.63 (2H, t, *J* = 7.0 Hz), 1.90 (1H, br. s), 1.72 (2H, m); ^{13}C NMR (125 MHz, $CDCl_3$) δ 148.0, 141.0, 128.3, 127.3, 126.0, 112.5, 62.2, 31.5, 31.1 ppm.

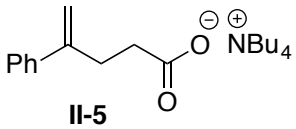

II-5

Analytical data for **tetrabutylammonium 4-phenylpent-4-enoate** (**II-5**): pale yellow oil; ^{1}H NMR (500 MHz, $CDCl_3$) δ 7.43 (2H, d, *J* = 7.5 Hz), 7.26-7.23 (2H, m), 7.18 (1H, m), 5.22 (1H, br. s), 5.07 (1H, d, *J* = 0.5 Hz), 3.34 (8H, AB quartet, *J* = 8.5 Hz), 2.83-2.80 (2H, m), 2.39-2.36 (2H, m), 1.66-1.60 (8H, m), 1.39 (8H, sextet, *J* = 7.5 Hz), 0.96 (12H, t, *J* = 7.5 Hz); ^{13}C NMR (125 MHz, $CDCl_3$) δ 177.9, 149.0, 141.8, 128.0, 126.9, 126.1, 111.1, 58.9, 37.2, 32.3, 24.1, 19.8, 13.7 ppm. IR (film) 3082, 2961, 2875, 1761, 1652, 1585 (s), 1455, 1387, 1153, 1028, 889, 781 cm^{-1}.

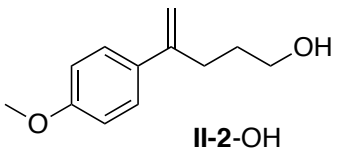

II-2-OH

Analytical data for **4-(4-methoxyphenyl)pent-4-en-1-ol** (**II-2**-OH):[70] White solid, m.p. 46 ºC; ^{1}H NMR (500 MHz, $CDCl_3$) δ 7.35 (2H, dd, *J* = 6.5, 2.0 Hz), 6.86 (2H, dd, *J* = 6.5, 2.0 Hz), 5.21 (1H, br. s), 5.00 (1H, br. s), 3.79 (3H, s), 3.64 (2H, t, *J* = 6.5 Hz), 2.56 (2H, t, *J* = 7.0 Hz), 1.73-1.68 (2H, m), 1.46 (1H, br. s); ^{13}C NMR (125 MHz, $CDCl_3$) δ 159.0, 147.2, 133.3, 127.1, 113.6, 111.0, 62.4, 55.2, 31.6, 31.2 ppm.

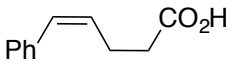

II-12

Analytical data for **(*Z*)-5-phenylpent-4-enoic acid** (**II-12**):[71] pale yellow oil; ^{1}H NMR (500 MHz, $CDCl_3$) δ 7.32 (2H, t, *J* = 8.0 Hz), 7.26-7.20 (3H, m), 6.48 (1H, d, *J* = 11.5 Hz), 5.62 (1H, m), 2.69-2.62 (2H, m), 2.48 (2H, ddd, *J* = 1.5, 7.5, 9.0 Hz); ^{13}C NMR (125 MHz, $CDCl_3$) δ 179.4, 137.0, 130.4, 129.8, 128.7, 128.2, 126.8, 34.1, 23.7 ppm.

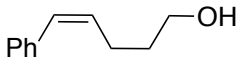

II-12-OH

Analytical data for **(*Z*)-5-phenylpent-4-en-1-ol** (**II-12**-OH):[72] colorless oil; ^{1}H NMR (500 MHz, $CDCl_3$) δ 7.35-7.20 (5H, m), 6.44 (1H, d, *J* = 11.5 Hz), 5.66 (1H, dt, *J* = 7.0, 11.5 Hz), 3.64 (2H, t, *J* = 6.5 Hz), 2.41 (2H, dq, *J* = 2.0, 7.5 Hz), 1.71 (2H, quint, *J* = 7.0 Hz), 1.52 (1H, br s); ^{13}C NMR (125 MHz, $CDCl_3$) δ 137.4, 132.0, 129.4, 128.7, 128.1, 126.6, 125.9, 62.3, 32.8, 24.8 ppm.

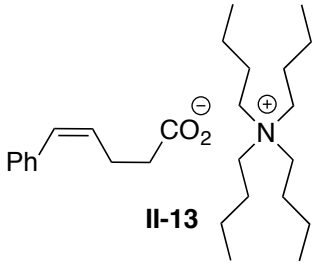

II-13

Analytical data for **tetrabutylammonium (*Z*)-5-phenylpent-4-enoate** (**II-13**): pale yellow oil; ^{1}H NMR (500 MHz, $CDCl_3$) δ 7.30 (2H, d, *J* = 7.5 Hz), 7.26-7.23 (2H, m), 7.13 (1H, m), 6.30 (1H, d, *J* = 12.0 Hz), 3.31 (8H, AB quartet, *J* = 8.5 Hz), 2.65 (2H, ddd, *J* = 1.5, 7.5, 15.5 Hz), 2.32 (2H, m), 1.60 (8H, m), 1.38 (8H, sextet, *J* = 7.5 Hz), 0.94 (12H, t, *J* = 7.5 Hz); ^{13}C NMR (125 MHz, $CDCl_3$) δ 177.9, 138.0, 134.2, 128.8, 127.9, 127.8, 126.0, 58.7, 38.6, 26.3, 24.0, 19.7, 13.7 ppm. IR (film) 3010, 2962 (s), 2876, 1760, 1648, 1587, 1490, 1381, 1152, 1029, 892, 770, 700 cm^{-1}.

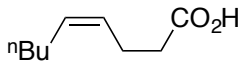

II-14

Analytical data for **(*Z*)-non-4-enoic acid** (**II-14**):[80] colorless oil; ^{1}H NMR (500 MHz, $CDCl_3$) δ 11.50 (1H, br s), 5.42 (2H, m), 5.32 (1H, m), 2.37 (4H, m) 2.03 (2H, q, *J* = 6.5 Hz), 1.30 (4H, m), 0.87 (3H, t, *J* = 6.5 Hz); ^{13}C NMR (125 MHz, $CDCl_3$) δ 179.9, 131.9, 126.9, 34.2, 31.8, 26.9, 22.5, 22.3, 14.0 ppm.

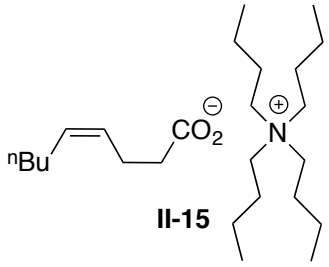

II-15

Analytical data for **tetrabutylammonium (*Z*)-non-4-enoate** (**II-15**): colorless oil; ^{1}H NMR (500 MHz, $CDCl_3$) δ 5.40 (1H, m), 5.26 (1H, m), 3.36 (8H, AB quartet, *J* = 8.0 Hz), 2.35 (2H, dd, *J* = 7.0, 16.0 Hz), 2.18 (2H, dd, *J* = 6.0, 9.0 Hz), 2.02 (2H, m), 1.63 (8H, m), 1.40 (8H, sextet, *J* = 7.0 Hz), 1.27 (4H, m), 0.97 (12H, t, *J* = 7.5 Hz), 0.84 (3H, t, *J* = 6.5 Hz); ^{13}C NMR (125 MHz, $CDCl_3$) δ 178.5, 130.7, 129.0, 58.8, 39.1, 32.1, 26.9, 25.2, 24.1, 22.4, 19.8, 14.0, 13.7 ppm. IR (film) 3001, 2962, 2874, 1652, 1576, 1458, 1395, 1296, 1155, 1096, 885, 737 cm^{-1}.

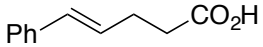

II-16

Analytical data for **(*E*)-5-phenylpent-4-enoic acid** (**II-16**):[74] crystalline white solid, recrystallized from hot ethyl acetate, m.p. 89 ºC (lit.[71] 86.6 ºC); ^{1}H NMR (500 MHz, $CDCl_3$) δ 11.92 (1H, br s),

7.39-7.23 (5H, m), 6.48 (1H, d, *J* = 16.0 Hz), 6.27-6.22 (1H, m), 2.58 (4H, m); ^{13}C NMR (125 MHz, $CDCl_3$) δ 179.7, 137.2, 131.2, 128.5, 127.9, 127.2, 126.0, 33.8, 27.8 ppm.

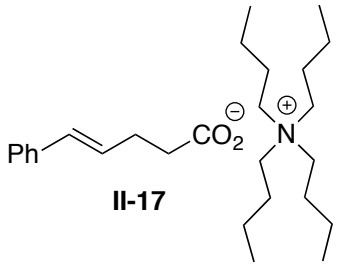

II-17

Analytical data for **tetrabutylammonium (*E*)-5-phenylpent-4-enoate** (**II-17**): pale yellow oil; ^{1}H NMR (500 MHz, $CDCl_3$) δ 7.28 (2H, d, *J* = 7.0 Hz), 7.21 (2H, t, *J* = 7.5 Hz), 7.10 (1H, m), 6.34 (2H, m), 3.33 (8H, AB quartet, *J* = 8.0 Hz), 2.52 (2H, m), 2.32 (2H, dd, *J* = 5.5, 8.0 Hz), 1.60 (8H, m), 1.40 (8H, sextet, *J* = 7.5 Hz), 0.95 (12H, t, *J* = 7.0 Hz); ^{13}C NMR (125 MHz, $CDCl_3$) δ 177.9, 138.4, 132.6, 128.6, 128.3, 126.3, 125.8, 58.7, 38.6, 30.8, 24.0, 19.7, 13.7 ppm. IR (film) 3058, 2961 (s), 2875 (s), 2740, 1766, 1649, 1575 (s), 1424 (s), 1384, 1153, 1068, 965, 880, 740 (s) cm^{-1}.

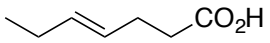

II-18

Analytical data for **(*E*)-hept-4-enoic acid** (**II-18**):[81] colorless oil; ^{1}H NMR (500 MHz, $CDCl_3$) δ 11.64 (1H, br s), 5.51 (1H, dtt, *J* = 1.5, 6.5, 13.5 Hz), 5.38 (1H, dtt, *J* = 1.5, 6.5, 13.5 Hz), 2.40 (2H, dt, *J* = 1.0, 8.0 Hz), 2.27-2.32 (2H, m), 1.98 (2H, dquint. *J* = 1.5, 7.5 Hz), 0.94 (3H, t, *J* = 7.5 Hz); ^{13}C NMR (125 MHz, $CDCl_3$) δ 179.8, 133.6, 126.5, 34.2, 27.5, 25.5, 13.7 ppm.

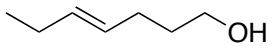

II-18-OH

Analytical data for **(*E*)-hept-4-en-1-ol** (**II-18**-OH):[76] colorless oil; ^{1}H NMR (500 MHz, $CDCl_3$) δ 5.46 (1H, dtt, *J* = 1.5, 6.5, 9.0 Hz), 5.37 (1H, dtt, *J* = 1.0, 6.5, 9.0 Hz), 3.60 (2H, t, *J* = 6.0 Hz), 2.04 (2H, ddd, *J* = 1.5, 7.5, 15.0.), 1.96 (2H, m), 1.73 (1H, br s), 1.59 (2H, quint, *J* = 7.0 Hz), 0.93 (3H, t, *J* = 7.5 Hz); ^{13}C NMR (125 MHz, $CDCl_3$) δ 132.7, 128.4, 62.4, 32.4, 28.8, 25.5, 13.9 ppm.

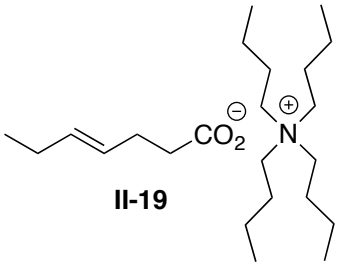

II-19

Analytical data for **tetrabutylammonium (*E*)-hept-4-enoate** (**II-19**): colorless oil; ^{1}H NMR (500 MHz, $CDCl_3$) δ 5.40 (2H, m), 3.32 (8H, AB quartet, *J* = 8.5 Hz), 2.28-2.24 (2H, m), 2.21-2.18 (2H, m), 1.90 (2H, m), 1.61 (8H, m), 1.36 (8H, sextet, *J* = 7.5 Hz), 0.94 (12H, t, *J* = 7.5 Hz), 0.87 (3H, t, *J* = 7.5 Hz); ^{13}C NMR (125 MHz, $CDCl_3$) δ 178.1, 131.0, 129.8, 58.7, 29.9, 25.5, 24.0, 19.7, 13.9, 13.6 ppm. IR (film) 2963 (s), 2875 (s), 2742, 1758, 1651, 1543 (s), 1444, 1382, 1248, 1103, 1035, 966, 886, 740 cm^{-1}.

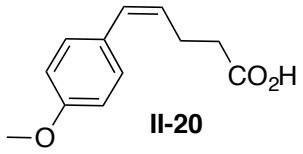

II-20

Analytical data for **(*Z*)-5-(4-methoxyphenyl)pent-4-enoic acid** (**II-20**):[77] Recrystallized from hot ethyl acetate. White solid, m.p. 67 ºC (lit.[77] 64-65 ºC); ^{1}H NMR (500 MHz, $CDCl_3$) δ 11.60 (1H, br s), 7.20 (2H, d, *J* = 9.0 Hz), 6.87 (2H, dd, *J* = 3.0, 9.0 Hz), 6.40 (1H, d, *J* = 11.5 Hz), 5.20 (1H, dt, *J* = 7.5, 11.5 Hz), 3.80 (3H, s), 2.65 (2H, ddd, *J* = 1.5, 7.0, 8.5 Hz), 2.49 (2H, dd, *J* = 7.5, 15.0 Hz); ^{13}C NMR (125 MHz, $CDCl_3$) δ 179.4, 158.4, 129.9, 129.8, 129.7, 128.3, 55.2, 34.2, 23.7 ppm.

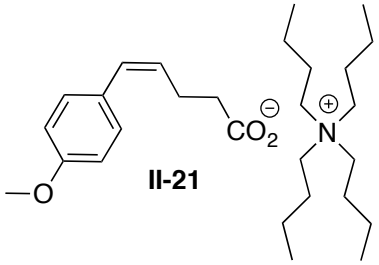

II-21

Analytical data for **tetrabutylammonium (*Z*)-5-(4-methoxyphenyl)pent-4-enoate** (**II-21**): pale yellow oil; ^{1}H NMR (500 MHz, $CDCl_3$) δ 7.24 (2H, d, *J* = 8.5 Hz), 6.78 (2H, m), 6.22 (1H, d, *J* = 12.0 Hz), 5.63 (1H, dt, *J* = 7.0, 11.5 Hz), 3.75 (3H, s), 3.32 (8H, AB quartet, *J* = 8.5 Hz), 2.63 (2H, ddd, *J* = 1.5, 7.5, 9.0 Hz), 2.30 (2H, dd, *J* = 7.5, 9.5 Hz), 1.60 (8H, m), 1.38 (8H, sextet, *J* = 7.5 Hz), 0.94 (12H, t, *J* = 7.5 Hz); ^{13}C NMR (125 MHz, $CDCl_3$) δ 177.9, 157.8, 132.7, 130.8, 130.0, 127.1, 113.3, 58.7, 55.2, 39.0, 26.5, 24.0, 19.7, 13.7 ppm. IR (film) 3175, 2961 (s), 2875, 1761, 1650, 1591 (s), 1511 (s), 1465, 1382, 1247, 1176, 1031, 842, 739 cm^{-1}.

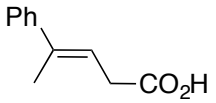

II-22

Analytical data for **(*E*)-4-phenylpent-3-enoic acid** (**II-22**):[78,79] White solid, m.p. 75 ºC (lit.[79] 76-77 ºC); ^{1}H NMR (500 MHz, $CDCl_3$) δ 11.12 (1H, br s), 7.42 (2H, d, *J* = 7.0 Hz), 7.34 (2H, t, *J* = 7.0 Hz), 7.23 (1H, m), 5.95 (1H, dt, *J* = 1.5, 7.5 Hz), 3.33 (2H, d, J = 7.5 Hz), 2.10 (3H, s); ^{13}C NMR (125 MHz, $CDCl_3$) δ 178.3, 142.9, 138.7, 128.2, 127.2, 125.8, 118.3, 34.1, 16.2 ppm.

The *E*-geometry was established based on NOESY experiment.

NOESY data: (a) Irradiation at 5.95 ppm shows enhancement at 7.42 and 3.33 ppm, (b) Irradiation at 3.33 ppm shows enhancement at 5.95 and 2.10 ppm and, (c) Irradiation at 2.10 ppm shows enhancement at 3.33 and 7.42 ppm.

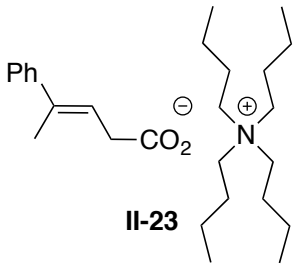

II-23

Analytical data for **tetrabutylammonium (*E*)-4-phenylpent-3-enoate** (**II-23**): pale yellow oil; ^{1}H NMR (500 MHz, $CDCl_3$) δ 7.40 (2H, dd, *J* = 1.0, 7.5 Hz), 7.22 (2H, t, *J* = 7.5 Hz), 7.11 (1H, t, *J* = 7.5 Hz), 6.27 (1H, dt, *J* = 1.0, 7.0 Hz), 3.29 (8H, AB quartet, *J* = 8.5 Hz), 3.16 (2H, d, *J* = 7.0 Hz), 2.00 (3H, s), 1.58 (8H, m), 1.37 (8H, sextet, *J* = 7.5 Hz), 0.94 (12H, t, *J* = 7.0 Hz); ^{13}C NMR (125 MHz, $CDCl_3$) δ 176.3, 144.3, 132.8, 127.8, 126.8, 125.8, 125.6, 58.7, 39.3, 24.0, 19.7, 15.9, 13.7

ppm. IR (film) 3011, 2965 (s), 2876, 1770 (w), 1595 (s), 1464, 1377, 1153, 1061, 873, 757, 699 cm^{-1}.

iii. Synthesis of isotopically labeled substrates:

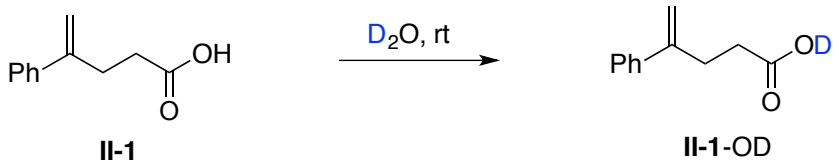

II-1 **II-1**-OD

4-phenylpent-4-enoic acid-*d*$_1$ (**II-1**-OD): Alkenoic acid **II-1**[69] (50 mg, 0.28 mmol) was suspended in D_2O (2 mL) in a 10 mL round bottom flask attached to a condenser. The resulting suspension was warmed over a steam bath for 20 min and the suspension was concentrated to dryness using a rotary evaporator. Another 2 mL of D_2O was added to the residue and the process was repeated three more times. Finally, the solid obtained was dried under vacuum (250 mtorr) for 12 h.

Analytical data for **II-1**-OD: white solid, m.p. 95 °C; NMR data is identical to previously reported data for the unlabeled substrate.[37,69] ^{1}H NMR (500 MHz, $CDCl_3$) δ 7.39 (2H, d, *J* = 7.5 Hz), 7.33 (2H, t, *J* = 7.5 Hz), 7.27 (1H, m), 5.31 (1H, br s), 5.10 (1H, br s), 2.84 (2H, t, *J* = 7.0 Hz), 2.54 (2H, t, *J* = 7.0 Hz); ^{13}C NMR (125 MHz, $CDCl_3$) δ 179.4, 146.5, 140.4, 128.4, 127.7, 126.1, 113.0, 32.9, 30.1 ppm. IR (film) 3100-2200 (br), 1697, 1625, 1443, 1411, 1312, 1218, 1026, 900, 779, cm^{-1}.

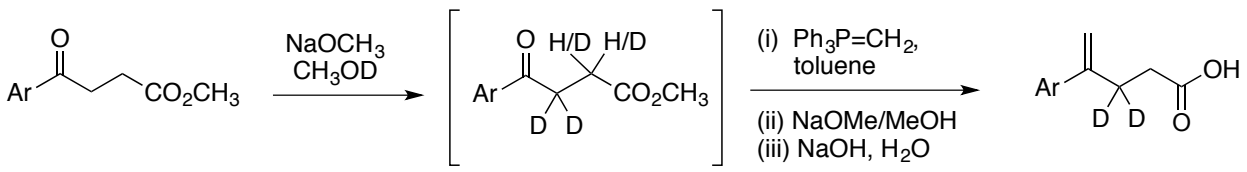

(3,3-*d*$_2$) -4-phenylpent-4-enoic acid (**II-1**-D_2)**:**

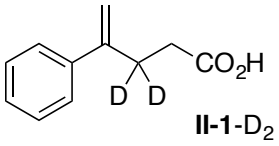

II-1-D_2

Recrystallized 4-oxo-4-phenylbutanoic acid[82] (500 mg, 2.80 mmol) was dissolved in 2 mL of methanol in a 10 mL round bottom flask. The solution was cooled at 0 ºC using an ice bath. To this cold solution, thionyl chloride (0.22 mL, 2.95 mmol, 1.05 equiv) was added drop wise over 15 min. The reaction mixture was stirred for 30 min at 0 ºC. It was then diluted with DCM (10 mL) and poured in a separatory funnel and washed with ice-cold 10% aq. $NaHCO_3$ solution (5 mL). The organics were washed with brine (2 mL), separated, dried over anhydrous Na_2SO_4 and concentrated to obtain the corresponding methyl ester. It was used for the next step without any further purification.

Crude methyl-4-oxo-4-phenylbutanoate (535 mg, 2.78 mmol) obtained above was dissolved in CH_3OD (2.5 mL) along with catalytic amount of $NaOCH_3$ (26 mg, 0.47 mmol, 0.17 equiv). The reaction mixture was stirred for 12 h at room temperature. The solvent was partially removed using a rotary evaporator and 2.5 mL of CH_3OD were introduced to the reaction flask. The mixture was allowed to stir for 12 h more after which the reaction mixture was diluted with DCM (10 mL) and poured in a separatory funnel containing 5 mL of ice-cold saturated aq. NH_4Cl solution. The organics were washed quickly (<2 min) with the satd. aq. NH_4Cl solution and then

with brine solution (5 mL). The organics were separated, dried over anhydrous Na_2SO_4, concentrated and dried under vacuuo to obtain the corresponding α-dideuterated keto-ester. It was then subjected to the next step immediately without further purification.

A 25 mL flame dried flask was charged with methyltriphenylphosphonium bromide (1.01 g, 2.83 mmol, 1.1 equiv) and dry toluene (7.5 mL). The resulting suspension was cooled to 0 ºC on an ice bath and 1.0 M NaHMDS in THF (2.83 mL, 2.83 mmol, 1.1 equiv) was added drop wise. The suspension turned clear with a bright yellow color. The resulting ylide solution was then stirred for 30 min at 0 ºC and then cooled further to -78 ºC (dry ice/acetone bath). To this cold reaction mixture, a solution of crude methyl-4-oxo-4-phenylbutanoate-3,3-d_2 (500 mg, 2.57 mmol, 1.0 equiv in 1 mL toluene) obtained above, was added at once. The reaction was eventually warmed to room temperature over a period of 1 h and then placed in a pre-heated oil bath at 70 ºC. Heating was continued for 8 h after which the reaction mixture was cooled to room temperature and poured in a separatory funnel containing saturated aq. NH_4Cl solution (10 mL). The organics were washed with brine, separated, dried over anhydrous Na_2SO_4, concentrated and the product was dissolved in 20% ethyl acetate in hexanes (30 mL) and filtered through a pad of silica (5 cm height, 2.5 cm diameter) using a frit funnel. The resulting solution of dideuterated alkenoic ester was concentrated using a rotary evaporator, dissolved in CH_3OH (5 mL) and treated with 20 mol% $NaOCH_3$. The reaction mixture was stirred for 8 h at room temperature. This was necessary to remove the undesired labeling at the α-carbon of the ester functionality. The reaction mixture was then concentrated to a volume of 2 mL followed by addition of NaOH (308 mg, 7.71 mmol, 3.0 equiv) pre-dissolved in water (1 mL). After stirring for further 8 h, the resulting solution was cooled on an ice bath and treated with conc. HCl until the pH of the solution was 2. The solution was diluted with ethyl acetate (10 mL) and poured in a separatory funnel containing brine solution (5 mL). The organics were then washed with 10% aq. HCl followed by brine (2 mL).

Finally, the solution was dried over anhydrous Na_2SO_4, concentrated and the crude product (**II-1**-D_2) was subjected to purification using silica gel flash chromatography with 25% ethyl acetate in hexanes as eluent. Pure product (3,3-*d*$_2$)-4-phenylpent-4-enoic acid (299 mg, **II-1**-D_2) was obtained as a white powder in 65% yield from its corresponding crude α-dideuterated keto-ester. It was further purified by recrystallization from hot 20% ethyl acetate in hexanes. Recrystallized product (230 mg) was collected in 2 crops in 50 % isolated yield (90% deuterium incorporation).

Note: All intermediates were verified by crude ^{1}H NMR analysis and completion of reaction was judged by TLC and ^{1}H NMR. The intermediates may be purified if necessary, however H-D exchange was observed in case of α-dideutero keto ester upon purification by silica gel column chromatography.

Analytical data for (3,3-*d*$_2$)-4-phenylpent-4-enoic acid (**II-1**-D_2): White crystalline plates, mp. 82 ºC; ^{1}H NMR (500 MHz, $CDCl_3$) δ 11.40 (1H, br s), 7.39 (2H, d, *J* = 7.5 Hz), 7.39 (2H, m), 7.33 (2H, m), 7.27 (1H, ddd, *J* = 1.0, 6.0, 8.5 Hz), 5.32 (1H, br s), 5.10 (1H, br s), 2.83 (0.2H, m, 10% residual CH_2), 2.51 (2H, m); ^{13}C NMR (125 MHz, $CDCl_3$) δ 179.4, 146.4, 140.4, 128.4, 127.7, 126.1, 113.0, 32.8, 29.7 (quint, *J* = 19.9 Hz) ppm. IR (film) 3100-2600 (br), 2360, 2330, 1955, 1894, 1813, 1696 (s), 1621, 1442, 1410, 1306, 1077, 902, 831, 779, 698 cm^{-1}. HRMS (ESI) Calculated Mass for $C_{11}H_9D_2O_2$: ($[M-H]^-$) = 177.0890, Found ($[M-H]^-$) = 177.0890.

(3,3-*d*$_2$)-4-(4-methoxyphenyl)pent-4-enoic acid (**1e**-D_2)**:**

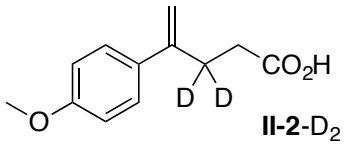

II-2-D_2

The same procedure described above for **II-1**-D_2 was employed for the synthesis of **II-2**-D_2. Using 500 mg of 4-(4-methoxyphenyl)-4-oxobutanoic acid,[82] 260 mg (52% overall yield) of pure **II-2**-D_2 was obtained (82% deuterium incorporation).

Analytical data for (3,3-*d*$_2$)-4-(4-methoxyphenyl)pent-4-enoic acid (**II-2**-D_2): White crystalline solid, mp. 131 ºC; ^{1}H NMR (500 MHz, $CDCl_3$) δ 11.06 (1H, br s), 7.32 (2H, dd, *J* = 2.0, 7.0 Hz), 6.85 (2H, dd, *J* = 2.0, 7.0 Hz), 5.24 (1H, br s), 5.01 (1H, br s), 3.80 (3H, s), 2.80 (0.36H, m, 18% residual CH_2), 2.50 (2H, m); ^{13}C NMR (125 MHz, $CDCl_3$) δ 178.7, 159.3, 145.7, 132.7, 127.1, 113.8, 111.4, 55.3, 32.8, 30.1 (quint, *J* = 19.0 Hz) ppm. IR (film) 3100-2600 (br), 2360, 2330, 1955, 1894, 1813, 1696 (s), 1621, 1442, 1410, 1306, 1077, 902, 831, 779, 698 cm^{-1}. HRMS (ESI) Calculated Mass for $C_{12}H_{11}D_2O_3$: ($[M-H]^-$) = 207.0996, Found ($[M-H]^-$) = 207.0999.

General procedure for synthesis of ^{18}O labeled alkenoic acids:[83]

^{18}O-labeled water was purchased as a normalized 99% ^{18}O solution (1% ^{16}O) from Cambridge Isotope Laboratories, Inc.

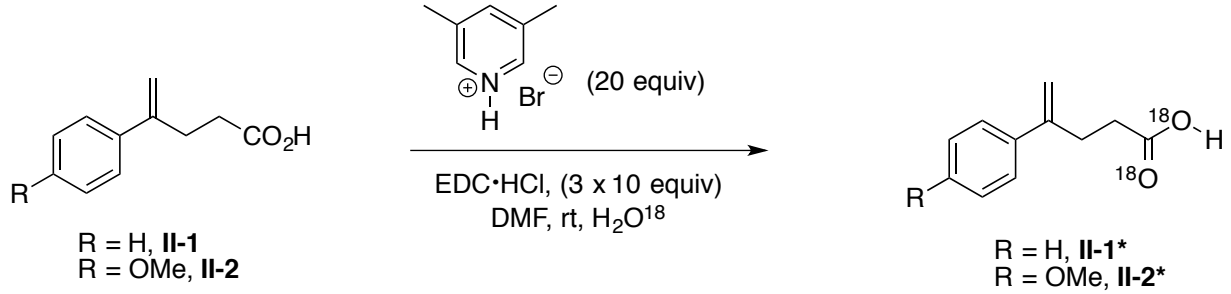

R = H, **II-1**
R = OMe, **II-2**

R = H, **II-1***
R = OMe, **II-2***

3 5-lutidine hydrogen bromide was prepared as follows:

Freshly distilled 3 5-lutidine (1mL) was placed in a 50 mL flame dried two neck flask under argon atmosphere. Diethyl ether (15 mL) was added and the solution was cooled to 0 ºC using an ice bath. Dry HBr gas (made by reacting anhydrous NaBr with conc. H_2SO_4) was bubbled through this cold solution (vigorously stirred) for 2 min at a rate such that the temperature of the reaction mixture was maintained below 2-5 ºC. The desired hydrobromide salt precipitated as a white solid. It was filtered under nitrogen atmosphere and washed with diethyl ether (10 mL) followed by pentanes (10 mL). The resulting solid was dried under vacuuo prior to use. This procedure gave 1.64 g of the desired salt in quantitative yield.

The 3,5-dimethylpyridine hydrobromide prepared above (425 mg, 4.52 mmol, 20 equiv) was suspended in dry DMF (2 ml) under nitrogen. To this solution, EDC•HCl (430 mg, 1.12 mmol, 10 equiv, dried under vacuum for 5h prior to use), $^{18}OH_2$ (112 μL, 99%, 5.7 mmol, 50 equiv) and the alkenoic acid (0.11 mmol) were added in sequence. The mixture was stirred at room temperature for 18 h under argon atmosphere. A second portion of dry EDC•HCl (215 mg, 1.12

mmol, 10 equiv) was added and the mixture was stirred for another 8 h at room temperature. Finally, a third portion of dry EDC•HCl (215 mg, 1.12 mmol, 10 equiv) was added and stirring was continued for another 15 hours. The reaction was diluted by adding 10 mL ethyl acetate, washed with 0.1 M citric acid (3 x 10 ml) followed by brine (5 mL). The organics were separated, dried over anhydrous Na_2SO_4, concentrated and subjected to purification using silica gel flash chromatography with 25% ethyl acetate in hexanes as eluent. The alkenoic acids were then recrystallized from hot ethyl acetate: hexanes (1:5).

4-phenylpent-4-enoic-1,1-$^{18}O_2$ acid (II-1*):

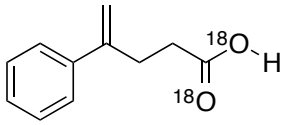

II-1*

Analytical data for 4-phenylpent-4-enoic-1,1-$^{18}O_2$ acid (**II-1***): White crystalline plates, mp. 89 ºC, NMR data is identical to the unlabeled substrate;[37,69] ^{1}H NMR (500 MHz, $CDCl_3$) ^{1}H NMR (500 MHz, $CDCl_3$) δ 11.40 (1H, br s), 7.39 (2H, d, *J* = 7.5 Hz), 7.39 (2H, m), 7.33 (2H, m), 7.27 (1H, ddd, *J* = 1.0, 6.0, 8.5 Hz), 5.32 (1H, br s), 5.10 (1H, br s), 2.83 (2H, m), 2.51 (2H, m); ^{13}C NMR (125 MHz, $CDCl_3$) δ 179.4, 146.4, 140.4, 128.4, 127.7, 126.1, 113.0, 32.8, 29.7 ppm. IR (film) 3300-2600 (br), 1954, 1891, 1674(s), 1625, 1444, 1411, 1265, 1026, 901, 779, 703 cm^{-1}. HRMS (ESI) Calculated Mass for $C_{11}H_{11}{}^{18}O_2$: ($[M-H]^-$) = 179.0849, Found ($[M-H]^-$) = 179.0852.

4-(4-methoxyphenyl)pent-4-enoic-1,1-$^{18}O_2$ acid (II-2*):

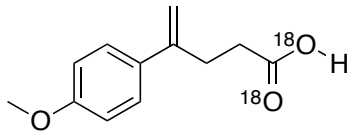

II-2*

Analytical data for 4-(4-methoxyphenyl)pent-4-enoic-1,1-$^{18}O_2$ acid (**II-2***): White crystalline solid, mp. 131 ºC, NMR data is identical to the unlabeled substrate;[37] ^{1}H NMR (500 MHz, $CDCl_3$) δ 11.06 (1H, br s), 7.32 (2H, dd, *J* = 2.0, 7.0 Hz), 6.85 (2H, dd, *J* = 2.0, 7.0 Hz), 5.24 (1H, br s), 5.01 (1H, br s), 3.80 (3H, s), 2.80 (2H, m), 2.50 (2H, m); ^{13}C NMR (125 MHz, $CDCl_3$) δ 178.7, 159.3, 145.7, 132.7, 127.1, 113.8, 111.4, 55.3, 32.8, 30.1 ppm. IR (film) 3000-2550 (br), 1904, 1795, 1668 (s), 1623, 1515, 1423, 1254, 1030, 895, 840 cm^{-1}. HRMS (ESI) Calculated Mass for $C_{12}H_{13}O^{18}O_2$: ($[M-H]^-$) = 209.0955, Found ($[M-H]^-$) = 209.0956.

II.5.3. Halocyclization reactions.

General Procedure:

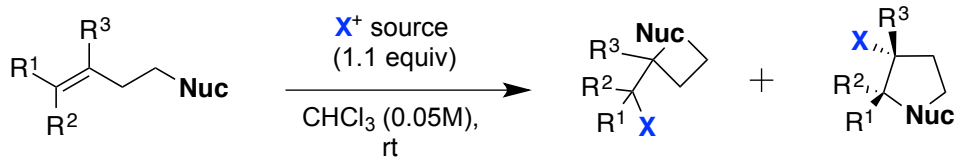

Unless otherwise mentioned, all reactions were performed at room temperature at 0.05 M substrate concentration in amylene stabilized $CHCl_3$. The reactions were conducted in absence of light to avoid radical halogenation. Reactions were initially ran using 0.1 mmol of the substrate and then scaled up at 1.0 mmol scale.

In a 10 mL flame dried round bottom flask, 1.0 mmol of the substrate was dissolved in $CHCl_3$ (50 mL, amylene stabilized) at room temperature under argon atmosphere. The flask was then wrapped with an aluminum foil and placed in dark. To this homogenous solution, 1.10 mmol of the halogenating reagent was added and then reaction was continued to stir until complete consumption of the starting material (as judged by TLC and ^1H NMR analysis). Upon completion of the reaction, the contents were poured in a separatory funnel containing 50 mL of ice-cold solution of 10% aq. sodium sulfite (Na_2SO_3). The organics were then washed with brine solution (10 mL), separated, dried over anhydrous Na_2SO_4, filtered, concentrated and then subjected to crude ^1H NMR analysis using undecane (0.05 M) as internal standard. Purification was then commenced using silica gel flash chromatography with ethyl acetate and hexanes as eluent.

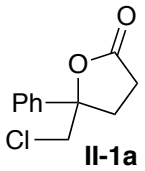

II-1a

Analytical data for **5-(chloromethyl)-5-phenyldihydrofuran-2(3H)-one** (**II-1a**):[37] colorless oil; ^{1}H NMR (500 MHz, $CDCl_3$) δ 7.39-7.31 (5H, m), 3.71 (1H, d, *J* = 11.5 Hz), 3.67 (1H, d, *J* = 11.5 Hz), 2.77 (2H, m), 2.52 (2H, m); ^{13}C NMR (125 MHz, $CDCl_3$) δ 175.4, 140.6, 128.7, 128.5, 124.7, 86.3, 40.9, 32.2, 28.9 ppm.

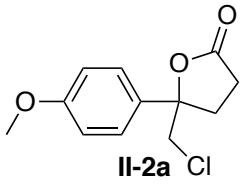

II-2a

Analytical data for **5-(chloromethyl)-5-(4-methoxyphenyl)dihydrofuran-2(3H)-one** (**II-2a**):[37] colorless oil; ^{1}H NMR (500 MHz, $CDCl_3$) δ 7.31 (2H, d, *J* = 8.5.), 6.90 (2H, d, *J* = 8.5.), 3.80 (3H, s), 3.79 (1H, d, *J* = 12.0 Hz), 3.73 (1H, d, *J* = 12.0 Hz), 2.76 (2H, m), 2.49 (2H, m); ^{13}C NMR (125 MHz, $CDCl_3$) δ 175.7, 159.8, 132.5, 126.2, 114.2, 87.0, 55.3, 52.2, 31.2, 29.0 ppm.

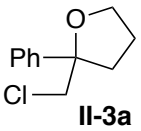

II-3a

Analytical data for **2-(chloromethyl)-2-phenyltetrahydrofuran** (**II-3a**): colorless oil; ^{1}H NMR (500 MHz, $CDCl_3$) δ 7.42-7.39 (2H, m), 7.34 (2H, t, *J* = 7.5 Hz), 7.26 (1H, m), 4.07 (1H, dd, *J* = 7.0, 15.0 Hz), 3.92 (1H, dd, *J* = 7.0, 15.0 Hz), 3.70 (2H, m), 2.41 (1H, dt, *J* = 8.0, 12.5 Hz), 2.20 (1H, ddd, *J* = 5.5, 8.0, 13.0 Hz), 2.07-1.99 (1H, m), 1.87-1.79 (1H, m); ^{13}C NMR (125 MHz, $CDCl_3$) δ

143.7, 127.9, 127.0, 125.3, 85.6, 68.4, 52.1, 35.3, 25.8 ppm. IR (film) 3060, 2954, 2875, 1601, 1493, 1449, 1301, 1217, 1132, 1060 (s), 1027, 986, 763, 727, 701 cm^{-1}. HRMS (ESI) Calculated Mass for $C_{11}H_{14}ClO$: ($[M+H]^+$) = 197.0733, Found ($[M+H]^+$) = 197.0733.

Note: Chloroether **II-3a** is highly volatile. Based on ^1H NMR, the yields for chloroetherification of **II-3** were >90%, however the isolated yields ranged from 30-55%. Following the general procedure described above, compound **II-3a** was purified via silica gel flash chromatography using dichloromethane and pentanes (1:5) as eluents. The purified fractions were concentrated using rotary evaporator (pressure should not be lower than 90 mtorr) with the flask immersed under ice-water bath. Complete removal of residual dichloromethane led to poor isolated yields (10-15%).

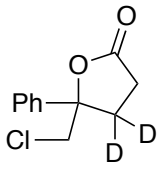

II-1a-D_2

Analytical data for **5-(chloromethyl)-5-phenyldihydrofuran-2(3H)-one-4,4-*d*$_2$** (**II-1a**-D_2): colorless oil; ^1H NMR (500 MHz, $CDCl_3$) δ 7.39-7.32 (5H, m), 3.83 (1H, d, *J* = 12.0 Hz), 3.75 (1H, d, *J* = 12.0 Hz), 2.77 (1H, d, *J* = 18.0 Hz), 2.52 (1H, d, *J* = 18.0 Hz); ^{13}C NMR (125 MHz, $CDCl_3$) δ 175.7, 140.6, 128.8, 128.7, 124.9, 87.0, 52.1, 31.2 (quint, *J* = 19.5 Hz), 28.8 ppm. IR (film) 3068, 3032, 2961, 2410, 2366, 2251, 1955, 1782 (broad and strong), 1653, 1496, 1449, 1255, 1169, 1037, 930, 702 cm^{-1}. HRMS (ESI) Calculated Mass for $C_{11}H_{10}D_2ClO_2$: ($[M+H]^+$) = 213.0651, Found ($[M+H]^+$) = 213.0650.

8-chloro-3,5-dimethyl-6-oxabicyclo[3.2.1]oct-2-en-7-one (**II-6a**-Cl)**:**

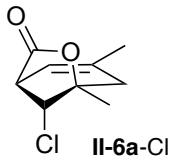

II-6a-Cl

Analytical data for 8-chloro-3,5-dimethyl-6-oxabicyclo[3.2.1]oct-2-en-7-one (**II-6a**-Cl): Pale yellow oil, ^{1}H NMR (500 MHz, $CDCl_3$) δ 5.39 (1H, m.), 4.09 (1H, d, *J* = 4.5 Hz.), 3.23 (1H, dd, *J* = 4.5, 6.5 Hz.), 2.44 (1H, d, *J* = 19.0 Hz.), 2.23 (1H, d, *J* = 19.0 Hz.), 1.74 (3H, br s.), 1.47 (3H, s.); ^{13}C NMR (125 MHz, $CDCl_3$) δ 171.5, 137.8, 114.2, 84.5, 58.5, 45.3, 38.8, 21.8 ppm. IR (film) 3007, 2978, 2840, 1780 (s), 1653, 1445, 1384, 1152, 928, 867 cm^{-1}. HRMS (ESI) Calculated Mass for $C_9H_{12}ClO_2$: ($[M+H]^+$) = 187.0526, Found ($[M+H]^+$) = 187.0522.

5-chloro-3,5-dimethyl-7-oxabicyclo[4.2.0]oct-2-en-8-one (**II-6b**-Cl)**:**

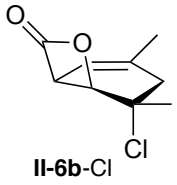

II-6b-Cl

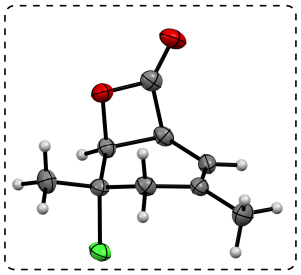

crystal structure of **II-6b**-Cl

Analytical data for 5-chloro-3,5-dimethyl-7-oxabicyclo[4.2.0]oct-2-en-8-one (**II-6b**-Cl): Pale yellow crystalline solid, mp = 46 ºC, ^{1}H NMR (500 MHz, $CDCl_3$) δ 5.45 (1H, m.), 4.56 (1H, dd, *J* = 1.5, 5.0 Hz.), 4.17 (1H, t, *J* = 6.0 Hz.), 2.42 (1H, dt, *J* = 1.5, 2.5, 17.0 Hz.), 2.33 (1H, d, *J* = 2.0, 17.0 Hz.), 1.78 (3H, s.), 1.70 (3H, s.); ^{13}C NMR (125 MHz, $CDCl_3$) δ 166.9, 137.4, 111.0, 73.0, 64.0, 50.1, 39.5, 27.0, 23.8 ppm. IR (film) 3010, 2978, 2935, 1835 (s), 1670, 1448, 1380, 1255, 1121, 876

cm^{-1}. HRMS (ESI) Calculated Mass for $C_9H_{12}ClO_2$: ($[M+H]^+$) = 187.0526, Found ($[M+H]^+$) = 187.0525.

8-bromo-3,5-dimethyl-6-oxabicyclo[3.2.1]oct-2-en-7-one (**II-6a**-Br**):**

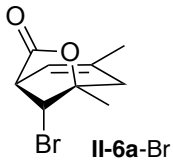

II-6a-Br

Analytical data for 8-bromo-3,5-dimethyl-6-oxabicyclo[3.2.1]oct-2-en-7-one (**II-6a**-Br): Pale yellow oil, ^{1}H NMR (500 MHz, $CDCl_3$) δ 5.53 (1H, d, *J* = 7.0 Hz.), 4.19 (1H, d, *J* = 4.5 Hz.), 3.22 (1H, dd, *J* = 4.5, 7.0 Hz.), 2.48 (1H, d, *J* = 18.5 Hz.), 2.27 (1H, d, *J* = 18.5 Hz.), 1.73 (3H, br s.), 1.46 (3H, s.); ^{13}C NMR (125 MHz, $CDCl_3$) δ 171.9, 137.6, 115.6, 84.7, 49.3, 45.4, 39.4, 22.0, 21.7 ppm. IR (film) 3055, 2978, 2912, 1783 (s), 1656, 1446, 1383, 1271, 1196, 1148, 1070, 925, 868 cm^{-1}. HRMS (ESI) Calculated Mass for $C_9H_{12}BrO_2$: ($[M+H]^+$) = 231.0021, Found ($[M+H]^+$) = 231.0021.

5-bromo-3,5-dimethyl-7-oxabicyclo[4.2.0]oct-2-en-8-one (**II-6b**-Br**):**

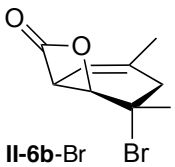

II-6b-Br

Analytical data for 5-bromo-3,5-dimethyl-7-oxabicyclo[4.2.0]oct-2-en-8-one (**II-6b**-Br): Pale crystalline solid, decomposes upon heating above 45 ºC, ^{1}H NMR (500 MHz, $CDCl_3$) δ 5.51 (1H, d, *J* = 6.5 Hz.), 4.78 (1H, d, *J* = 5.0 Hz.), 4.20 (1H, t, *J* = 6.0 Hz.), 2.46 (2H, m.), 1.93 (3H, s.), 1.81 (3H, s.); ^{13}C NMR (125 MHz, $CDCl_3$) δ 167.1, 138.3, 111.1, 73.5, 59.2, 50.5, 40.6, 28.3, 23.9 ppm.

IR (film) 3048, 2974, 2932, 2873, 1833 (s), 1778, 1713, 1447, 1381, 1257, 1176, 1120, 1064, 867, 816 cm^{-1}. HRMS (ESI) Calculated Mass for $C_9H_{12}BrO_2$: ($[M+H]^+$) = 231.0021, Found ($[M+H]^+$) = 231.0020.

8-iodo-3,5-dimethyl-6-oxabicyclo[3.2.1]oct-2-en-7-one (**II-6a**-I**):**

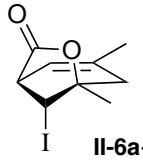

II-6a-I

Analytical data for 8-iodo-3,5-dimethyl-6-oxabicyclo[3.2.1]oct-2-en-7-one (**II-6a**-I): Pale yellow oil, ^{1}H NMR (500 MHz, $CDCl_3$) δ 5.55 (1H, d, *J* = 7.0 Hz.), 4.24 (1H, d, *J* = 4.5 Hz.), 3.17 (1H, dd, *J* = 4.5, 7.0 Hz.), 2.51 (1H, d, *J* = 18.5 Hz.), 2.32 (1H, d, *J* = 18.5 Hz.), 1.73 (3H, br s.), 1.46 (3H, s.); ^{13}C NMR (125 MHz, $CDCl_3$) δ 172.5, 137.4, 118.3, 85.2, 46.3, 40.7, 27.0, 22.4, 21.8 ppm. IR (film) 3047, 2976, 2910, 1783 (s), 1656, 1445, 1384, 1305, 1184, 1143, 1066, 924, 862, 697 cm^{-1}. HRMS (ESI) Calculated Mass for $C_9H_{12}IO_2$: ($[M+H]^+$) = 278.9882, Found ($[M+H]^+$) = 278.9884.

8-chloro-3,5-dimethyl-6-oxabicyclo[3.2.1]oct-2-ene (**II-8a**-Cl**):**

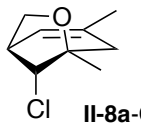

II-8a-Cl

Analytical data for 8-chloro-3,5-dimethyl-6-oxabicyclo[3.2.1]oct-2-ene (**II-8a**-Cl): colorless oil, ^{1}H NMR (500 MHz, $CDCl_3$) δ 5.52 (1H, d, *J* = 7.0 Hz.), 3.92 (2H, m.), 3.84 (1H, d, *J* = 6.5 Hz.), 2.75 (1H, dt, *J* = 4.0, 6.5 Hz.), 2.32 (1H, d, *J* = 18.5 Hz.), 1.95 (1H, d, *J* = 18.5 Hz.), 1.67 (3H, br s.), 1.30 (3H, s.); ^{13}C NMR (125 MHz, $CDCl_3$) δ 135.1, 120.6, 79.9, 74.3, 61.6, 43.1, 41.9, 22.9, 21.9

ppm. IR (film) 3027, 2935, 2866, 1708, 1645, 1600, 1493, 1447, 1345, 1055, 972, 760, 700 cm^{-1}. HRMS (ESI) Calculated Mass for $C_9H_{14}ClO$: ($[M+H]^+$) = 173.0733, Found ($[M+H]^+$) = 173.0736.

8-bromo-3,5-dimethyl-6-oxabicyclo[3.2.1]oct-2-ene (**II-8a**-Br**):**

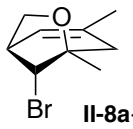

II-8a-Br

Analytical data for 8-bromo-3,5-dimethyl-6-oxabicyclo[3.2.1]oct-2-ene (**II-8a**-Br): colorless oil, ^1H NMR (500 MHz, $CDCl_3$) δ 5.53 (1H, dd, *J* = 1.5, 7.0 Hz.), 3.97 (1H, d, *J* = 3.0 Hz.), 3.92 (1H, m.), 3.85 (1H, d, *J* = 7.0 Hz.), 2.77 (1H, dt, *J* = 4.0, 7.0 Hz.), 2.37 (1H, d, *J* = 17.5 Hz.), 2.00 (1H, d, *J* = 17.5 Hz.), 1.66 (3H, br s.), 1.30 (3H, s.); ^{13}C NMR (125 MHz, $CDCl_3$) δ 134.9, 121.7, 80.0, 74.5, 53.2, 43.8, 42.1, 22.9, 21.9 ppm. IR (film) 2962, 2927, 2869, 1833 (w), 1718, 1666, 1451, 1414, 1379, 1249, 1114 (s), 1029, 815 cm^{-1}. HRMS (ESI) Calculated Mass for $C_9H_{14}BrO$: ($[M+H]^+$) = 217.0228, Found ($[M+H]^+$) = 217.0226.

5-bromo-3,5-dimethyl-7-oxabicyclo[4.2.0]oct-2-ene (**II-8b**-Br**):**

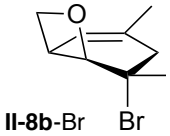

II-8b-Br

Analytical data for 5-bromo-3,5-dimethyl-7-oxabicyclo[4.2.0]oct-2-ene (**II-8b**-Br): colorless oil, ^1H NMR (500 MHz, $CDCl_3$) δ 5.11 (1H, br s.), 4.58 (1H, d, *J* = 4.0 Hz.), 3.79 (1H, m.), 3.36 (1H, m.), 2.77 (1H, d, *J* = 19.0 Hz.), 2.50 (1H, d, *J* = 19.5 Hz.), 2.02 (3H, s.), 1.69 (3H, s.); ^{13}C NMR (125 MHz, $CDCl_3$) δ 131.9, 116.7, 65.8, 65.4, 61.5, 43.6, 42.5, 34.1, 23.0 ppm. IR (film) 3020, 2920,

2801, 1711, 1600, 1462, 1444, 1319, 1204, 1050, 1012, 749 cm^{-1}. HRMS (ESI) Calculated Mass for $C_9H_{14}BrO$: ($[M+H]^+$) = 217.0228, Found ($[M+H]^+$) = 217.0228.

8-iodo-3,5-dimethyl-6-oxabicyclo[3.2.1]oct-2-ene (**II-8a**-I**):**

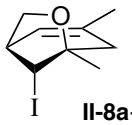

II-8a-I

Analytical data for 8-iodo-3,5-dimethyl-6-oxabicyclo[3.2.1]oct-2-ene (**II-8a**-I): pale yellow oil, ^1H NMR (500 MHz, $CDCl_3$) δ 5.55 (1H, d, *J* = 6.0 Hz.), 3.98 (1H, d, *J* = 3.5 Hz.), 3.89 (2H, m.), 2.76 (1H, m.), 2.41 (1H, d, *J* = 18.0 Hz.), 2.07 (1H, d, *J* = 18.0 Hz.), 1.66 (3H, s.), 1.33 (3H, s.); ^{13}C NMR (125 MHz, $CDCl_3$) δ 134.6, 123.8, 80.6, 74.7, 45.0, 43.2, 31.3, 23.0, 21.9 ppm. IR (film) 2967, 2983, 2866, 1724, 1607, 1448, 1378, 1334, 1211, 1096, 1012, 916, 810, 729 cm^{-1}. HRMS (ESI) Calculated Mass for $C_9H_{14}IO$: ($[M+H]^+$) = 265.0089, Found ($[M+H]^+$) = 265.0088.

8-chloro-3,5-dimethyl-N-phenyl-6-oxabicyclo[3.2.1]oct-2-en-7-imine (**II-9a**-Cl**):**

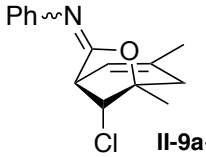

II-9a-Cl
(*E*:*Z* = 1:1)

Analytical data for 8-chloro-3,5-dimethyl-N-phenyl-6-oxabicyclo[3.2.1]oct-2-en-7-imine (**II-9a**-Cl): inseparable mixture of *E* and *Z* isomers (~1:1) colorless oil, ^1H NMR (500 MHz, $CDCl_3$) δ 7.29-7.25 (3H, m), 7.10-7.03 (5H, m.), 6.84 (2H, d, *J* = 7.5 Hz), 5.64 (1H, d, *J* = 6.5 Hz.), 5.37 (1H, d, *J* = 6.5 Hz.), 4.16 (1H, d, *J* = 4.5 Hz.), 4.08 (1H, d, *J* = 4.5 Hz.), 3.36 (1H, dd, *J* = 4.5, 7.0 Hz.), 3.22 (1H, dd, *J* = 4.5, 7.0 Hz.), 2.45-2.18 (4H, m.), 1.74 (6H, m.), 1.50 (3H, s.), 1.41 (3H, s.); ^{13}C NMR

(125 MHz, $CDCl_3$) δ 164.7, 160.5, 148.1, 145.7, 138.5, 137.2, 136.1, 132.5, 129.3, 129.2, 129.2, 129.2, 128.8, 128.7, 128.7, 124.4, 124.2, 123.9, 123.5, 123.5, 123.5, 123.5, 121.4, 121.4, 121.4, 117.1, 116.1, 85.8, 83.9, 77.5, 77.5, 77.3, 77.0, 59.7, 59.3, 46.2, 41.7, 39.8, 39.8, 30.9, 26.5, 25.5, 22.3, 22.2, 22.1, 22.1, 21.4 ppm. IR (film) 3295, 3060, 2923, 1775, 1707, 1652, 1600, 1541, 1498, 1442, 1322, 1265, 1178, 1074, 754, 692 cm^{-1}. HRMS (ESI) Calculated Mass for $C_{15}H_{17}ClNO$: ($[M+H]^+$) = 262.0999, Found ($[M+H]^+$) = 262.0999.

Note: The complex nature of NMR spectrum can be attributed not only to the inseparable isomeric (*E* and *Z*) forms, but also to the rotamers along the N-Ph bond. To validate this hypothesis, a solution of 20 mg of **II-9a**-Cl in 1 mL THF/H_2O (1:1) was treated with 1μL of 12M HCl for 12h at ambient temperature. The resulting hydrolysis followed by purification, furnished 9 mg (63% yield) of pure **II-6a**-Cl with spectral and physical properties as reported above.

8-bromo-3,5-dimethyl-N-phenyl-6-oxabicyclo[3.2.1]oct-2-en-7-imine (**II-9a**-Br**):**

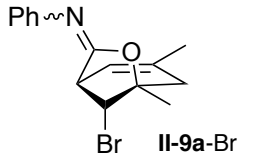

II-9a-Br
(*E*:*Z* = 1:1)

Analytical data for 8-bromo-3,5-dimethyl-N-phenyl-6-oxabicyclo[3.2.1]oct-2-en-7-imine (**II-9a**-Br): pale yellow oil, ^1H NMR (500 MHz, $CDCl_3$) δ 7.28-7.25 (3H, m), 7.10-7.02 (5H, m.), 6.84 (2H, d, *J* = 8.0 Hz), 5.66 (1H, d, *J* = 6.5 Hz.), 5.39 (1H, d, *J* = 7.0 Hz.), 4.21 (1H, d, *J* = 4.0 Hz.), 4.13 (1H, d, *J* = 4.0 Hz.), 3.36 (1H, dd, *J* = 4.5, 7.0 Hz.), 3.22 (1H, dd, *J* = 4.5, 7.0 Hz.), 2.49-2.22 (4H, m.), 1.75 (6H, m.), 1.50 (3H, s.), 1.42 (3H, s.); ^{13}C NMR (125 MHz, $CDCl_3$) δ 164.5, 160.2, 147.8, 145.5, 138.2, 137.0, 135.8, 132.2, 129.0, 128.5, 124.2, 124.0, 123.6, 123.3, 121.2, 116.9, 115.9, 85.6, 83.7, 59.4, 59.0, 46.0, 41.4, 39.6, 39.5, 32.2, 30.7, 26.2, 25.4, 22.1, 21.9, 21.9, 21.2 ppm. IR

(film) 3160, 2975, 2913, 2856, 1780, 1659, 1600, 1544, 1443, 1324, 1247, 1149, 1081, 925, 755 cm^{-1}. HRMS (ESI) Calculated Mass for $C_{15}H_{17}BrNO$: ($[M+H]^+$) = 306.04935, Found ($[M+H]^+$) = 306.04937.

8-iodo-3,5-dimethyl-N-phenyl-6-oxabicyclo[3.2.1]oct-2-en-7-imine (II-9a-I):

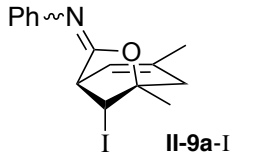

II-9a-I
(*E*:*Z* = 1:1)

Analytical data for 8-iodo-3,5-dimethyl-N-phenyl-6-oxabicyclo[3.2.1]oct-2-en-7-imine (**II-9a**-I): pale yellow oil, ^1H NMR (500 MHz, $CDCl_3$) δ 7.30-7.25 (3H, m), 7.08-7.03 (5H, m.), 6.84 (2H, d, *J* = 7.5 Hz), 5.69 (1H, d, *J* = 6.5 Hz.), 5.42 (1H, d, *J* = 7.0 Hz.), 4.25 (1H, d, *J* = 4.0 Hz.), 4.18 (1H, d, *J* = 4.0 Hz.), 3.33 (1H, dd, *J* = 4.0, 7.0 Hz.), 3.18 (1H, dd, *J* = 4.0, 7.0 Hz.), 2.54-2.30 (4H, m.), 1.75 (6H, m.), 1.51 (3H, s.), 1.43 (3H, s.); ^{13}C NMR (125 MHz, $CDCl_3$) δ 165.1, 160.9, 147.9, 145.5, 136.6, 135.4, 133.4, 129.1, 129.0, 128.5, 124.7, 123.9, 123.6, 123.3, 121.2, 120.7, 120.1, 119.8, 86.5, 84.4, 47.2, 42.6, 41.5, 41.4, 28.3, 27.8, 22.6, 22.4, 21.8, 21.8, 21.3 ppm. IR (film) 3054, 2969, 2915, 2850, 1771, 1654, 1599, 1538, 1442, 1327, 1245, 1180, 925, 757 cm^{-1}. HRMS (ESI) HRMS (ESI) Calculated Mass for $C_{15}H_{17}INO$: ($[M+H]^+$) = 354.03549, Found ($[M+H]^+$) = 354.03549.

5-chloro-7-oxabicyclo[4.2.0]oct-2-en-8-one (**II-10b**-Cl**):**

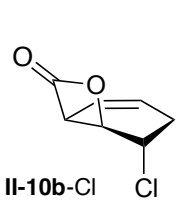

II-10b-Cl

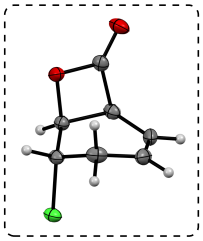

crystal structure of **II-10b**-Cl

Analytical data for 5-chloro-7-oxabicyclo[4.2.0]oct-2-en-8-one (**II-10b**-Cl): Pale yellow oil, ^{1}H NMR (500 MHz, $CDCl_3$) δ 6.03 (1H, dt, *J* = 4.5, 9.5.), 5.87 (1H, dd, *J* = 7.5, 9.0 Hz.), 4.79 (1H, m.), 4.48 (1H, d, *J* = 3.0 Hz.), 4.28 (1H, t, *J* = 6.0 Hz.), 2.63 (2H, m.); ^{13}C NMR (125 MHz, $CDCl_3$) δ 166.0, 127.5, 118.1, 70.6, 50.6, 49.0, 27.6 ppm. IR (film) 3050, 2957, 2854, 1826 (s), 1646, 1429, 1367, 1269, 1232, 1105 (s), 902, 863, 683 cm^{-1}. HRMS (ESI) Calculated Mass for $C_7H_8ClO_2$: ($[M+H]^+$) = 159.0213, Found ($[M+H]^+$) = 159.0212.

5-bromo-7-oxabicyclo[4.2.0]oct-2-en-8-one (**II-10b**-Br**):**

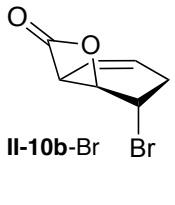

II-10b-Br

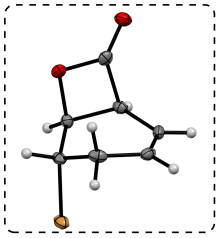

crystal structure of **II-10b**-Br

Analytical data[84] for 5-bromo-7-oxabicyclo[4.2.0]oct-2-en-8-one (**II-10b**-Br):[84] White crystalline solid, mp = 99 ºC (lit.[84] 97 ºC) ^{1}H NMR (500 MHz, $CDCl_3$) δ 6.04 (1H, dt, *J* = 5.0, 10.0.), 5.89 (1H, dd, *J* = 7.0, 9.5 Hz.), 4.92 (1H, m.), 4.53 (1H, d, *J* = 3.0 Hz.), 4.27 (1H, t, *J* = 6.0 Hz.), 2.71 (2H, m.); ^{13}C NMR (125 MHz, $CDCl_3$) δ 166.0, 128.2, 118.3, 70.6, 49.1, 41.4, 27.9 ppm.

8-iodo-6-oxabicyclo[3.2.1]oct-2-en-7-one (II-10a-I):

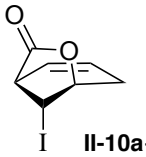

II-10a-I

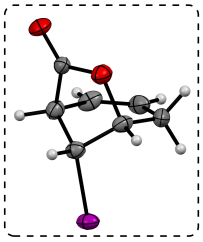

crystal structure of **II-10a**-Cl

Analytical data for 8-iodo-6-oxabicyclo[3.2.1]oct-2-en-7-one (**II-10a**- I): White solid, decomposes above 47 ºC, ^{1}H NMR (500 MHz, $CDCl_3$) δ 5.89 (1H, d, *J* = 9.5.), 5.82 (1H, dd, *J* = 8.5, 8.5 Hz.), 4.73 (1H, m.), 4.54 (1H, t, *J* = 4.5 Hz.), 3.17 (1H, dd, *J* = 5.0, 6.5 Hz.), 2.81 (1H, dd, *J* = 2.5, 19.5 Hz.), 2.57 (1H, d, *J* = 19.5 Hz.); ^{13}C NMR (125 MHz, $CDCl_3$) δ 171.9, 127.4, 124.1, 78.3, 43.4, 30.1, 17.0 ppm. IR (film) 3046, 2926, 1772 (s), 1537, 1412, 1333, 1220, 1145, 1083, 919, 690 cm^{-1}. HRMS (ESI) Calculated Mass for $C_7H_8IO_2$: ($[M+H]^+$) = 250.9569, Found ($[M+H]^+$) = 250.9568.

5-iodo-7-oxabicyclo[4.2.0]oct-2-en-8-one (II-10b-I):

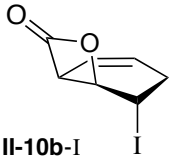

II-10b-I

Analytical data for 5-iodo-7-oxabicyclo[4.2.0]oct-2-en-8-one (**II-10b**-I): white solid with a purple tint of liberated iodine indicating possible decomposition. Stored at -20 ºC as a 0.1 M solution in $CHCl_3$ or DCM in dark. Product is stable at room temperature for about 2-3 h and undergoes rapid decomposition upon heating above 30 ºC, ^{1}H NMR (500 MHz, $CDCl_3$) δ 5.95 (1H, dt, *J* = 4.5, 10.0.), 5.87 (1H, m.), 4.86 (1H, dd, *J* = 3.0, 5.5 Hz.), 4.47 (1H, dd, *J* = 3.5, 3.5 Hz.), 4.21 (1H, t, *J* = 6.0 Hz.), 2.61 (2H, m.); ^{13}C NMR (125 MHz, $CDCl_3$) δ 165.8, 129.2, 118.1, 71.6, 48.7, 28.5, 19.7

ppm. IR (film) 3052, 2964, 1811 (s), 1652, 1426, 1358, 1127, 845 cm^{-1}. HRMS (ESI) Calculated Mass for $C_7H_8IO_2$: ($[M+H]^+$) = 250.9569, Found ($[M+H]^+$) = 250.9566.

***syn*-5-chloro(phenyl)methyl)dihydrofuran-2(3H)-one (II-12b-Cl):**

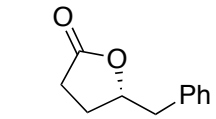

II-12b-Cl

Analytical data for *syn*-5-chloro(phenyl)methyl)dihydrofuran-2(3H)-one (**II-12b**-Cl): colorless oil, ^1H NMR (500 MHz, $CDCl_3$) δ 7.45-7.41 (2H, m.), 7.38-7.32 (3H, m.), 4.96 (1H, d, *J* = 5.0 Hz), 4.90-4.86 (1H, m.), 2.46-2.37 (1H, m.), 2.29-2.15 (2H, m.), 2.13-2.05 (1H, m.); ^{13}C NMR (125 MHz, $CDCl_3$) δ 176.2, 136.1, 129.1, 128.8, 128.0, 81.9, 63.6, 28.0, 24.5 ppm. IR (film) 3032, 2916, 1781, 1444, 1411, 1332, 1165, 1153, 1035, 924, 875 cm^{-1}. HRMS (ESI) Calculated Mass for $C_{11}H_{12}ClO_2$: ($[M+H]^+$) = 211.0526, Found ($[M+H]^+$) = 211.0525.

***syn*-5-bromo(phenyl)methyl)dihydrofuran-2(3H)-one (6b-Br):**

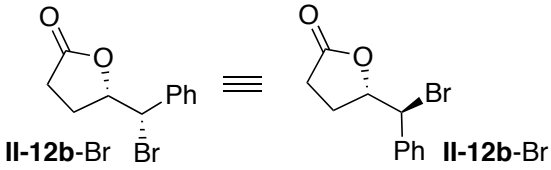

II-12b-Br

II-12b-Br

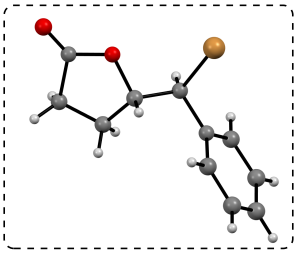

crystal structure of **II-12b**-Br

Analytical data[61] for *syn*-5-bromo(phenyl)methyl)dihydrofuran-2(3H)-one (**II-12b**-Br): white crystalline solid, mp = 131 ºC, (lit.[61] 126-129 ºC), ^1H NMR (500 MHz, $CDCl_3$) δ 7.45-7.42 (2H, m.),

7.36-7.30 (3H, m.), 4.97 (1H, d, *J* = 5.5 Hz), 4.90 (1H, ddd, *J* = 1.0, 5.5, 6.5 Hz.), 2.50-2.34 (2H, m.), 2.26-2.19 (1H, m.), 2.04 (1H, dddd, *J* = 7.0, 8.5, 10.0, 13.5 Hz.); ^{13}C NMR (125 MHz, $CDCl_3$) δ 176.0, 136.8, 128.8, 128.4, 81.9, 55.2, 28.3, 25.6 ppm.

***syn*-5-iodo(phenyl)methyl)dihydrofuran-2(3H)-one (II-12b-I):**

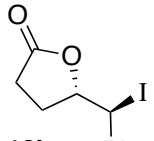

II-12b-I

Analytical data[61] for *syn*-5-iodo(phenyl)methyl)dihydrofuran-2(3H)-one (**II-12b**-I): pale crystalline solid, decomposes above 85 ºC, (lit.[61] mp = 90-94 ºC), ^{1}H NMR (500 MHz, $CDCl_3$) δ 7.44-7.43 (2H, m.), 7.32-7.26 (3H, m.), 5.10 (1H, d, *J* = 6.0 Hz), 4.65 (1H, dd, *J* = 7.5, 7.0 Hz.), 2.51-2.47 (2H, m.), 2.30-2.23 (1H, m.), 1.99-1.91 (1H, m.); ^{13}C NMR (125 MHz, $CDCl_3$) δ 175.7, 139.1, 128.9, 128.7, 128.5, 82.8, 34.1, 28.7, 26.9 ppm.

***syn*-5-(1-chloropentyl)dihydrofuran-2(3H)-one (II-14b-Cl):**

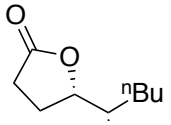

II-14b-Cl

Analytical data for *syn*-5-(1-chloropentyl)dihydrofuran-2(3H)-one (**II-14b**-Cl): colorless oil, ^{1}H NMR (500 MHz, $CDCl_3$) δ 4.67 (1H, ddd, *J* = 2.5, 6.0, 8.0 Hz.), 3.92 (1H, dt, *J* = 3.0, 7.5 Hz.), 2.65 (1H, ddd, *J* = 6.0, 11.0, 17.0 Hz.), 2.50 (1H, ddd, *J* = 7.0, 10.5, 17.5 Hz.), 2.37-2.30 (1H, m.), 2.23-2.16 (1H, m.), 1.81 (2H, dd, *J* = 7.0, 7.5 Hz.), 1.57-1.49 (1H, m.), 1.42-1.25 (3H, m.), 0.89 (3H, t, *J* = 7.0 Hz.); ^{13}C NMR (125 MHz, $CDCl_3$) δ 176.6, 80.5, 64.5, 33.8, 28.6, 28.1, 24.5, 22.1, 13.8 ppm.

IR (film) 2957, 2872, 1778 (s), 1596, 1460, 1419, 1254, 1179, 1121, 1052, 915, 802 cm^{-1}. HRMS (ESI) Calculated Mass for $C_9H_{16}ClO_2$: ($[M+H]^+$) = 191.0839, Found ($[M+H]^+$) = 191.0841.

***syn*-5-(1-bromopentyl)dihydrofuran-2(3H)-one (II-14b-Br):**

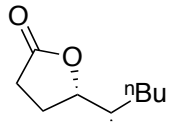

II-14b-Br

Analytical data for *syn*-5-(1-bromopentyl)dihydrofuran-2(3H)-one (**II-14b**-Br): colorless oil, ^1H NMR (500 MHz, $CDCl_3$) δ 4.62 (1H, ddd, *J* = 3.0, 6.5, 8.0 Hz.), 4.02 (1H, ddd, *J* = 3.0, 5.5, 8.5 Hz.), 2.66 (1H, ddd, *J* = 5.5, 10.5, 16.0 Hz.), 2.51 (1H, ddd, *J* = 8.0, 10.5, 18.5 Hz.), 2.40-2.32 (1H, m.), 2.20-2.12 (1H, m.), 1.90-1.86 (2H, m.), 1.59-1.50 (1H, m.), 1.42-1.24 (3H, m.), 0.88 (3H, t, *J* = 7.0 Hz.); ^{13}C NMR (125 MHz, $CDCl_3$) δ 176.5, 80.9, 58.0, 34.2, 29.7, 28.2, 25.3, 21.9, 13.8 ppm. IR (film) 2958, 2871, 1780 (s), 1459, 1419, 1355, 1176, 1052, 1018, 913, 795 cm^{-1}. HRMS (ESI) Calculated Mass for $C_9H_{16}BrO_2$: ($[M+H]^+$) = 235.0334, Found ($[M+H]^+$) = 235.0332.

***syn*-5-(1-iodopentyl)dihydrofuran-2(3H)-one (II-14b-I):**

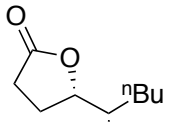

II-14b-I

Analytical data[85] for *syn*-5-(1-iodopentyl)dihydrofuran-2(3H)-one (**II-14b**-I): colorless oil, ^1H NMR (500 MHz, $CDCl_3$) δ 4.32 (1H, ddd, *J* = 3.0, 7.0, 10.5 Hz.), 4.12 (1H, dt, *J* = 4.5, 8.0 Hz.), 2.66 (1H, ddd, *J* = 4.5, 10.5, 15.5 Hz.), 2.53 (1H, ddd, *J* = 8.5, 10.5, 19.0 Hz.), 2.40 (1H, dddd, *J* = 4.5,

7.5, 10.5, 13.0 Hz.), 2.11-2.03 (1H, m.), 1.88 (1H, ddd, *J* = 4.5, 10.0, 14.5 Hz.), 1.75 (1H, ddd, *J* = 4.5, 10.0, 14.0 Hz.), 1.58-1.50 (1H, m.), 1.39-1.23 (3H, m.), 0.89 (3H, t, *J* = 7.5 Hz.); ^{13}C NMR (125 MHz, $CDCl_3$) δ 176.4, 81.8, 39.1, 35.3, 31.7, 28.6, 26.8, 21.8, 13.8 ppm. IR (film) 2956, 2871, 1779 (s), 1459, 1348, 1181, 1050, 991, 912, 805 cm^{-1}. HRMS (ESI) Calculated Mass for $C_9H_{16}IO_2$: ($[M+H]^+$) = 283.0195, Found ($[M+H]^+$) = 283.0199.

***anti*-5-chloro-6-phenyltetrahydro-2H-pyran-2-one (II-16a-Cl):**[86]

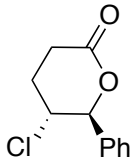

II-16a-Cl

Analytical data[86] for *anti*-5-chloro-6-phenyltetrahydro-2H-pyran-2-one (**II-16a**-Cl): white waxy solid, ^{1}H NMR (500 MHz, $CDCl_3$) δ 7.41-7.34 (3H, m.), 7.31-7.30 (2H, m.), 5.46 (1H, d, *J* = 6.0 Hz.), 4.30 (1H, dt, *J* = 4.5, 6.0 Hz.), 2.94 (1H, ddd, *J* = 7.0, 8.5, 16.0 Hz.), 2.69 (1H, dt, *J* = 5.5, 12.0 Hz.), 2.36-2.29 (1H, m.), 2.23-2.16 (1H, m.), 2.16 (1H, dt, *J* = 6.5, 12.5 Hz.); ^{13}C NMR (125 MHz, $CDCl_3$) δ 169.1, 137.0, 129.0, 128.8, 126.2, 85.2, 56.2, 27.2, 26.6 ppm.

***anti*-5-bromo-6-phenyltetrahydro-2H-pyran-2-one (II-16a-Br):**[61]

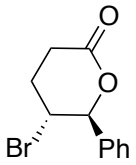

II-16a-Br

Analytical data[61] for *anti*-5-bromo-6-phenyltetrahydro-2H-pyran-2-one (**II-16a**-Br): white solid, mp = 101 ºC (lit.[61] 104-106 ºC), ^{1}H NMR (500 MHz, $CDCl_3$) δ 7.41-7.34 (3H, m.), 7.31-7.30 (2H, m.),

5.46 (1H, d, *J* = 6.0 Hz.), 4.30 (1H, dt, *J* = 4.5, 6.0 Hz.), 2.94 (1H, ddd, *J* = 7.0, 8.5, 18.0 Hz.), 2.69 (1H, dt, *J* = 5.5, 18.0 Hz.), 2.36-2.29 (1H, m.), 2.23-2.16 (1H, m.), 2.16 (1H, ddd, *J* = 6.5, 12.5, 14.5 Hz.); ^{13}C NMR (125 MHz, $CDCl_3$) δ 169.0, 137.2, 129.0, 128.8, 126.4, 85.5, 47.2, 28.3, 27.5 ppm.

***anti*-5-(1-bromopentyl)dihydrofuran-2(3H)-one (II-16b-Br):**[61,84]

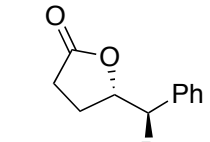

II-16b-Br

Analytical data[61,84] for *anti*-5-(1-bromopentyl)dihydrofuran-2(3H)-one (**II-16b**-Br): White solid, ^{1}H NMR (500 MHz, $CDCl_3$) δ 7.44-7.40 (2H, m.), 7.36-7.29 (3H, m.), 5.00 (1H, d, *J* = 7.0 Hz.), 4.92-4.88 (1H, m.), 2.53-2.45 (3H, m.), 2.29-2.19 (1H, m.); ^{13}C NMR (125 MHz, $CDCl_3$) δ 176.0, 137.0, 129.1, 128.8, 128.2, 81.6, 55.4, 28.6, 26.4 ppm.

***anti*-5-iodo-6-phenyltetrahydro-2H-pyran-2-one (II-16b-I):**[61]

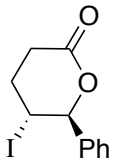

II-16a-I

Analytical data[61] for *anti*-5-iodo-6-phenyltetrahydro-2H-pyran-2-one (**II-16a**-I): white solid, decomposes above 70 ºC (lit.[61] mp = 68-76 ºC), ^{1}H NMR (500 MHz, $CDCl_3$) δ 7.40-7.36 (3H, m.), 7.31-7.29 (2H, m.), 5.53 (1H, d, *J* = 8.0 Hz.), 4.40 (1H, dt, *J* = 5.0, 8.5 Hz.), 2.82 (1H, dt, *J* = 7.0, 18.0 Hz.), 2.69 (1H, dt, *J* = 7.0, 18.0 Hz.), 2.47-2.32 (2H, m.); ^{13}C NMR (125 MHz, $CDCl_3$) δ 169.1, 137.6, 129.2, 128.7, 126.8, 87.1, 30.5, 24.3 ppm.

***anti*-5-(1-iodopentyl)dihydrofuran-2(3H)-one (II-16b-I):**

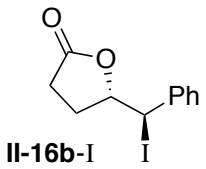

II-16b-I

Analytical data[61,87] for *anti*-5-(1-iodopentyl)dihydrofuran-2(3H)-one (**II-16b**-I): White solid, ^{1}H NMR (500 MHz, $CDCl_3$) δ 7.40-7.39 (2H, m.), 7.31-7.25 (3H, m.), 5.11 (1H, d, *J* = 8.0 Hz.), 4.89-4.85 (1H, m.), 2.64-2.48 (3H, m.), 2.17-2.09 (1H, m.); ^{13}C NMR (125 MHz, $CDCl_3$) δ 176.1, 139.1, 128.9, 128.7, 128.2, 82.5, 34.3, 29.3, 28.9 ppm.

***anti*-5-chloro-6-ethyltetrahydro-2H-pyran-2-one (II-18a-Cl):**

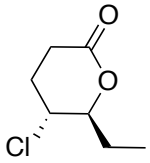

II-18a-Cl

Analytical data for *anti*-5-chloro-6-ethyltetrahydro-2H-pyran-2-one (**II-18a**-Cl): Compound **II-18a**-Cl could not be separated chromatographically from its regioisomer, **II-18b**-Cl. The assignments are based on 2D NMR experiments and the reported analytical data for the corresponding bromolactones.[88,89] ^{1}H NMR (mixture of **II-18a**-Cl: **II-18b**-Cl = 1.0:1.6) assignments are only made for protons from **II-18a**-Cl that were distinctly resolved (500 MHz, $CDCl_3$) δ 4.26 (1H, dt, *J* = 4.0, 8.0 Hz.), 3.98 (1H, ddd, *J* = 5.0, 7.5 Hz.), 2.78 (1H, td, *J* = 7.0, 14.5 Hz.), 1.03 (3H, t, *J* = 7.5 Hz.); ^{13}C NMR (125 MHz, $CDCl_3$) δ 169.8, 84.6, 54.0, 28.4, 27.9, 26.4, 9.0 ppm.

***anti*-5-(1-chloropropyl)dihydrofuran-2(3H)-one (II-18b-Cl):**

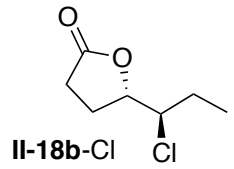

II-18b-Cl

Analytical data for *anti*-5-(1-chloropropyl)dihydrofuran-2(3H)-one (**II-18b**-Cl): colorless oil, ^{1}H NMR (500 MHz, $CDCl_3$) δ 4.51 (1H, dd, *J* = 7.0, 14.0 Hz.), 3.90 (1H, ddd, *J* = 3.5, 6.5, 10.0 Hz.), 2.62-2.48 (2H, m.), 2.40-2.33 (1H, m.), 2.20-2.12 (1H, m.), 1.93 (1H, dddd, *J* = 3.5, 7.0, 10.5, 14.5 Hz.), 1.67 (1H, septet, *J* = 7.5 Hz.), 1.06 (3H, t, *J* = 7.5 Hz.); ^{13}C NMR (125 MHz, $CDCl_3$) δ 176.4, 81.0, 65.5, 28.2, 27.4, 24.4, 10.5 ppm. IR (film) 2971, 2937, 2886, 1783 (s), 1459, 1421, 1336, 1176 (s), 1120, 1023, 914, 800 cm^{-1}. HRMS (ESI) Calculated Mass for $C_7H_{12}ClO_2$: ($[M+H]^+$) = 163.0526, Found ($[M+H]^+$) = 163.0525.

***anti*-5-bromo-6-ethyltetrahydro-2H-pyran-2-one (II-18a-Br):**

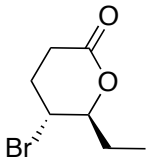

II-18a-Br

Analytical data for *anti*-5-bromo-6-ethyltetrahydro-2H-pyran-2-one (**II-18a**-Br): colorless oil, ^{1}H NMR (500 MHz, $CDCl_3$) δ 4.37 (1H, dt, *J* = 3.5, 8.0 Hz.), 4.05 (1H, dt, *J* = 5.0, 8.0 Hz.), 2.76 (1H, td, *J* = 7.0, 17.5 Hz.), 2.55 (1H, td, *J* = 7.0, 17.5 Hz.), 2.47-2.41 (1H, m.), 2.27 (1H, ddd, *J* = 7.5, 7.5, 14.5 Hz.), 1.96 (1H, dddd, *J* = 3.5, 7.5, 11.0, 15.0 Hz.), 1.75 (1H, septet, *J* = 7.5 Hz.), 1.03 (3H, t, *J* = 7.5 Hz.); ^{13}C NMR (125 MHz, $CDCl_3$) δ 169.9, 84.8, 45.0, 29.3, 28.9, 26.8, 8.9 ppm. IR

(film) 2971, 2893, 1741, 1461, 1336, 1176, 1021, 990, 914, 800 cm^{-1}. HRMS (ESI) Calculated Mass for $C_7H_{12}BrO_2$: ($[M+H]^+$) = 207.0020, Found ($[M+H]^+$) = 207.0021.

***anti*-5-(1-bromopropyl)dihydrofuran-2(3H)-one (II-18b-Br):**

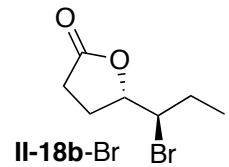

II-18b-Br

Analytical data for *anti*-5-(1-bromopropyl)dihydrofuran-2(3H)-one (**II-18b**-Br): colorless oil, ^1H NMR (500 MHz, $CDCl_3$) δ 4.54 (1H, dd, *J* = 7.0, 14.5 Hz.), 3.99 (1H, ddd, *J* = 3.5, 7.5, 9.0 Hz.), 2.66-2.49 (2H, m.), 2.49-2.42 (1H, m.), 2.19-2.11 (1H, m.), 2.06 (1H, dddd, *J* = 3.5, 7.5, 11.0, 14.5 Hz.), 1.86-1.77 (1H, m.), 1.08 (3H, t, *J* = 7.5 Hz.); ^{13}C NMR (125 MHz, $CDCl_3$) δ 176.3, 81.0, 59.4, 28.4, 27.8, 25.9, 11.5 ppm. IR (film) 2977, 2912, 2854, 1783 (s), 1449, 1411, 1330, 1174, 1110, 1023, 904, 804 cm^{-1}. HRMS (ESI) Calculated Mass for $C_7H_{12}BrO_2$: ($[M+H]^+$) = 207.0020, Found ($[M+H]^+$) = 207.0024.

***anti*-5-iodo-6-ethyltetrahydro-2H-pyran-2-one (II-18a-I):**

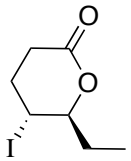

II-18a-I

Analytical data for *anti*-5-chloro-6-ethyltetrahydro-2H-pyran-2-one (**II-18a**-I): Compound **II-18a**-I could not be separated chromatographically from its regioisomer, **II-18b**-I. The assignments are based on 2D NMR experiments and the reported analytical data for the corresponding bromolactones.[88,89] ^1H NMR (mixture of **II-18a**-I : **II-18b**-I = 1:5) assignments are only made for

protons from **II-18a**-I that were distinctly resolved (500 MHz, $CDCl_3$) δ 4.44 (1H, dddd, *J* = 3.0, 7.5, 9.0, 10.5 Hz.), 4.09 (1H, ddd, *J* = 5.0, 9.0, 14.0 Hz.), 2.40-2.32 (1H, m.), 0.99 (3H, t, *J* = 6.0 Hz.); ^{13}C NMR (125 MHz, $CDCl_3$) δ 169.9, 85.9, 31.9, 30.8, 27.7, 22.0, 8.7 ppm.

***anti*-5-(1-iodopropyl)dihydrofuran-2(3H)-one (II-18b-I):**

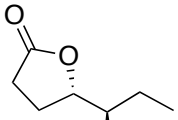

II-18b-I

Analytical data for *anti*-5-(1-iodopropyl)dihydrofuran-2(3H)-one (**II-18b**-I): colorless oil, ^1H NMR (500 MHz, $CDCl_3$) δ 4.38 (1H, dd, *J* = 7.5, 14.5 Hz.), 4.04 (1H, ddd, *J* = 3.5, 9.0, 12.5 Hz.), 2.62-2.46 (3H, m.), 2.04-1.90 (2H, m.), 1.83-1.74 (1H, m.), 1.04 (3H, t, *J* = 7.0 Hz.); ^{13}C NMR (125 MHz, $CDCl_3$) δ 176.3, 81.8, 41.4, 29.1, 28.9, 28.7, 13.6 ppm. IR (film) 2967, 2934, 2877, 1782 (s), 1457, 1419, 1325, 1179 (s), 1035, 912, 796 cm^{-1}. HRMS (ESI) Calculated Mass for $C_7H_{12}IO_2$: ($[M+H]^+$) = 254.9882, Found ($[M+H]^+$) = 254.9882.

***syn*-5-chloro-6-phenyltetrahydro-2H-pyran-2-one (II-12b-Cl):**

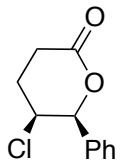

II-12a-Cl

Analytical data for *syn*-5-chloro-6-phenyltetrahydro-2H-pyran-2-one (**II-12a**-Cl): colorless oil, ^{1}H NMR (500 MHz, $CDCl_3$) δ 7.41-7.33 (5H, m.), 5.60 (1H, d, *J* = 2.0 Hz.), 4.48 (1H, dd, *J* = 3.5, 5.5 Hz.), 2.99 (1H, dddd, *J* = 8.0, 11.0, 18.5, 18.5 Hz.), 2.74 (1H, ddd, *J* = 2.5, 7.5, 18.5 Hz.), 2.52 (1H, dddd, *J* = 3.0, 7.0, 11.0, 14.5 Hz.), 2.42-2.36 (1H, m.); ^{13}C NMR (125 MHz, $CDCl_3$) δ 168.9, 136.2, 128.6, 128.3, 125.9, 82.1, 57.5, 28.6, 25.2 ppm. IR (film) 3010, 2929, 1710, 1615, 1530, 1240, 1184, 1041, 835 cm^{-1}. HRMS (ESI) Calculated Mass for $C_{11}H_{12}ClO_2$: ($[M+H]^+$) = 211.05258, Found ($[M+H]^+$) = 211.05254.

***syn*-5-bromo-6-phenyltetrahydro-2H-pyran-2-one (II-12a-Br):**

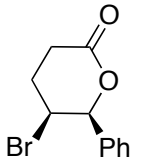

II-12a-Br

Analytical data[61] for *syn*-5-chloro-6-phenyltetrahydro-2H-pyran-2-one (**II-12a**-Br): pale oil, ^{1}H NMR (500 MHz, $CDCl_3$) δ 7.39-7.32 (5H, m.), 5.47 (1H, d, *J* = 1.5 Hz.), 4.56 (1H, dd, *J* = 3.0, 5.0 Hz.), 3.01 (1H, dddd, *J* = 8.0, 11.0, 18.5, 18.5 Hz.), 2.75 (1H, ddd, *J* = 2.0, 7.5, 18.5 Hz.), 2.60 (1H, dddd, *J* = 3.5, 7.5, 11.0, 14.5 Hz.), 2.48-2.42 (1H, m.); ^{13}C NMR (125 MHz, $CDCl_3$) δ 168.8, 137.0, 128.5, 128.3, 125.6, 81.9, 51.0, 29.3, 26.3 ppm.

***anti*-5-chloro-6-(4-methoxyphenyl)tetrahydro-2H-pyran-2-one (II-20a-Cl):**

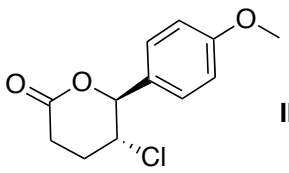

II-20a-Cl

Analytical data for *anti*-5-chloro-6-(4-methoxyphenyl)tetrahydro-2H-pyran-2-one (**II-20a**-Cl): white solid, ^{1}H NMR (500 MHz, $CDCl_3$) δ 7.23 (2H, d, *J* = 9.0 Hz.), 6.90 (2H, d, *J* = 9.0 Hz.), 5.38 (1H, d, *J* = 6.5 Hz.), 4.25 (1H, ddd, *J* = 4.5, 6.5, 11.0 Hz.), 3.80 (3H, s.), 2.92 (1H, td, *J* = 8.0, 18.0 Hz.), 2.67 (1H, td, *J* = 6.5, 18.5 Hz.), 2.39-2.32 (1H, m.), 2.16 (1H, ddd, *J* = 6.5, 13.5, 13.5 Hz.); ^{13}C NMR (125 MHz, $CDCl_3$) δ 169.3, 160.0, 129.0, 127.7, 114.1, 85.0, 56.3, 55.3, 27.4, 27.0 ppm. IR (film) 3015, 2958, 2919, 2839, 1746, 1614, 1516, 1455, 1250, 1178, 1030, 835 cm^{-1}. HRMS (ESI) Calculated Mass for $C_{12}H_{14}ClO_3$: ($[M+H]^+$) = 241.0632, Found ($[M+H]^+$) = 241.0635.

***syn*-5-chloro-6-(4-methoxyphenyl)tetrahydro-2H-pyran-2-one (II-20b-Cl):**

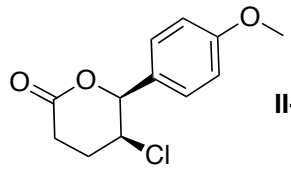

II-20b-Cl

Analytical data for *syn*-5-chloro-6-(4-methoxyphenyl)tetrahydro-2H-pyran-2-one (**II-20b**-Cl): low melting white solid, ^{1}H NMR (500 MHz, $CDCl_3$) δ 7.29 (2H, d, *J* = 8.5 Hz.), 6.91 (2H, d, *J* = 8.5 Hz.), 5.54 (1H, d, *J* = 2.0 Hz.), 4.43 (1H, m.), 3.80 (3H, s.), 2.98 (1H, dddd, *J* = 7.5, 10.5, 18.5, 18.5 Hz.), 2.72 (1H, ddd, *J* = 2.0, 7.5, 18.5 Hz.), 2.50 (1H, dddd, *J* = 3.5, 7.5, 11.0, 14.5 Hz.), 2.41-2.35 (1H, m.); ^{13}C NMR (125 MHz, $CDCl_3$) δ 169.0, 159.7, 128.3, 127.3, 113.7, 81.9, 57.8, 55.3, 28.6, 25.2 ppm. IR (film) 3002, 2917, 2850, 1741, 1618, 1516, 1462, 1348, 1252, 1176,

1109, 1059, 911, 731 cm^{-1}. HRMS (ESI) Calculated Mass for $C_{12}H_{14}ClO_3$: ($[M+H]^+$) = 241.0632, Found ($[M+H]^+$) = 241.0631.

***anti*-5-bromo-6-(4-methoxyphenyl)tetrahydro-2H-pyran-2-one** (**II-20a**-Br**):**

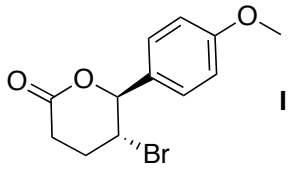

II-20a-Br

Analytical data for *anti*-5-bromo-6-(4-methoxyphenyl)tetrahydro-2H-pyran-2-one (**II-20a**-Br): white solid, ^{1}H NMR (500 MHz, $CDCl_3$) δ 7.23 (2H, d, *J* = 9.0 Hz.), 6.90 (2H, d, *J* = 9.0 Hz.), 5.46 (1H, d, *J* = 7.0 Hz.), 4.32 (1H, ddd, *J* = 4.5, 7.0, 11.5 Hz.), 3.80 (3H, s.), 2.91 (1H, td, *J* = 7.5, 18.0 Hz.), 2.68 (1H, td, *J* = 6.5, 18.5 Hz.), 2.43 (1H, dddd, *J* = 4.5, 6.5, 8.0, 11.5 Hz.), 2.27 (1H, ddd, *J* = 6.5, 13.5, 13.5 Hz.); ^{13}C NMR (125 MHz, $CDCl_3$) δ 169.2, 160.1, 129.3, 127.8, 114.1, 85.3, 55.3, 47.4, 28.6, 28.0 ppm.

Analytical data for **II-20a**-Br is in accord with the literature data,[77] however the reported relative stereochemistry (*syn*) does not match the ^{1}H coupling constants and NOE results. Our assignment of the relative stereochemistry of **II-20a**-Br is based on NOE results and ^{1}H coupling constants and comparison of the spectral data to compounds **II-20a**-Cl, **II-20b**-Cl, **II-20b**-Br and **II-20a**-I.[90]

***syn*-5-bromo-6-(4-methoxyphenyl)tetrahydro-2H-pyran-2-one** (**II-20b**-Br**):**

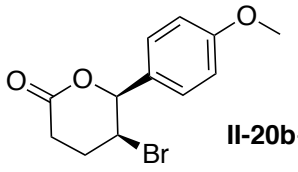

II-20b-Br

Analytical data for *syn*-5-bromo-6-(4-methoxyphenyl)tetrahydro-2H-pyran-2-one (**II-20b**-Br): colorless oil, ^{1}H NMR (500 MHz, $CDCl_3$) δ 7.27 (2H, d, *J* = 8.5 Hz.), 6.90 (2H, d, *J* = 8.5 Hz.), 5.41 (1H, br s.), 4.51 (1H, m.), 3.80 (3H, s.), 3.00 (1H, dddd, *J* = 8.0, 10.5, 18.5, 18.5 Hz.), 2.74 (1H, ddd, *J* = 1.5, 7.5, 18.5 Hz.), 2.56 (1H, dddd, *J* = 3.0, 7.0, 10.5, 14.5 Hz.), 2.47-2.42 (1H, m.); ^{13}C NMR (125 MHz, $CDCl_3$) δ 168.9, 159.7, 129.2, 127.0, 113.6, 81.8, 55.3, 51.5, 29.2, 26.3 ppm. IR (film) 3031, 2926, 2850, 1735, 1721, 1612, 1515, 1251, 1180, 1033, 919, 733 cm^{-1}. HRMS (ESI) Calculated Mass for $C_{12}H_{14}BrO_3$: ($[M+H]^+$) = 285.01263, Found ($[M+H]^+$) = 285.01263.

***syn*-5-(bromo(4-methoxyphenyl)methyl)dihydrofuran-2(3H)-one** (**II-20c**-Br**):**

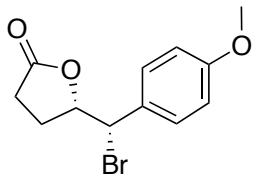

II-20c-Br

Analytical data for *syn*-5-(bromo(4-methoxyphenyl)methyl)dihydrofuran-2(3H)-one (**II-20c**-Br): white solid, ^{1}H NMR (500 MHz, $CDCl_3$) δ 7.36 (2H, d, *J* = 9.0 Hz.), 6.85 (2H, d, *J* = 9.0 Hz.), 4.96 (1H, d, *J* = 5.5 Hz.). 4.90-4.85 (1H, m.), 3.79 (3H, s.), 2.52-2.35 (2H, m.), 2.22 (1H, dddd, *J* = 5.5, 7.5, 10.0, 13.5 Hz.), 2.03 (1H, dddd, *J* = 7.0, 8.5, 10.0, 13.5 Hz.); ^{13}C NMR (125 MHz, $CDCl_3$) δ 176.0, 160.0, 129.7, 129.5, 114.2, 82.2, 55.3, 55.2, 28.3, 25.7 ppm. IR (film) 3001, 2905, 2848,

1725, 1611, 1513, 1464, 1249, 1179, 1034, 909.6, 733 cm^{-1}. HRMS (ESI) Calculated Mass for $C_{12}H_{14}BrO_3$: ($[M+H]^+$) = 285.01263, Found ($[M+H]^+$) = 285.01261.

***anti*-5-iodo-6-(4-methoxyphenyl)tetrahydro-2H-pyran-2-one (II-20a-I):**

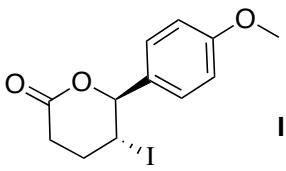

II-20a-I

Analytical data[90] for *anti*-5-iodo-6-(4-methoxyphenyl)tetrahydro-2H-pyran-2-one (**II-20a**-I): colorless oil, ^{1}H NMR (500 MHz, $CDCl_3$) δ 7.23 (2H, d, *J* = 9.0 Hz.), 6.89 (2H, d, *J* = 9.0 Hz.), 5.47 (1H, d, *J* = 8.0 Hz.), 4.36 (1H, td, *J* = 5.0, 8.5 Hz.), 3.80 (3H, s.), 2.81 (1H, td, *J* = 6.5, 18.0 Hz.), 2.70 (1H, td, *J* = 7.0, 18.5 Hz.), 2.52-2.46 (1H, m.), 2.39 (1H, ddd, *J* = 8.0, 15.5, 15.5 Hz.); ^{13}C NMR (125 MHz, $CDCl_3$) δ 169.4, 160.1, 129.8, 128.2, 114.0, 86.9, 55.3, 31.0, 30.7, 24.8 ppm.

***syn*-5-iodo-6-(4-methoxyphenyl)tetrahydro-2H-pyran-2-one (II-20b-I):**

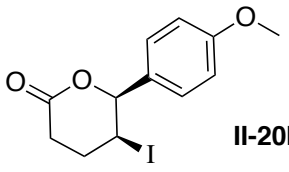

II-20b-I

Analytical data for *syn*-5-iodo-6-(4-methoxyphenyl)tetrahydro-2H-pyran-2-one (**II-20b**-I): colorless oil, ^{1}H NMR (500 MHz, $CDCl_3$) δ 7.23 (2H, d, *J* = 9.0 Hz.), 6.89 (2H, d, *J* = 9.0 Hz.), 4.80 (1H, d, *J* = 2.0 Hz.), 4.60 (1H, dd, *J* = 3.0, 6.0 Hz.), 3.80 (3H, s.), 3.00 (1H, dddd, *J* = 8.5, 11.0, 19.0, 19.0 Hz.), 2.78 (1H, ddd, *J* = 2.0, 7.0, 19.0 Hz.), 2.54-2.41 (2H, m.); ^{13}C NMR (125 MHz, $CDCl_3$) δ

168.8, 159.6, 130.7, 126.5, 113.6, 82.1, 55.3, 33.5, 30.7, 28.3 ppm. IR (film) 3009, 2929, 2856, 1709, 1163, 1516, 1260, 1145, 1034, 990, 829 cm^{-1}. HRMS (ESI) Calculated Mass for $C_{12}H_{14}IO_3$: ($[M+H]^+$) = 332.9988, Found ($[M+H]^+$) = 332.998772.

***syn*-5-(iodo(4-methoxyphenyl)methyl)dihydrofuran-2(3H)-one (II-20c-I):**

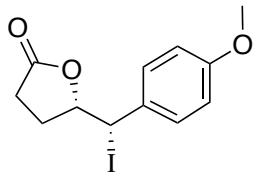

6'c-I

Compound **II-20c**-I could not be purified by known analytical methods. This iodolactone is unstable at room temperature and decomposes rapidly upon work up of the reaction mixture. Its identity was confirmed based on crude ^1H NMR analysis. Distinctly resolved protons are as

Figure II-31. Crude ^1H NMR spectrum for **II-20c**-I.

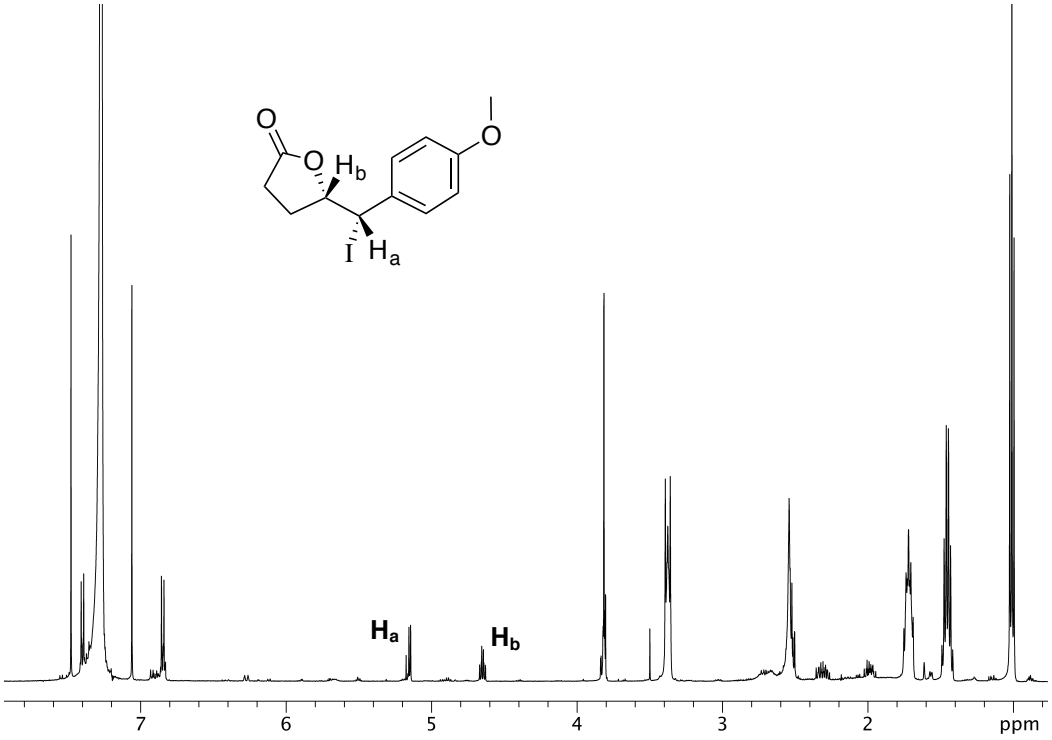

follows: ^{1}H NMR (500 MHz, $CDCl_3$) δ 7.37 (2H, d, *J* = 9.0 Hz.), 6.82 (2H, d, *J* = 9.0 Hz.), 5.12 (1H, d, *J* = 5.5 Hz.). 4.62 (1H, ddd, *J* = 5.5, 7. 0, 12.5 Hz.), 3.78 (3H, s.), 2.28 (1H, dddd, *J* = 5.5, 8.0, 10.0, 16.0 Hz.), 1.95 (1H, dddd, *J* = 7.0, 9.0, 12.5, 16.0 Hz.) ppm. Figure II-31 depicts the crude ^{1}H NMR spectrum for **II-20c**-I.

5-methyl-5-phenylfuran-2(5*H*)-one (II-22a):

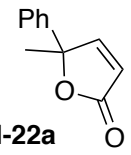

II-22a

Analytical data[78,91] for 5-methyl-5-phenylfuran-2(5*H*)-one (**II-22a**): colorless oil, ^{1}H NMR (500 MHz, $CDCl_3$) δ 7.62 (2H, d, *J* = 5.5 Hz.), 7.36-7.28 (5H, m.), 6.03 (1H, d, *J* = 5.5 Hz.), 1.81 (3H, s.); ^{13}C NMR (125 MHz, $CDCl_3$) δ 171.2, 159.2, 138.2, 127.8, 127.3, 123.7, 118.3, 88.0, 25.3 ppm.

4-chloro-5-methyl-5-phenyldihydrofuran-2(3H)-one (II-22b-Cl**):**

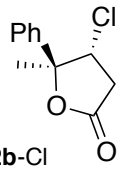

II-22b-Cl

Analytical data for 4-chloro-5-methyl-5-phenyldihydrofuran-2(3H)-one (**II-22b**-Cl): colorless oil, ^{1}H NMR (500 MHz, $CDCl_3$) δ 7.40-7.31 (5H, m.), 4.67 (1H, dd, *J* = 3.5, 6.5 Hz.), 2.94 (1H, dd, *J* = 6.5, 17.5 Hz.), 2.77 (1H, dd, *J* = 3.0, 17.5 Hz.), 1.81 (3H, s.); ^{13}C NMR (125 MHz, $CDCl_3$) δ 172.8, 141.8, 129.0, 128.5, 124.1, 88.9, 62.2, 39.4, 25.5 ppm. IR (film) 3062, 3003, 2938, 1789, 1602, 1496, 1447, 1380, 1217, 1133, 1073, 956, 768 cm^{-1}. HRMS (ESI) Calculated Mass for $C_{11}H_{12}ClO_2$: ($[M+H]^+$) = 211.0526, Found ($[M+H]^+$) = 211.0525.

The relative stereochemistry was established by NOE studies:

a. Irradiation at 4.67 ppm shows enhancement at 2.94 and 7.42 ppm.

b. Irradiation at 1.81 ppm shows enhancement at 2.77 and 7.42 ppm.

4-bromo-5-methyl-5-phenyldihydrofuran-2(3H)-one (II-22b-Br**):**

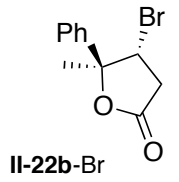

II-22b-Br

Analytical data[92] for 4-bromo-5-methyl-5-phenyldihydrofuran-2(3H)-one (**II-22b**-Br): colorless oil, ^{1}H NMR (500 MHz, $CDCl_3$) δ 7.39-7.32 (5H, m.), 4.70 (1H, dd, *J* = 4.0, 7.0 Hz.), 3.09 (1H, dd, *J* = 7.0, 18.5 Hz.), 2.91 (1H, dd, *J* = 4.0, 18.5 Hz.), 1.86 (3H, s.); ^{13}C NMR (125 MHz, $CDCl_3$) δ 173.0, 141.1, 129.0, 128.5, 124.1, 88.4, 52.5, 40.2, 27.6 ppm.

4-iodo-5-methyl-5-phenyldihydrofuran-2(3H)-one (II-22b-I**):**

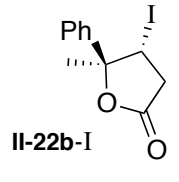

II-22b-I

Analytical data[78] for 4-iodo-5-methyl-5-phenyldihydrofuran-2(3H)-one (**II-22b**-I): colorless oil, ^{1}H NMR (500 MHz, $CDCl_3$) δ 7.43-7.31 (5H, m.), 4.63 (1H, t, *J* = 6.5 Hz.), 3.18 (1H, dd, *J* = 7.5, 18.0 Hz.), 2.99 (1H, dd, *J* = 6.5, 18.5 Hz.), 1.91 (3H, s.); ^{13}C NMR (125 MHz, $CDCl_3$) δ 173.5, 140.7, 128.9, 128.4, 124.3, 88.1, 42.1, 30.5, 27.7 ppm.

4-(1-phenylvinyl)oxetan-2-one (**II-22c**)**:**

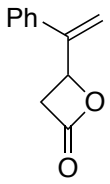

II-22c

Analytical data for 4-(1-phenylvinyl)oxetan-2-one (**II-22c**): colorless oil, ^{1}H NMR (500 MHz, $CDCl_3$) δ 7.40-7.31 (5H, m.), 5.61 (1H, br s.), 5.55 (1H, br s.), 5.35 (1H, dd, *J* = 4.5, 5.0 Hz.), 3.73 (1H, dd, *J* = 6.0, 16.5 Hz.), 3.22 (1H, dd, *J* = 4.5, 16.5 Hz.); ^{13}C NMR (125 MHz, $CDCl_3$) δ 167.5, 144.0, 136.4, 128.8, 128.6, 126.0, 114.3, 70.1, 44.9 ppm. IR (film) 3059, 2928, 2853, 1831 (s), 1787, 1718, 1575, 1496, 1446, 1406, 1268, 1131, 947, 897, 712 cm^{-1}. HRMS (ESI) Calculated Mass for $C_{11}H_{11}O_2$: ($[M+H]^+$) = 175.0759, Found ($[M+H]^+$) = 175.0764.

5-(chloromethyl)-5-(4-methoxyphenyl)dihydrofuran-2(3H)-one-4,4-*d*$_2$ (**II-2a**-D_2):

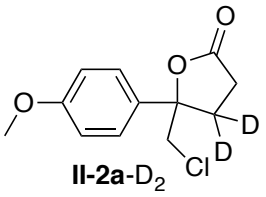

II-2a-D_2

Analytical data for 5-(chloromethyl)-5-(4-methoxyphenyl)dihydrofuran-2(3H)-one-4,4-*d*$_2$ (**II-2a**-D_2): colorless oil; ^{1}H NMR (500 MHz, $CDCl_3$) δ 7.30 (2H, d, *J* = 8.5.), 6.90 (2H, d, *J* = 8.5.), 3.80 (3H, s), 3.79 (1H, d, *J* = 12.0 Hz), 3.70 (1H, d, *J* = 12.0 Hz), 2.75 (1H, d, *J* = 18.0 Hz), 2.51 (1H, d, *J* = 18.0 Hz); ^{13}C NMR (125 MHz, $CDCl_3$) δ 175.8, 159.7, 132.4, 126.2, 114.1, 86.9, 55.3, 52.1, 30.9 (quint, *J* = 19.5 Hz), 28.9 ppm. IR (film) 3004, 2959, 2839, 2558, 2423, 2249, 2073, 1893, 1783 (s), 1612, 1515 (s), 1463, 1254, 1180, 1034, 835 cm^{-1}. HRMS (ESI) Calculated Mass for $C_{12}H_{12}D_2ClO_3$: ($[M+H]^+$) = 243.0757, Found ($[M+H]^+$) = 243.0756.

II.6. Quantum mechanical modeling studies.

Full optimizations for all conformations of the 'halenium ion' acceptors and the corresponding 'Lewis base-halenium ion' complexes were performed using density functional calculations at the B3LYP/6-31G*/SM8($CHCl_3$) level in the Spartan-10 software running on Macintosh and Linux platforms. To confirm that each structure was a true minimum, vibrational analyses were performed. The *HalA* (Cl) values were calculated using the energies obtained from a full geometry optimization of the structures in simulated chloroform at B3LYP/6-31G*/SM8 level of theory. Alternatively, when the *gas phase* energies of the same structures were corrected for solvation in simulated chloroform using the SM8 model available in the Spartan code to run single point (i.e. B3LYP/6-31G*/SM8) calculations, the resulting data led to the same conclusion. To verify convergence and consistency of the optimizations, a number of examples were re-optimized from multiple starting points; energetic variations of 0.02 kcal/mol or less were found among these calculated structures. Relative enthalpies $\Delta H°_{rel}$ were calculated for the *gas phase* structures by including zero-point and thermal corrections to 298.15 K. All transition state structures were validated as first-order stationary points (i.e. a single imaginary frequency) by vibrational analysis. All values are in kcal/mol, eV or hartrees. Importantly, neither the vibration nor the solvation corrections introduced differences between relative E° and relative H° values that were large enough to reorder the relative energy structures; thus, either set of data led to the same conclusions.

REFERENCES

REFERENCES

(1) Patai, S. *Frontmatter*; John Wiley & Sons, Ltd., 2010.

(2) Crudden, Cathleen M.; Edwards, D. *Eur. J. Org. Chem.* **2003**, *2003*, 4695.

(3) Jacobsen, E. N.; Pfaltz, A.; Yamamoto, H. *Comprehensive Asymmetric Catalysis*; Springer: Berlin, New York, 1999.

(4) Faul, M. M.; Evans, D. A. In *Asymmetric Oxidation Reactions*; Katsuki, T., Ed.; Oxford University Press: London, 2001, p 115.

(5) Ojima, I. *Catalytic asymmetric synthesis*; 2nd ed.; Wiley-VCH: New York, 2000.

(6) Sweeney, J. B. *Chem. Soc. Rev.* **2002**, *31*, 247.

(7) van Summeren, R. P.; Romaniuk, A.; Ijpeij, E. G.; Alsters, P. L. *Catal. Sci. Technol.* **2012**, *2*, 2052.

(8) van Pee, K. H.; Unversucht, S. *Chemosphere* **2003**, *52*, 299.

(9) Tan, C. K.; Zhou, L.; Yeung, Y. Y. *Synlett* **2011**, 1335.

(10) Roberts, I.; Kimball, G. E. *J. Am. Chem. Soc.* **1937**, *59*, 947.

(11) Murai, K.; Fujioka, H. *Heterocycles* **2013**, *87*, 763.

(12) J, C.; L, Z. *Synthesis* **2014**, *46*, 586.

(13) Hennecke, U. *Chem. Asian. J.* **2012**, *7*, 456.

(14) Denmark, S. E.; Kuester, W. E.; Burk, M. T. *Angew. Chem. Int. Ed.* **2012**, *51*, 10938.

(15) De Luca, L.; Giacomelli, G.; Masala, S.; Porcheddu, A. *J. Org. Chem.* **2003**, *68*, 4999.

(16) Chen, G.; Ma, S. *Angew. Chem. Int. Ed.* **2010**, *49*, 8306.

(17) Castellanos, A.; Fletcher, S. P. *Chem. Eur. J.* **2011**, *17*, 5766.

(18) Brunel, Y.; Rousseau, G. *J. Org. Chem.* **1996**, *61*, 5793.

(19) Yousefi, R.; Ashtekar, K. D.; Whitehead, D. C.; Jackson, J. E.; Borhan, B. *J. Am. Chem. Soc.* **2013**, *135*, 14524.

(20) Williams, D. L.; Bienvenu.E; Dubois, J. E. *J. Chem. Soc.* **1969**, 517.

(21) Solling, T. I.; Radom, L. *Int. J. Mass. Spectrom.* **1999**, *185*, 263.

(22) Poutsma, M. L. *J. Am. Chem. Soc.* **1965**, *87*, 4285.

(23) Olah, G. A.; Westerma.Pw; Melby, E. G.; Mo, Y. K. *J. Am. Chem. Soc.* **1974**, *96*, 3565.

(24) Olah, G. A.; Peterson, P. E. *J. Am. Chem. Soc.* **1968**, *90*, 4675.

(25) Olah, G. A.; Bollinger, J. *J. Am. Chem. Soc.* **1967**, *89*, 4744.

(26) Olah, G. A.; Bollinge, J. M. *J. Am. Chem. Soc.* **1968**, *90*, 947.

(27) Olah, G. A.; Bollinge, J. M.; Brinich, J. *J. Am. Chem. Soc.* **1968**, *90*, 6988.

(28) *Halogen Bonding: Fundamentals and Applications*; Metrangolo, P.; Resnati, G., Eds.; Springer-Verlag: Berlin, 2008.

(29) McManus, S. P.; Peterson, P. E. *Tetrahedron Lett.* **1975**, 2753.

(30) Haubenstock, H.; Sauers, R. R. *Tetrahedron* **2005**, *61*, 8358.

(31) Haubenstock, H.; Sauers, R. R. *Tetrahedron* **2004**, *60*, 1191.

(32) Fahey, R. C.; Schubert, C. *J. Am. Chem. Soc.* **1965**, *87*, 5172.

(33) Fahey, R. C.; McPherso.Ca *J. Am. Chem. Soc.* **1969**, *91*, 3865.

(34) Fahey, R. C. *J. Am. Chem. Soc.* **1966**, *88*, 4681.

(35) Denmark, S. E.; Burk, M. T.; Hoover, A. J. *J. Am. Chem. Soc.* **2010**, *132*, 1232.

(36) Bienvenu.E; Dubois, J. E.; Pearson, D. W.; Williams, D. L. *J. Chem. Soc.* **1970**, 1275.

(37) Whitehead, D. C.; Yousefi, R.; Jaganathan, A.; Borhan, B. *J. Am. Chem. Soc.* **2010**, *132*, 3298.

(38) Blackmond, D. G. *Angew. Chem. Int. Ed.* **2005**, *44*, 4302.

(39) Poutsma, M. L. *Science* **1967**, *157*, 997.

(40) Tarbell, D. S.; Bartlett, P. D. *J. Am. Chem. Soc.* **1937**, *59*, 407.

(41) Bartlett, P. D.; Tarbell, D. S. *J. Am. Chem. Soc.* **1936**, *58*, 466.

(42) Bogle, X. S.; Singleton, D. A. *J. Am. Chem. Soc.* **2011**, *133*, 17172.

(43) McManus, S. P.; Ware, D. W. *Tetrahedron Lett.* **1974**, 4271.

(44) Ohta, B. K.; Hough, R. E.; Schubert, J. W. *Org. Lett.* **2007**, *9*, 2317.

(45) Cristol, S. J.; Stermitz, F. R.; Ramey, P. S. *J. Am. Chem. Soc.* **1956**, *78*, 4939.

(46) Rao, T. S.; Jukar, R. N.; Dangat, V. T. *Curr. Sci.* **1986**, *55*, 483.

(47) Ashtekar, K. D.; Marzijarani, N. S.; Jaganathan, A.; Holmes, D.; Jackson, J. E.; Borhan, B. *J. Am. Chem. Soc.* **2014**, *136*, 13355.

(48) Struble, M. D.; Scerba, M. T.; Siegler, M.; Lectka, T. *Science* **2013**, *340*, 57.

(49) Wang, Y. M.; Wu, J.; Hoong, C.; Rauniyar, V.; Toste, F. D. *J. Am. Chem. Soc.* **2012**, *134*, 12928.

(50) Braddock, D. C.; Hermitage, S. A.; Kwok, L.; Pouwer, R.; Redmond, J. M.; White, A. J. P. *Chem. Commun.* **2009**, 1082.

(51) Bennet, A. J.; Brown, R. S.; McClung, R. E. D.; Klobukowski, M.; Aarts, G. H. M.; Santarsiero, B. D.; Bellucci, G.; Bianchini, R. *J. Am. Chem. Soc.* **1991**, *113*, 8532.

(52) Neverov, A. A.; Brown, R. S. *J. Org. Chem.* **1996**, *61*, 962.

(53) Snyder, S. A.; Treitler, D. S.; Brucks, A. P. *J. Am. Chem. Soc.* **2010**, *132*, 14303.

(54) Klopman, G. *J. Am. Chem. Soc.* **1968**, *90*, 223.

(55) Tomoda, S. *Chem. Rev.* **1999**, *99*, 1243.

(56) Singleton, D. A.; Szymanski, M. J. *J. Am. Chem. Soc.* **1999**, *121*, 9455.

(57) Singleton, D. A.; Thomas, A. A. *J. Am. Chem. Soc.* **1995**, *117*, 9357.

(58) Akdag, A.; Worley, S. D.; Acevedo, O.; McKee, M. L. *J. Chem. Theory Comput.* **2007**, *3*, 2282.

(59) Mizar, P.; Burrelli, A.; Gunther, E.; Softje, M.; Farooq, U.; Wirth, T. *Chem. Eur. J.* **2014**, *20*, 13113.

(60) Grunwald, E. *J. Am. Chem. Soc.* **1951**, *73*, 5458.

(61) Denmark, S. E.; Burk, M. T. *Proc. Natl. Acad. Sci. U. S. A.* **2010**, *107*, 20655.

(62) The SciFinder® prediction displays a pKa of 4.65 for **1f** using Advanced Chemistry Development (ACD/Labs) Software V11.02 (© 1994-2014 ACD/Labs)

(63) Brown, A. R.; Uyeda, C.; Brotherton, C. A.; Jacobsen, E. N. *J. Am. Chem. Soc.* **2013**, *135*, 6747.

(64) Jensen, K. H.; Pathak, T. P.; Zhang, Y.; Sigman, M. S. *J. Am. Chem. Soc.* **2009**, *131*, 17074.

(65) Blackman, M. L.; Royzen, M.; Fox, J. M. *J. Am. Chem. Soc.* **2008**, *130*, 13518.

(66) Marenich, A. V.; Olson, R. M.; Kelly, C. P.; Cramer, C. J.; Truhlar, D. G. *J. Chem. Theory Comput.* **2007**, *3*, 2011.

(67) Kuck, D.; Schneider, J.; Grutzmacher, H. F. *J. Chem. Soc.-Perkin Trans. 2* **1985**, 689.

(68) Grossel, M. C.; Cheetham, A. K.; James, D.; Newsam, J. M. *J. Chem. Soc.-Perkin Trans. 2* **1980**, 471.

(69) Braddock, D. C.; Cansell, G.; Hermitage, S. A. *Chem. Commun.* **2006**, 2483.

(70) Takemiya, A.; Hartwig, J. F. *J. Am. Chem. Soc.* **2006**, *128*, 6042.

(71) Tan, C. K.; Zhou, L.; Yeung, Y. Y. *Org. Lett.* **2011**, *13*, 2738.

(72) Zheng, T.; Narayan, R. S.; Schomaker, J. M.; Borhan, B. *J. Am. Chem. Soc.* **2005**, *127*, 6946.

(73) Jefford, C. W.; Wang, Y. *J. Chem. Soc.-Chem. Commun.* **1987**, 1513.

(74) Perkins, R. J.; Xu, H. C.; Campbell, J. M.; Moeller, K. D. *Beilstein J. Org. Chem.* **2013**, *9*, 1630.

(75) Less, S. L.; Handa, S.; Millburn, K.; Leadlay, P. F.; Dutton, C. J.; Staunton, J. *Tetrahedron Lett.* **1996**, *37*, 3515.

(76) Odinokov, V. N.; Vakhidov, R. R.; Shakhmaev, R. N.; Zorin, V. V. *Chemistry of Natural Compounds* **1996**, *32*, 912.

(77) Tan, C. K.; Le, C. C.; Yeung, Y. Y. *Chem. Commun.* **2012**, *48*, 5793.

(78) Garnier, J. M.; Robin, S.; Rousseau, G. *Eur. J. Org. Chem.* **2007**, 3281.

(79) Song, S.; Zhu, S. F.; Yang, S.; Li, S.; Zhou, Q. L. *Angew. Chem. Int. Ed.* **2012**, *51*, 2708.

(80) Francisco, C. G.; Freire, R.; Hernandez, R.; Salazar, J. A.; Suarez, E.; Delamora, G. A. G.; Noguez, J. A.; Acosta, A.; Jimeno, O. *Steroids* **1983**, *41*, 267.

(81) Nagase, R.; Matsumoto, N.; Hosomi, K.; Higashi, T.; Funakoshi, S.; Misaki, T.; Tanabe, Y. *Org. Biomol. Chem.* **2007**, *5*, 151.

(82) Mahmoodi, N. O.; Jazayri, M. *Synth. Commun.* **2001**, *31*, 1467.

(83) Seyfried, M. S.; Lauber, B. S.; Luedtke, N. W. *Org. Lett.* **2010**, *12*, 104.

(84) Armstrong, A.; Braddock, D. C.; Jones, A. X.; Clark, S. *Tetrahedron Lett.* **2013**, *54*, 7004.

(85) Gurjar, M. K.; Purandare, A. V. *Indian J. Chem. Sect B-Org. Chem. Incl. Med. Chem.* **1988**, *27*, 554.

(86) Abe, H.; Fukazawa, N.; Kobayashi, T.; Ito, H. *Tetrahedron* **2013**, *69*, 2519.

(87) Wang, M.; Gao, L. X.; Mai, W. P.; Xia, A. X.; Wang, F.; Zhang, S. B. *J. Org. Chem.* **2004**, *69*, 2874.

(88) Paull, D. H.; Fang, C.; Donald, J. R.; Pansick, A. D.; Martin, S. F. *J. Am. Chem. Soc.* **2012**, *134*, 11128.

(89) Snider, B. B.; Johnston, M. I. *Tetrahedron Lett.* **1985**, *26*, 5497.

(90) Fang, C.; Paull, D. H.; Hethcox, J. C.; Shugrue, C. R.; Martin, S. F. *Org. Lett.* **2012**, *14*, 6290.

(91) Meyers, A. I.; Spohn, R. F. *J. Org. Chem.* **1985**, *50*, 4872.

(92) Tan, C. K.; Er, J. C.; Yeung, Y. Y. *Tetrahedron Lett.* **2014**, *55*, 1243.